Geochemistry of the Rosebery Ore Deposit

by

Winfried Naschwitz, Diplom Mineraloge

Submitted in fulfilment of the
requirements of the degree of
Doctor of Philosophy

graduating 1985

UNIVERSITY OF TASMANIA
HOBART
1985

To the best of my knowledge this thesis
contains no material by another author,
except where due reference is made

March, 1985

Table of Contents

List of Figures

List of Tables

ABSTRACT

The Rosebery ore deposit is located in the Cambrian Mt. Read Volcanic Belt at the west coast of Tasmania. Two tabular Zn-Pb-Cu(-Ag-Au) orebodies of the deposit are hosted next to each other in a 45° east dipping sedimentary horizon and belong to the massive sulphide deposits which were generated within pyroclastics during a period of reduced volcanism.

In the Rosebery area the calc-alkaline Mt. Read Volcanics are divided into rhyolitic pyroclastics and overlying andesitic to rhyolitic lavas. The ash flow tuff in the footwall of the ore deposit is uniformly welded. The volcanic rocks in the hanging wall consist mostly of a mixed sequence of unwelded and welded pyroclastics. In the mine area the two pyroclastic units are separated by the 70-150 m wide ore-bearing sedimentary horizon which includes siltstone and associated reworked tuff and tuff.

The footwall and to a minor degree the hanging wall have been subjected to hydrothermal alteration. In the field, this alteration is marked by plagioclase-free quartz-sericite(-chlorite) schists which exhibit two different facies: siliceous augen schists and thinly cleaved K-feldspar bearing schists.

Geochemically the collected rock samples fall into two groups: altered and unaltered volcanics. This classification is made possible by cluster analysis despite the large chemical variation within each group. In addition, an almost perfect separation into these two groups can be achieved by discriminant analysis when the chemistry of the schists is compared to that of the unaltered pyroclastics. On a univariate basis geochemical differences exist for a large number of elements. A clear pattern of enrichment (SiO_2, K_2O, Rb, S) and depletion (Al_2O_3, Na_2O, TiO_2, CaO, Sr, Zr, Y, Nb) can be contour-plotted for a smaller number of elements which show a statistically significant difference between altered and unaltered rocks. Both geological and geochemical alteration extend for $\leq$ 2 km in N-S direction and have a maximal E-W width of about 700 m. However the geochemical approach is more successful in detecting the hanging wall alteration and in defining the hydrothermal channel in the footwall.

Based on underground geology and geochemistry, there is evidence for a separate hydrothermal vent for each of the two orebodies apart from the alteration halo on the surface which belongs entirely to the vent below the

larger southern orebody. In the immediate footwall of the northern orebody a central area of $\geq$ 300 m across is totally devoid of feldspars, as below the southern orebody. This aureole of intense alteration is largely composed of siliceous augen schists with an increased amount of disseminated mineralization which is clearly reflected in the chemical distribution patterns of the ore forming metals including sulphur. Based on constant rock volume the element mobilization pattern in this part differs slightly from that of the surface alteration. Most importantly CaO is not depleted, SiO_2 shows a stronger enrichment and the decrease in Zr and TiO_2 is more pronounced. A good spatial relationship exists between the sulphide enrichment in the footwall schists and the maximum ore grade in the overlying orebody. This footwall zone is surrounded by moderately altered pyroclastics containing albitic feldspars which range from clear euhedra to relics.

Additional exploration methods based on REE distribution and whole rock oxygen isotope analyses and the composition of phyllosilicates produce less satisfactory results than major and conventional trace element chemistry. Some of the original features of hydrothermal oxygen isotope and REE chemistry and mineral compositions have been partly obliterated due to re-equilibration during the Devonian Tabberabberan orogeny.

Based on contoured metal zonations and also drill core logging, the northern orebody can be shown to be essentially divided into a Cu-Fe rich bottom part and a Pb-Zn rich top half. This distribution is complicated by the occurrence of smaller amounts of Pb-Zn ore in the bottom part and Cu-Fe ore in the top half. This zonation can be best explained by the deposition of a blanket of galena-sphalerite ore during the initial stage of hydrothermal activity and subsequent introduction and/or replacement by chalcopyrite-pyrite ore by hydrothermal solutions at an increased temperature. Boundary conditions for the hydrothermal fluids can be established based on the sulphide mineral assemblage in the ore and the silicate mineral assemblage in the alteration zone.

INTRODUCTION

The Zn-Pb-Cu(Ag-Au) bearing massive sulphide deposit at Rosebery (145°32′ E, 41°46′ S, fig.1) lies 30 km inland from the west coast of Tasmania, 170 m above sea level in rugged terrain with dense rainforests. The deposit, consisting of two adjacent orebodies is hosted in a mainly sedimentary horizon within a pile of acid pyroclastics which are part of the Cambrian Mt. Read Volcanic Belt. Based on Reid & Meares (1981), the total amount of the original ore amounted to approximately 18 million tonnes of 5.2% Pb, 16.6% Zn, 0.7% Cu, 159 ppm Ag and 3.3 ppm Au. At the end of January 1984, 6.4 million tonnes of ore reserves remain, grading 4.9% Pb, 15.8% Zn, 0.77% Cu, 135 ppm Ag and 3.5 ppm Au. The production in the twelve months until the end of June 1984 was 478000 tonnes (J.W. Farquhar, pers. comm.).

The ore was discovered by T. McDonald in 1893 who found alluvial gold and galena-sphalerite boulders (Easterbrook, 1962). By 1898, Harcourt Smith (1898) reported 29 mines operating in the Rosebery area.

Originally the Rosebery ore deposit was considered to be a Devonian replacement ore (e.g. Hills, 1915a, b; Finucane, 1932a, b). Hall & Solomon (1962) raised the possibility of a Cambrian ore deposition during or after volcanic activity. The syngenetic exhalative-volcanic origin of the ore deposit was firmly established by Braithwaite (1969) who carried out an extensive investigation of the mine geology. The results of his Ph. D. thesis which is referred to frequently in this thesis were published in Braithwaite (1972, 1974). Loftus-Hills & Solomon (1967) studied the Co and Ni content in pyrite as indicators of magmatic-hydrothermal activity of respectively Cambrian and Devonian age. Stanton & Rafter(1966), Solomon et al. (1969) and Green et al. (1981) investigated the sulphur isotope chemistry. The mineralogy and geochemistry of the host rock and its comparison to other sediment horizons in the vicinity was examined by Gee (1970), Eastoe (1973) and Smith (1975).

The general geology of the Rosebery area and the origin of the volcanic rocks has been discussed by many authors, partly mentioned in chap. 5.1.-5.3.,6.

This project was taken up in the final stages of G.R. Green's Ph.D. thesis, which was submitted at the end of 1983. His work concentrated on

the regional geology, zonation of the southern orebody, including trace element distribution of the immediate footwall and ore genesis including sulphur isotope chemistry. He also evaluated the influence of the Devonian greenschist metamorphism on the hydrothermal mineralogy. Most of his work has been published in Green et al. (1981).

The principal aim of this study was to test exploration methods for massive sulphide deposits on an existing case. As such it was in its beginning greatly influenced by the publication of Beus and Grigorian (1977) and Levinson (1980) stressing the importance of lithogeochemistry in outlining the target areas for ore deposits. In addition to the Russian studies, geochemical alteration studies of massive sulphide deposits have been mainly published from the Archaean and Palaeozoic deposits in Canada, from the Miocene Kuroko deposits in Japan and some of the Australian deposits in the Palaeozoic Tasman geosyncline (chap.12.2.2). Further incentives were provided by the fact that Rosebery and Que River, some 20 km to the north are the only major Pb-Zn-Cu-Ag(-Au) producers with economic amounts of Au in Australia (Legge et al., 1984). A study combining geology, geochemistry and mineral composition was employed in order to compare the results and eliminate the less efficient exploration methods. This aim required an understanding of the ore forming processes and in particular of the zonation of the ore in relation to the centres of the hydrothermal activity.

Sampling on the surface was severely restricted away from the Rosebery township by dense vegetation. Drill core sampling in the immediate footwall below the northern orebody was limited by the usually short extension of drill holes. Drilling on most levels was conducted away from the ore and stopped immediately below the ore or shortly after reaching the footwall schists. Specimens and samples referred to are quoted in brackets. Drill holes referred to are preceeded by "DDH", surface maps are based on the Australian Map Grid (A.M.G.). Data manipulation was carried out on a Burroughs B6800.

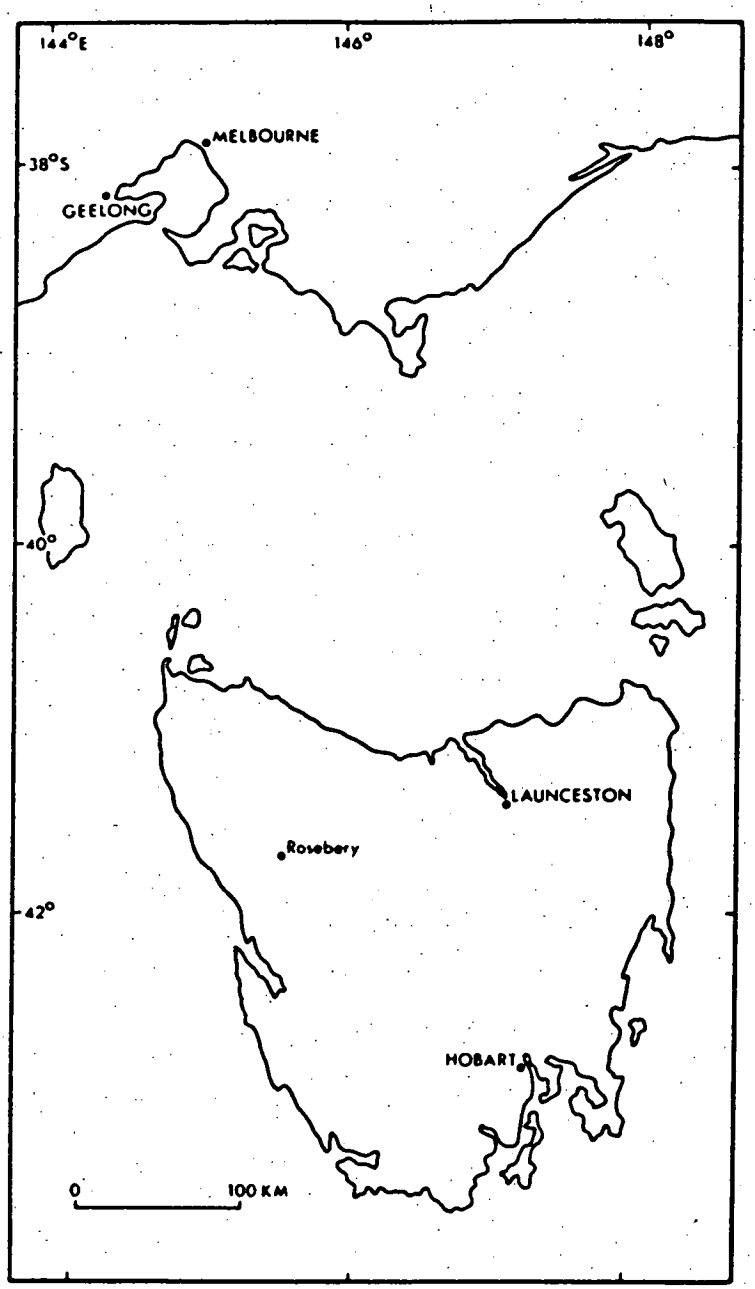

Fig.1: Location of Tasmania

ACKNOWLEDGEMENTS

The Electrolytic Zinc Company of Australasia Pty Ltd, West Coast Operations, at Rosebery made this project possible by permitting access to all facilities and records. Also the company financed the oxygen isotope analyses and part of the trace element analyses, whilst accommodation was provided during my field work. I am most grateful for this support. I am indebted to the geological staff at Rosebery which helped me find my way through records, coresheds, underground and bush, and also contributed to my understanding of the ore deposit by discussion and offering new ideas. My particular thanks go the the late J.G. Druett, J. McDonald, J.H.A. Mill, G.D. Iliff, D.A.C. Archibald, J.W. Howarth, T.C. Lees, J.W. Farquhar, R.A. Hawley, R. J. Reid.

I am most sincerely grateful to my supervisor Dr. J.C. van Moort, without his unrelenting moral and intellectual support I would not have completed this project. My thanks extend to staff and post-graduate students of the Geology Department of the University of Tasmania for discussion and criticism. Among these Dr. R.J. Ford never hesitated to give his advice on matters of mineralogy and petrography, P. Robinson provided help for chemical analyses, Dr. N.C. Higgins introduced me to the REE analysis, Dr. A.J. Crawford read part of the thesis and helped to improve the English, J.P. Pongratz drafted most of the manual diagrams and S. Stephens made the thin sections.

Prof. A.A. Levinson, University of Calgary, suggested the examination of the REE distribution. Dr. B.M. Brown and G.D. McPherson from the Department of Mathematics of the University of Tasmania gave their advice on statistical problems. Dr. R.K. Allen and B.W. Marriott from the Computing Centre helped me to circumvent the traps and snares of a main frame computer system and contributed largely to my working knowledge of computing. The friendly and helpful attitude of the staff of the Computing Centre made hardware breakdowns much more bearable. W. Jablonski of the Central Science Laboratory of the University introduced me to the microprobe and gave a helping hand when things went wrong. Thank you to all of them and others I might have missed.

Above all I would like to thank my parents who have supported me in many ways through all these years of study to see their only child settle at the opposite side of the globe.

The same gratitude I extend to my wife Jennifer for putting up with a disrupted life, typing the thesis, proof reading and polishing up my English.

1. Definition of massive sulphide deposits.

Massive sulphide deposits are a major source for the production of Pb, Zn, Cu and sometimes Au and Ag, and occur world wide, mostly in clusters, as conformable and stratiform orebodies. Their sulphide content can exceed 60 wt % (Sangster & Scott, 1976). Underneath the massive tabular to lenticular shaped orebodies, crosscutting stockworks or disseminated ore can extend into the footwall. The term "massive sulphide deposits" includes two different groups of deposits.

a. The volcanic massive sulphide deposits associated with volcanic rocks and sediments represent the majority of deposits. They have been formed during periods of quiescence in orogenic belts and at sites of sea floor spreading as lenticular orebodies.

b. The sediment hosted massive sulphide deposits are embedded as tabular orebodies in epiclastic or chemical sediments along rift structures in an ensialic environment. They will not be discussed explicitly.

From the oldest massive sulphide deposits in the Archaean to the youngest in the Miocene, they share many common characteristics in relation to the shape and zonation of their orebodies, their host rock and the alteration imposed upon the host rock. This suggests a general genetic process that has persisted through time with little variation, and is now accepted as a submarine exhalative deposition by metal-bearing hot fluids.

Despite the unifying similarities among the massive sulphide deposits, recognizable variations remain which serve to distinguish between certain types.

2. Classification of massive sulphide deposits.

Several authors have attempted to classify the massive sulphide deposits. They used metal compositions, host rock lithology and tectonic setting as main criteria.

Sawkins (1972, 1976) stressed the importance of tectonics as a control of ore formation and devised a four fold division into:

a. Kuroko-type deposits related to plate convergence.

b. Cyprus-type deposits related to plate divergence.

c. Besshi-type deposits related to incipient plate convergence, but uncertain.

d. Sullivan-type deposits related to intercratonic tensional rifting.

Sangster & Scott (1976) suggested a three fold division based on North American massive sulphide deposits:

a. Deposits predominantly associated with volcanics in the Noranda district (Quebec), Flin Flon and Snow Lake area (Manitoba) and near Jerome (Arizona).

b. Deposits in mixed volcanic-sedimentary terrain peripheral to volcanic centres in the Flin Flon, Noranda and Manitouwadge area (Ontario).

c. Deposits in predominantly sedimentary rocks such as the siltstone and argillite hosted Sullivan mine in British Columbia.

Solomon (1976) used a different approach. His classification is based on the overall Cu/Pb/Zn ratio of some fifty ore deposits resulting in three different types:

a. Zn-Pb-Cu type: Major ore minerals in order of abundance are pyrite, sphalerite, galena and chalcopyrite with minor amounts of tetrahedrite, pyrrhotite and bornite. Barite usually occurs with this type of mineralization.

b. Zn-Cu type: Pyrite, pyrrhotite, sphalerite and chalcopyrite with minor amounts of arsenopyrite and magnetite. Deposits of both types can hold economic amounts of gold and silver.

c. Cu type: Pyrite and chalcopyrite with minor amounts of pyrrhotite and sphalerite and economic concentrations of gold.

He further concluded that more than 90% of type a. deposits overlie at least to some extent felsic (dacitic-rhyolitic) volcanics. As for type b., most ore deposits still have a felsic volcanic footwall, however this changes with type c. This type shows greater affinity towards mafic volcanics in the footwall.

Hutchinson (1973, 1980) and Klau & Large (1980) put the emphasis on the tectonic setting as the main controlling factor for the variation in the occurrence of massive sulphide deposits as Sawkins had. Yet they chose different characteristics for their classification. Hutchinson employed a combination of metal composition, spatially associated volcanics and sediments, age and tectonic environment (volcanic hosted and sediment hosted). Listed below are the first and last characteristics only from Hutchinson (1980):

A. Volcanogenic group.

a. Primitive type Zn-Cu-(Ag-Au) at consuming margin of island arc.

b. Polymetallic type Pb-Zn-Cu-(Ag-Au) at sites of back-arc spreading.

c. Cupreous pyrite type Cu-(Au) at sites of oceanic rifting.

d. Kieslager type Cu-Zn-(Au) in fore-arc trough.

B. Sedimentary group.

e. Clastic hosted type Pb-Zn-(Ag) in aulacogenic trough.

f. Carbonate hosted type Zn-Pb-(Ag) on shelf or in fault controlled basin.

Klau & Large supported a broad division into deposits with close association to:

a. Mafic volcanics in ophiolitic sequences and immature island arcs.

b. Felsic volcanics in immature and mature island arcs, and greenstone belts with cratonic rifting.

c. Sediments associated with cratonic rifting.

Tab. 1 shows the correlation amongst the discussed classifications in relation to their tectonic setting.

Tectonic setting	Klau & Large, 1980	Sangster & Scott, 1976	Hutchinson, 1980	Solomon, 1976	Sawkins, 1976
Oceanic rifting at accreting margin			Cupreous pyrite type	Cu type	Cyprus type
Immature island arc	Deposits in mafic volcanics		Kieslager type		Besshi type
Mature island arc	Deposits in felsic volcanics		Polymetallic type	Zn-Pb-Cu type	Kuroko type
Greenstone belt		Deposits in volcanic sequences	Primitive type	Zn-Cu type	Kuroko type
		Deposits in volcanic sedimentary sequences			
Cratonic rifting	Deposits in sediments	Deposits in sedimentary sequences	Clastic hosted type		Sullivan type
			Carbonate hosted type		

Tab. 1: Classification of massive sulphide deposits

3. Massive sulphide deposits in relation to time and tectonics.

An understanding of the tectonic mechanisms that lead to the formation of massive sulphide deposits stands at the beginning of every exploration project. The knowledge of the geological environments that preferably host massive sulphide deposits, and their change in time, assist in defining a prospective target area.

3.1. Zn-Cu type deposits in the Archaean greenstone belts.

Greenstone belts were formed in the early stages of crustal evolution. Basic and ultrabasic volcanic rocks derived from partial melting of the mantle erupted repeatedly onto or between thin continental rafts of lower density granitoid material in zones of instability along "oceanic rifts" (Hutchinson, 1980). Troughs were formed through gravitational subsidence which in turn caused deformation by synkinematic compression. Within these subsiding troughs, the reworking of ultramafic-mafic "oceanic" crust resulted in tholeiitic and intermediate-felsic calc-alkaline suites comparable to modern tectonic mechanisms along consuming plate margins. It also led to an enrichment of metals in the differentiated rocks.

The oldest known (3.8×10^9 y) mineralization of this type, mostly pyrrhotite-chalcopyrite occurs in the Isua Belt of West Greenland (Appel, 1980). Some of the earliest deposits can be found on the West Australian Archaean shield. Among five to six larger known deposits in this area Mons Cupri (Miller & Gair, 1975) and the Big Stubby Zinc Deposit (Reynolds et al., 1975) form an exception, as they contain substantial amounts of galena, and barite in the latter, which is unusual when compared with the majority of early massive sulphide deposits. Both are estimated to be older than 3×10^9 years. The Big Stubby Zinc Deposit is associated with felsic fragmental volcanism within a three phased mafic to felsic cycle. Mons Cupri is hosted in rhyolitic pyroclastics.

The vast majority of primitive Zn-Cu deposits lie on the Canadian shield. Most of the mineralization occurs in the Superior Province and also to some extent in the Slave Province. The deposits are slightly younger in age ($2750\text{-}2650 \times 10^6$ y). Galena and barite, which are thought to form under a more evolved environment, are virtually absent. Sangster (1972, 1980), Sangster & Scott (1976) and Franklin et al. (1981) covered

the North American massive sulphide deposits and their characteristics extensively.

They are spatially related with felsic volcanics and in some cases with rhyolite domes. Within the tholeiitic and calc-alkaline volcanic series of the Abitibi Belt (Ontario-Quebec), only about 5% consists of rhyolitic rocks, with basalt and andesite constituting about 70% (Descarreaux, 1973). Spence and de Rosen-Spence (1975) divided the stratigraphy of Noranda Camp into five alternating cycles of andesitic and rhyolitic volcanism, the latter forming the footwall of the majority of deposits, especially in the third cycle. Commonly the pyroclastic host rock is brecciated to more than 30% due to eruptions. The massive sulphide deposits of the Manitouwadge District, north of Lake Superior, are situated in a mixed greenstone-metasedimentary sequence.

3.2 Zn-Cu type deposits in the Proterozoic.

The number of volcanic massive sulphide deposits formed during the Proterozoic appears to be considerably smaller than during the Archaean. The deposits are virtually absent from the Middle Proterozoic (fig. 2), a time of tectonic quiescence (Watson, 1973) when the formerly mobile belts had previously been welded to older massifs in order to form large cratons. A different tectonic style, continental rifting on a thickened sialic crust, followed the Archaean granitic plutonism. This new environment could have been less favourable for the production of massive sulphide deposits. Extensive rifting may have led to sediment troughs accompanied by tholeiitic or bimodal volcanism. The large sediment hosted Pb-Zn rich Sullivan Deposit, (Kanasewich, 1968), and the sediment hosted Broken Hill Deposit, associated with amphibolite and gneiss (Johnson & Klingner, 1975) were formed in this period.

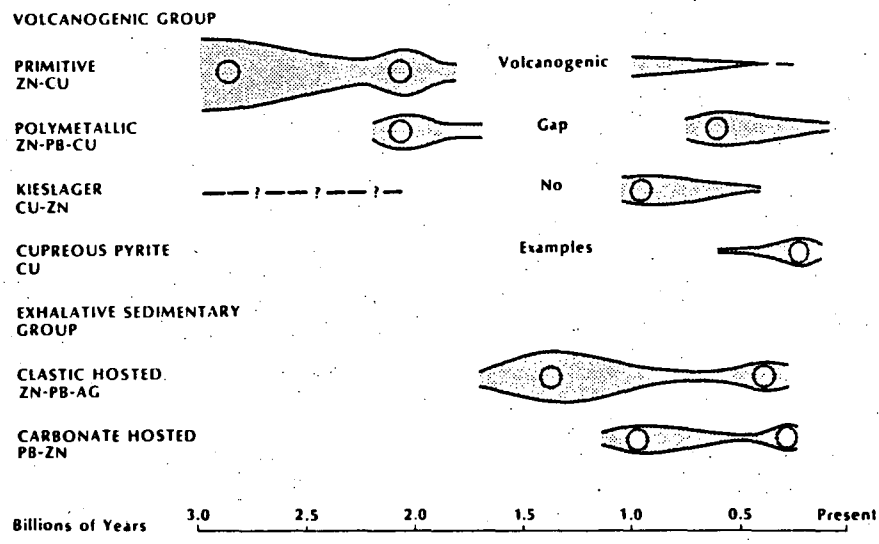

Fig. 2: Distribution in time of massive sulphide deposits (after Hutchinson, 1980)

Volcanic Zn-Cu type deposits have been reported from four different areas; the Churchill Province (Manitoba), Wisconsin, Arizona and the Svecokarelides. The deposits in the Proterozoic greenstone belts of the Flin Flon-Snow Lake area (Koo & Mossman, 1975), in the volcanic belt of Wisconsin (Banks & Robello, 1969) and near Jerome, Arizona, (Anderson & Nash, 1972) are very similar to the Canadian Archaean deposits. The deposits in the four mineralized districts of the Svecokarelian shield are highly metamorphosed and deformed, and the proportion of metasediments involved is larger than in previously described examples. They are still regarded as spatially related to felsic metavolcanics. Notably, deposits of the Bergslagen district and the Pyhasalmi Deposit in the Pyhasalmi-Pielaves district can average up to 3.5% Pb. The Åsen deposit in the Skellefte district includes barite (Frietsch et al., 1979; Latvalahti, 1979; Rickard et al., 1979; Huhtala, 1979; Helovuori, 1979; Rickard & Zweifel, 1975).

3.3. Massive sulphide deposits in the Upper Proterozoic and Phanerozoic.

The later Proterozoic saw the onset of lateral plate tectonics with the interaction of oceanic and continental plates. Many authors explain these younger massive sulphide deposits in the context of modern plate tectonics. Zn-Pb-Cu type deposits are related to volcanic island arcs and back-arc basins, and Cu type deposits to sea floor rifting.

Beginning with the latter, their formation has been thought to be at or near sites of ocean floor spreading within abyssal tholeiitic oceanic crust. The most favourable horizons are either the base or the top of the pillow lavas. After lateral transport and obduction along plate boundaries (Hutchinson, 1973) they became what is commonly known as the Cyprus type deposits within ophiolitic complexes.

Deposits are known from the Troodos massive in Cyprus (Constantinou & Govett, 1972, 1973), from other ophiolitic complexes within the alpine belt in Turkey (Wallace et al., 1972; Suffel & Hutchinson, 1973) and in the Oman Mountains (Hassan et al., 1979). Older deposits exist from the Lower Ordovician in Newfoundland. Several deposits exist in the Notre Dame area (Bachinski, 1977). The York Harbour deposit contains substantial amounts of sphalerite (Duke & Hutchinson, 1974). Scheibner & Markham (1976) mentioned several small deposits in the Silurian New England-Lachlan fold belt of New South Wales. Another deposit, possibly from the Upper Proterozoic, occurs in Bleida, Morocco (Leblanc et al., 1978).

There is uncertainty concerning a whole range of metamorphic Cu-rich Cu-Zn type deposits that are associated with metasediments and basic metavolcanics. These are the Japanese deposits of the Sanbagawa terrain, the Besshi deposits (Kanehira & Tatsumi, 1970), the alpine Kieslager (Derkmann & Klemm, 1977) and some of the deposits in the Norwegian Caledonides, in particular Lokken (Vokes, 1976; Vokes et al., 1976). Sillitoe (1972) tried to explain the Besshi deposits by transportation of a Cyprus type deposit from a spreading center onto a consuming plate margin. Mitchell & Bell (1973) regarded them as a product of the early stages of island arc evolution on oceanic crust. Klau & Large (1980) also applied this explanation to the Kieslager.

The most important type of massive sulphide deposits during this period are the Zn-Pb-Cu type deposits assumed to be connected mainly with

felsic volcanics of the calc-alkaline series in mature island arcs. Miyashiro (1975) showed that the calc-alkaline volcanic rocks increased proportionally with the thickening of the crust along island arcs and active continental margins. Hutchinson (1973) considered the difference between the Devonian Zn-Cu type deposit of West Shasta and the Triassic Zn-Pb-Cu type deposit of East Shasta in the Californian Cordilleran belt as an expression of island arc evolution. Apart from the Pb content, modern Zn-Pb-Cu type deposits commonly hold considerable amounts of barite.

The Miocene Kuroko deposits are located in the Japanese Green Tuff Belt, a volcanic-sedimentary sequence of several thousand metres. The region of the Green Tuff represents a horst-graben system in the inner belt of the island arc of Japan. The initial andesitic volcanism turned felsic in the later stages of subsidence due to rifting. The volcanic activity during this last stage produced calc-alkaline rhyolitic-dacitic tuff which hosts the massive sulphide deposits. These deposits are closely associated with brecciated rhyolitic lava domes and tend to be overlain by mudstone which indicates a discontinuity in volcanic activity (Sato, 1977). Similar Zn-Pb-Cu type deposits without rhyolitic domes in their vicinity occur in the Cambrian intermediate-felsic calc-alkaline Mt. Read Volcanics at Tasmania's west coast (chap.5, 8.2), and in the Silurian Lachlan fold belt as part of the Tasman geosyncline (Malone et al., 1975; Davis, 1975; Malone, 1979). The orebodies at Rosebery and Woodlawn are closely associated with shale lenses, contained in felsic tuffs. At Captains Flat the southern part of the ore deposit is also associated with sediments. The Pb-Zn rich orebodies at Buchans, Newfoundland, occur in the first dacite sequence of four Silurian calc-alkaline andesite-dacite-rhyolite cycles (Thurlow et al., 1975). The polymetallic Avoca ore deposits in the Caledonian province of Ireland occur in calc-alkaline rhyolitic tuff. They are laterally associated with mudstones and dolomitic sediments and can be overlain by a thin band of graphitic shale (Platt, 1977).

In the Scandinavian part of the Ordovician Caledonides, only a few deposits in middle Norway, around Bleikvassli, belong to the polymetallic Zn-Pb-Cu type. They are found in metasediments with units of felsic volcanics (Vokes, 1976; Vokes & Gale, 1976). The Caledonian Zn-Pb-Cu type deposits of New Brunswick occur in a highly deformed caldera structure 50 km across which contains sediments and a bimodal rhyolitic-basaltic suite. Most of the deposits are located in sedimentary horizons and are associated with rhyolitic ash flow tuff or brecciated felsic lava domes (Harley,

1979). The pyrite-rich low base metal deposits of the Devonian-Carboniferous Iberian geosyncline are all emplaced in felsic volcanics in a volcanic-sedimentary complex of up to 800 m thickness. Acid volcanics, mainly pyroclastics, outnumber in volume the basic volcanics, which are mostly spilitic lavas. The amount of intermediate volcanic rocks is insignificant (Schermerhorn, 1970; Strauss & Madel, 1974; Strauss et al., 1977). The tectonic environments of the deposits described in this paragraph are not well understood.

4. Common characteristics among massive sulphide deposits.

Apart from the correlation with volcanic activity there exist many more features that are shared by most volcanic massive sulphide deposits. They are most easily recognized in little deformed and metamorphosed deposits and have been discussed widely in literature.

4.1. Location of deposition.

Massive sulphide orebodies are conformably emplaced in horizons that indicate a break or a change in volcanic activity. Generally volcanism seems to be in the waning stages. Deposition appears to be controlled by faults and regional lineaments and their intersections. These channels enable the metal-bearing hot solutions to rise to the sea floor and thus generate clusters of orebodies, as indicated for the deposit in Cyprus (Adamides, 1975), the Hokuroku district, Japan, (Scott, 1978) and Mt. Lyell, Tasmania (Solomon & Elms, 1965). Autobrecciation of the felsic footwall, Sangster's "millrock", is probably an indication of the close relationship between explosion centres and sulphide mineralization. Brecciated volcanics are known from the Canadian Archaean deposits (Sangster, 1972), Newfoundland (Thurlow et al., 1975) and the Kuroko deposits (Horikoshi & Sato, 1970). Rhyolitic domes in the immediate footwall have been reported from the Kuroko deposits (Date & Tanimura, 1974) and deposits in the Noranda Camp (Spence & de Rosen-Spence, 1975).

4.2. Sulphide and gangue mineralization.

The orebodies vary in shape from bulbous lenses to elongated tabular sheets. Contemporaneous slumping and brecciation as well as post-depositional deformation can lead to changes in their shape.

Generally the major sulphide components are ubiquitous pyrite, pyrrhotite, chalcopyrite, galena and sphalerite. The relative proportions depend on the deposit type. Apart from a broad Cu-Zn-Pb zonation from the base to the top of the massive sulphide lens, fine banding down to millimetre thickness can be observed.

The Cyprus type deposits are mainly composed of a Cu-rich zone, although sphalerite occasionally occurs in various proportions. The chalcopyrite content can reach up to 20% (Hutchinson & Searle, 1971). The Cyprus deposits in particular have their own zonation with conglomeratic ore in the upper part, and pyrite-quartz ore in the lower part. The sulphide content increases from bottom to top (Constantinou & Govett, 1973).

The general lack of Pb in the Archaean deposits apart from some exceptions (see chap. 3) has been explained in terms of Pb development as a result of radiogenic decay and crustal fractionation (Hutchinson, 1973). Barite is present in many modern Zn-Pb-Cu type deposits, usually in the upper zone or as a separate layer above the sulphide ore. The occurrence of gypsum or anhydrite is rare. Apart from the Kuroko ores, gypsum has been reported from Vanua Levu, Fiji (Colley & Rice, 1975). The increase in sulphate gangue minerals in modern polymetallic deposits may have its origin in higher oxygen levels in the evolving atmosphere (Sangster & Scott, 1976). A further indication of increased oxidation levels is the presence of haematite in ferruginous cherts, while Archaean Canadian deposits contain magnetite. Ferruginous chert, which is a late stage exhalite, tends to cap a deposit and extends beyond its limits, and can include Mn-rich layers of carbonate.

Pyrrhotite is most common in the Precambrian deposits and usually nonexistent in the Miocene Kuroko type deposits, which could be regarded as further evidence for an early less oxidising environment. Occasional larger occurrences of pyrrhotite in the Kuroko type deposits and from Precambrian deposits have been described as post-depositional metamorphic products due to heat induced release of sulphur from pyrite. In the Archaean deposits pyrrhotite is present in the massive ore and also in the crosscutting stockwork below, together with chalcopyrite and pyrite. The mineralization of the stockwork varies from sparsely disseminated ore to massive stringers, and rarely extends laterally beyond the massive ore, remaining within the alteration zone. Occasionally these stringers can be followed down to several hundred metres of depth.

The absence of both stockwork and alteration zone, particularly around the highly metamorphosed and deformed deposits of the Norwegian Caledonides was explained by Vokes (1976) in four different ways:

a. Deposition away from the feeder channel depending on the density of the emanating metal-bearing hydrothermal fluids (Sato, 1972).

b. Slumping and turbidity current transport of unconsolidated sulphides down the palaeoslope.

c. Transport of consolidated coherent sulphide bodies during tectonic movements.

d. Folding and other deformational movements.

All four mechanisms, single or combined, are thought to be able to produce distal orebodies in contrast to proximal orebodies above their feeder channel.

4.3. Alteration.

The footwall alteration zone below a deposit represents the channel which hydrothermal solutions followed on their ascent to the seafloor. In the Noranda Camp, the alteration is well defined and pipe-like or funnel-shaped. Vertically it can extend to more than 1000 m into the footwall, as in the case of the Vauze mine (Spence, 1975). Generally the alteration decreases, from a hydrothermal mineral assemblage in the centre, to a peripheral zone that shows a minor alteration and a partly preserved primary texture. Sericite, quartz and chlorite dominate the centre in varying proportions and can be associated with stockwork ore. Feldspar emerges towards the marginal zone.

Hanging wall alteration has been observed from a few massive sulphide deposits. These are the Amulet mine (Spence and de Rosen-Spence, 1975), the Kuroko deposits (Shirozu, 1974), Woodlawn (Petersen & Lambert, 1979), Madenkoy (Cagatay & Boyle, 1980), the deposits in New Brunswick (Govett, 1983) and Rosebery (this study).

5. Regional geology of western Tasmania

The Rosebery ore deposit lies on Tasmania's west coast. The deposit is situated within the Cambrian Mt. Read volcanic belt, which was part of the early Tasman geosyncline. This Palaeozoic orogenic zone stretches from Tasmania to Queensland along the Australian east coast. Fragments of this zone have also been identified in New Zealand and Antarctica (Griffiths, 1971; Solomon & Griffiths, 1972; Solomon 1981), as shown in fig.3.

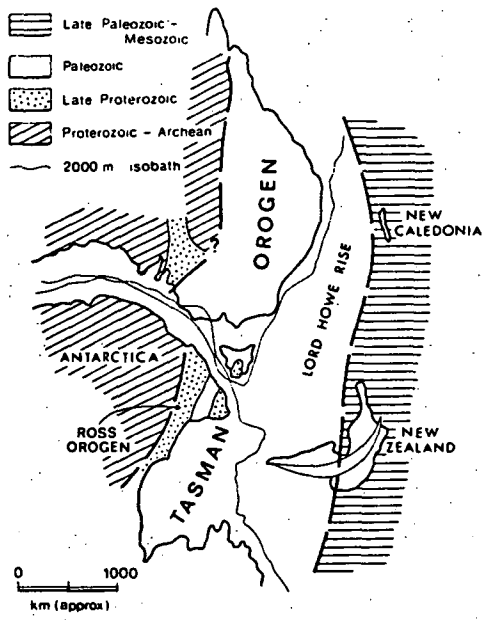

Fig. 3: Reconstruction of the continental crust prior to opening of the Tasman Sea (after Solomon, 1981)

The Mt. Read Volcanics were named by Banks & Solomon (1961) and defined by Campana & King (1963). They represent the eastern flank of the Dundas Trough, a synclinorium between the weakly metamorphosed Rocky Cape geanticline to the west and the Tyennan Nucleus to the east.

The lithology of the Dundas Trough can be divided roughly into a western sedimentary part and an eastern volcanic dominated part with a general decrease in age from west to east. The geology of the Dundas Trough (fig.4) has been studied intensively during the last few decades, and has been summarized recently by Corbett (1981).

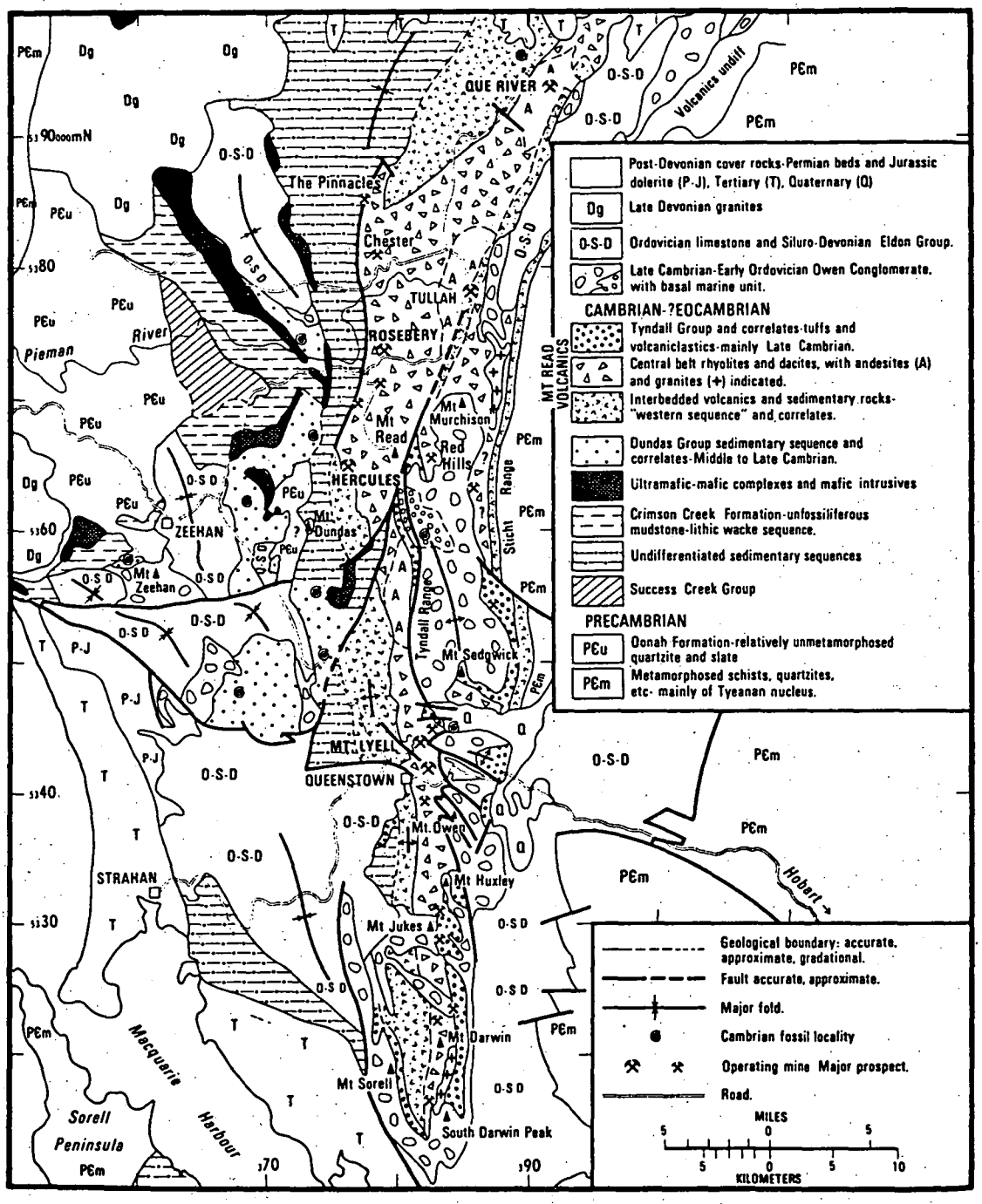

Fig.4: Geological map of central western Tasmania showing distribution of the Mt. Read Volcanics and the major mines within the volcanic belt (after Corbett, 1981)

5.1. Western sedimentary part of the Dundas Trough.

The sedimentation in the subsiding Dundas Trough began with the Success Creek Group, a sequence of quartz sandstone, mudstone and minor amounts of dolomite. These sediments unconformably overlie Proterozoic basement (Brown, 1980). They are succeeded by mudstones or argillites and lithic graywacke of the Crimson Creek Formation with minor proportions of locally scattered mafic lava. Ultramafic ophiolitic intrusions have been recognized in and above the Crimson Creek Formation at the contact with the Dundas Group. The contact is not well exposed, however, the sediments of the Dundas Group are believed to overlie the Crimson Creek Formation.

The rock pile of the Dundas Group occupies the central part of the Dundas Trough. Lithic-volcanic wacke, conglomerate, quartz wacke, siltstone and flysch type slate are interbedded. In some areas mafic volcanics, including tholeiitic pillow lavas and felsic tuffs identical to the Mt. Read Pyroclastics also occur. Marine fossils from several localities have been dated as middle to late Middle Cambrium (Jago, 1979).

5.2. Eastern volcanic-dominated part of the Dundas Trough.

The Dundas Group passes into a sequence of mudstone and graywacke, interbedded with felsic tuff, small amounts of pillow lavas, gabbroic intrusions and ultramafic bodies. The amount of felsic tuff increases towards the Mt. Read Volcanics. Part of this sequence has been correlated to the Dundas Group. According to Corbett (1981) this sequence represents the western zone of the Mt. Read volcanic belt, which he divided into three zones. Trilobite fossils found in the northern part of the western sequence suggest an age of late Late Middle Cambrian (Gee et al., 1970).

The Mt. Read volcanic belt is about 10 km wide. It stretches almost continuously in north-south direction over 100 km from Eliott Bay in the south-west of Tasmania. Its northern-most extension continues in north-easterly direction towards Fossey Mountain and Dial Range Trough (Williams et al., 1975) bending around the Tyennan Nucleus.

In the central zone, the second of Corbett's three lithological subdivisions, sediments are rare. At Mt. Lyell, trilobites of late Middle Cambrian age were found in the overlying Tyndall Group (Jago et al., 1972).

Rhyolitic-dacitic volcanics dominate over andesitic-basaltic volcanics, which do not amount to more than 15% in proportion (Corbett, 1981). Both suites are of calc-alkaline affinity and are altered keratophyres and spilites (Solomon, 1964; White, 1975). Their trace element chemistry suggests a continental margin type environment (Anderson, 1972). The volcanics occur as ash fall and ash flow tuffs, as volcanic breccias and as lavas. Larger areas of andesitic rocks, intrusive and extrusive in character, exist around Que River, in the Tullah-Mt. Black area and near the Tyndall Range. Granitic intrusions are present at Mt. Murchison, with an estimated age of > 515 $\pm$ 15 million y (McDougall & Leggo, 1965), and South Darwin, dated as 511 million y (Black & Adams, 1980). The time correlation between the western and central zone is not clear. The central zone may be contemporaneous or younger.

At Rosebery, extending several kilometres north and south, the central zone of the Mt. Read Volcanics is fault bounded by the Rosebery Group. The Rosebery Group, a series of sediments and tuffs, has been correlated to the Success Creek Group by Loftus-Hills et al. (1967). Brathwaite (1969) described it as younger than Crimson Creek Argillites and the Dundas Group. However Williams et al. (1975) and Green (in Wallace and Green, 1982) argue that the Rosebery Group could be equivalent to the Dundas Group. The sharp contact to the west led Corbett (1981) to the conclusion of an existing rift or elongated cauldron structure. Green et al. (1981) emphasised a cauldron subsidence in connection with ignimbrite eruptions.

The eastern flank and particularly the southern half of the central Mt. Read arc is overlain by the Tyndall Group, the third lithological zone. This last zone is comprised of tuffs, lavas and sediments of late Middle Cambrian age (Jago, 1979). The Lake Beatrice sequence, a narrow sequence of siliceous clastic sediments between the central Mt. Read Volcanics and the Tyennan region is regarded by Corbett (1981) as the eastern equivalent of the Mt. Read arc western zone.

Between the Cambro-Ordovician Jukesian Orogeny and the Middle Devonian Tabberabberan Orogeny several thousand metres of clastic and chemical sediments were deposited unconformably (Campana & King, 1963) on top of the Cambrian rocks. The Tabberabberan Orogeny produced folds, faults and greenschists. Part of the sediment pile and particularly post-Devonian sediments have been eroded by Tertiary uplifting. During the Pleistocene,

part of Tasmania's west coast was covered by glaciers and subsequently by tillites.

5.3. Tectonic models.

The existence of ultramafic complexes and a belt of Andean type calc-alkaline volcanics in the Dundas Trough between two continental regions has led to a number of controversial plate tectonic models. Some of these models also incorporate in their concept a second smaller trough-nucleus combination, the Adamsfield Trough and Jubilee Block, further to the east. A summary of the principal tectonic models can be seen in fig. 5.

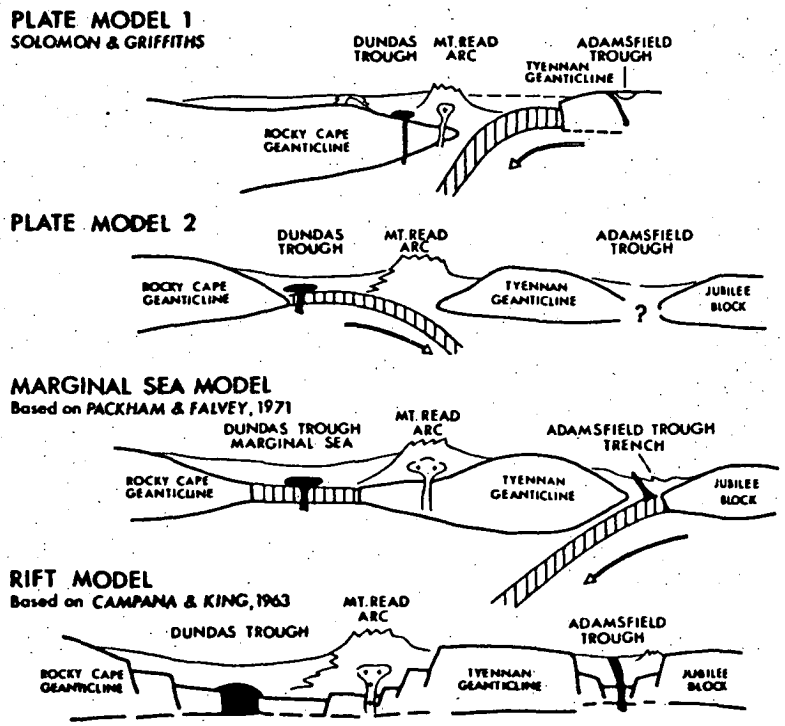

Fig. 5: Possible tectonic models of west Tasmania
(after Corbett et al., 1972)

Campana & King (1963) proposed early graben structures along rifts within a geosyncline as the main cause for subsidence. Packham & Falvey (1971) considered the Dundas Trough to be a marginal spreading sea, while westward dipping ocean crust subduction occurred in the Adamsfield Trough. Solomon & Griffiths (1972) suggested that initial crustal stretching

accounted for the emplacement of ophiolite complexes. A subsequent westward dipping oceanic crust was produced by the westward moving Tyennan Nucleus, which resulted in the formation of the Mt. Read volcanic arc. At the time of the collision of the Tyennan Craton with the Mt. Read volcanic arc, ultramafic diapirs intruded into the intracratonic basin of the Adamsfield Trough along thrust faults. Corbett et al. (1972) argued for an original proximity between the Mt. Read volcanic arc and the Tyennan Nucleus. Oceanic crust with ophiolites of the marginal basin type at its western end was subducted eastward. Another model favouring an eastward dipping subduction subsequent to crustal spreading, by Solomon & Griffiths (1974) and White (1975) tried to explain the occurrence of ultramafic complexes by obduction of oceanic crust. Crook (1979) and Green (1983) also preferred an eastward dipping subduction model.

5.4. Mineralization of the central Mt. Read volcanic belt.

Mineralization within the Mt. Read volcanic belt occurs over a distance of approximately 85 km from South Darwin in the south to Que River in the north. The majority of ore deposits, and in particular the economic deposits, are situated in the central zone, and fall into four locally distinct groups from south to north (Solomon, 1981) as shown in fig. 4:

a. South Darwin-Mt. Lyell group

b. Hercules-Rosebery-Pinnacles group

c. Farrell group

d. Que River-Hellyer Group

According to Campana et al. (1958) the ore deposits south of Red Hills are mainly disseminated and rich in Cu. To the north the massive stratiform Pb-Zn rich type dominates except for the Chester mine.

5.4.1. South Darwin-Mt. Lyell group.

The following deposits are partly taken from Green (1975) and are ordered from south to north:

a. Prince Darwin: Pyrite-chalcopyrite in haematite-magnetite gangue,

b. East Darwin: Pyrite-chalcopyrite in siliceous schists,

c. Lake Jukes: Haematite-bornite veins,

d. Jukes Proprietory: chalcopyrite-pyrite in chlorite schists,

e. Mt. Lyell: This mining field holds over a dozen ore deposits in hydrothermally altered volcanics as massive or disseminated sulphides. The combined amount of 90 million tonnes of ore (1.2% Cu) have been mined. The major components are pyrite, chalcopyrite and bornite with minor sphalerite and galena (Reid, 1975; Reid & Meares, 1981).

5.4.2. Hercules-Rosebery-Pinnacles group.

The following deposits are again ordered from south to north:

Hercules: The general characteristics are very similar to Rosebery, which will later be discussed in detail. The massive sulphide ore is emplaced in sericitic host rock which is capped by a horizon of black shale. The surrounding felsic pyroclastics are intensely altered in the footwall of the deposit. Mining operations have produced 2 million tonnes of ore with an average grade of 0.5% Cu, 5.4% Pb, 16.9% Zn, 172 ppm Ag and 3.5 ppm Au (Hall, 1967; Burton, 1975; Reid & Meares, 1981). Four out of five abandoned prospects between Hercules and Rosebery - the Dallwitz prospect, Grand centre, Koonya and Rosebery Lode - may all be associated with one shale horizon. The Dallwitz prospect holds sphalerite in calcite filled gash veins. Grand Centre, Koonya and Rosebery Lode contain massive sphalerite-pyrite-galena-chalcopyrite ore (Eastoe, 1973). The host rock shale of the Dalmeny Pb-Zn ore lies 300 m to the east of the interpolated shale horizon. The Jupiter mine, another small massive sulphide deposit just north of Williamsford, probably lies stratigraphically on a different level in schistose volcanic rocks (Green, 1983). The age and origin of a number of small abandoned mines (Salisbury & Chamberlain, Black P.A) in the Rosebery area are not well known.

Rosebery: See Chap.6, 9

Chester: Consists mainly of massive pyrite. Low contents of Cu, Pb and Zn are also present. The abandoned deposit is associated with quartz-sericite alteration (Corbett, 1981; Solomon, 1981).

Pinnacles: The abandoned mine is comprised of small massive lenses, stringer veins and disseminated ore of pyrite, sphalerite, galena, chalcopyrite and barite. The deposit is associated with sedimentary units within acid volcanics comprising autobrecciated lavas and tuffs with intercalated chert (Collins, 1981).

The deposits of this group are thought to lie on the same stratigraphic level and are situated close to the western boundary of the central Mt. Read volcanic belt.

5.4.3. Farrell group.

This group of Devonian deposits is spread over a distance of 8 km between Tullah and Mt. Murchison and is associated with the Farrell Slates. The deposits form several sub parallel lenticular fissure lodes averaging 1.2 m in width, and steeply dipping west. The main sulphide minerals are galena, sphalerite, pyrite, chalcopyrite and tetrahedrite in quartz and siderite gangue. Ag is present in galena and as ruby silver and argentite (Hall et al., 1953; Hall and Solomon, 1962; Solomon, 1965 and Burton, 1975).

Based on the similarity of Rosebery and Farrell $\delta^{34}S$ values, Solomon et al. (1969) considered a volcanogenic origin a distinct possibility for the Farrell sulphur.

5.4.4. Que River-Hellyer.

This mine includes several sub-parallel sulphide lenses of which the sphalerite-pyrite-galena dominated P/Q-lens is the largest. Apart from the S-lens (pyrite-chalcopyrite-sphalerite-galena mineralization of stringers and disseminations), the remaining smaller lenses resemble the P/Q-lens in metal composition. The deposit holds 5 million tonnes of ore containing on

average 0.4% Cu, 7.0% Pb, 12.5% Zn, 171 ppm Ag and 3.4 ppm Au. The mine sequence, mainly altered dacitic tuffs and lavas, is hosted in a large pile of andesitic volcanics (Wallace in Wallace & Green, 1982; Skey, 1984). In 1983 a new ore deposit, the Hellyer Prospect was discovered three km north of Que River. It is a high-grade polymetallic massive sulphide deposit with over 10 million tonnes of ore. Barite and fuchsite alteration is associated with the ore deposit as in the case of Que River (Skey, 1984; Sise & Jack, 1984).

6. Geology of the Rosebery area.

The geology of the Rosebery area has been extensively discussed since the beginning of this century, and numerous interpretations and re-interpretations of the stratigraphy, structure and stratigraphic nomenclature have been put forward (Hall et al., 1953; Banks & Solomon, 1961; Loftus-Hills et al., 1967; and Brathwaite, 1969). Brathwaite's (1969) classification of the Mt. Read Volcanics in the Rosebery area has been widely accepted, and is used in this study.

He distinguished two different lithologies within the Mt. Read Volcanics: The Primrose Pyroclastics, in the western part of the area, which includes the footwall pyroclastics, the ore-bearing host rock shale and the massive pyroclastics. The footwall pyroclastics contain the footwall schists of the alteration zone below the orebody. The massive pyroclastics are part of the hanging wall above the ore horizon and grade eastward into the Mt. Black Volcanics. The latter are dominated by lavas and have been described as keratophyres. Solomon (1964) reintroduced the terms keratophyre and quartz keratophyre and explained them after the terms had already been used by Twelvetrees & Petterd (1899).

The geology of the Rosebery area as part of the Mt. Read volcanic belt is shown on the geological map (fig. 6a, b) compiled during this study. The dominant feature is the hydrothermal alteration zone which is petrographically defined by schists. To the west, this zone adjoins a second, different alteration style of massive siliceous rocks which extend north-south over several kilometres. The total alteration area is contained within the Primrose Pyroclastics which are succeeded to the east by the lavas of the Mt. Black Volcanics. The Mt. Read Volcanics including the Primrose Pyroclastics and Mt. Black Volcanics are faulted on their western margin against the Rosebery Group (Corbett, 1981), a mixed sequence of sediments and volcanics, dipping and facing west (Loftus-Hills et al., 1967).

Solomon et al. (1976) inferred an anticlinal structure in the Mt. Read Volcanics at Rosebery, east of the fault contact against the Rosebery Group. The two major shale horizons, the east-dipping sedimentary host rock including black slate and the almost vertically-dipping shale horizon in the western limb of this anticline were considered as marker beds. Subsequent foliation measurements in the altered schists (Green et al.,

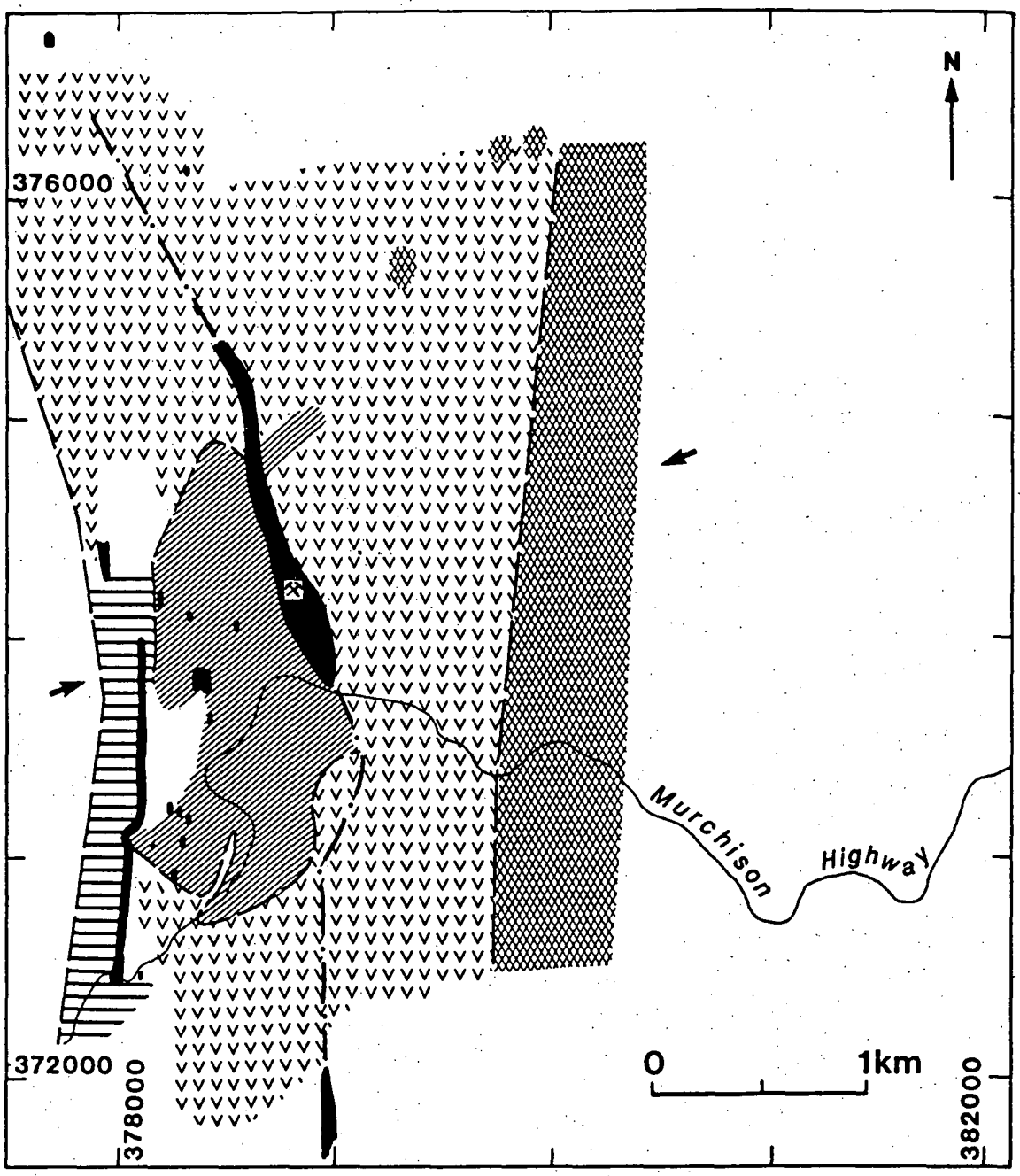

Fig. 6a: Simplified map of the alteration at Rosebery. A more comprehensive map (fig.6b) is enclosed in back pocket. Both maps are based on the Australian Map Grid (AMG). Arrows in fig.6a indicate the orientation of cross section in fig.7.

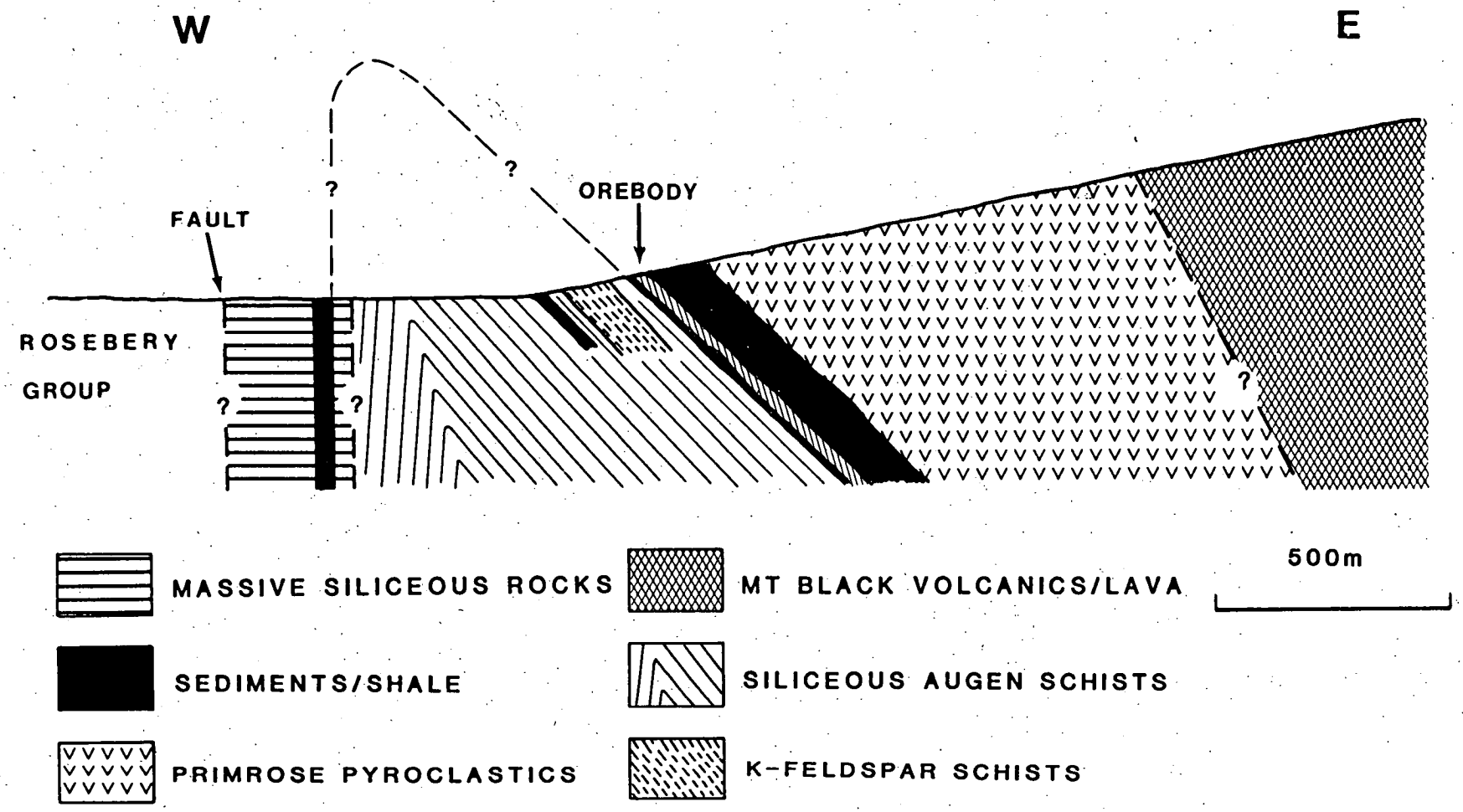

Fig. 7: Cross section through the alteration area at Rosebery

1981; this study) have confirmed this view, although the assumption of one continuous shale horizon prior to folding is doubtful (fig. 7). Fig. 7 represents an E-W cross section through the alteration zone, from the Rosebery Group to the Mt. Black Volcanics as mapped in this study.

6.1. Mapping area.

The area studied is entirely contained within the Mt. Read Volcanics. It extends north and south of the centrally located hydrothermal alteration zone. The occurrence of several smaller ore deposits and prospects has limited the area's southern extension. The western boundary is delineated by the Rosebery Group and dense bush. To the east, the area extends along the Murchison Highway up to its highest point on Mt. Black.

According to Brathwaite (1969), The stratigraphy of the Mt. Read Volcanics in the mine area is approximately:

massive pyroclastics	460 m
black slate	30 m
host rock	37 m
footwall schists/pyroclastics	640 m

Considering field evidence from this study, the proposed thickness for footwall and massive pyroclastics does not entirely agree with this description. Assuming a large anticlinal structure in the mine area, the thickness of the footwall pyroclastics and schists would amount to $\leq$ 500 m (fig. 7). The thickness of the massive pyroclastics varies from 500 m at the southern end of the deposit to 1000 m north of it, depending on the positioning of the boundary between massive pyroclastics and Mt. Black Volcanics.

6.2. Sediments.

A large number of shale lenses occur within the Primrose Pyroclastics. They vary in size considerably from centimetre range (fig. 8), to 1.5 km length and more than 100 m thickness, as in the case of the host rock (siltstone, reworked tuff and tuff), with overlying black slate.

Fig. 8: Shale inclusions in altered volcanics 378 400E, 373 570N (A.M.G.)

Bedding in the shale lenses is largely obscured by a pronounced slaty cleavage.

The majority of shale outcrop is from two horizons, both of which trend in northerly direction. The western shale horizon is flexed or faulted several times, but otherwise appears to be essentially continuous, at least within the Rosebery township area. The cleavage dip and the contact with the massive siliceous rocks are subvertical. According to Eastoe (1981) these shales face west. The eastern shale horizon is discontinuous apart from the ore-bearing host rock shale which generally dips 45°east and also faces east (Brathwaite, 1969). The cleavage is slightly steeper than the contact with the wall rock.

The shale at the Dalmeny Prospect, between Rosebery and Rosebery Lode (fig. 6b), lies approximately 300 m stratigraphically above the inferred horizon connecting the Rosebery host rock with a series of shale lenses which include some mineralization (chap. 5.4.2).

North of Rosebery the eastern shale horizon follows a NNW direction. Outcrop of both shale horizons is scant in this area along the west flank of Mt. Black. In an area 3 km NNW of Rosebery, there are 3 shale lenses exposed over an across-strike distance of 300 m. Eastoe (1981) regarded this locality as a possible hinge of a north plunging fold, assuming both shale horizons lie on the same stratigraphical level. The locality however does not match the extrapolated position of this fold hinge. Further north, at the Bastian Dam site, shale rafts tens of metres in length and up to 10 m thick were reported by Eastoe (1981). Rafts or smaller clasts of shale, considered as ripped up by the deposition of pyroclastics, are also exposed further south in the Rosebery area.

Between the two main shale horizons, a number of shale lenses of various size exist at different stratigraphical levels. Several outcrops were found, particularly in the Stitt River and in the area of the mine concentrator. Only the two eastern-most outcrops exhibit east dipping cleavage. The majority of these lenses have a subvertical cleavage. The recurrence of shale lenses at different levels is an indication of an unstable geological environment during this part of the Cambrian. It also casts some doubt on the assumed continuity of the major shale horizons, and the equivalence of their stratigraphical position.

6.2.1. Petrography of the sediments.

The shale lenses consist of green-grey to black shale, which is locally called black slate, in the ore-bearing host rock horizon. Occasionally feldspars and rounded and elongate remnants of feldspars up to 3 mm long are present (67892). The host rock horizon also contains slightly sheared tuff (Brathwaite, 1969; chap.9.5) and reworked tuff with a high proportion of phenocrysts. The major components are quartz and sericite in varying proportions. The grain size of the groundmass ranges from clay to silt. Pyrite (< 1 mm), carbonate and chlorite can be present in small amounts, and appear locally within the host rock shale in larger quantities (e.g. DDH 1121). Accessory minerals are zircon, tourmaline, sphene, apatite, rutile and fluorite (Brathwaite, 1969). Non-carbonate carbon in black slate averages 0.3% (Gee, 1970).

6.3. Massive siliceous rocks.

A band of altered, mostly massive grey-green to yellow-grey-green rocks dominates the area west of the western shale horizon. This unit has been termed massive siliceous rocks, as the SiO_2 content of ten analysed samples range from 74% to 83% (appendix 2), and average about 80%. South of Rosebery, in the Stitt River and around the concentrator, the massive siliceous rocks were also found to the east of the western shale horizon. According to mine geologists, these rocks have been traced north beyond Karlson's Knob (fig.6b) and south to Hercules.

In the area west of the concentrator (378400 E, 373950 N), a gradational transition from massive siliceous rocks through to weakly sheared rocks to schists can be seen. Weak schistosity in the massive siliceous rock is also developed locally along the Murchison Highway near the Williamsford Junction, where augen textures, produced by more intensive shearing occur (67911). In this area, folding of quartz veins several centimetres thick was observed. West of the railway bridge at the Stitt River, a distinct change from massive siliceous rocks to weakly sheared pyroclastics with striae takes place. Except for a small amount of feldspars, the petrography is identical to that of massive siliceous rocks as discussed below. On the flume track (378100 E, 374350 N) the massive siliceous rocks are intersected by a stockwork of quartz-carbonate veins.

To the east they grade into massive light grey carbonate-rich plagioclase-bearing rock.

The existence of massive siliceous rocks in the central schists and vice-versa, and also the transitional facies would suggest a similar origin for both rock types. In one case, the massive siliceous rocks clearly crosscut the schists as a 0.5 m wide dyke, perhaps indicating an intrusive character. This view is favoured by T.C. Lees, mine geologist (pers. comm.), who interprets the inclusions of massive siliceous rock in the schists as a fault zone within the anticlinal structure (fig. 7). Conversely the "intrusions" could be regarded as protrusions of rigid slabs of pre-existing massive siliceous rocks during late Tabberabberan folding. The differences in chemistry between the two rock types, although confined to a few elements (chap.8.3.1.3.3., 12.2.2.) indicates that these rocks must have had a slightly different alteration history.

6.3.1. Petrography of the massive siliceous rocks.

The mineral assemblage of the massive siliceous rocks is simple, with varying proportions of quartz and sericite as major components. Part of the massive siliceous rocks close to the eastern and western outcrop boundary show an inhomogeneous fragmented texture with grey-green schlieren surrounding lighter sections up to 1 cm length (e.g. 67893). In thin section, the lighter areas are seen to be composed mainly of quartz, and the grey-green schlieren are the usual quartz-sericite groundmass. Faint primary volcanic textures have been occasionally preserved (67842), as specified below. Minor quantities of carbonate and pyrite ($\leq$ 0.02 mm) occur (e.g. 67795, 67844). Some pyrite euhedra have slightly rounded edges. Carbonate overgrows quartz and sericite in the groundmass, and quartz in quartz-carbonate veins. The groundmass is fine sand-silt grain size. It contains coarse grained strained and fractured quartz megacrysts ($\leq$ 3 mm) and medium grained rounded quartz crystals which average 0.5 mm in diameter. Quartz veins are $\leq$ 1 mm thick.

Green (1983) cites unstrained vein quartz as evidence for a Devonian alteration for these rocks. This study could not confirm his findings. Only rounded quartz crystals show uniform extinction under crossed polars (e.g. 67836). Vein quartz and the megacrysts which occasionally show signs of resorption, exhibit undulatory extinction (e.g. 67844).

Relatively fresh feldspar ($\leq$ 1 mm) is present in minor amounts at the eastern edge, and towards the western limit of the outcrop (67893, 67842).

6.4. Central alteration zone.

The central hydrothermal alteration zone is clearly marked by schists. Loftus-Hills et al. (1967) recognized at Mt. Lyell that the resistance of former volcanic rocks towards subsequent deformation was reduced by the previous influence of hydrothermal fluids.

The alteration zone, approximately 1 km^2, covers the area around the concentrator and Rosebery township. About 300 m south of the Stitt River it merges into unaltered volcanics. This transition zone is poorly defined, and is exposed in cuttings along Gepp St. and on the Murchison Highway. The northern boundary is poorly exposed. It can at best be interpolated to occur somewhere between an open cut on the HEC maintenance track (375000 N, 378880 E) and the flume track (374330 N, 378150 E). To the west, the schists probably grade into the massive siliceous rocks as discussed above. The eastern limit is generally defined by the host rock shale, except for a restricted area above the shale horizon.

The contact from hydrothermally altered schists to unaltered pyroclastics is gradational. Primary depositional foliation in the surrounding welded pyroclastics contributes to the difficulties in outlining the alteration zone.

Despite some variation, two major lithological facies dominate this zone. One facies is represented by silica-rich grey to yellow-grey green schists, the other facies consists of fine grey to grey-green schists. Part of these siliceous schists have a more or less pronounced augen texture, resembling Brathwaite's (1969) mine sequence cherts. Two distinct areas of siliceous schist were recognized in the alteration zone. The western unit is exposed over roughly 1 km along strike and has a maximum thickness of about 400 m. Apart from these siliceous schists with varying degrees of augen texture, this unit also contains some massive siliceous rocks. The difference between the two alteration facies is shown in fig. 9. Further east a second band of siliceous augen schist appears to be part of the immediate footwall of the host rock. At the southern end of this area, coarse partly altered K-feldspars have been found (fig. 10).

Between the main adit and the open pit, a series of alternating strata of augen schist and fine schists is present. The fine schists occur as a 200 m wide band within the siliceous schists. The former are usually fine grained and thinly cleaved, and frequently they contain slightly to moderately altered K-feldspar These will be discussed in chap. 10.1. In places, a gradational transition exists from siliceous augen schist to fine schists.

South of the Stitt River, a lens of dark grey massive to slaty rocks is intersected by the Murchison Highway. The dark colour is caused by substantial amounts of biotite.

6.4.1. Petrography of the altered schists.

Remnants of pyroclastic features are sparse in the altered schists. Relic textures of pumice, glass shards and possibly welding were recognized in or close to the transition zone of the eastern limit of the hydrothermally altered area (e.g. 67885). Brathwaite (1969) also reported some evidence for pyroclastic textures within the schist.

The matrix composition of fine schists, as well as siliceous augen schists, varies from quartz-dominated to dense sericitic, with the phyllosilicates defining the foliation. The fine schists consist of large areas of densely packed, aligned sericite interspersed with fine quartz grains. In the case of the augen schists, bands of sericite drape oval inclusions ranging from millimetre to centimetre length, which consist mainly of quartz grains and some sericite grains (both $\leq$ 0.03 mm). Also, small aggregates about 1 mm across of clear subhedral quartz are scattered throughout the matrix, their longer axis aligned parallel to the cleavage. These aggregates may be of secondary origin. Medium sized quartz grains ($\leq$ 1 mm) are present in siliceous schists of the north-western part of the alteration zone. These schists are associated with massive siliceous rocks.

K-feldspars and feldspar relics are common in the fine schist, in contrast to the siliceous schists. The relics appear either as stretched pods of dense sericite (fig. 11c) or as pseudomorphous replacements of quartz with relatively large, unoriented sericite flakes which tend to overlap the quartz grains (67880). Fresh to moderately altered mottled

Fig.9: Comparison of alteration texture: siliceous augen schists (left) and massive siliceous rocks (right), length of black bar = 1cm

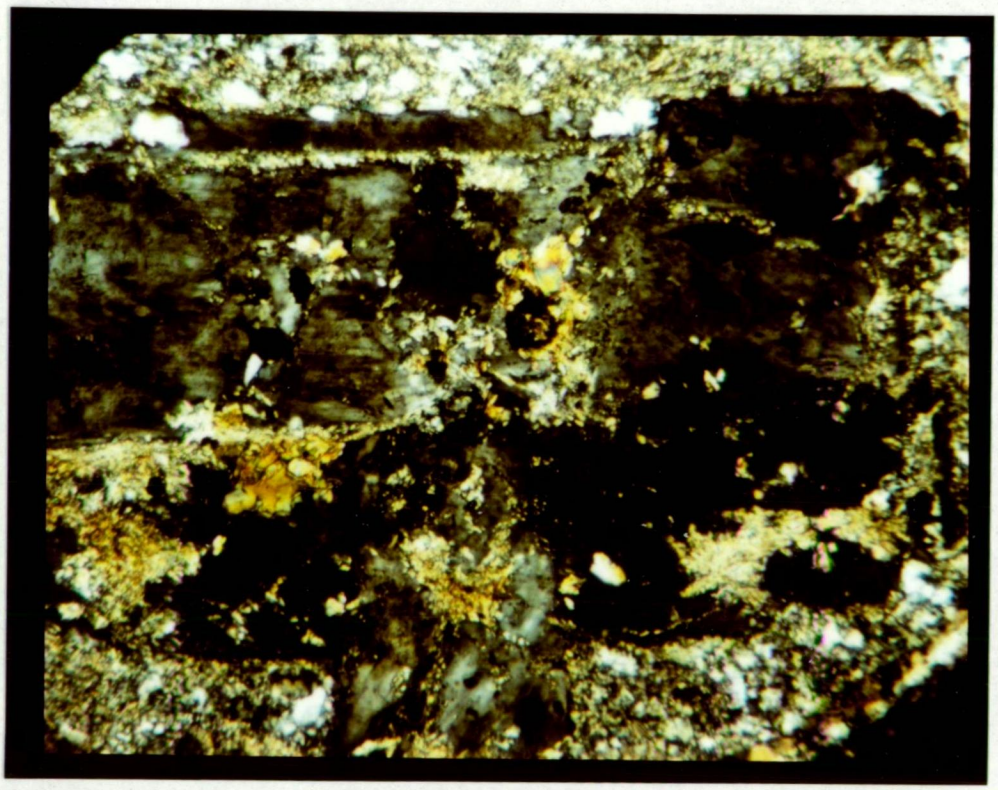

Fig.10: Mottled K-feldspar with biotite replacement (67885), field length 1.2 mm

K-feldspar is the only identifiable feldspar in the schists, and may be partly replaced by sericite and olive green pleochroic biotite (fig.10). K-feldspar in its original form can be up to 3 mm long and 1.5 mm wide. Polysynthetic twinning has been observed in a few crystals, suggesting a low temperature state of microcline (67905).

Chlorite and biotite can be present in varying but usually small amounts as part of the matrix. Larger amounts of olive green-brown biotite are present in the dark grey massive to slaty schists south of the Stitt River, together with fresh K-feldspar as mentioned above (67897).

Two generations of pyrite probably exist. Primary pyrite grains (singly or in small clusters) are easily recognized by their pressure shadows of quartz and occasionally quartz and chlorite. Second generation pyrite occurs in aggregates of clear secondary quartz, in altered K-feldspar, and in quartz veins (e.g. 67883).

Carbonate (5%) was found in one case as (Fe, Mn)CO_3 (67837). Individual grains overgrow quartz and sericite, and frequently form larger aggregates. Zircon, sphene, rutile and apatite are accessories (Brathwaite, 1969).

6.4.2. Petrography of the schists in the transition zone.

In the transition zone the pyroclastic rocks retain macroscopically part of their primary features. Under the microscope, however, sericite is strongly aligned. In contrast, sericite in unaltered pyroclastics shows only a weak orientation paralleling the primary texture. In fig.11a-d an idealized sequence of increasing alteration is portrayed.

6.5. Unaltered volcanics.

The hydrothermally altered schists are surrounded by relatively well preserved volcanic rocks of the Primrose Pyroclastics which are overlain to the east by the Mt. Black Volcanics. These rocks have been studied by Solomon (1964), Brathwaite (1969), Anderson (1972), Eastoe (1973, 1981), Fitzgerald (1974) and Green et al. (1981) in the area between Williamsford and Tullah.

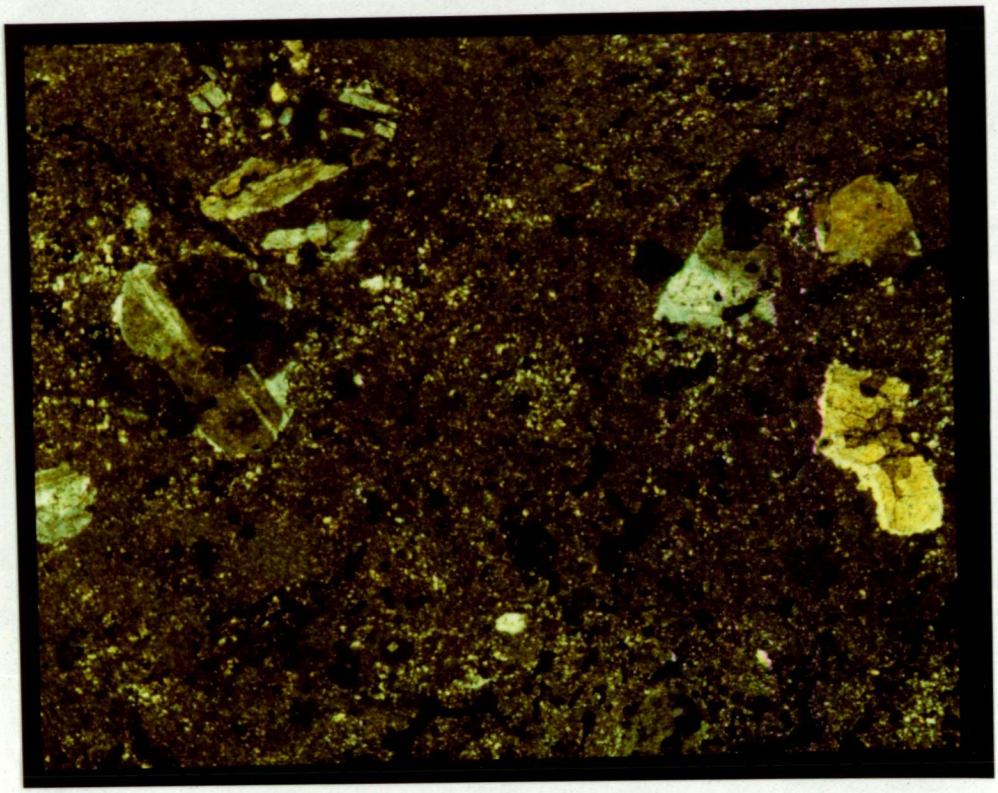

Fig.11a: Hydrothermally unaltered pyroclastic (67891), field length = 6 mm

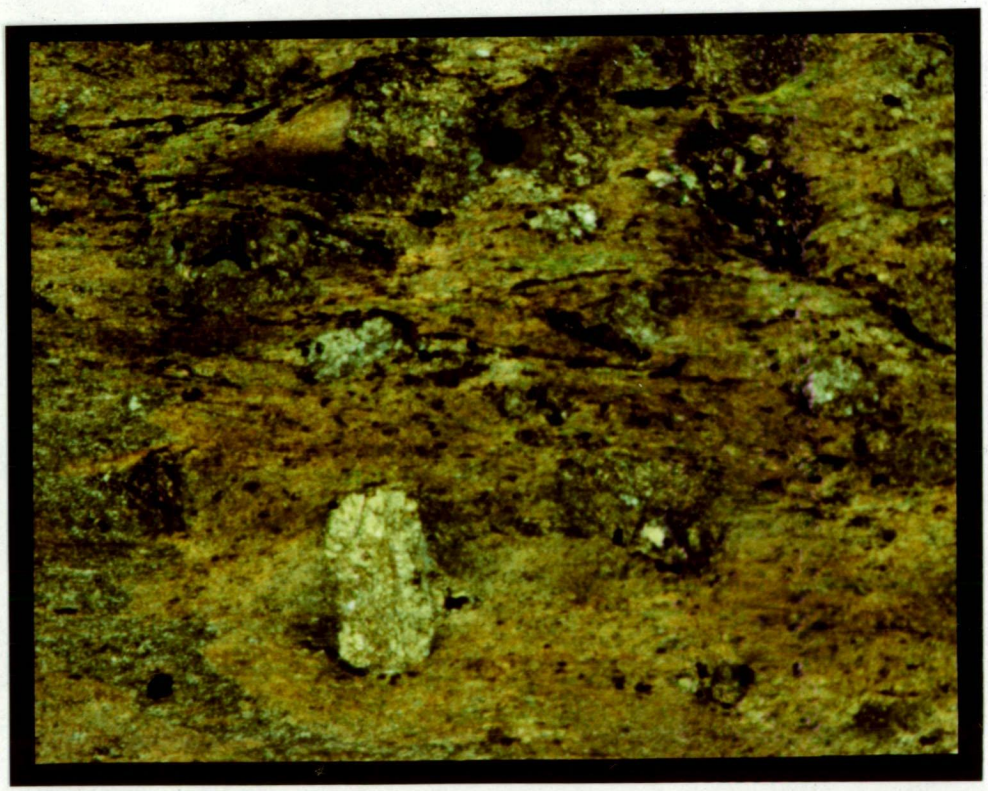

Fig.11b: Incipient hydrothermal alteration (67798), sericite alignment and beginning destruction of plagioclase, field length = 6 mm

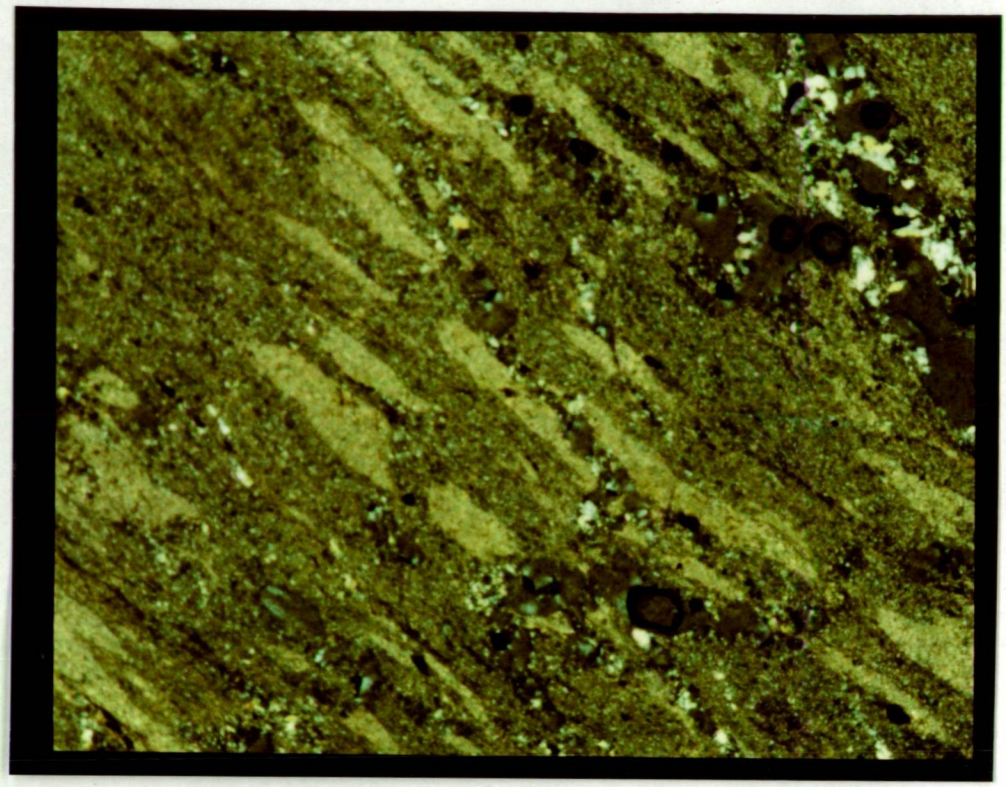

Fig.11c: Advanced hydrothermal alteration (67894) with sheared altered (sericitized) feldspars, field length = 6 mm

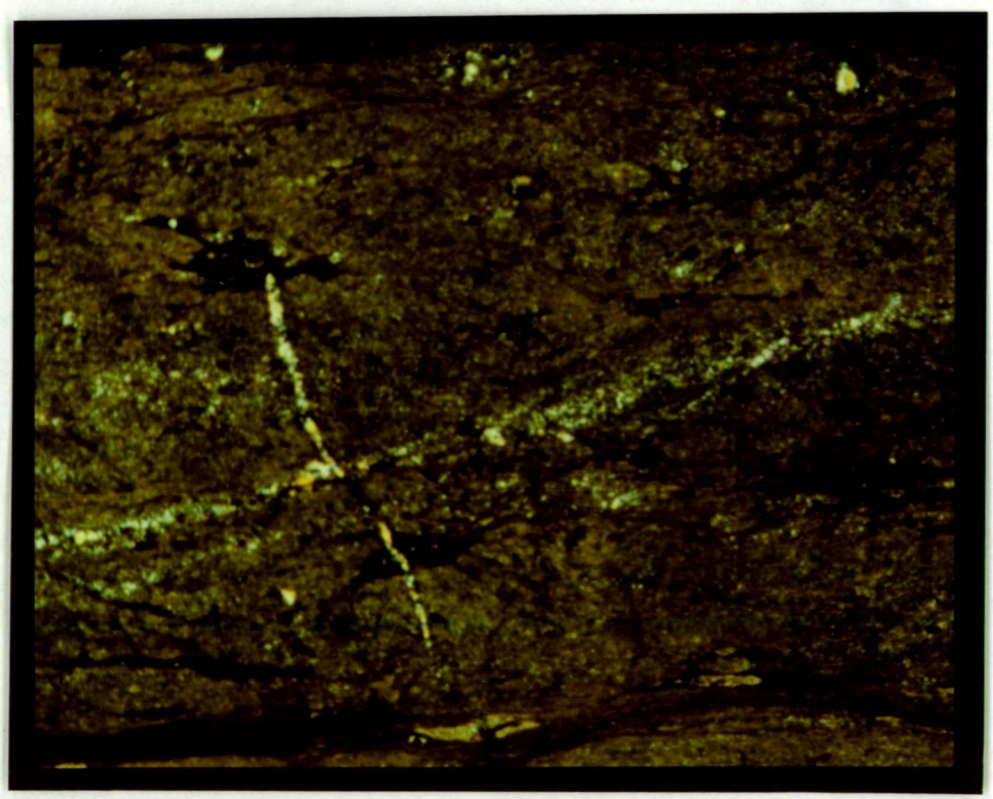

Fig.11d: Volcanic completely altered to siliceous schist with sericite and minor chlorite (67834), field length = 6 mm

6.5.1. Primrose Pyroclastics.

Brathwaite (1969) used the term footwall pyroclastics and massive pyroclastics to distinguish pyroclastics from below and above the ore horizon. According to him, these rocks are not clearly defined away from the mine.

Green et al. (1981) described the massive pyroclastics as a diverse sequence of mainly unwelded crystal tuff and volcanic breccia in the lower part and pumice tuff and agglomerate in the upper part. In contrast the footwall pyroclastics are welded vitric-crystal lapilli tuff and are uniform over a distance of 11 km. Green et al. (1981) list four criteria which help to distinguish between footwall and massive pyroclastics:

a. Numerous lenses of breccia with shale clasts occur only in the massive pyroclasts.

b. Quartz phenocrysts are restricted to the massive pyroclastics.

c. K-feldspars are restricted to the footwall pyroclastics.

d. Quartz-sericite schists are only well developed in the footwall pyroclastics.

Criteria b. and c. could not be confirmed by this study. Coarse quartz phenocrysts are more abundant in the massive pyroclastics, but are also present in the footwall pyroclastics (67797, DDH1121). Coarse plagioclase with K-feldspar rims, and fine to medium grained K-feldspar phenocrysts were found in the massive pyroclastics up to 200 m above the host rock shale horizon (67878). Criteria a. and d. were observed to be essentially correct.

Following Brathwaite (1969), the host rock shale horizon and its extension north and south have been regarded as the boundary between footwall and massive pyroclastics, marking a break in volcanic activity. The two types of pyroclastic rocks can be distinguished frequently by a reduced or absent primary foliation in the massive pyroclastics. This eutaxitic texture was probably created by welding and compaction during deposition as an ash flow tuff, as described by Smith (1960).

Between the shale horizons of the Rosebery deposit and Rosebery Lodes located approximately 1.5 km further south, the vaguely defined contact trends in north-south direction approximately 300 m west of the Dalmeny shale. North of the Rosebery host rock along the western flank of Mt. Black, the footwall pyroclastics continue to exhibit a welded texture which disappears at the northern end of the mapping area. The welded tuffs give way to the crystal-lithic ash fall tuffs of the massive pyroclastics, which include shale fragments in this area above the boundary. In the welded footwall pyroclastics along the western flank of Mt. Black, weathering has enhanced the compaction texture and thus produced a pseudo-cleavage which dips 50^{o} - 60^{o} east. This has also been recorded by Green et al. (1981).

In general, both pyroclastic units are vitric-crystal tuffs. The footwall pyroclastics are fairly uniform over most of the mapped area. Conversely, the massive pyroclastics display a variety of lithological facies. The main facies is vitric-crystal ash fall tuff with the occasional lithic fragment. Approximately 150 m east of the host rock shale and parallel to it, runs a band of crystal poor vitric ash fall tuff. It is exposed in the Stitt River and along the Murchison Highway where it can be traced over 400 m. Further up in the stratigraphy, welded vitric-crystal ash flow tuffs also with well developed fiamme (fig.12) alternate with ash fall tuffs. In one visibly bedded tuff a faint cross bedding might indicate a surge flow deposit (Cas & Wright, 1983) (67868). Towards the top of the massive pyroclastics volcanic agglomerates occur. The occasional strong alteration, or total lack, of feldspars, combined with extremely high quartz contents can certainly be attributed to post-depositional metasomatic processes (chap.8.3.1.3.1.).

6.5.1.1. Petrography of the Primrose Pyroclastics.

In some of the samples, the volcanoclastic textures have not been obliterated by greenschist metamorphism associated with the Devonian Tabberabberan Orogeny.

Recrystallized pumice relics occur as stringy quartz-sericite fragments. Remnants of unvesiculated glass are mostly recrystallized as well, and range from rounded ash particles ($\leq$ 0.5 mm) to vitric fragments. Rounded particles or fragments do not necessarily imply reworking, as

Fig. 12: Welded pyroclastics from the massive pyroclastics. Length of bar = 1 cm . Sample (67863)

rounding can also occur during transport in a hot pyroclastic cloud (Cas & Wright, 1983). Arcuate glass shards are also present in all stages of deformation (67838, 67847, 67848, 67863, 67908). Possible former glass blebs of irregular shape contain lobed quartz in a weak spherulitic arrangement (67852). All these features described are more easily recognized in the lower part of the massive pyroclastics, where welding is less pronounced than in the footwall pyroclastics. Mineralogically there is little difference between the two pyroclastic units. Both contain feldspar and quartz phenocrysts, which are more abundant in the massive pyroclastics. The matrix consists of quartz, sericite and possibly some plagioclase and K-feldspar. Matrix quartz has a grain size of 0.01 - 0.3 mm. Aggregates of clear secondary quartz or quartz, albite and K-feldspar (0.1 - 0.2 mm) are scattered in the matrix. Green pleochroic chlorite with anomalous blue interference colours is usually dispersed in fine grains throughout the matrix. It forms overlapping contacts with sericite. Larger patches of overgrowing chlorite occur infrequently.

The crystal content in both units varies quite considerably from 5% to more than 50% by volume particularly in a narrow layer just above the host rock horizon (e.g. 67838, 67955). In this band, the amount of quartz phenocryst can exceed that of plagioclase, usually the dominant crystal component. These coarse quartz phenocrysts ($\leq$ 3 mm) are rounded and fractured, and frequently show signs of resorption. Coarse plagioclase ($\leq$ 3 x 1.5 mm) is less fractured and has been variably sericitized (e.g. 68026). In footwall pyroclastics and massive pyroclastics up to 200 m east of the host rock horizon, clear and mottled rims of K-feldspar envelope sericitized plagioclase (e.g. 67878). Solomon (1964) first described the K-feldspar rims in the Rosebery area as a volcanic feature (chap. 10.1.3.). Epidote replacement of plagioclase occasionally is accompanied by carbonate and chlorite replacement (67818). From mineral contacts it is inferred that epidote is younger or coeval with chlorite, and both are post-carbonate. Spherulitic zoisite was found in two samples (67832, 67916). Carbonate and pyrite occur rarely, carbonate mainly in veins, and pyrite in quartz veins and as subhedra replacing plagioclase. Zircon, sphene and rutile are accessory minerals (see also Brathwaite, 1969).

6.5.2. Mt. Black Volcanics.

About 500 m east of Rosebery along the Murchison Highway the massive pyroclastics are succeeded by the Mt. Black Volcanics. These rocks are very dense and several different units with varying colours, from light to dark grey can be distinguished clearly along the highway. They are bounded by sharp to gradational contacts. Brathwaite (1969) first described this section and classified these rocks, based on their lithology, as lavas. He also introduced the name of Mt. Black Volcanics. Anderson (1972) mapped this section along the highway as rhyolitic quartz-feldspar porphyries and dacitic feldspar porphyries. Contrary to previous work, the boundary between massive pyroclastics and Mt. Black Volcanics is drawn in the present study further east, and the first appearances of lava are regarded as an intercalation of Mt. Black Volcanics in the massive pyroclastics. However the separation into lavas and pyroclastics is tentative in most cases due to the lack of preserved primary textures.

6.5.2.1. Petrography of the Mt. Black Volcanics.

The Mt. Black Volcanics are feldspar porphyries with up to 30% crystal content. The phenocrysts are dominantly albitic plagioclase ($\leq$ 3 x 1.5 mm). They have probably been affected by the Devonian greenschist metamorphism. Some rounded, occasionally resorbed quartz is also present. Commonly, the plagioclase phenocrysts are slightly fractured, and rounded to a minor degree. The feldspar alteration ranges from sparse sericitization to a more advanced replacement by epidote and chlorite, calcite or biotite. Epidote appears to overgrow chlorite (67827). In the matrix, chlorite (green and pleochroic with blue and purple interference colours) is present either as fine interspersed flakes or in larger patches. They overgrow crystals, matrix and veins.

The matrix is formed by a dense intergrowth of mainly quartz and sericite. Single laths of K-feldspar and albite (0.1 - 0.3 mm) and spherulitic bundles can form a substantial part of the matrix, and are slightly sericitized (67826). Sphene, rutile, zircon, apatite and pyrite are accessories (Brathwaite, 1969). Some 2000 m above the ore horizon, slightly rounded pyrite euhedra ($\leq$ 0.5 mm) amount to approximately 5% in volume of one section (67871). They occur singly or in clusters associated with chlorite and in plagioclase.

Small amygdales in the order of millimetres and less are filled with carbonate (67874) or quartz and chlorite (67827). The latter are zoned with chlorite in the centre surrounded by fine grained quartz.

7. Mode of Pyroclastic deposition.

Unaltered Primrose Pyroclastics retain some textural features useful in determining their origin. Compaction welding of glass fragments including pumice, and undeformed, unvesiculated glass shards and bedded lapilli indicate deposition as ash flows and as ash falls respectively. In many cases however, these features have been obliterated completely by subsequent metamorphic events. The occurrence of pumice and welding is interpreted as the result of terrestrial deposition, although these features have been reported from subaqueous volcanoclastic deposits. Ashfall deposits may be formed both subaqueously and subaerially.

As knowledge of the geological setting during the formation of the ore deposit is important for interpretation of the ore genesis, a brief discussion of the modes of pyroclastic deposition is included. Even before the idea of the Rosebery deposit as a submarine exhalative deposit in an island arc setting was accepted, there were speculations about the depositional environment of the Mt. Read Volcanics.

Solomon (1960) and Spry (1962) surmised that nuees ardentes could have produced some of the pyroclastic rocks in the Mt. Read volcanic belt. Solomon (1964) also briefly discussed subaerial and subaqueous deposition of glowing avalanches. Brathwaite (1969) preferred a subaerial environment for the pyroclastics around Rosebery, based on the occurrence of ignimbrites and absence of stratification. For the ore-bearing shale he envisaged a shallow water basin.

Green et al. (1981) assumed generally subaerial deposition for the welded footwall pyroclastics and a submarine environment for the massive pyroclastics. They used the absence of quartz nodules, megaflames and rootless vents as described by Francis & Howells (1973) and Wright & Coward (1977) for subaqueous ash flow tuffs as an additional argument for subaerial deposition of the footwall pyroclastics. Their evidence for largely submarine deposition of the massive pyroclastics include occasional undeformed shards, occasional grading of pyroclastic debris, and the presence of volcanic breccias with shale fragments and shale rafts. Green et al. explain minor welding in the massive pyroclastics by post-depositional weight compaction of cooled pumice and glass shards, as described by Fiske (1969).

Cas & Wright (1983) pointed out that for the subaqueously welded tuffs reported by Francis & Howell (1973) and Wright & Coward (1977), the actual water depth might not have exceeded 10 m, based on measurements of large scale cross-stratification. A pyroclastic flow apron is likely to have blanketed a shallow basin. The superheated trapped water escaped through rootless vents, or was contained in vesicles, hence the quartz nodules. Wright & Mutti (1981) re-examined the Dali ash in Rhodos and concluded that previously reported welding textures in the subaqueously emplaced pyroclastics were misinterpreted.

Carey & Sigurdson (1980) described the subaqueous extension of the Roseau ignimbrites in Domenica, lesser Antilles, as pyroclastic debris flow, in order to distinguish it from the terrestrial equivalent, with evidence of high emplacement temperatures of the Roseau ignimbrites. From the same island, Sparks et al. (1980) noted the underwater continuation of the Grande Savanne pyroclastic flow, comprising poorly vesiculated blocks and ash, offshore to a depth of up to 1000 m. They assumed subaqueous transport, at least partly as a hot debris flow with a velocity greater than the ablation rate, in order to retain the integrity of the submarine apron. No evidence was provided for welding. Their theoretical model, however, favours subaqueous welding over subaerial welding, which is in stark contrast to the encountered geology. The decreased viscosity of the juvenile glass due to higher water content more than offsets the loss in heat by mixing with water, and thus enables welding of the dense pyroclastic flow.

Cas & Wright (1983) summed up their literature review with the conclusion that most subaqueous pyroclastic flow deposits are the offshore extension of subaerially erupted flows, and that welding essentially occurs terrestrially.

Around Rosebery, several shale lenses of limited extent along strike, with a thickness of sometimes less than 1 cm, are interbedded with sheared volcanics at various stratigraphical levels. In association with the welded footwall pyroclastics this might indicate a lacustrine or lagoonal environment with rapid vertical tectonic and volcanic movements, as reported from Tuluma island (Reynolds & Best, 1976). The absence of features such as rootless vents in a heavily vegetated area should not be counted as a negative criterion. During or prior to the break in volcanic activity marked by the presence of the host rock shale, caldera subsidence

(chap.5.2) could have occurred, producing a basin several hundred metres deep.

The variety of lithologies in the massive pyroclastics probably reflects local environment in a resurging unstable volcanic arc. Apart from cold subaqueous compaction, a minor primary eutaxitic texture could also be the result of incipient welding at lower temperatures, as discussed by Smith (1960) and Sparks et al. (1978). The absence of pillows in the lavas from the Mt. Black Volcanics favours terrestrial deposition, which is in agreement with welded tuffs in the top part of the massive pyroclastics.

8. Geochemistry of the surface alteration.

8.1. Sampling.

A total of 101 samples of hard rock from the surface, including three duplicates were collected, each weighing approximately 1 kg. This amount is sufficient for a representative sample in the case of fine grained volcanic rocks (Govett, 1983). Four drill core samples close to the surface were also used to improve the sampling grid in the hanging wall which is covered by thick rainforest. Except for three samples affected by advanced weathering, the whole set was analysed for major and trace elements (tab.3) by XRF-analysis. The sulphur content was determined by titration using a LECO induction furnace. Major and trace element analyses are listed in appendix 2. Sample 67890 (host rock shale) and sample 67891 (ash flow tuff), south of the mapped area are not included in the following discussion.

The location of the majority of samples was concentrated in the hydrothermally altered schists and the surrounding footwall and massive pyroclastics. On the heavily timbered west and south flank of Mt. Black the sample density decreased due to lack of rock exposures. Several samples were also collected from the massive siliceous rocks and the Mt. Black Volcanics. The average sample coverage amounts to 6 samples/km^2, although sample density reaches up to 20 samples/km^2 in the altered and unaltered footwall pyroclastics in the vicinity of the ore deposit (fig.13) within the township of Rosebery. The decrease in the sampling density away from the population centre is due to dense vegetation and generally poor exposure of hard rock.

Dense vegetation and poor outcrop over large areas did not allow a systematic sampling pattern, apart from a rough subdivision into smaller areas including and surrounding the central hydrothermal alteration zone. The subdivision as shown in fig.13 is based on the same boundaries as fig. 6a. Three N-S striking units are defined. The central zone (B) is subdivided into a central schistose hydrothermal zone (B2), and unaltered footwall pyroclastic correlates along strike to the north and south (B1, B3). The central zone is bounded to the west by the massive siliceous rocks (A), and to the east by the host rock horizon and overlying massive pyroclastics (C). Above the orebody, the massive pyroclastics still show

signs of hydrothermal alteration (chap.6.4., 8.3.1.3.1.). Within each subarea, sampling was mainly based on the existence of rock exposures. The assumption of a random distribution factor is supported by a cluster analysis carried out on the surface samples (fig.32a, b, chap.8.3.2.1.2.). The samples within each group do not cluster according to their location. This contrasts with the duplicates, which were collected within a distance of 10 m and are very closely associated. Therefore a representatively uniform rock chemistry can be assumed for either group.

8.2. Geochemistry of the unaltered rocks (background).

According to the cluster analysis there is no evidence for a general difference between the rhyolitic rocks of the three unaltered lithological units; footwall pyroclastics, massive pyroclastics, and Mt. Black Volcanics. A large overlap exists among the units on a multivariate basis. Within the rhyolitic pyroclastics, out of 22 analysed elements, only the Fe and Ni content is statistically higher in the massive pyroclastics than in the footwall pyroclastics at the 0.01 significance level.

The AFM-diagram (fig.14) after Irvine & Baragar (1971) shows a calc-alkaline trend for the hydrothermally unaltered volcanics. White (1975) was able to demonstrate that the volcanic rocks from the southern end of the Mt. Read belt in Tasmania follow exactly the same trend.

Within the Primrose Pyroclastics only rocks of rhyolitic character >68% SiO_2 (Taylor, 1969) were found except for one sample at the western end of the sampled area, which is a dacite. In this study, the older classification according to Taylor (1969) was chosen over the updated classification by Peccerillio & Taylor (1976) in order to include all samples from the unaltered Primrose Pyroclastics as rhyolites. The lavas of the Mt. Black Volcanics contain dacites and andesites as well as the dominant rhyolites. The spatial distribution of these intermediate lavas does not reveal a systematic trend within the area under investigation.

Widespread metasomatism has affected the "unaltered" volcanics, as is most evident from silicification and the loss of Na and Ca. The deficiency of Ca in the Mt. Read Volcanics around Rosebery has already been recorded

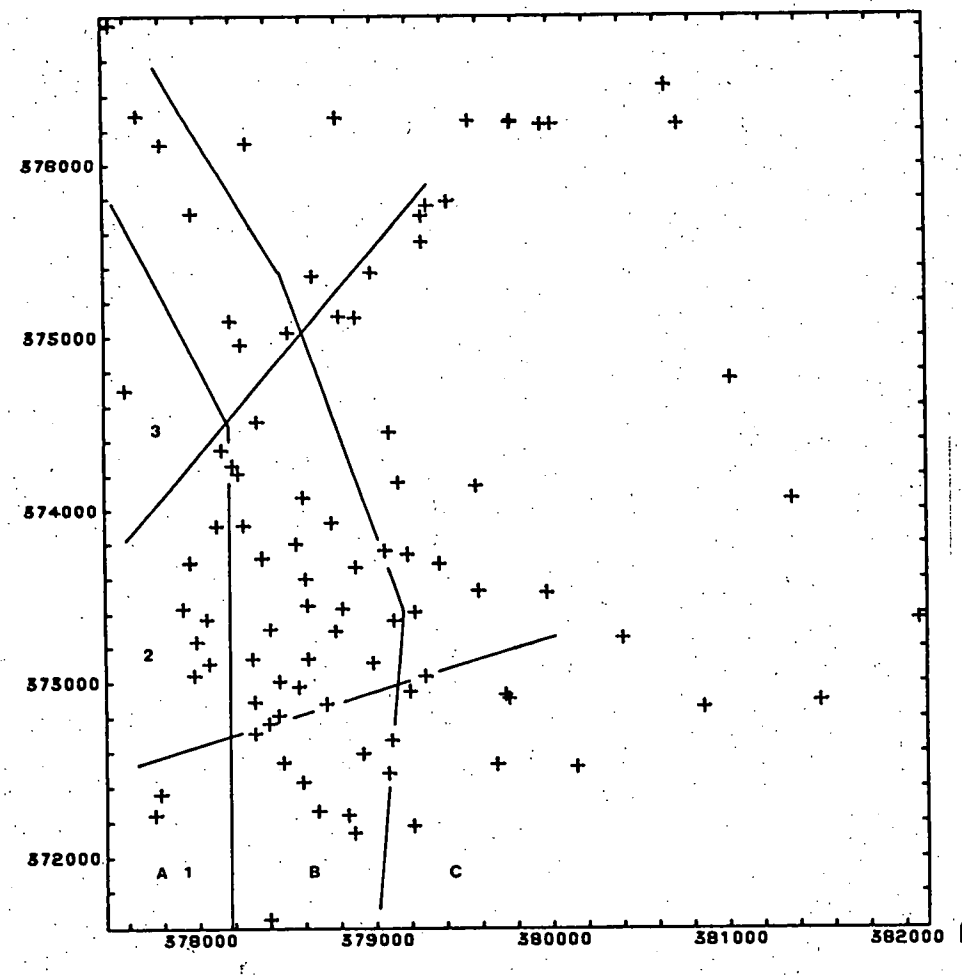

Fig.13: Sample distribution and sampling division in columns (A to C) and rows (1 to 3)

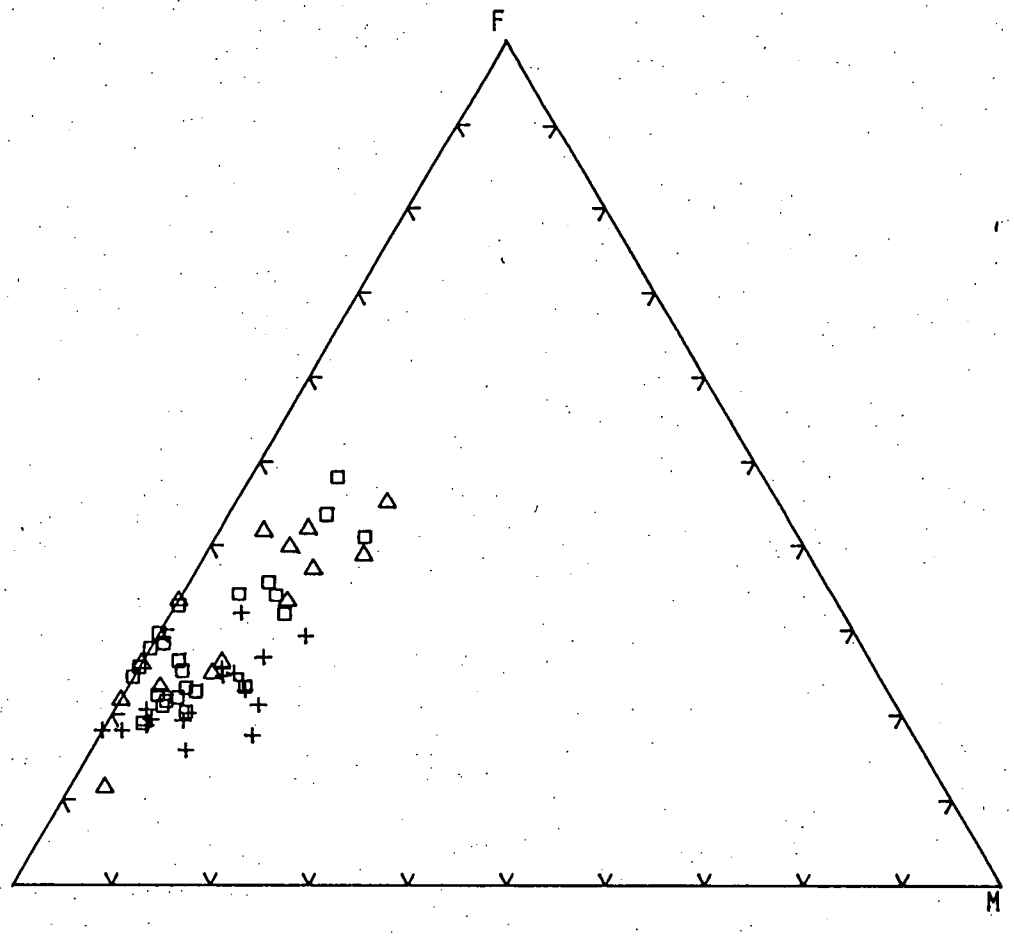

Fig.14: AFM diagram according to the method of Irvine & Baragar (1971), A: $Na_2O + K_2O$, F: FeO_t, M: MgO

by Eastoe (1981). In tab.2 the unaltered Mt. Read Volcanics from this study are compared to Cenozoic volcanics of the calc-alkaline suite from the Chilean Andes and New Zealand, and to felsic rocks within Archaean greenstones from the Marda complex in Western Australia. Both the Cambrian Mt. Read Volcanics and the felsic Archaean rocks are depleted in Ca with respect to the calc-alkakine suites of Chile and New Zealand. The rhyolitic Mt. Read Volcanics are also depleted in Na. Tatsumi & Clark (1972) also reported the problem of alteration in "unaltered" volcanics related to the Kuroko deposits. It is envisaged that two factors; age with its accumulated geological events, and hydrothermal fluids, could have changed the chemistry of the "unaltered" rocks to some extent.

8.3. Alteration geochemistry (target).

The geochemistry of the alteration (target area) and its comparison to the "unaltered" volcanics (background area) has been examined by statistical methods including uni- and multivariate analysis. This approach was necessary because of large chemical variations within altered and unaltered rocks. The geochemical halo of the hydrothermally altered area can be demonstrated to follow closely the mineralogical and petrographical zonation, by contour-plotting the distribution of various elements. Contouring was significantly improved by smoothing the already averaged data (chap.8.3.1.2.2.). The alteration was investigated in the following manner:

a. After recording the analytical data and co-ordinates on a data file, the inherent chemical grouping and random distribution within the target and background group were tested by cluster analysis.

b. The chemical clustering was subsequently compared with the petrographic grouping.

c. The samples within the groups were also considered in view of their position relative to the ore deposit.

d. The established target and background group were compared against each other on a univariate basis by analysis of variance including Duncan's test and the non-parametric Wilcoxon test.

	A	B	C	D	E	F	G	H	I	J	K	L	M
SiO_2	73.79	73.97	65.40	59.56	75.30	60.80	74.90	72.90	62.50	74.22	73.85	66.08	59.22
TiO_2	0.38	0.32	0.68	1.09	0.23	0.77	0.17	0.26	0.82	0.28	0.23	0.50	0.72
Al_2O_3	14.25	13.50	15.26	14.65	12.60	14.70	12.60	13.80	16.30	13.27	13.55	15.27	16.83
Fe_2O_3	2.42	0.12	6.00	8.00	2.13	7.59	1.00	1.70	5.60	1.90	1.92	4.54	7.17
MnO	0.06	0.09	0.10	0.17	0.08	0.11	0.05	0.06	0.11	0.05	0.05	0.08	0.13
MgO	0.59	0.49	1.77	2.67	0.20	3.50	0.30	0.50	2.50	0.28	0.30	2.04	3.78
CaO	0.33	0.23	1.91	4.62	0.30	5.50	0.90	1.50	4.90	1.59	1.53	4.29	6.77
Na_2O	3.06	2.24	3.16	3.18	3.90	3.60	3.60	3.80	3.00	4.24	3.71	3.60	3.27
K_2O	3.12	4.08	3.03	1.78	4.10	1.70	4.80	4.30	2.90	3.18	3.60	2.34	1.50
P_2O_5	0.05	0.05	0.11	0.26	0.02	0.23	0.03	0.08	0.18	0.05	0.05	0.13	0.12

A: rhyolite, Primrose Pyroclastics
B: rhyolite, Mt. Black Volcanics
C: dacite
D: andesite
E: rhyolite, Marda Complex (W. A.), Archaean
F: andesite, Marda Complex (W. A.), Archaean
G: rhyolite I, ignimbrite, Chilean Andes
H: rhyolite II, ignimbrite, Chilean Andes
I: dacite I, ignimbrite, Chilean Andes
J: rhyolite, lava, Taupo (N. Z.)
K: rhyolite, ignimbrite, Taupo (N. Z.)
L: dacite, lava, Taupo(N. Z.)
M: andesite, lava, Tongariro (N. Z.)

References:
A - D: Rosebery, this study
E - F: Hallberg et al., 1976
G - I: Pichler & Zeil, 1970
J - K: Ewart et al., 1968
L - M: Cole, 1979

Tab.2: Average composition of calc-alkaline volcanics

e. The distribution pattern of the analysed elements was studied using local and global contouring techniques.

f. A discriminant analysis was performed to compare the discriminatory power of a set of elements against a single element.

Step b. and f. are discussed together as multivariate statistics (chap. 8.3.2.) following the general description of the alteration based on single-element behaviour.

8.3.1. Univariate alteration geochemistry.

8.3.1.1. Theory of statistical tests.

The following discussion is based on Davis (1973), Hoel (1976) and Mendenhall et al. (1981). In this context the term "sample" has the statistical meaning of a group of observations.

8.3.1.1.1. Analysis of variance.

The analysis of variance is based on the F-distribution. This is a mathematical expression for the spread of ratios of sample variances taken from a normally distributed population. Three assumptions are required. The samples have to be drawn in a random way from populations which are normally distributed and also have equal variances.

The analysis of variance tests the equivalence of two or more samples on the hypotheses:

H_0: The samples and their parent populations are equivalent.
H_1: At least one sample is different.

In the two sample cases the results are in theory identical to that produced by a t-test.

The test is carried out by computing the F-statistic. This is the ratio of the mean square among samples

$$MS_A = \frac{\sum_{j=1}^{m} n_j (\bar{x}_{\cdot j} - \bar{x})^2}{m - 1}$$

over the mean square within replications

$$MS_W = \frac{\sum_{j=1}^{m} \sum_{i=1}^{n} (x_{ij} - \bar{x}_{\cdot j})^2}{N - m}$$

with N = nm being the total number of observations. The hypothesis H_0 is rejected if $F = \frac{MS_A}{MS_W}$ falls into the critical region. The critical region or region of rejection is defined as an area of low probability for F to occur, commonly 1-10%.

The analysis of variance was performed by the program package Teddybear (Wilson, 1978) which includes Duncan's test if more than two samples are involved. This test overcomes the failure of the analysis of variance to detect samples which do not differ significantly. Duncan's test compares the difference between sample means to a shortest significant range (Duncan, 1955) and rejects the H_0-hypothesis of equality between samples if the difference exceeds this range.

8.3.1.1.2. Wilcoxon rank sum test.

The Wilcoxon rank sum test belongs to the group of non-parametric tests. It can be shown to be equivalent to the Mann-Whittney U-test. They are applied to test the equivalence of samples which do not satisfy the requirements of normal distribution. If populations are normally distributed the ability of these tests to discriminate between them is almost as good as that of the parametric tests.

The test procedure for two independent random samples combines both samples, and ranks their observations successively. In a second step the rank sums (W) of each sample are calculated. For a two-tailed test the smaller of these two sums is used to test the equivalence of the two samples. The hypothesis H_0 will be rejected if W, the rank sum, falls into the rejection region which is obtained by establishing the probability of a predetermined W_0-value to occur. The calculation of the probability is based on a binomial distribution. For large samples (> 30 observations)

the program package SPSS (Nie et al., 1975) employs the normal approximation of the binomial distribution and transforms the W-statistic into a Z-statistic.

8.3.1.2. Theory of contour plotting.

8.3.1.2.1. Trend surface analysis.

The following discussion is based on Davis (1973), Krumbein & Graybill (1965), Koch & Link (1971) and Agterberg (1974).

Trend surface analysis relies on a mathematical model in the form of a regression analysis such as

$$\hat{y} = f(x_1, x_2, \ldots x_n ; b_1, b_2 \ldots b_n) + e$$

with independent variables x_i and b_i as estimators for the parameters B_i. The term e represents a random error which follows a normal distribution.

The aim is to minimize the difference $\sum_{i=1}^{n} e^2 = \sum_{i=1}^{n} (\hat{y}_i - y_i)^2$ between the estimated value $\hat{y}_i$ and the observed value y_i for the variables x_{ij}. This is achieved with the help of the least square procedure, and the estimated parameters b_i are obtained by a set of linear equations which can be expressed in matrix notation:

$$B\underline{x} = \underline{y}$$

Two important measures for the significance of the obtained equations are the goodness of fit and the F-ratio.

$$R^2 = \frac{SS_{Reg}}{SS_{Tot}} \qquad F = \frac{MS_{Reg}}{MS_{Res}} .$$

The goodness of fit, R^2, indicates the explained variation due to curve fitting. The F-ratio determines which independent variable is to be included in the stepwise determination of the regression equation as performed by the program package SPSS.

8.3.1.2.2. Gridding by weighted moving averages.

The preferred method of local fitting by the program package Surface II (Sampson, 1978) in this study (chap. 8.3.1.3.4.) was based on interpolating contours between grid nodes (fig.15a). These were calculated from the original observations by a search algorithm which selects a specified number (n = 8) of original data points within a certain distance. The data points are weighted (multiplied) by the squared inverse of distance ($\frac{1}{d^2}$) from the grid node, which was calculated from the eight nearest data points (fig.15b). Tests with other specifications and search algorithms that draw points from subdivided areas eg. quadrants, did not change the results.

A two-phase gridding was finally selected with an initial pass creating local slopes through each data point, based on n nearest data points, and a final pass computing the grid nodes by averaging the slopes' projections at each node (fig.16a, b). This method slightly reduces the noise on the unsmoothed contour plot but otherwise produces an identical surface when compared to a one-phase weighted moving average gridding.

As a final step the grid matrix was smoothed in one pass by averaging squares of 11 columns x 11 rows over each grid node (fig. 17).

Local fitting does not provide statistics about the significance of a fit for the final surface. However error analyses based on smoothed grid values show a narrow, linear band of these grid values when plotted against the original data in the case of the major elements, and a wider band for trace elements. To demonstrate the process of contour plotting, the distribution of raw data, the unsmoothed and smoothed contoured surface is presented for Na_2O (fig.31a, b, c). In addition, the trend surface based on a cubic regression analysis is shown for comparison (fig.31e).

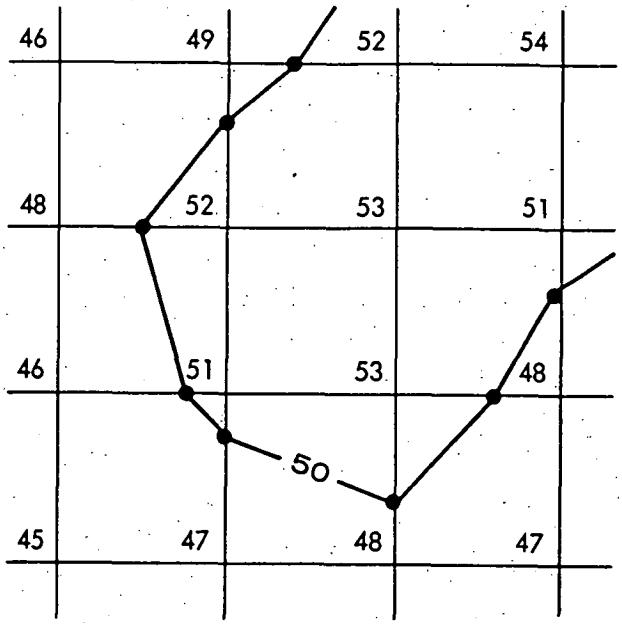

Fig.15a: Path of a contour line drawn through a regular grid. Value of the contour line is 50 (After Sampson, 1978).

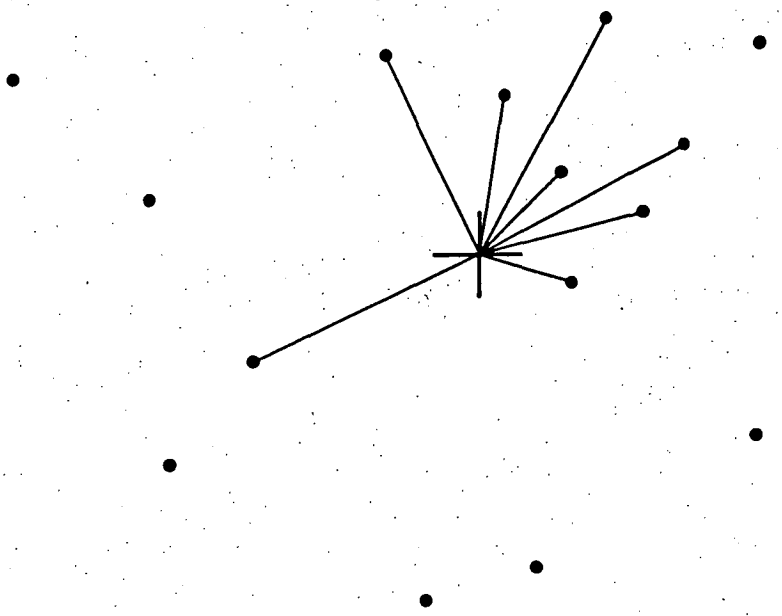

Fig.15b: Search pattern used by 'NEAR' to find the eight closest values to a grid node being estimated (after Sampson, 1978).

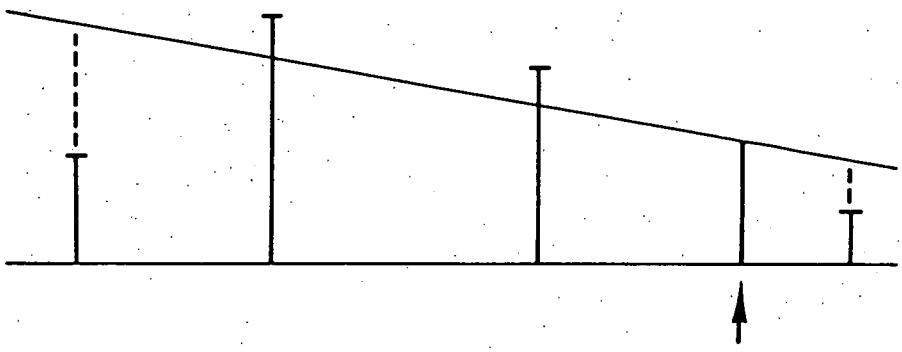

Fig. 16a: Local dip at a data point (shown by arrow) is found by fitting a least-squares surface to surrounding data points, subject to the constraint that the plane passes through the point (after Sampson, 1978).

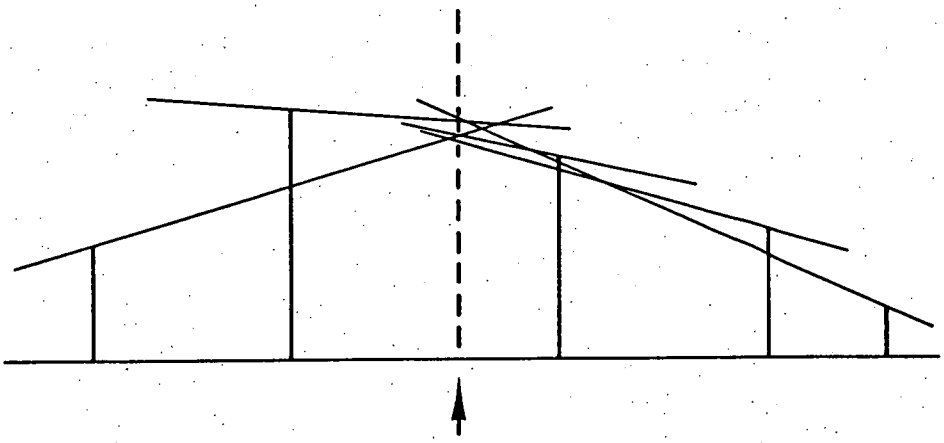

Fig. 16b: Local dips at control points are projected to a grid node to be estimated (arrow). The value assigned to this node is a weighted average of the dip projections (after Sampson, 1978).

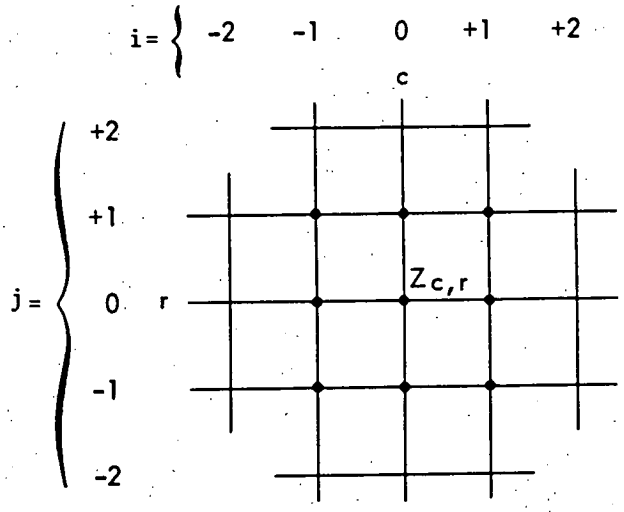

Fig. 17: Smoothing of a grid matrix by replacing the value $Z_{c,r}$ at a grid node with an average of the values at neighbouring nodes (after Sampson, 1978).

8.3.1.2.3. Comparison of local and global surface fitting.

The program package Surface II was used to contour the alteration halo for 22 major and trace elements. A local fit was chosen over a global fit, although tests with trend surface analyses were conducted to determine its power of detecting the anomaly. Fitting a trend through the original data did not result in a significant surface. For further examinations, a grid matrix based on the element Na was created by a weighted moving average algorithm, as discussed above. Subsequently the unsmoothed and smoothed grid matrix was read into a SPSS-program for performing a two-dimensional cubic stepwise regression analysis. The trend surface analysis in Surface II is not implemented at the University of Tasmania. From the resulting equation, a new grid matrix was calculated and fed back into the Surface II package. As it turned out, the regression analysis only produced a significant fit ($R^2 = 0.57$) when the smoothed grid matrix was used as a data base. The resulting surface revealed (fig. 31e) a very simplified anomaly. Trend surface analysis did not provide any advantages and therefore was not pursued any further.

8.3.1.3. Geochemical alteration pattern.

The geochemical alteration patterns are in good agreement with the geological findings (fig. 6a, b, chap. 6). However the geochemistry is more effective in defining the path of the hydrothermal solution. The chemical distribution pattern of the alteration halo of many elements points to the ore deposit and could provide a fast method of pinpointing an unknown orebody. In addition geochemistry proved to be more sensitive to hanging wall alteration than the study of hand specimen and thin sections.

The central halo in the footwall of the ore deposit is influenced in two ways, firstly by samples from the hanging wall with an alteration chemistry as demonstrated by the cluster analysis, and secondly by the massive siliceous rocks. These represent a second style of alteration (chap. 6.3.) west of the altered schists and are included in the general group of altered rocks, based on their comparable geochemistry to schists.

8.3.1.3.1. Influence of the hanging wall alteration.

Several samples from the hanging wall and in particular from a 100 - 300 m wide strata just above the host rock shale, cannot be distinguished chemically from altered footwall rocks. In some of these cases textural evidence favours an unaltered status but this is not entirely conclusive. As suggested in chap.6.5.1.1., the chemistry of these rocks might reflect a stratum of originally crystal-poor pyroclastics. Conversely two further samples up to 2 km stratigraphically above the ore horizon which appear macroscopically unaltered, fall into the altered cluster. This chemical behaviour is not paralleled in the lateral direction away from the ore deposit. This could be interpreted as a diminished continuation of the hydrothermal alteration after the deposition of the ore, by hot fluids migrating into the hanging wall.

The chemical haloes usually protrude several hundred metres into the hanging wall. To test the influence of the samples immediately above the ore, they were included in subsequent statistical tests in the altered and unaltered groups. This had no noticeable affect on the results, which are listed in tab.3 and 4, with the exception of Fe_2O_3, which showed a slightly improved separation when the samples concerned were assigned to the altered schists. Tab.3 and 4 are based on this chemical approach, in order to explain the alteration halo as seen by the contouring program. The samples in doubt were included in the altered group. Also, contour plots were based on quadrant search (see above) to overcome the gap in the sample distribution above the host rock. This method did not change the halo, and the contoured alteration in the hanging wall remained the same.

8.3.1.3.2. Influence of the chemistry of the massive siliceous rocks.

The overall chemistry of the massive siliceous rocks (MS) with their texturally different style of alteration is comparable to that of the altered schists (SCH). Both rock types cluster in the altered group, although the massive siliceous rocks are more closely linked together at a lower level of heterogeneity (fig.32a, chap.8.3.2.1.2.). On a univariate basis, statistically significant differences exist for several elements between the two rock types (tab.4).

To test the influence of the massive siliceous rocks on the shape of the geochemical haloes at the western margin of the mapped area, three different cases were studied by contouring the haloes for Na_2O, K_2O and SiO_2 excluding the massive siliceous rocks:

a. Na_2O: MS and SCH are statistically equivalent but statistically lower than unaltered rocks (UA) (fig. 31d).
(MS = SCH) < UA

b. K_2O: MS are equivalent to SCH and UA, SCH are higher than UA (fig. 19b).
(MS =SCH) and (MS = UA) and (SCH > UA)

c. SiO_2: SCH and UA are equivalent but lower than MS (fig. 20b).
(SCH =UA) < MS

The new contour plots show only minor changes to the shape of the alteration haloes, demonstrating their robust behaviour.

8.3.1.3.3. Statistical significance of the alteration.

In order to explain the geochemical alteration patterns as accurately as possible in statistical terms, a three-step approach was pursued:

a. Altered rocks including schists and massive siliceous rocks were compared against unaltered rhyolitic pyroclastics.

b. Schists, the centrally located type of altered rock, were compared against unaltered pyroclastics.

c. All three rock types were compared on an equal basis.

The basic statistics of each group are listed in tab. 3 and the results of the comparison among groups are listed in tab. 4 and briefly discussed with the contour plots. Step a. and b. were tested by analysis of variance, a robust statistical procedure (Garrett, 1983), and Wilcoxon's rank sum test. A t-test (not listed) was also carried out and produced consistently identical results to the analysis of variance. Step c. was tested by analysis of variance only, including Duncan's multiple range

test. As indicated in tab.4 the analysis of variance based on a completely randomized design with one variable (Mendenhall et al., 1981) is slightly better in discriminating between groups than Duncan's multiple range test. Wilcoxon's rank sum test in the two-group cases of step a. and b. was used as a measure of double checking elements with deviations from a normal distribution. This test is also more robust to inequality of group variances with sample sizes used in this study (Brown, 1982) when compared to the t-test. In most cases these deviations could be reduced significantly by taking the square root, the logarithm of 10, or both, from the original data, as specified in tab.4 (see also appendix 3).

Apart from those ambiguous samples discussed in chap.8.3.1.3.1. only samples with a clear cut geological and geochemical adherence to one group were included in the statistical tests, except for one sample (67889) where geological evidence and location determined the group. Thus eight samples from the transition zone (chap.6.4.2.) were excluded from the statistical tests. They are however included in the control group in the discriminant analysis and listed at the end of tab. 7 (chap. 8.3.2.2.2.). In an additional test case, the inclusion of felsic rocks of the Mt. Black Volcanics (lavas), immediately adjacent to the massive pyroclastics in the hanging wall, a pyroclastic rock (67868) which was chemically altered only, and a dacite from the western end of the sampling area (67818) did not change the results of the statistical tests noticeably. The results listed in tab.4 are based on a comparison between altered and unaltered pyroclastics.

	SiO_2	TiO_2	Al_2O_3	Fe_2O_3	MnO	MgO	CaO	Na_2O	K_2O	P_2O_5	Nb	Zr	Y	Sr	Rb	Pb	Zn	Cu	Ni	Co	Ba	S
	<-----------------------%----------------------->										<-----------------ppm----------------->											%
Unaltered pyroclastics																						
x	73.79	0.38	14.25	2.42	0.06	0.59	0.33	3.06	3.12	0.05	16	265	34	185	144	15	53	8	4	3.3	1100	0.01
s.e.	0.52	0.02	0.26	0.13	0.01	0.07	0.07	0.18	0.17	0.01	0.4	7	1.7	15	10	3.4	11	1	0.2	0.3	74	0.01
s	3.07	0.11	1.53	0.77	0.07	0.40	0.41	1.06	0.99	0.06	2.6	39	10	89	61	19	60	6	1	2	413	0.04
M	73.79	0.37	14.08	2.31	0.03	0.59	0.17	3.00	3.22	0.03	16	259	33	188	141	9	34	6	4	3.5	1054	0.01
min	68.13	0.20	11.41	1.10	0.01	0.05	0.02	1.08	0.60	0.01	12	199	18	43	26	2	12	2	3	1	314	0.00
max	79.56	0.70	17.40	4.37	0.32	1.28	2.00	6.01	4.48	0.31	21	359	59	381	338	108	316	26	6	11	2307	0.19
n	35	35	35	35	35	35	35	35	35	35	35	35	35	35	35	32	32	32	32	32	31	32
Schists																						
x	74.66	0.27	13.07	3.31	0.17	0.87	2.20	0.31	4.53	0.03	14	217	29	21	215	15	73	8	4	3	1181	0.29
s.e.	0.58	0.02	0.36	0.41	0.06	0.17	0.09	0.07	0.23	0.01	0.7	12	1.4	3.5	11	3	20	1	0.4	0.4	161	0.23
s	2.78	0.09	1.72	1.96	0.31	0.83	0.41	0.35	1.08	0.04	3.3	56	7	17	52	12	86	4	1.5	2	700	1.00
M	74.72	0.27	12.89	2.35	0.07	0.70	0.04	0.15	4.74	0.03	14	236	28	14	208	12	40	6	4	3	953	0.01
min	70.81	0.10	9.28	0.52	0.01	0.05	0.01	0.15	2.73	0.01	8	90	19	3	146	1.7	18	3	2.3	1	539	0.00
max	80.83	0.44	17.1	8.22	1.34	3.96	1.44	1.51	6.23	0.16	19	305	43	56	327	36	393	20	9	7	3513	4.37
n	23	23	23	23	23	23	23	23	23	23	23	23	23	23	23	18	18	18	19	19	19	19
Massive siliceous rocks																						
x	79.28	0.08	12.23	1.41	0.07	0.18	0.19	0.59	3.79	0.04	13	101	33	11	197	23	23	10	5	2	640	0.15
s.e.	1.01	0.01	0.60	0.18	0.03	0.06	0.18	0.27	0.17	0.03	1	5	7	4	19	7	5	5	0.3	0.4	84	0.06
s	3.20	0.04	1.88	0.56	0.11	0.18	0.57	0.85	0.55	0.08	3	17	21	13	59	21	14	14	1	1	251	0.19
M	79.69	0.06	11.43	1.24	0.01	0.07	0.01	0.21	3.47	0.02	13	96	28	3.7	176	15	20	5	4	2	572	0.06
min	74.29	0.02	10.07	0.44	0.01	0.05	0.01	0.15	3.25	0.01	9	79	11	2	152	2	5	3	4	1	426	0.01
max	82.98	0.14	15.25	2.12	0.33	0.58	1.80	2.74	4.87	0.26	18	137	88	40	350	66	50	45	6	4	1272	0.54
n	10	10	10	10	10	10	10	10	10	10	10	10	10	10	10	9	9	9	9	8	9	9
Altered rocks																						
x	76.06	0.21	12.82	2.73	0.14	0.66	0.20	0.39	4.30	0.04	13	181	30	18	210	17	57	8	4	3	1007	0.25
s.e.	0.62	0.02	0.31	0.33	0.05	0.13	0.08	0.10	0.17	0.01	0.6	12	2	3	9	3	14	2	0.3	0.3	121	0.16
s	3.59	0.12	1.78	1.88	0.27	0.77	0.45	0.55	1.00	0.05	3	72	13	16	54	16	74	8	1.4	2	642	0.82
M	75.97	0.24	12.58	2.07	0.06	0.57	0.03	0.15	4.10	0.01	13	187	28	12	193	12	35	6	4	3	765	0.02
min	70.81	0.02	9.28	0.44	0.01	0.05	0.01	0.15	2.73	0.01	8	79	11	2	146	2	5	3	2	1	426	0.00
max	82.98	0.44	17.10	8.22	1.34	3.96	1.80	2.74	6.23	0.26	19	305	88	56	350	66	393	45	9	7.4	3513	4.37
n	33	33	33	33	33	33	33	33	33	33	33	33	33	33	33	27	27	27	28	27	28	28

x = mean
s.e. = standard error
s = standard deviation
M = median
min = minimum value
max = maximum value
n = number of observations

Tab. 3: Statistics of individual rock groups

	SiO_2	TiO_2	Al_2O_3	Fe_2O_3	MnO	MgO	CaO	Na_2O	K_2O	P_2O_5	Nb	Zr	Y	Sr	Rb	Pb	Zn	Cu	Ni	Co	Ba	S
Comparison of unaltered rocks and schists																						
Analysis of variance																						
F	1.21	15.72	7.51	4.27	4.48	1.99	15.94	259.89	26.00	0.19	8.01	15.16	4.51	137.50	21.48	0.24	2.17	0.12	4.23	0.08	0.04	9.47
P	0.28	0.00	0.01	0.04	0.04	0.16	0.00	0.00	0.00	0.66	0.01	0.00	0.04	0.00	0.00	0.62	0.15	0.73	0.05	0.77	0.84	0.00
p	0.64	0.99	0.57	0.00	0.12	0.57	0.07	0.23	0.69	0.41	0.19	0.09	0.13	0.00	0.06	0.13	0.57	0.25	0.98	0.63	0.41	0.03
Wilcoxon's rank sum test																						
W	743	456	507	772	802	750	444	279	934	651	541	480	554	278	946	484	531	477	427	487	470	615
P	0.31	0.00	0.01	0.14	0.05	0.26	0.00	0.00	0.00	0.64	0.03	0.00	0.05	0.00	0.00	0.61	0.15	0.72	0.19	0.88	0.76	0.02
Comparison of unaltered rocks and altered* rocks																						
Analysis of variance																						
F	7.93	35.33	12.75	0.11	1.56	0.07	24.89	244.37	24.01	1.34	12.53	36.15	2.81	199.06	23.93	0.00	0.19	0.03	0.58	1.14	1.81	17.45
P	0.01	0.00	0.00	0.74	0.22	0.79	0.00	0.00	0.00	0.25	0.00	0.00	0.10	0.00	0.00	0.99	0.66	0.87	0.45	0.29	0.18	0.00
p	0.38	0.01	0.39	0.00	0.04	0.61	0.02	0.87	0.97	0.63	0.19	0.00	0.35	0.00	0.04	0.13	0.13	0.79	0.92	0.91	0.34	0.03
Wilcoxon's rank sum test																						
W	1340	741	861	1107	1220	1104	765	581	1459	1042	900	765	967	563	1500	868	802	792	842	744	731	1083
P	0.01	0.00	0.00	0.70	0.31	0.67	0.00	0.00	0.00	0.20	0.00	0.00	0.04	0.00	0.00	0.38	0.90	0.78	0.85	0.31	0.10	0.00
Comparison of unaltered rocks, schist and massisve siliceous rocks																						
Analysis of variance																						
F	13.22	62.66	7.35	9.09	2.99	7.95	14.48	123.57	14.50	1.75	6.65	55.57	1.55	101.00	12.18	0.57	8.04	0.53	4.97	1.91	6.52	9.99
P	0.00	0.00	0.00	0.00	0.06	0.00	0.00	0.00	0.00	0.18	0.00	0.00	0.22	0.00	0.00	0.57	0.00	0.59	0.01	0.16	0.00	0.00
p	0.85	0.64	0.69	0.00	0.18	0.79	0.19	0.07	0.10	0.67	0.38	0.00	0.00	0.00	0.13	0.17	0.50	0.09	0.87	0.82	0.61	0.05
D 0.10	SU		MS		MU	SU		MS		MU,MS	MS		MSU	MS	MS	MSU	SU	MSU	MU	MS,SU	SU	MS
D 0.05					MSU		MS		MU,MS	MSU										MSU		
D 0.01				MU															SU			
norm				SQRT	LOG		LOG	SQRT		LOG				SQRT	SQRT	<--SQRT(LOG)->			SQRT	SQRT	LOG	LOG

altered*: schists and massive siliceous rocks combined
F: F-ratio
W: ranked sum
P: significance level according to F-ratio and ranked sum (W)
p: significance level of groups having equal variances
D 0.01 - D 0.10: significance level in Duncan's multiple range test 1-10 %
M: massive siliceous rocks
S: schists
U: unaltered rocks
eg. SU: schists and unaltered rocks are "equal" at indicated level of significance
norm: transformation of data to a normal distribution by taking the square root (SQRT) and/or the logarithm of 10 (LOG).

Tab. 4: Statistical comparison between rock groups

8.3.1.3.4. Contoured geochemical data.

In the following sub-chapters, a number of alteration haloes are shown for elements which have been affected by hydrothermal fluids. Most of these haloes can be explained in statistical terms as described at the beginning of each discussion. First enriched elements and their haloes are discussed, followed by elements with a depletion halo. The description of the major elements is based on measurements of oxide-%, while ppm are used for trace elements. The statistical results which are referred to are listed in tab.3, 4. Significant depletion or enrichment is based on the 0.01 probability level. The frame of the contour plots is the same as in fig.6a, and the ore-bearing host rock horizon is marked. The co-ordinates, horizontal (E) and vertical (N) are based on the Australian Map Grid (A.M.G.).

8.3.1.3.4.1. Manganese (MnO) (fig.18).

On a two group basis, comparing altered with unaltered rock, Mn does not reveal a significant difference. The analysis of variance comparing schist and unaltered rocks reveals a significant enrichment at the 0.04 level which Duncan's test fails to detect. The enrichment halo of Mn is not very well developed and concentrates on a narrow zone in the footwall.

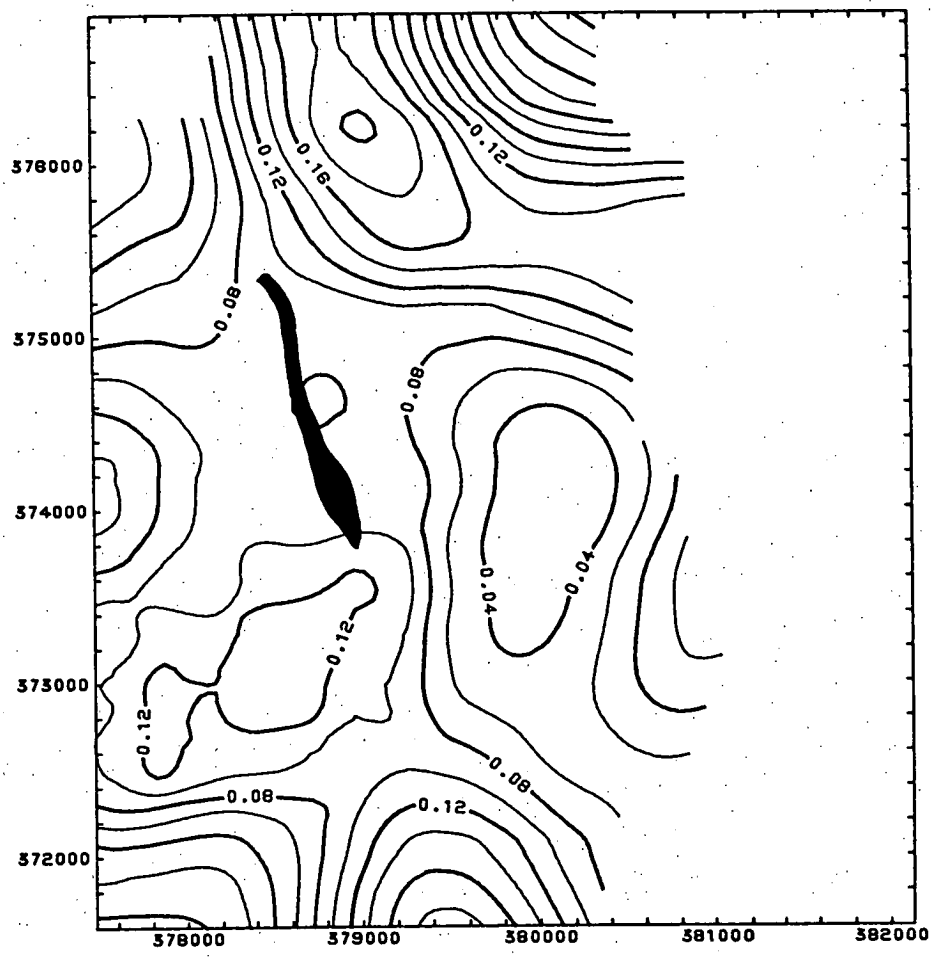

Fig. 18: Smoothed distribution of MnO in %. Host rock marked by shaded area

8.3.1.3.4.2. Potassium (K_2O) (fig.19a, b).

The K content in the altered rocks, comprising schists and massive siliceous rocks, is significantly higher than the amount of K in the unaltered pyroclastics. If considered separately, only the schists are significantly enriched in K. Fig.19b shows the contoured surface without the influence of the massive siliceous rocks.

The K enrichment is due to the generally increased amount of sericite in the alteration zone, and the presence of K-feldspar.

The large variation in the K content of the schists can be partly explained by the occurrence of K-feldspar (chap.6.4.) which causes the bulk content of K_2O to exceed 6%. There are also a few samples with uncharacteristically low quantities of K_2O in the transition zone and in unaltered volcanics close to the schists. These lower values probably affect the grid nodes in the area of the schists. The K halo clearly extends into the hanging wall.

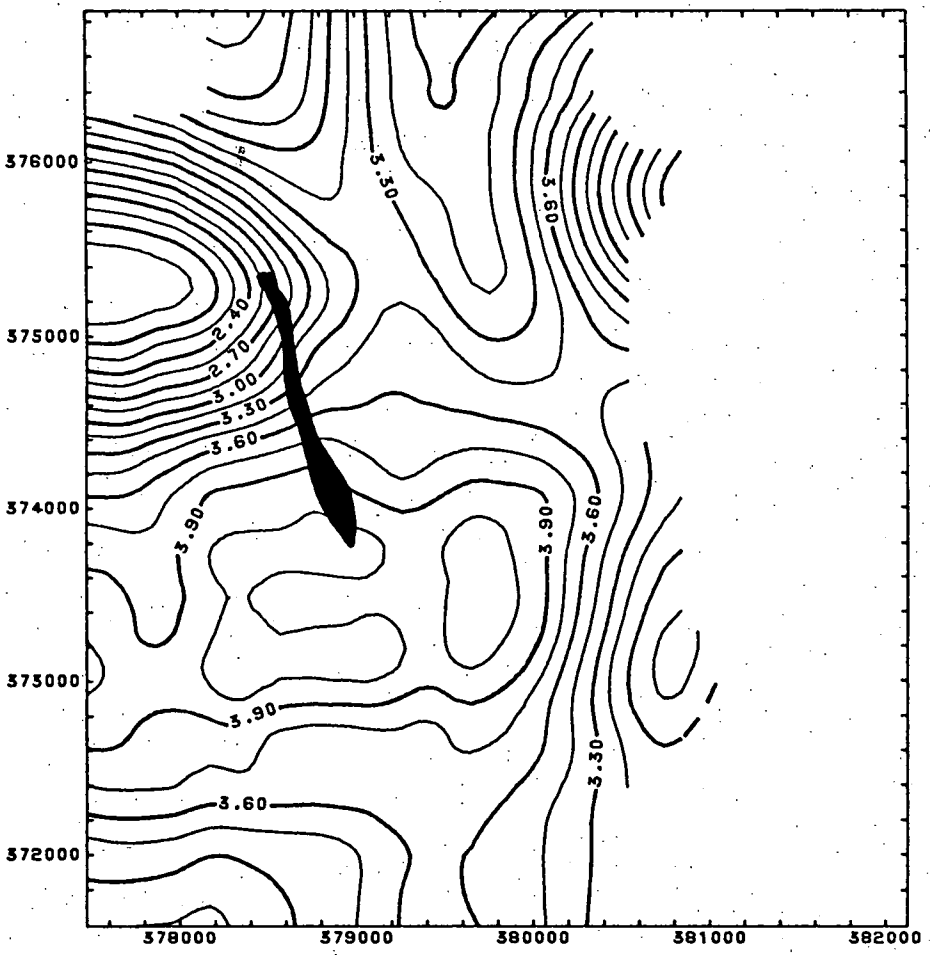

Fig.19a: Smoothed distribution of K_2O in %

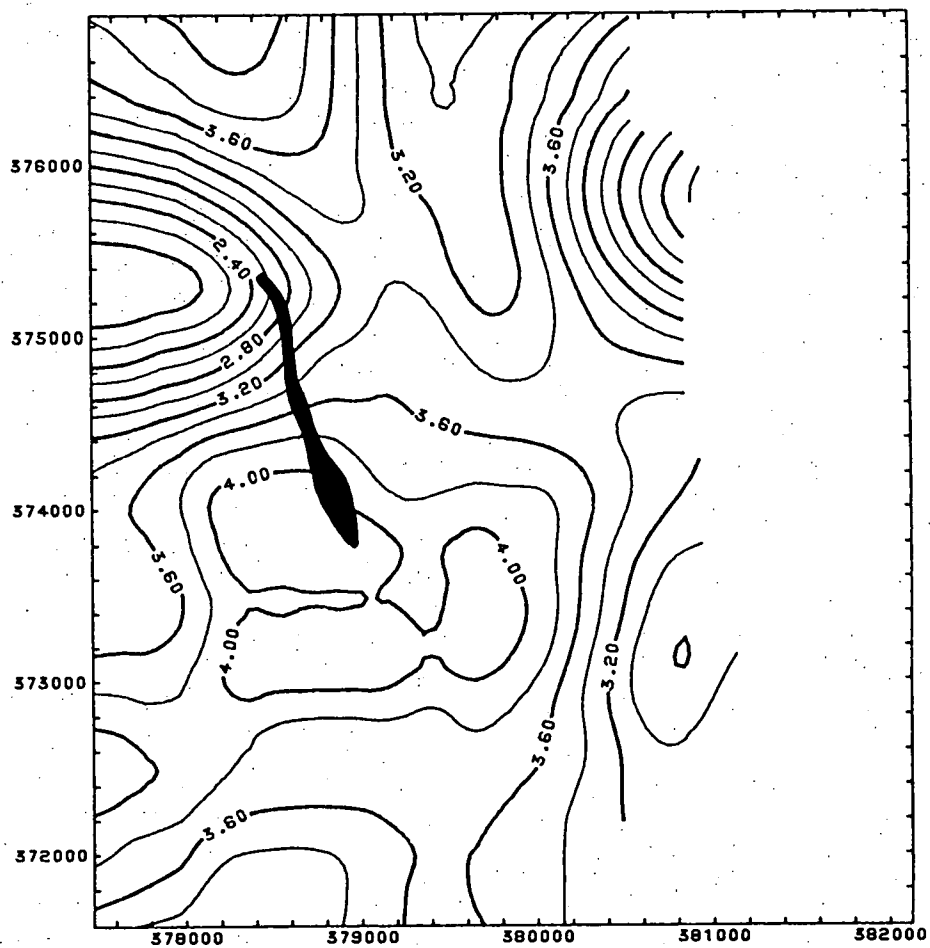

Fig.19b: Smoothed distribution of K_2O in %, massive siliceous rocks are excluded

8.3.1.3.4.3. Silicon (SiO_2) (fig. 20a, b).

The amount of Si is significantly increased in the altered rocks, although there is no difference between the schists and the unaltered volcanics (tab. 3, 4).

The reason for the Si halo extending across the schists into the hanging wall is two-fold. Firstly the average Si content is still slightly higher than that of the unaltered volcanics, especially in the centre of the schists. Secondly, samples from the latter group, in the vicinity of the alteration zone, have unusually high Si contents. Fig. 20b shows the Si halo, without the influence of the massive siliceous rocks.

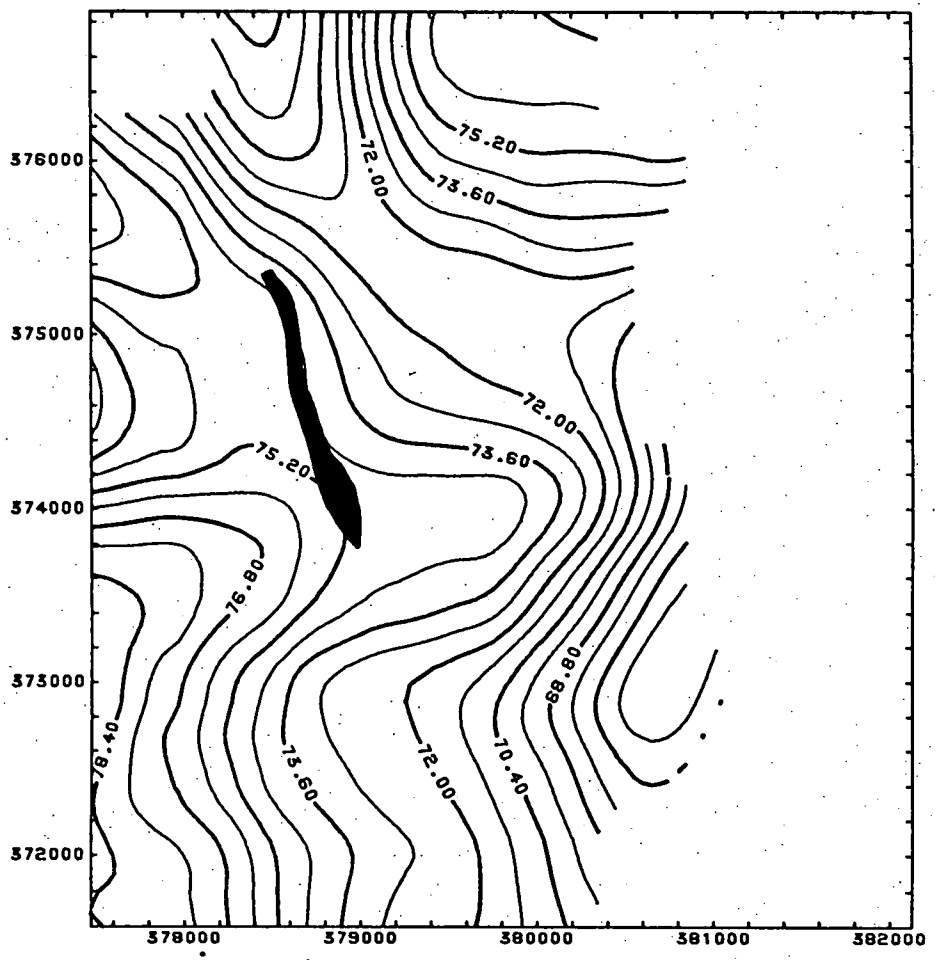

Fig. 20a: Smoothed distribution of SiO_2 in %

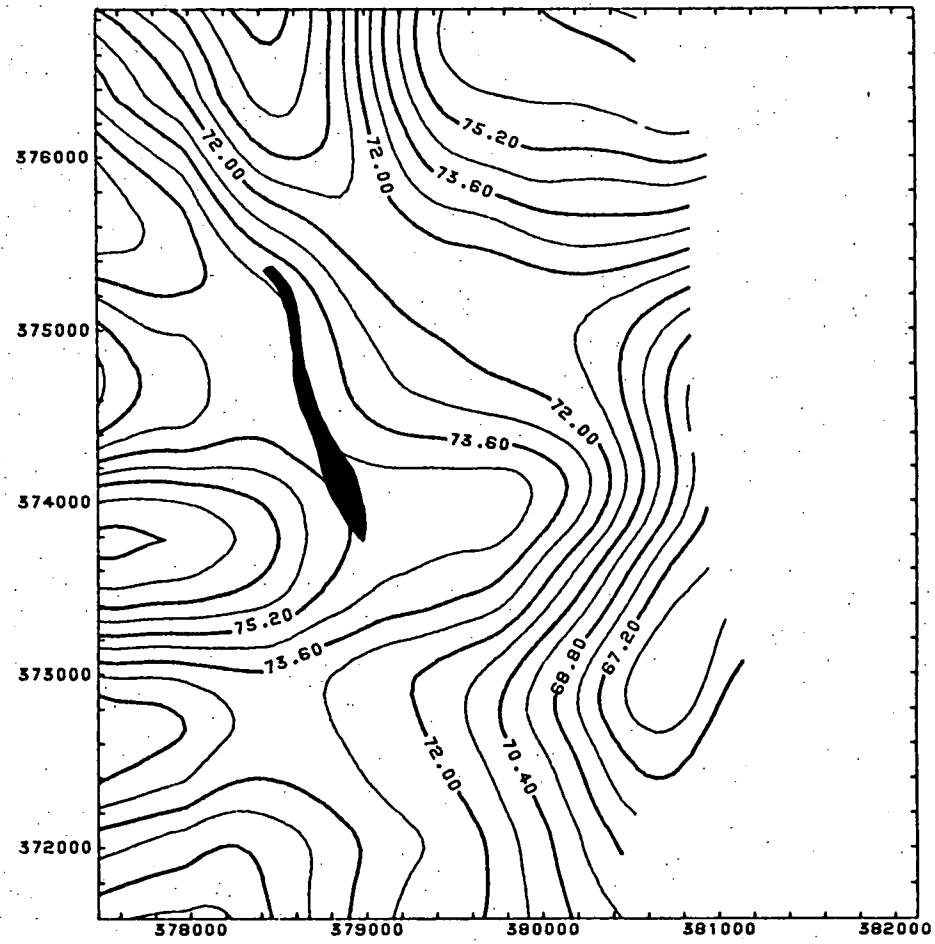

Fig. 20b: Smoothed distribution of SiO_2 in %, massive siliceous rocks are excluded

8.3.1.3.4.4. Rubidium (Rb) (fig.21).

Schists and altered rocks are significantly enriched in Rb including the massive siliceous rocks in contrast to K. Apart from this difference the chemical relationship of the two elements is evident from the similar shape of their alteration haloes.

In the case of Rb one sample (67853) had to be removed from the original data set, because its extreme value distorted a large part of the shape of the alteration.

8.3.1.3.4.5. Lead (Pb) (fig.22).

The enrichment pattern of Pb in the altered rocks cannot be accounted for in statistical terms because of strong variation within groups. The average Pb content is higher in the massive siliceous rocks, although this does not explain the increase of Pb in the central part of this group. A systematic enrichment within the altered rock group could explain this pattern.

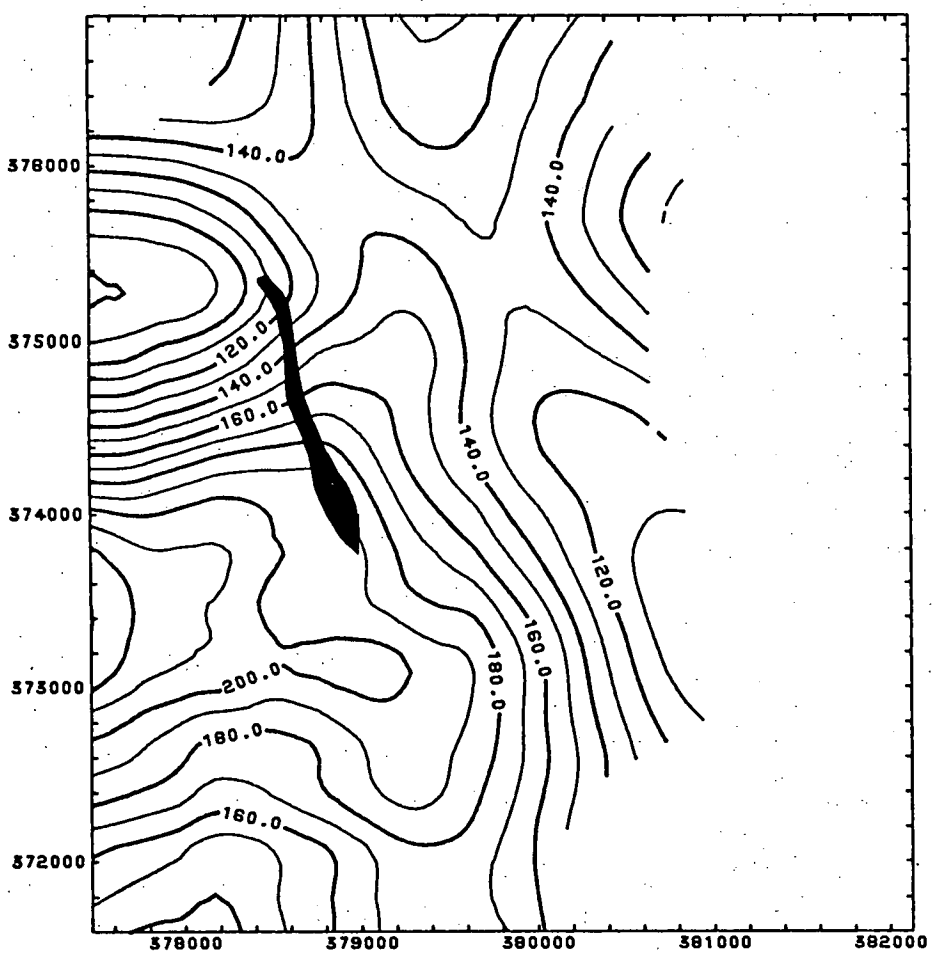

Fig. 21: Smoothed distribution of Rb in ppm

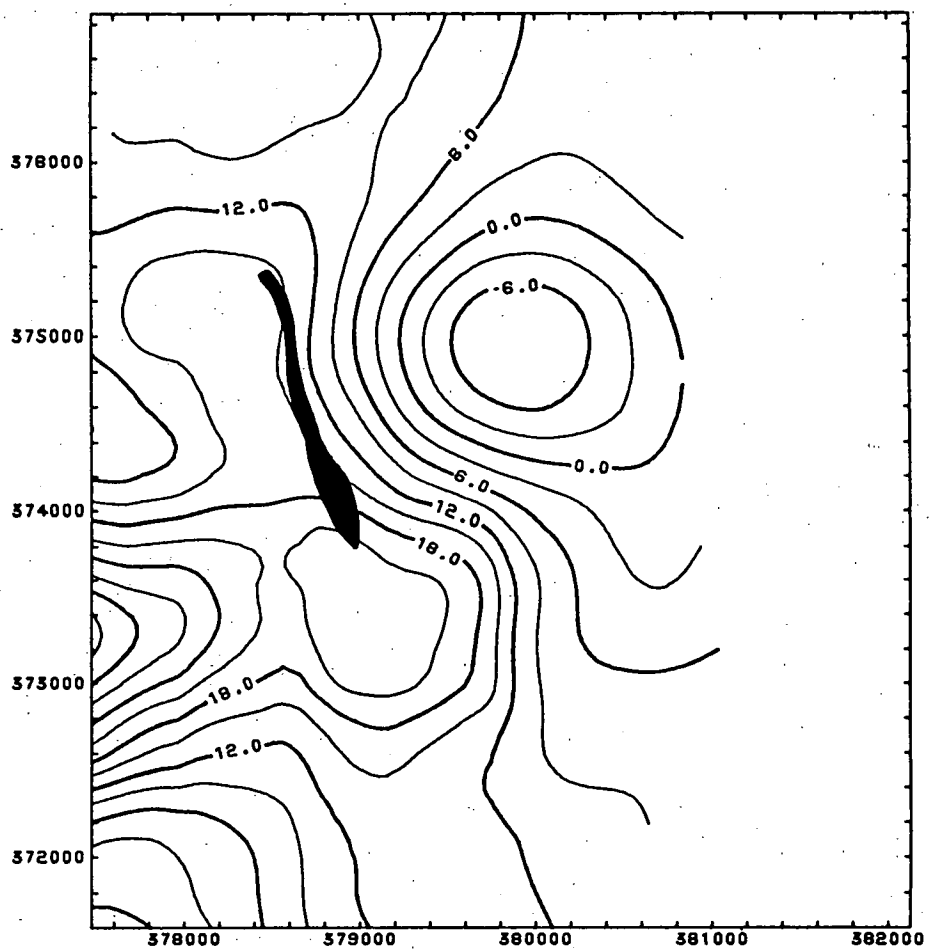

Fig. 22: Smoothed distribution of Pb in ppm

8.3.1.3.4.6. Sulphur (S) (fig.23).

The alteration pattern of S exhibits a significant enrichment in schists and massive siliceous rocks. The S halo relies on a few high values within the alteration zone and remains entirely on the footwall side of the ore horizon.

8.3.1.3.4.7. Titanium (TiO_2) (fig.24).

Statistically there is no agreement among the three rock groups. The amount of Ti decreases from the unaltered volcanics across the schists to the massive siliceous rocks. The alteration halo extends far into the hanging wall, and also reflects the strong depletion in the massive siliceous rocks. The mobility of Ti, a so-called immobile element, will be discussed in chap. 12.2.2.

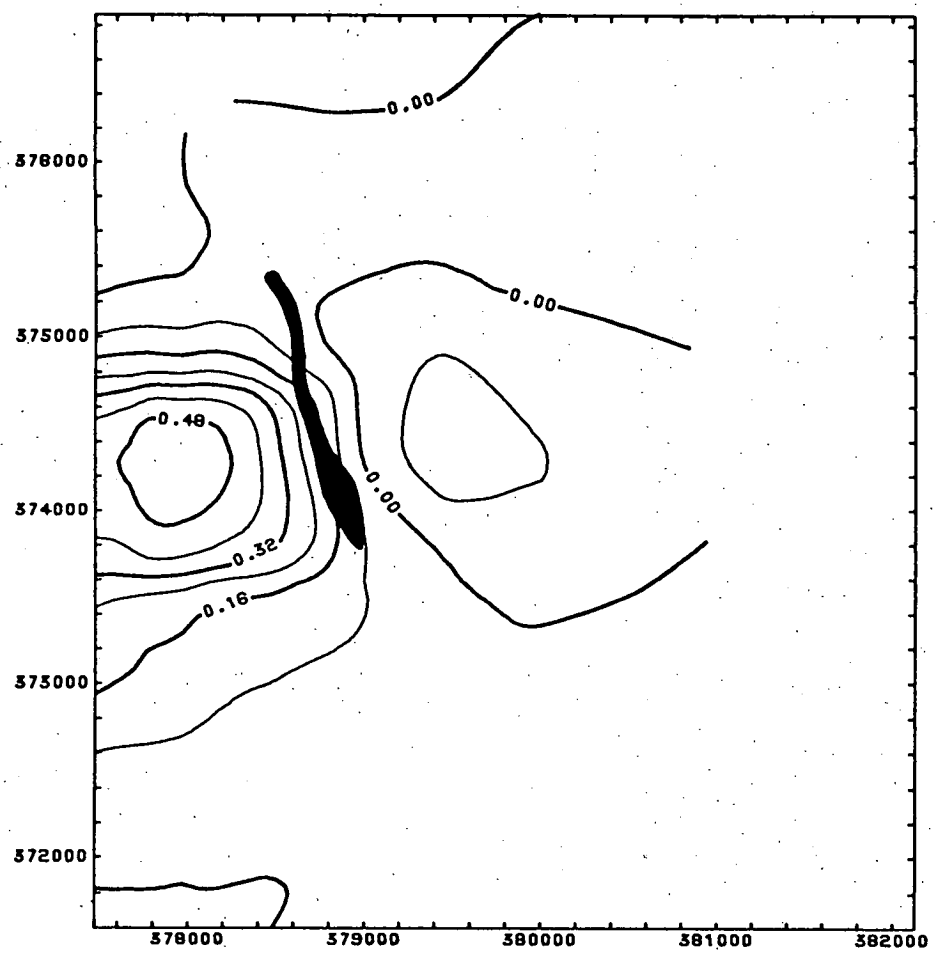

Fig. 23: Smoothed distribution of S in %

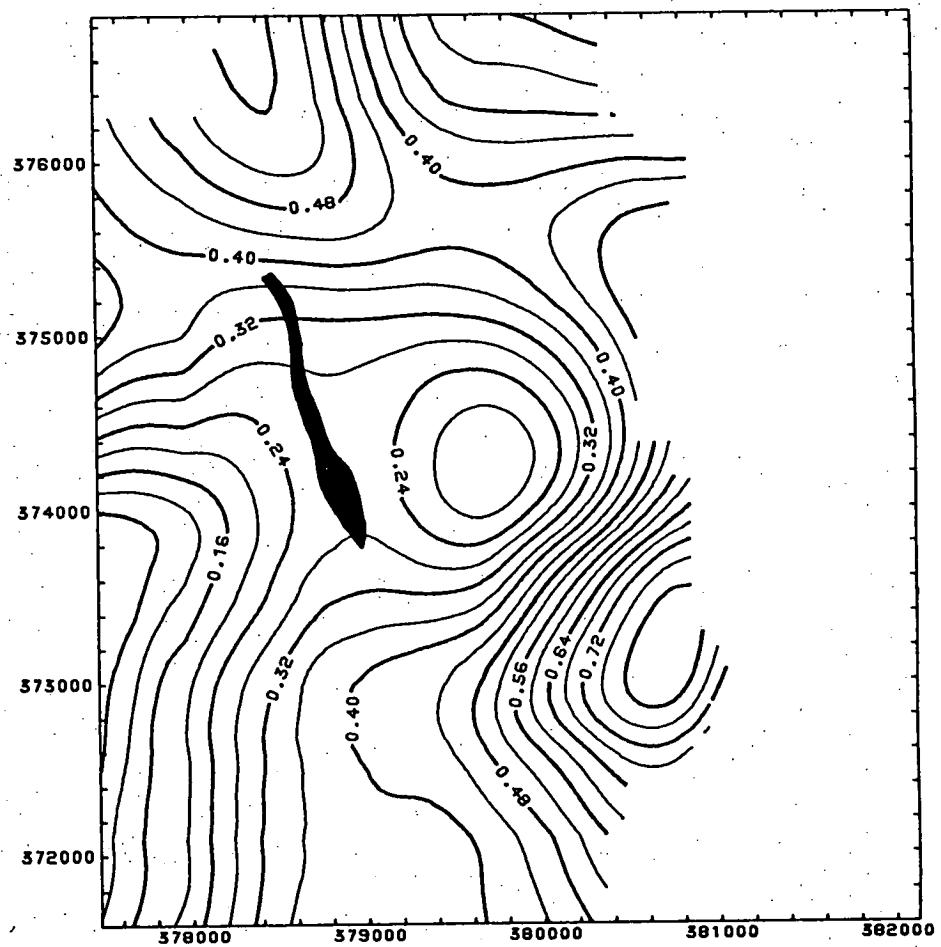

Fig. 24: Smoothed distribution of TiO_2 in %

8.3.1.3.4.8. Aluminium (Al_2O_3) (fig. 25).

The Al content is significantly lower in the altered rocks, and this also applies to both subgroups, schists and massive siliceous rocks.

The shape of the Al-halo is similar to that of Ti and Si (see previous chapter). This could suggest a relationship between the depletion of Al and Ti and conversely the enrichment of Si. The mobilization of elements in real terms is discussed in chap. 12.2.2.

8.3.1.3.4.9. Calcium (CaO) (fig. 26).

A significant decrease exists in the Ca content of the altered rocks, including schist and massive siliceous rocks, due to the removal of plagioclase as the major Ca-bearing phase. This depletion does not reach as far into the hanging wall as for the previously discussed elements.

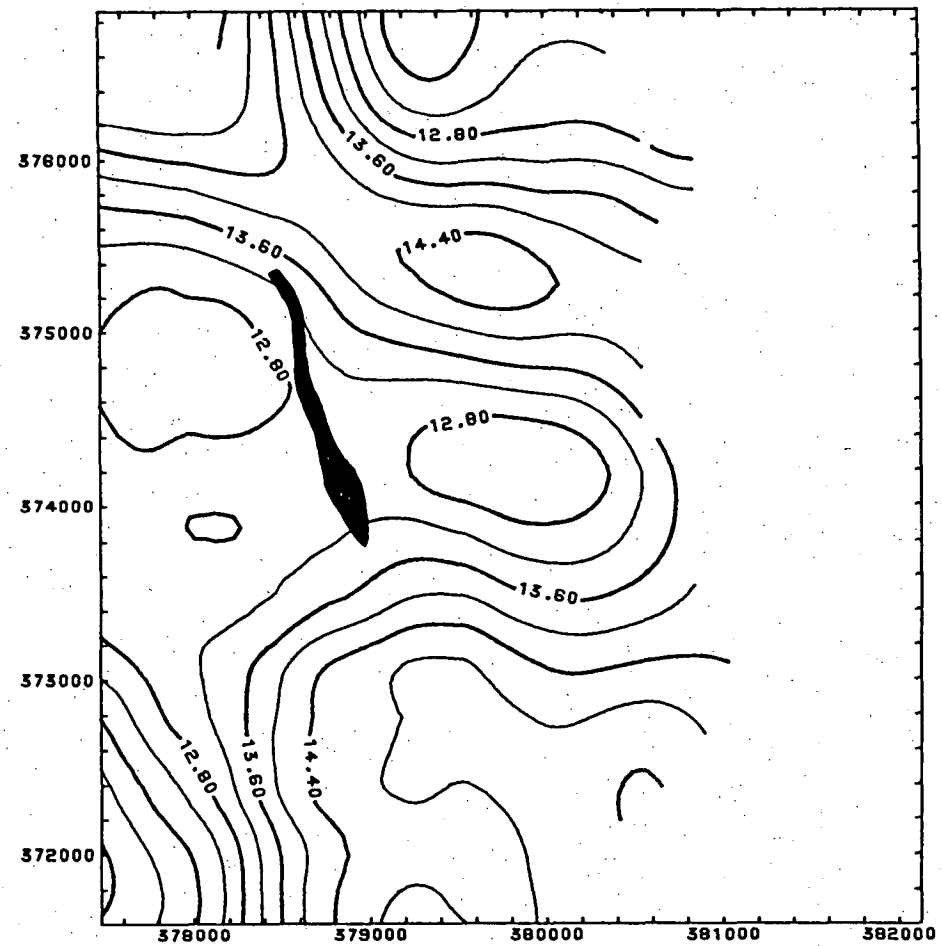

Fig. 25: Smoothed distribution of Al_2O_3 in %

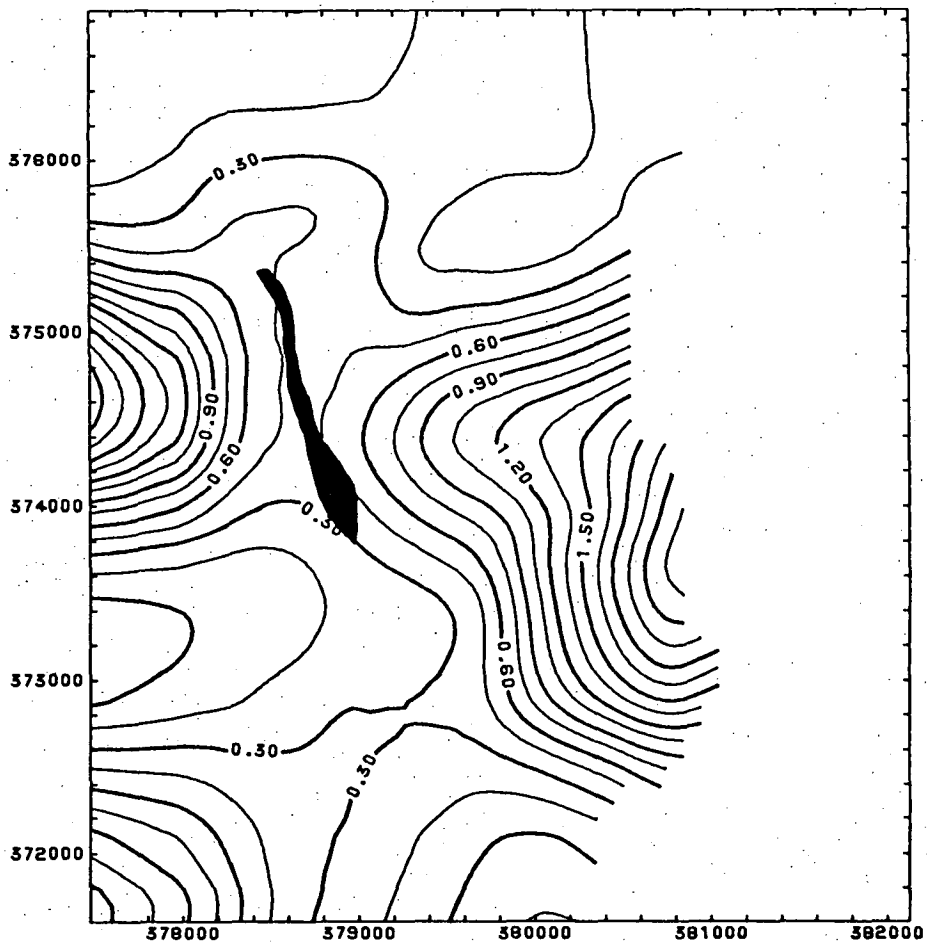

Fig. 26: Smoothed distribution of CaO in %

8.3.1.3.4.10. Strontium (Sr) (fig.27).

The alteration pattern for Sr is statistically more pronounced than that of Ca. The depletion halo reflects the close chemical relationship between the two elements.

8.3.1.3.4.11. Yttrium (Y) (fig.28).

The Y content exhibits a pattern of minor depletion. This halo is not strongly supported by the statistical tests. Their use is limited in this case by the large background variation. It can only be assumed that a systematic trend exists within the altered rocks.

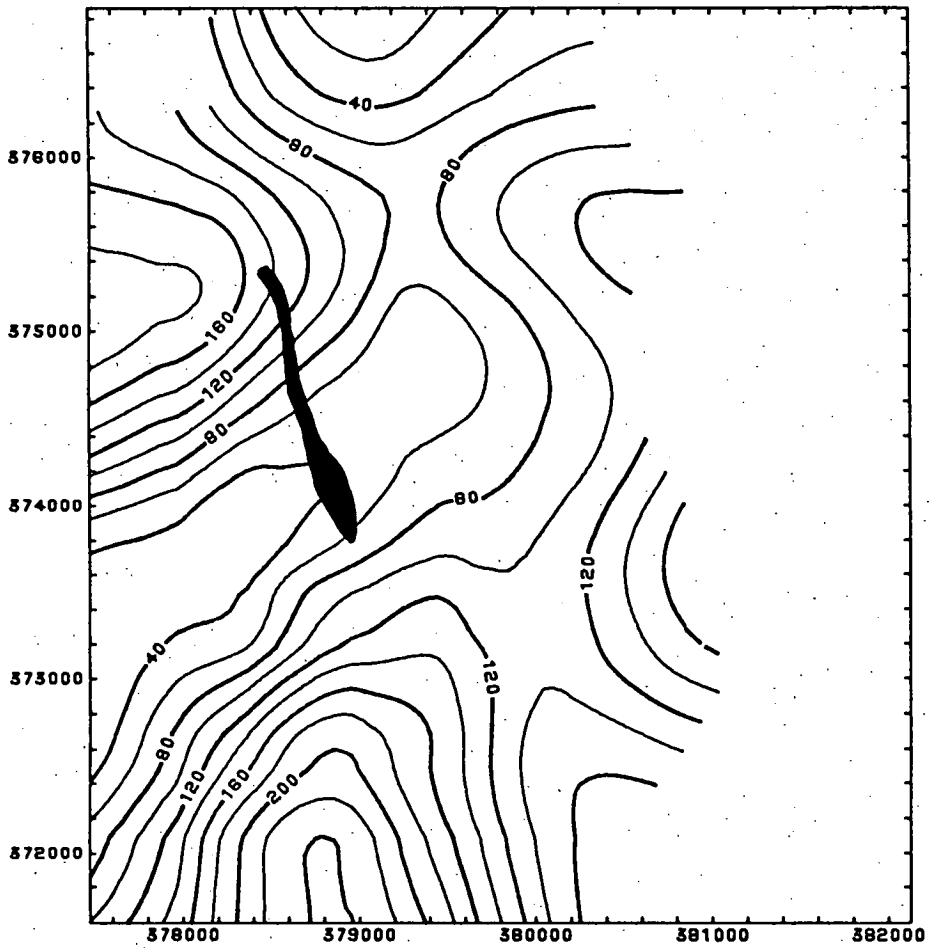

Fig.27: Smoothed distribution of Sr in ppm

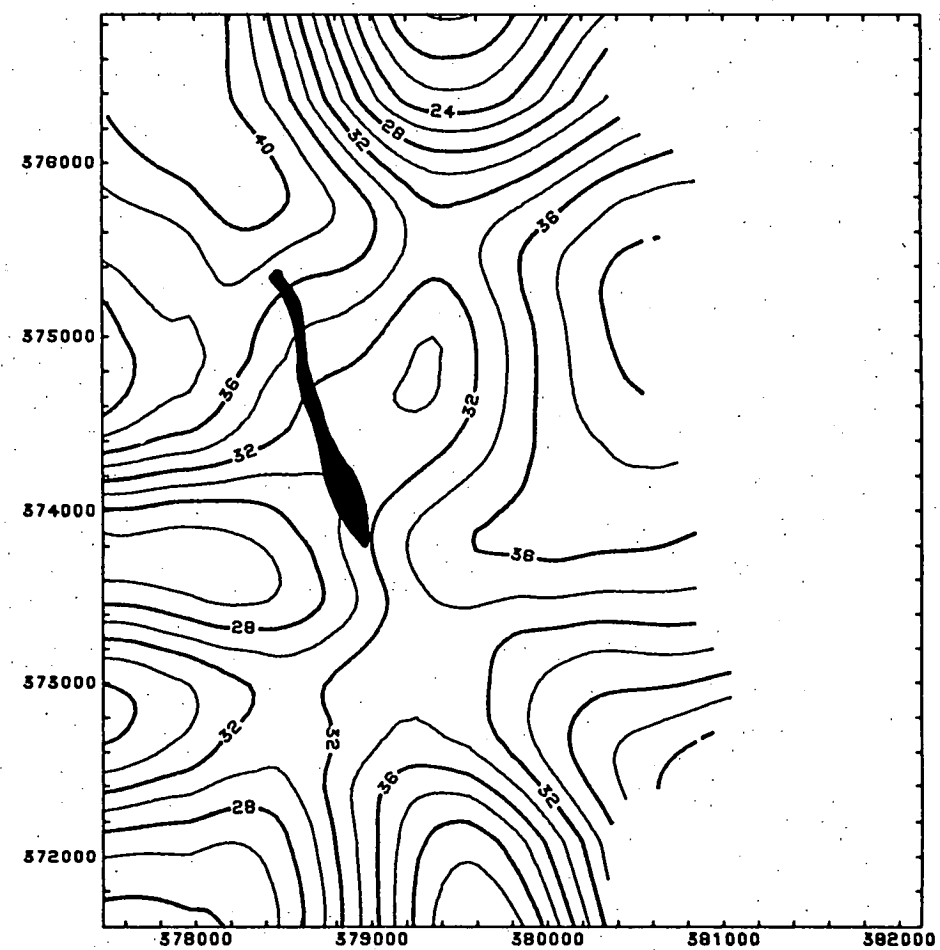

Fig.28: Smoothed distribution of Y in ppm

8.3.1.3.4.12. Niobium (Nb) (fig. 29).

Nb like Y exhibits a weakly depleted alteration halo. The decrease of the Nb content on both a two group and a three group basis is however statistically significant.

The halo is entirely confined to the footwall of the ore horizon.

8.3.1.3.4.13. Zirconium (Zr) (fig. 30).

Zr is the only element apart from Ti that shows a significant difference among all three rock groups. As for Ti, the depletion proceeds from unaltered volcanics across the schists to the massive siliceous rocks.

The implications of the removal of Zr and its host mineral, zircon, on the hydrothermal element exchange will be discussed in chap. 12.

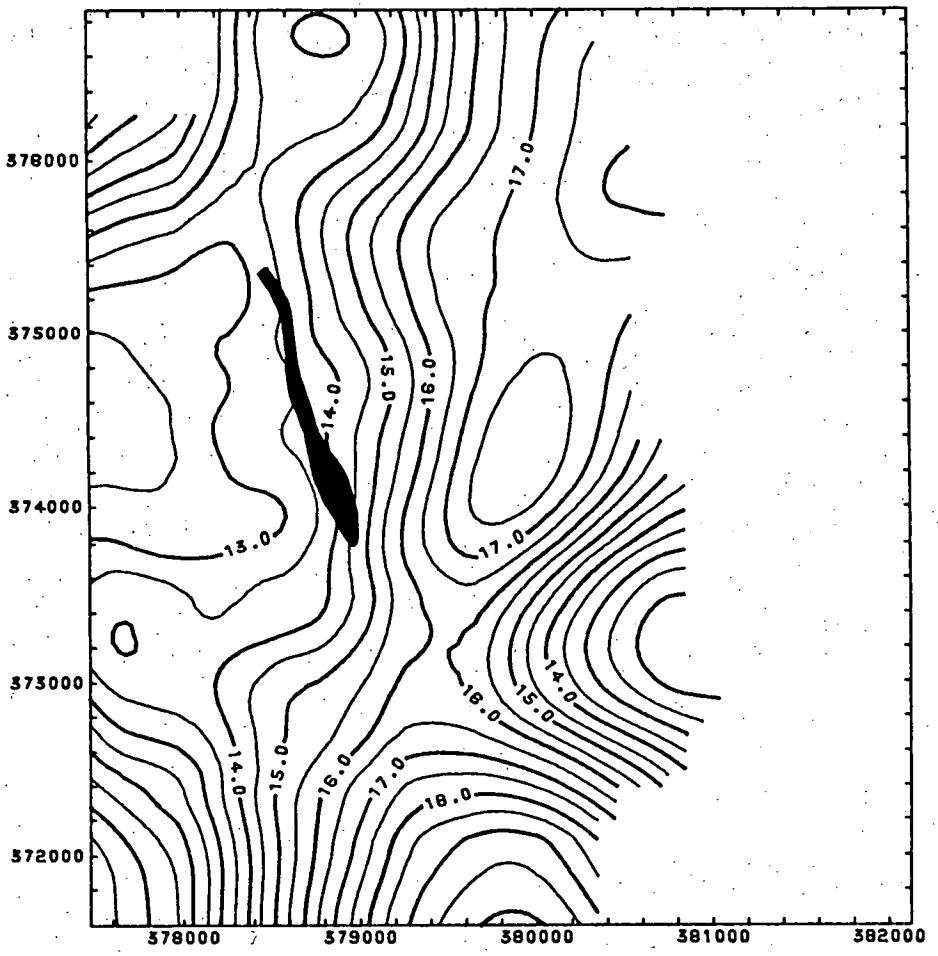

Fig. 29: Smoothed distribution of Nb in ppm

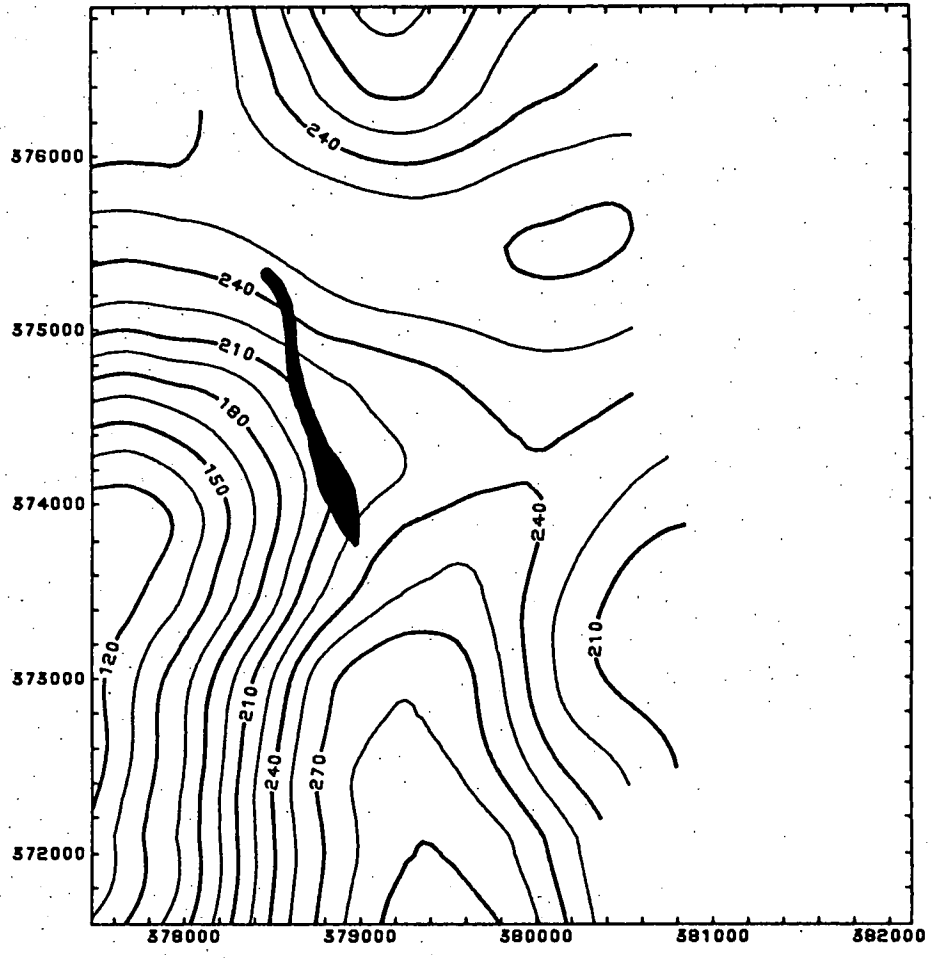

Fig. 30: Smoothed distribution of Zr in ppm

8.3.1.3.4.14. Sodium (Na_2O) (fig.31a-e).

Albite, and therefore sodium, is completely removed from the altered rocks. The smoothed Na_2O halo (fig.31c) follows closely the outline of the petrographic alteration and extends into the hanging wall as well. It is statistically supported by a significant depletion in both schists and massive siliceous rocks.

Na is the third test case of the influence of the massive siliceous rocks on the general shape of the alteration halo. The result can be seen in fig.31d. Fig.31a shows the distribution of the raw data. Fig.31b represents the original contoured halo prior to smoothing, and the contour plot in fig.31e is the result of a trend surface analysis based on the smoothed gridded data for performing the regression analysis.

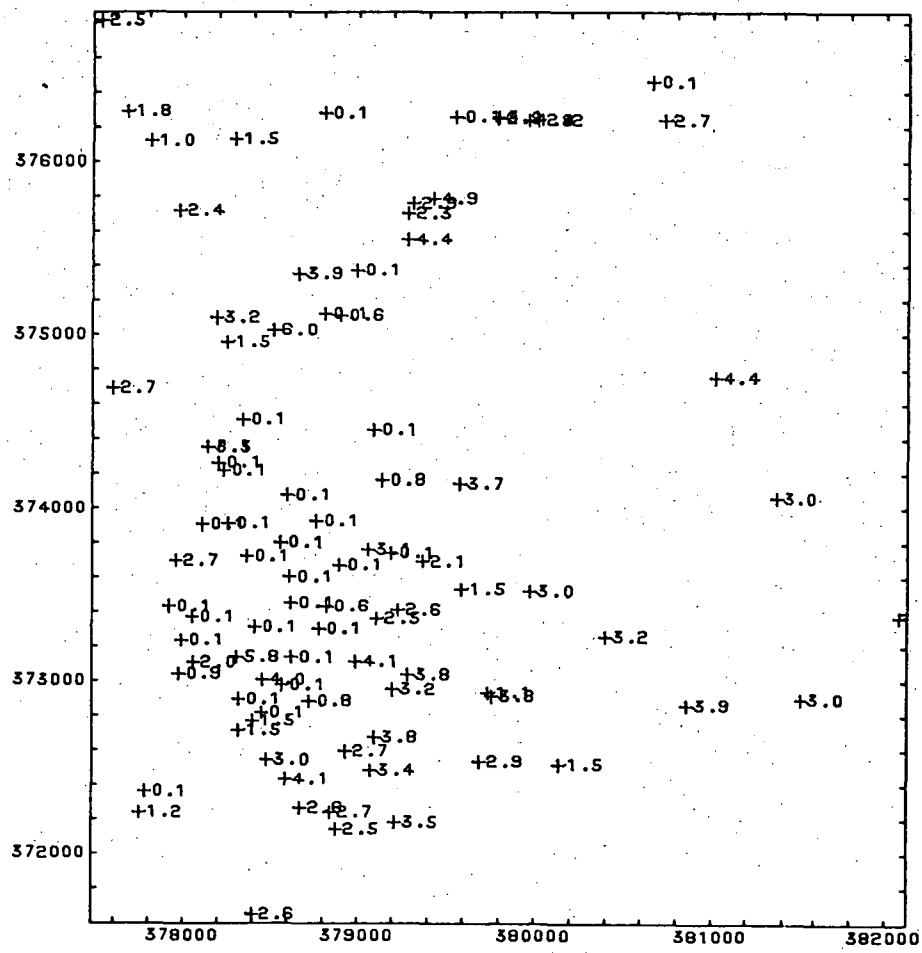

Fig.31a: Distribution of raw data for Na_2O in %

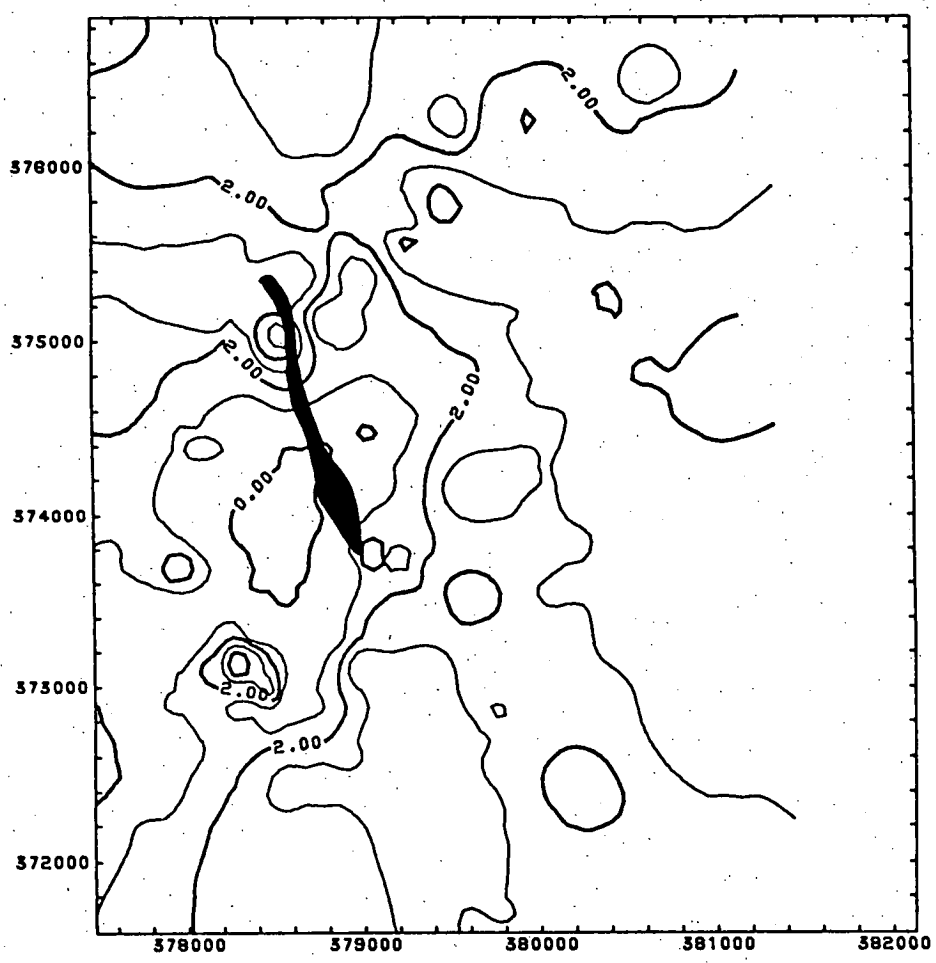

Fig. 31b: Unsmoothed distribution of Na_2O in %

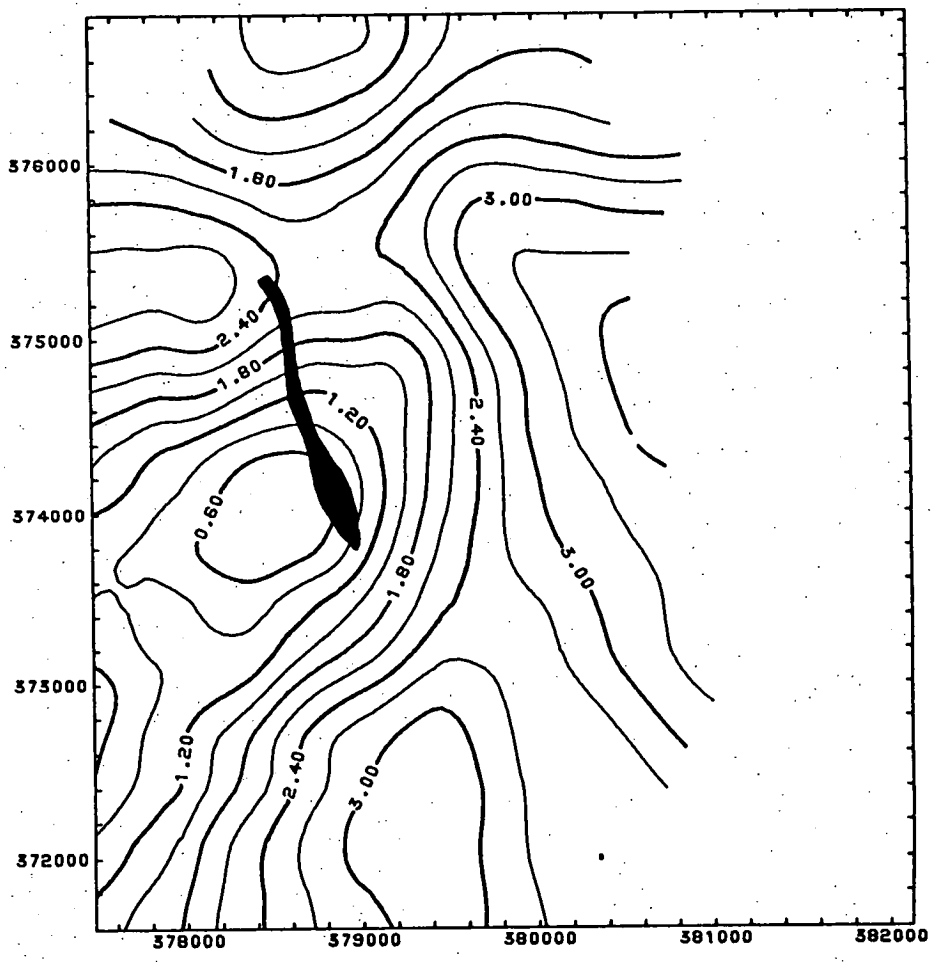

Fig. 31c: Smoothed distribution of Na_2O in %

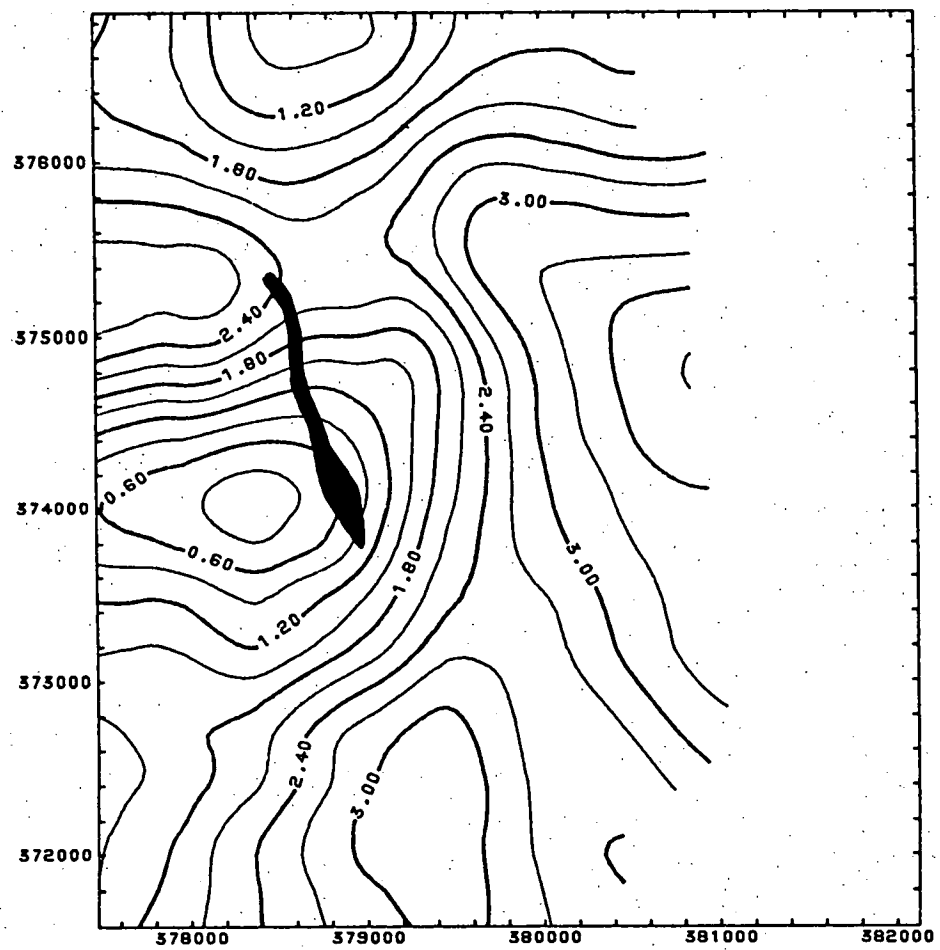

Fig. 31d: Smoothed distribution of Na_2O in %, massive siliceous rocks are excluded

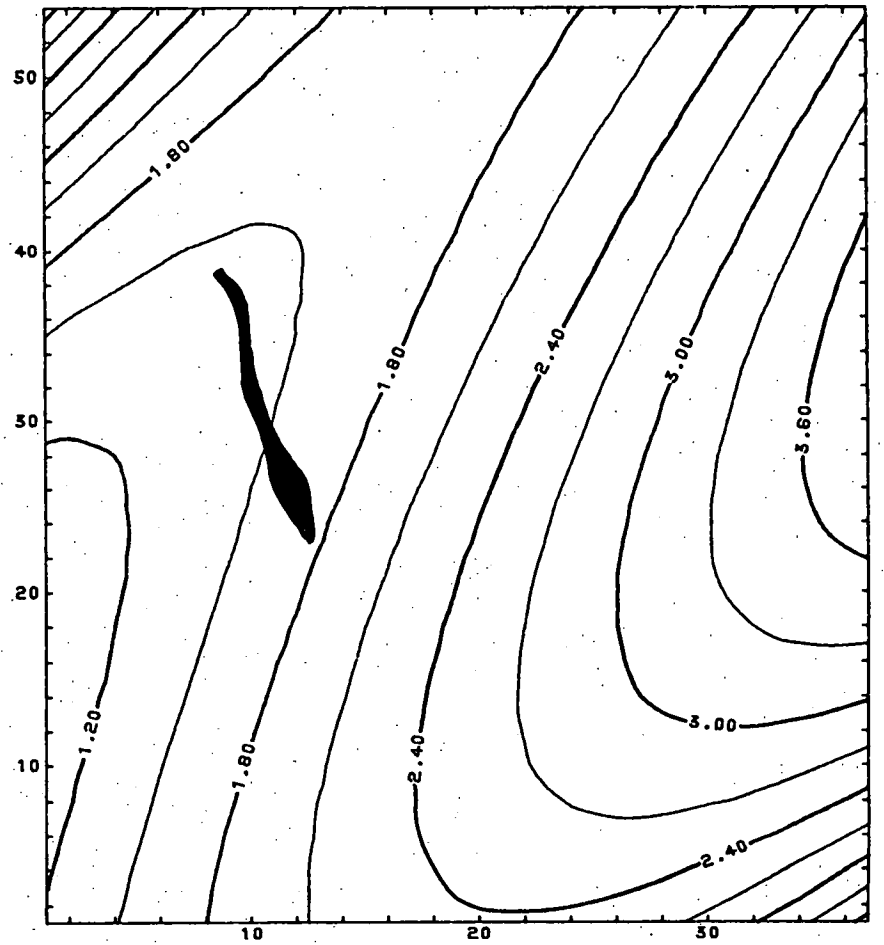

Fig. 31e: Distribution of Na_2O based on trend surface analysis. Coordinates are expressed in rows (horizontal) and columns (vertical) of the grid matrix

8.3.1.3.4.15. Summary.

The study of the geochemical distribution patterns revealed four different cases:

a. The most coherent patterns of depletion or enrichment exist for those elements with statistically significant differences at the 0.01 level between the altered groups comprising schists and massive siliceous rocks, and the group of unaltered pyroclastics.

b. Conversely, there are haloes which cannot be explained in statistical terms, because considerable variation occurs within groups and this variation is apparently directed towards the centre of the hydrothermal alteration.

c. A third class of elements including Fe (Fe_2O_3), Co, Ni and P (P_2O_5) exists with unexplained geochemical patterns which are presumably influenced by the different state of fractionation in the unaltered volcanics. The Mt. Black Volcanics include intermediate rocks which give rise to higher concentrations in the above mentioned elements, and thus create a relative depletion in the western part of the sampled area.

d. The elements of the fourth class - Mg (MgO), Zn, and Cu are neither statistically different, nor do they develop a systematic distribution pattern. The only exception is Ba with a depletion halo which is confined to the massive siliceous rocks.

Attempts at contouring element ratios, e.g. K/Na and K/Rb ratios (van Moort, 1982) and modified alteration indices by Ishikawa et al. (1976) and Saeki & Date (1980), did not improve or enlarge the alteration halo. Date et al. (1979) noted that these alteration indices mostly rely on the Na_2O content. Generally, the chemical haloes appear to be larger than the alteration zone outlined by geological criteria. This is largely caused by the higher sample density in the altered rocks, which influences the gridding process, and thus creates a slightly biased zonation.

8.3.2. Multivariate alteration geochemistry.

None of the elements discussed in the previous chapter, including Na, the best discriminator, provide a complete separation between altered and unaltered rocks. To improve the two-way classification, multivariate statistical methods were employed. Based on an array of properties for each observation they should overcome spurious larger univariate deviations. The most common multivariate procedures are cluster analysis and discriminant analysis. The second method is better suited to improve discrimination among groups, as will be discussed below, and has been applied in some cases for geochemical purposes (Govett, 1972; Marcotte & David, 1981; Fedikow & Turek, 1983 and Amor & Nichol, 1983). Van den Boom et al. (1980) used a method called PATREC1 which is related to a non-parametric discriminant analysis. The importance of the cluster analysis lies more at the starting level of the alteration study by providing a broad basis for a geochemical classification.

Both methods are discussed here together separated from the trend surface analysis, because the independent variables are "real" geochemical data rather than geographical co-ordinates.

Cluster analysis and discriminate analysis have a fundamentally different approach. The classification of the first method is internally based, and relies on natural clusters inherent in the properties of the observations to be studied. The results of the cluster analysis are presented as a dendrogram with the most similar observations linked together at a low level of heterogeneity (fig. 32a, b). The second method requires a prior knowledge about the grouping of already existing observations (Davis, 1973). The resulting discriminant function serves to allocate new observations and those already grouped, to clusters, forming univariate sample distributions which are separated by a maximum distance (fig. 33). The theoretical background of both multivariate methods is discussed below in more detail.

The trace elements Pb, Zn, Cu, Ni, Co and Ba were excluded from multivariate analysis due to poor discriminatory power as well as S which lacked a broadly based enrichment within the alteration area.

8.3.2.1. Cluster analysis.

8.3.2.1.1. Theory.

Cluster analysis as described by Tatsuoka (1974) and Massart & Kaufmann (1983) is based on measures of similarity. The most common measure of similarity between observation l and m is the Euclidian distance

$$D = (\sum_{j=1}^{n}(x_{lj} - x_{mj})^2)^{1/2}$$

with j dimensions of chemical variables. The observations are subsequently linked to form larger clusters, depending on their similarity or distances apart. Several rules have been developed to determine the criteria which select the clusters to be merged, including single observations. They are discussed by Massart & Kaufmann (1983). This method of forming clusters with an increasing number of observations is called an agglomerative hierarchical procedure. Ward's method, which was used in this study, belongs to this general type, but derives its criteria for linking clusters only after this process has been completed. This method is recommended by program CLUSTAN (Wishart, 1978) for small samples.

Ward's method, also named error sum of squares method for its analogy to analysis of variance (chap.8.3.1.1.1.), calculates the heterogeneity of each cluster

$$E_k = \sum_{j=1}^{n}\sum_{i=1}^{m}(y_{ijk} - \bar{y}_{\cdot jk})^2$$

by calculating the sum of the squared distance $_k$ for each new cluster k with m observations, n variables and the centroid $\bar{y}_{\cdot jk}$.

Only those clusters that provide a minimum increase in heterogeneity are merged:

$$E_{(p,q)} = E_p - E_q \text{ is minimum.}$$

8.3.2.1.2. Results.

The procedure for small samples (n < 150) was pursued in program CLUSTAN (Wishart, 1978). Standardized data were used to compensate for different scales of major (oxide %) and trace elements (ppm). The first cluster pattern proved to be stable during two subsequent relocation runs. The error sum of squares can thus be reduced by reassessing the probability of each observation belonging to a certain cluster, and relocating the observation if a higher probability towards another cluster can be found. The non-hierarchical clustering method based on density, also included in the recommended procedure (Wishart, 1978) turned out to be inferior to Ward's method.

A reasonable separation into two main clusters, altered rocks and unaltered, based on the chemical variables is provided at a high level of heterogeneity (fig. 32a). Several observations can be regarded as misclassified from a geological view point. To be precise, four observations (67810, 67812, 67866 and 67868) are in the altered group, and two more observations (67824 and 67828) lie in the unaltered group but are closely associated at a low level of heterogeneity with misclassified altered rocks. Among these observations are volcanics with macroscopically primary textures, collected immediately above the host rock horizon and also up to 2 km into the hanging wall. This has already been discussed in chap. 8.3.1.3.1. It has also been pointed out that the way the observations are clustered at a low level of heterogeneity does not suggest a bias in sampling. In addition the more basic volcanics from different locations are closely linked together. This is also the case for most of the massive siliceous rocks.

The number of misclassifications was marginally reduced (fig. 32b) by converting the distribution of all variables to normal. This also helps to compare the results of the cluster analysis to those of the discriminant analysis where normal distribution is a prerequisite. In this case the massive siliceous rocks were separated into two subclusters at opposite ends, and also a new observation (67853) which has no connection to the alteration was introduced into the altered group. On the whole the second cluster analysis is not considered an improvement over the original one.

In order to avoid misclassification by correlated variables, a principal component analysis was performed prior to classification in a

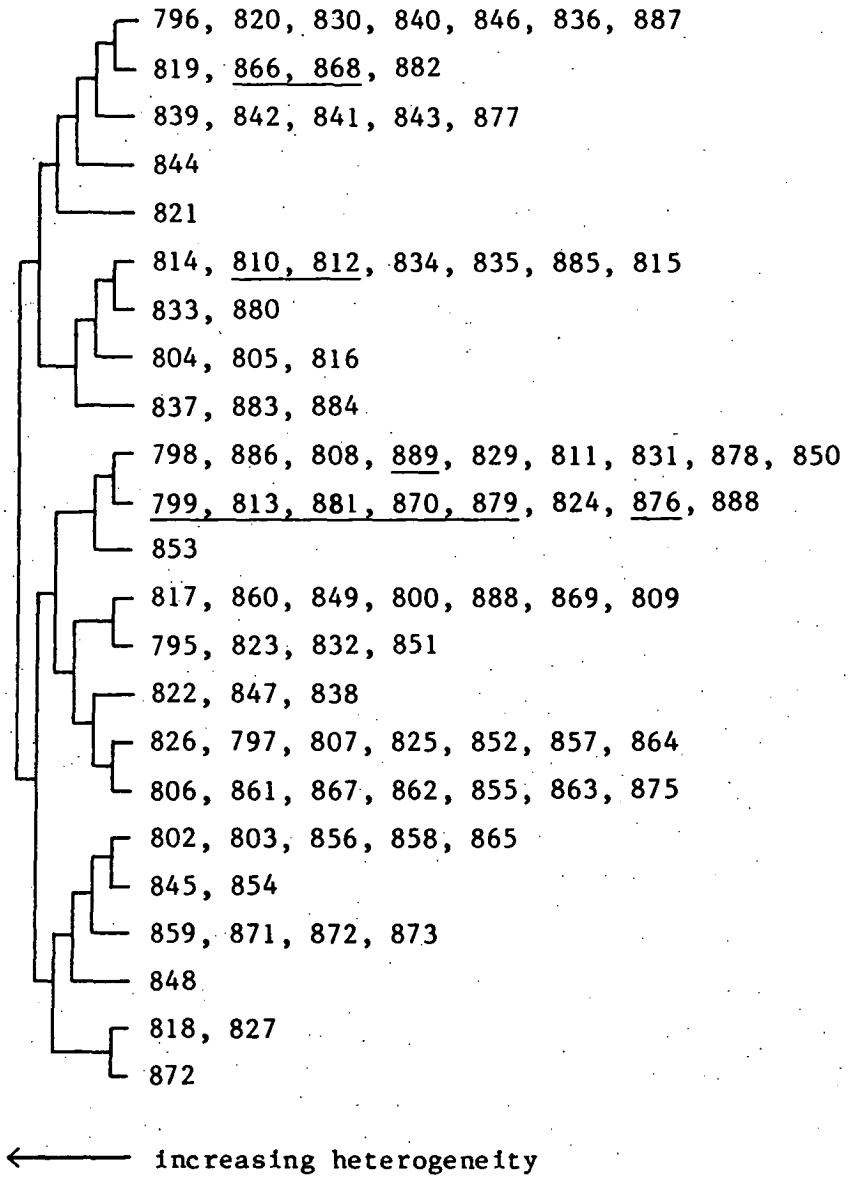

- catalog sample number is found by adding 67000

Fig. 32a: Cluster analysis: dendrogram based on normalized data, observations are combined to clusters below heterogeneity coefficient = 1.0, underlined observations are misclassified from a geological viewpoint

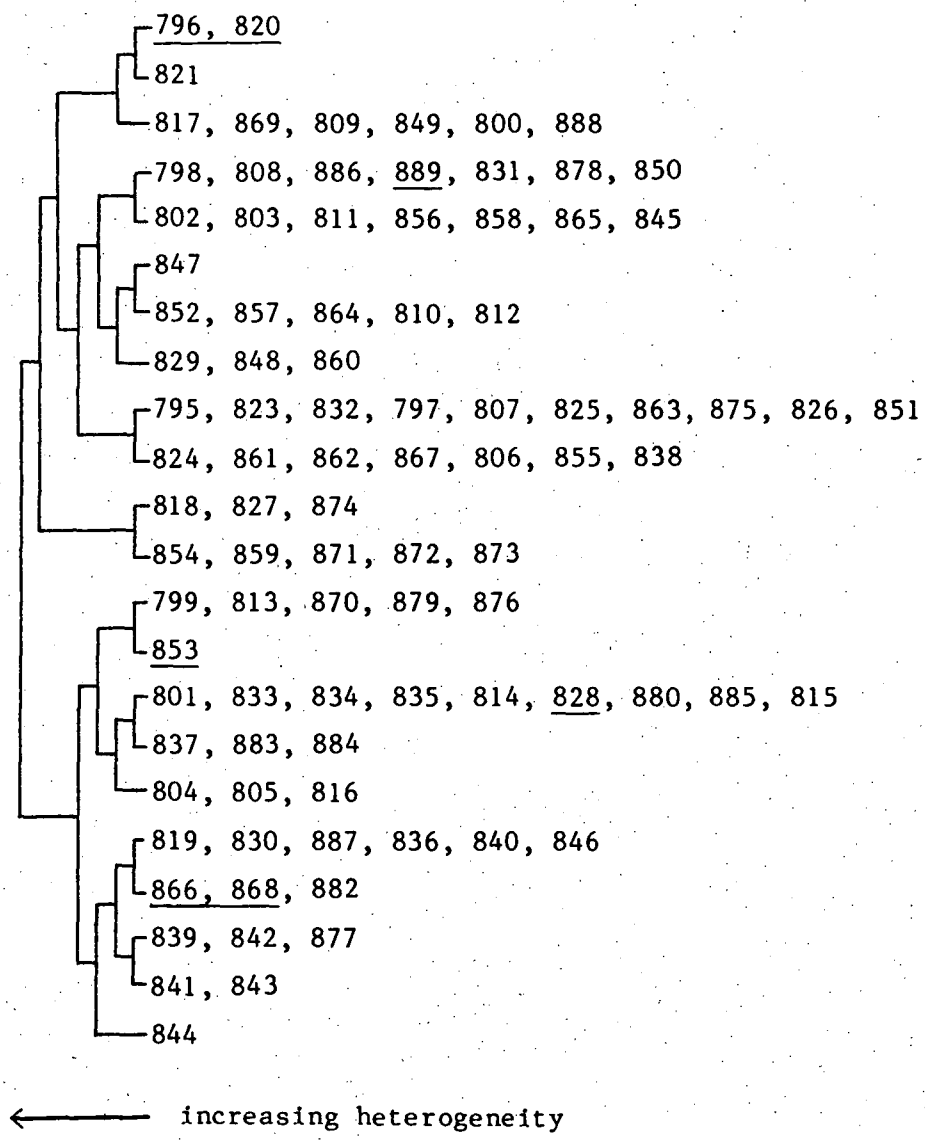

- catalog sample number is found by adding 67000

Fig. 32b: Cluster analysis: dendrogram based on normalized data with normal distribution, observations are combined to clusters below heterogeneity coefficient = 1.5, underlined observations are misclassified from a geological viewpoint

second trial. Massart & Kaufmann(1983) demonstrated a distortion of similarities by introducing an additional dimension which was linearly dependent on the original set.

Principal component analysis transforms a set of correlated variables into a new set of uncorrelated variables, the principal components. These are a linear combination of the original variables, and are computed by way of maximization as the eigen-vectors of the covariance matrix similar to discriminant analysis (see next chapter). The original variation is now explained by the length (or eigen-values) of the eigen-vectors (Chatfield & Collins, 1980).

The sizes of the first three principal components were used for classification instead of the standardized original variables. Clustering was slightly different at a low level of heterogeneity. The overall grouping into two clusters however did not improve at all. This can be explained by looking at the eigen-values, and the percentage of their contribution to the variation of the original data (tab. 5).

	Original Data		Normalised Data	
Component	Eigen Value	Cumulative Variance	Eigen Value	Cumulative Variance
1	4.53	30.20	5.05	33.67
2	2.82	48.97	2.80	52.32
3	2.32	64.41	2.30	67.63
4	1.14	72.00	1.02	74.46
5	0.93	78.17	0.80	79.97
6	0.72	82.98	0.65	84.12
7	0.63	87.19	0.61	88.21
8	0.50	90.50	0.50	91.52
9	0.40	93.13	0.40	94.20
10	0.35	95.48	0.34	96.46
11	0.28	97.38	0.20	97.77
12	0.15	98.40	0.13	98.63
13	0.14	99.31	0.10	99.30
14	0.09	99.94	0.08	99.82
15	0.01	100.00	0.03	100.00

Tab. 5: Eigen-values of Principal Component Analysis

Original Data

	Si	Ti	Al	Fe	Mn	Mg	Ca	Na	K	P	Nb	Zr	Y	Sr
Si														
Ti	-0.8													
Al	-0.7	0.5												
Fe	-0.7	0.5	0.1											
Mn	-0.1	0.1	-0.1	0.2										
Mg	-0.6	0.5	0.2	0.5	0.0									
Ca	-0.5	0.4	0.1	0.3	0.1	0.5								
Na	-0.4	0.4	0.3	0.0	-0.2	0.0	0.3							
K	0.1	-0.2	0.2	-0.1	0.2	-0.2	-0.4	-0.6						
P	-0.4	0.6	0.2	0.3	0.1	0.2	0.3	0.2	-0.2					
Nb	0.0	0.0	0.5	-0.3	-0.2	-0.3	-0.3	0.2	0.3	-0.1				
Zr	-0.4	0.5	0.7	0.1	-0.1	0.1	0.1	0.4	0.2	0.0	0.6			
Y	-0.2	0.2	0.3	0.0	0.0	0.0	0.2	0.1	0.0	0.3	0.3	0.2		
Sr	-0.3	0.4	0.3	0.0	-0.1	0.2	0.4	0.8	-0.5	0.2	0.0	0.4	0.1	
Rb	0.0	-0.1	0.3	-0.1	0.1	-0.1	-0.3	-0.4	0.7	-0.1	0.2	0.1	0.0	-0.4

Normalized data

Si														
Ti	-0.8													
Al	-0.7	0.6												
Fe	-0.7	0.6	0.2											
Mn	-0.4	0.3	0.0	0.4										
Mg	-0.5	0.5	0.3	0.4	0.2									
Ca	-0.5	0.5	0.1	0.3	0.3	0.3								
Na	-0.4	0.4	0.4	0.0	-0.1	0.1	-0.6							
K	0.1	-0.1	0.2	-0.1	0.0	-0.1	-0.4	-0.5						
P	-0.5	0.6	0.3	0.3	0.3	0.2	0.4	-0.3	-0.2					
Nb	0.0	0.0	0.5	-0.3	-0.3	-0.1	0.1	0.3	0.3	0.1				
Zr	-0.4	0.6	-0.7	0.1	0.0	0.2	0.2	0.4	0.2	0.2	0.6			
Y	-0.3	0.2	0.3	0.1	0.0	0.0	0.2	0.2	0.0	0.3	0.3	0.3		
Sr	-0.4	0.5	0.3	0.0	0.0	0.2	0.7	0.9	-0.5	0.3	0.1	0.4	0.2	
Rb	0.0	0.1	0.3	-0.1	0.0	-0.1	-0.4	-0.5	0.8	-0.1	0.3	0.1	0.0	-0.5

Tab.6: Major and trace element correlation for original (top) and normally distributed (bottom) data of surface rocks

The first three principal components only account for approximately two thirds of the variation. The addition of subsequent principal components only gradually increases the explained variation. For this reason no attempt was made to interpret the principal component analysis. Because of the lack of strong correlations between the original variables, it is considered sufficient to examine the correlation matrix (tab.6) to learn more about the interaction of variables.

8.3.2.2. Discriminant analysis.

8.3.2.2.1. Theory.

The theoretical discussion relies on Seal (1968), Papula (1975), Tatsuoka (1970) and Le Maitre (1982). The aim of discriminant analysis is to find the parameters of a linear function, which helps to maximize the separation of predetermined groups (in this study two) by projecting the multivariate observation vectors onto the linear function. This is graphically demonstrated in fig.33 for a simplified two-variate space.

Mathematically this can be achieved by maximizing the ratio of between-groups to within-groups mean of squares (chap.8.3.1.1.1.) or simply the sum of squares, because the degrees of freedom are a constant for a given problem.

$$L = \frac{SS_B}{SS_W}$$

As each observation can be expressed as a Z-score, similarly the sum of squares within and between groups can be reduced to 1 variable.

$$Z = \sum_{j=1}^{n} v_j x_j = \underline{v}\,\underline{x}$$

For simplicity this conversion is expressed in matrix notation.

$$SS_W = \underline{v}\,W\,\underline{v} \qquad SS_B = \underline{v}\,B\,\underline{v}$$

W represents the covariance matrix within groups, and B the covariance matrix between groups, based on the original n variables.

The maximization of $L = \frac{\underline{v}\, B\, \underline{v}}{\underline{v}\, W\, \underline{v}}$ can be achieved by equating all $\frac{dL}{dv}$ to zero. This results in a set of n linear equations:

$$(b_{i1}, b_{i2} \cdots b_{in})\ \underline{v} = L(w_{i1}, w_{i2} \cdots w_{in})\ \underline{v}$$

which can be written in matrix form as

$$B\ \underline{v} = L\ W\ \underline{v} \qquad \text{or} \qquad W^{-1}\ B\ \underline{v} = L\ \underline{v}$$

In order to avoid scaling of $\underline{v}$, the constraint of $\underline{v}.\underline{v} = 1$ is added.

The solution of this problem is known as the determination of the eigen-vectors, and subsequently the eigen-values, of matrix $W^{-1}\ B$ as long as W is non-singular. The equation $(W^{-1}\ B - L\ J)\ \underline{v} = 0$ has non-trivial solutions if L's can be found so that

$$| W^{-1}\ B - L\ J | = 0$$

Graphically the maximization is to look for a vector which keeps its orientation when subjected to a transformation by the matrix $W^{-1}\ B$.

Discriminant analysis requires normally distributed observations, and the equivalence of covariance matrices, for groups to be compared. According to Marriott (1974), discriminant analysis is reasonably robust for sample distributions which deviate from normality, provided the residuals are not correlated with the original grouped data. The assumption of equal dispersion matrices is a more serious requirement. If it is not fulfilled, the surface which separates the groups and is perpendicular in the ideal case to the discriminant function (fig. 33), can be distorted.

8.3.2.2.2. Results.

The SPSS program package was employed to perform a stepwise discriminant analysis. By analogy to trend surface analysis (chap. 8.3.1.2.1), a variable is included if the separation is significantly improved. The default F-values were used as upper and lower limits. Method Wilks maximizes the difference between groups by taking into account

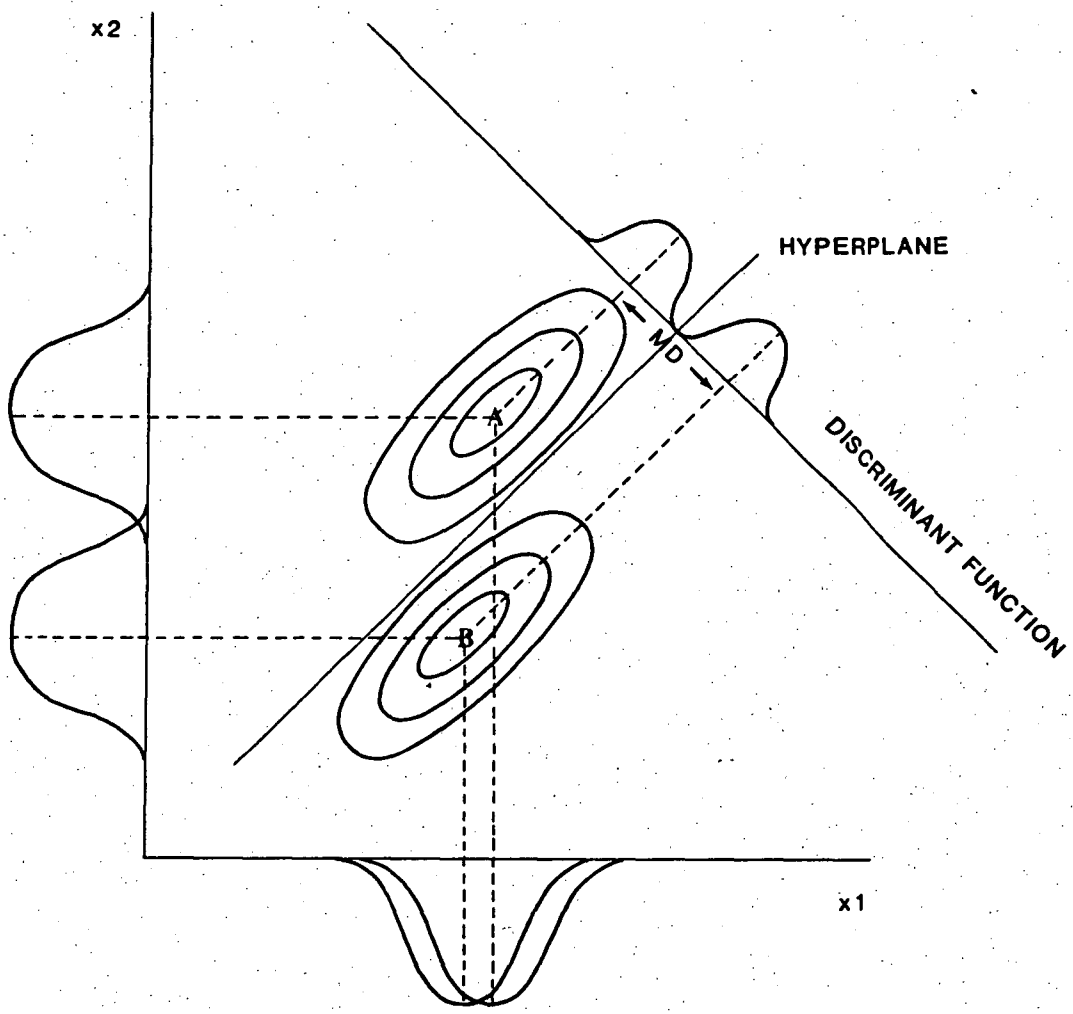

Fig.33: Geometric interpretation of discriminant analysis with two groups (A, B) defined by two variables (X_1, X_2). Projection of group centroids on discriminant function are separated by the Mahalanobis distance (MD)

the homogeneity within groups as discussed above. Method Mahal maximizes the Mahalanobis distance (fig.33) between two groups (Nie et al., 1975). Both methods produced the same discrimination functions.

The discrimination between groups was carried out on a similar basis as for the univariate analysis of variance (chap.8.3.1.3.3.). Unaltered pyroclastics were discriminated firstly against schists, and then against altered rocks including schists and massive siliceous rocks. The prior grouping was based on geological evidence, in order to avoid a biased geochemical discrimination (Le Maitre, 1982). This meant the ambiguous observations immediately above the host rock (chap.8.3.1.3.1) were either grouped according to textural evidence or placed into the control group. Also, one dacite from the western end of the sampling area (67818) was included in the unaltered pyroclastics. These different approaches were applied to a full set of elements, as used for the cluster analysis, and to a reduced number of elements which had previously (tab.4, chap.8.3.1.3.3.) shown a significant difference between groups at the 0.01 probability level.

The elements Pb, Zn, Cu, Co, Ni and Ba were not included due to their poor discriminatory power. The element S wes ignored because the significant differences between groups relies on few observations with extremely high concentrations. The minimum number of grouped observations was 55 cases. This is above the minimum recommended size of two to three times the number of variables (Tatsuoka, 1970).

Only small variations occur among the different trials conducted, with the lowest correct classification being 94%. Generally the full set of variables achieved slightly better classification results. In contrast to cluster analysis, all observations from the schists were classified correctly. The control group contained the Mt. Black Volcanics (lavas), the massive siliceous rocks when the unaltered rocks were discriminated against schists, and samples from the transition zone. The large majority of massive siliceous rocks classified as altered rocks, and all Mt. Black Volcanics as unaltered. The rocks from the transition zone fell into both groups. The discriminant analyses were based on data transformed to approximately normal distributions as discussed in chap.8.3.1.3.3. and cited in the appendix. Variables with some deviations from normality did not show a correlation between residuals and grouped data. Only three trials however, comply with the more important requirement of equivalent

covariance matrices as discussed in the previous chapter. These three cases are explained below in more detail. They can also be considered representative for the remaining trials, owing to the fact that no large differences exist as stated above. The discriminant scores and the projection of the grouped observations onto the discriminant function is shown in tab.7 and fig.34 respectively. The cases to be discussed are:

a. Trial a. is based on a complete set of variables with the ambiguous hanging wall observations included in the unaltered group. The approximate F-value for equivalence of covariance is 1.40 with a significance level of 0.06. 97% of the grouped observations are correctly classified. The hanging wall observations in question are evenly split into the altered and unaltered group. The standardized discriminant function reveals a strong influence of MnO_2 despite the fact that MnO_2 is the least powerful discriminator in the function. This could be explained by considering the correlation matrix in tab. 6 (chap.8.3.2.1.2) which does not reveal any correlation between MnO_2 and other elements. Conversely the negative parameter for Al_2O_3 which is depleted in the schists could be caused by correlations with other elements, which affects the shape of the multivariate cloud of observations, and therefore the discriminant function. The direction of the discriminant vector is also influenced by the position of the cloud centroids, especially if their relative univariate distances vary markedly (Dr. B.M. Brown, pers comm.). A strong correlation between SiO_2 and Al_2O_3 including Zr could be the cause for the change in direction.

b. Trial b. is identical to a. apart from a smaller selected set of variables. The approximate F-value for equality of covariance is 1.91 with a significance level of 0.04. 95% of the grouped observations are correctly classified. Except for one observation from a higher stratigraphic level in the hanging wall, the allocation remains essentially the same.

c. Trial c. included the observation from the immediate hanging wall in the control group, otherwise trial c. is identical to trial b. The approximate F-value is 1.84 with a significance level of 0.01. 98% of the grouped observations are correctly classified. All observations from the immediate hanging wall are allocated to the

Tab.7: Discriminant scores and classification

	a			b			c		
Sample	Actual group	Assigned group	Discrim. score	Actual group	Assigned group	Discrim. score	Actual group	Assigned group	Discrim. score
67818	unaltered	unaltered	2.04	unaltered	unaltered	1.49	unaltered	unaltered	2.04
67802	"	"	0.55	"	"	0.57	"	"	1.08
67808	"	"	0.83	"	"	1.12	"	"	1.32
67817	"	"	1.58	"	"	2.47	"	"	3.36
67795	"	"	1.74	"	"	0.94	"	"	1.41
67832	"	"	1.30	"	"	0.98	"	"	1.50
67797	"	"	0.20	"	"	0.05	"	"	0.00
67806	"	"	2.09	"	"	1.05	"	"	1.24
67807	"	"	0.18	"	"	-0.30	"	"	0.17
67831	"	"	1.18	"	"	1.48	"	"	1.53
67849	"	"	2.37	"	"	1.56	"	"	1.99
67850	"	"	0.76	"	"	1.22	"	"	1.54
67851	"	"	1.65	"	"	1.59	"	"	2.50
67858	"	"	1.82	"	"	1.70	"	"	1.71
67869	"	"	0.79	"	"	0.74	"	"	0.91
67800	"	"	2.41	"	"	2.17	"	"	2.57
67885	"	"	2.39	"	"	2.38	"	"	3.08
67809	"	"	0.85	"	"	1.37	"	"	2.08
67822	"	"	1.05	"	"	1.16	"	"	0.71
67823	"	"	0.90	"	"	0.61	"	"	1.31
67803	"	"	0.80	"	"	0.06	"	"	0.63
67811	"	"	2.86	"	"	2.37	"	"	2.73
67829	"	"	1.44	"	"	1.39	"	"	1.53
67847	"	"	1.90	"	"	1.61	"	"	1.26
67848	"	"	1.48	"	"	1.91	"	"	2.31
67852	"	"	1.61	"	"	1.22	"	"	1.69
67854	"	"	2.19	"	"	1.77	"	"	2.69
67858	"	"	1.09	"	"	0.78	"	"	1.41
67860	"	"	1.80	"	"	2.64	"	"	2.77
67861	"	"	1.14	"	"	0.99	"	"	0.46
67863	"	"	1.96	"	"	1.42	"	"	1.54
67875	"	"	1.25	"	"	0.80	"	"	0.79
67878	"	"	1.92	"	"	1.81	"	"	1.98
67886	"	"	0.41	"	"	0.74	"	"	0.75
67838	"	"	2.91	"	"	2.87	"	"	1.77
67913	"	"	2.36	"	"	2.22	"	"	1.96
67865	"	"	0.61	"	"	0.43	"	"	1.35
67868	"	"	-0.72	"	schists	-2.09	"	schists	-2.55
67801	schists	schists	-2.12	schists	"	-2.76	schists	"	-4.07
67819	"	"	-2.76	"	"	-3.20	"	"	-3.78
67820	"	"	-2.25	"	"	-1.75	"	"	-4.02
67833	"	"	-3.94	"	"	-3.26	"	"	-4.25
67835	"	"	2.67	"	"	-2.54	"	"	-3.86
67837	"	"	-3.56	"	"	-2.66	"	"	-3.97
67814	"	"	-1.63	"	"	-1.08	ungrpd	"	-1.69
67816	"	"	-4.01	"	"	-2.89	"	"	-4.46
67870	"	"	-2.97	"	"	-2.40	schists	"	-3.15
67876	"	"	-1.64	"	"	-1.54	"	"	-3.07
67877	"	"	-3.20	"	"	-2.74	"	"	-3.33
67879	"	"	-1.60	"	"	-1.03	"	"	-1.28
67880	"	"	-1.78	"	"	-1.39	"	"	-2.13
67881	"	"	-2.63	"	"	-2.43	"	"	-3.70
67882	"	"	-3.04	"	"	-2.29	"	"	-3.19
67883	"	"	-3.33	"	"	-2.37	"	"	-3.43
67885	"	"	-3.31	"	"	-3.75	"	"	-4.25
67815	"	"	-3.09	"	"	-3.06	"	"	-4.15
67889	"	"	-1.98	"	"	-1.06	"	"	-1.48
67824	unaltered	unaltered	0.19	unaltered	unaltered	-0.15	ungrpd	"	-1.04
67828	"	schists	-2.87	"	schists	-1.80	"	"	-3.49
67810	"	"	-1.14	"	"	-1.21	"	"	-3.28
67812	"	unaltered	1.65	"	unaltered	0.43	"	"	-1.30
67796	ungrpd	"	-0.45	ungrpd	schists	0.11	"	"	-2.03
67830	"	schists	-3.80	"	unaltered	-3.30	"	unaltered	-4.73
67836	"	"	-3.12	"	"	-2.07	"	schist	-3.08
67840	"	"	-2.74	"	schists	-2.49	"	"	-3.69
67841	"	"	-4.21	"	"	-2.84	"	"	-3.83
67843	"	"	-5.73	"	"	-3.01	"	"	-3.88
67844	"	"	-1.67	"	"	-1.12	"	"	-2.54
67846	"	"	-3.10	"	"	-2.71	"	"	-3.93
67887	"	"	-3.68	"	"	-3.36	"	"	-4.29
67842	"	"	-0.99	"	unaltered	0.27	"	unaltered	0.66
67826	"	unaltered	-0.31	"	"	-0.05	"	"	-0.50

67827	ungrpd	unaltered	2.27	ungrpd	unaltered	2.41	ungrpd	unaltered	3.47
67856	"	"	1.15	"	"	0.70	"	"	1.53
67867	"	"	1.76	"	"	1.48	"	"	1.14
67871	"	"	2.89	"	"	2.43	"	"	2.85
67872	"	"	2.48	"	"	1.93	"	"	2.49
67873	"	"	2.63	"	"	2.18	"	"	2.99
67874	"	"	3.04	"	"	1.11	"	"	3.47
67825	"	"	1.21	"	"	0.98	"	"	0.54
67853	"	"	1.99	"	"	-0.35	"	"	-0.56
67855	"	"	1.60	"	"	1.70	"	"	1.20
67859	"	"	0.42	"	"	1.21	"	"	1.91
67862	"	"	1.41	"	"	0.81	"	"	0.30
67864	"	"	1.47	"	"	1.82	"	"	1.20
67798	"	"	0.67	"	"	0.24	"	"	0.16
67845	"	"	3.28	"	"	2.65	"	"	5.26
67813	"	schists	-1.76	"	schists	-2.20	"	schists	-3.09
67839	"	unaltered	0.34	"	unaltered	1.25	"	unaltered	1.54
67821	"	"	0.97	"	"	1.69	"	"	1.01
67804	"	schists	-3.87	"	schists	-2.86	"	schists	-2.89
67866	"	"	-2.53	"	"	-1.80	"	"	-3.09
67799	"	"	out of range	"	"	-1.62	"	"	-3.85

Trial a

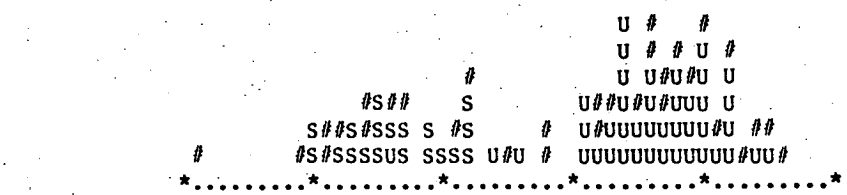

Group centroids S (-2.71) U (1.22)

Standardized discriminant function: $Z = -0.53\ MnO + 0.43\ TiO_2 + 0.67\ CaO - 0.58\ K_2O - 0.55\ Al_2O_3 + 0.57\ Na_2O + 0.72\ Nb + 0.34Rb$

Unstandardized discriminant function: $Z = -1.06\ MnO + 4.38\ TiO_2 + 1.21\ CaO - 0.55\ K_2O - 0.32\ Al_2O_3 + 1.26\ Na_2O + 0.25\ Nb + 0.15\ Rb - 3.50$

Trial b

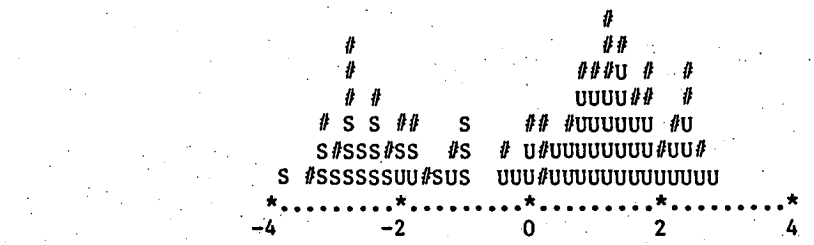

Group centroids S (-2.35) U (1.06)

Standardized discriminant function: $Z = 0.42\ CaO - 0.37\ K_2O + 0.64\ Na_2O + 0.52\ Nb$

Unstandardized discriminant function: $Z = 0.76\ CaO - 0.35\ K_2O + 1.44\ Na_2O + 0.18 - 2.38$

Trial c

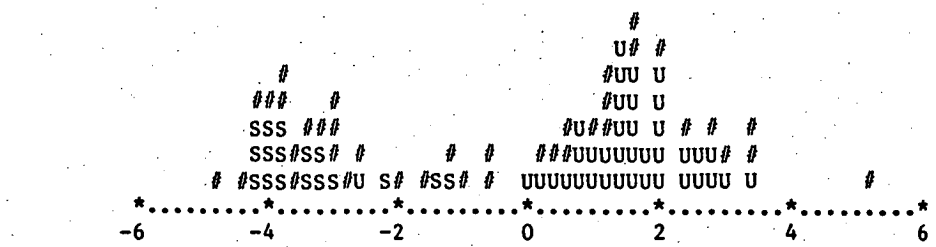

Group centroids S (-3.36) U (1.50)

Standardized discriminant function: $Z = 0.44\ TiO_2 - 0.45K_2O + 0.63\ Na_2O + 0.66\ Nb - 0.36\ Zr + 0.33\ Sr$

Unstandardized discriminant function: $Z = 4.51\ TiO_2 - 0.44\ K_2O + 1.83\ Na_2O + 0.23\ Nb - 0.01\ Zr + 0.10\ Sr - 5.92$

Fig. 34: Group histograms based on standardized discriminant function for trial a, b, c, (one character = one observation)
U = unaltered pyroclastics, S = schists, # = ungrouped

altered group. As in trial a., Zr, another depleted element causes a negative parameter in the discriminant function.

The percentage of correctly classified observations compares well with those from literature quoted above. Compared with cluster analysis from this study, the classification is slightly improved. Discriminant analysis also supports the univariate alteration patterns by demonstrating a good agreement between geological evidence and broadly based multi-element geochemical behaviour. This can be seen in fig. 35.

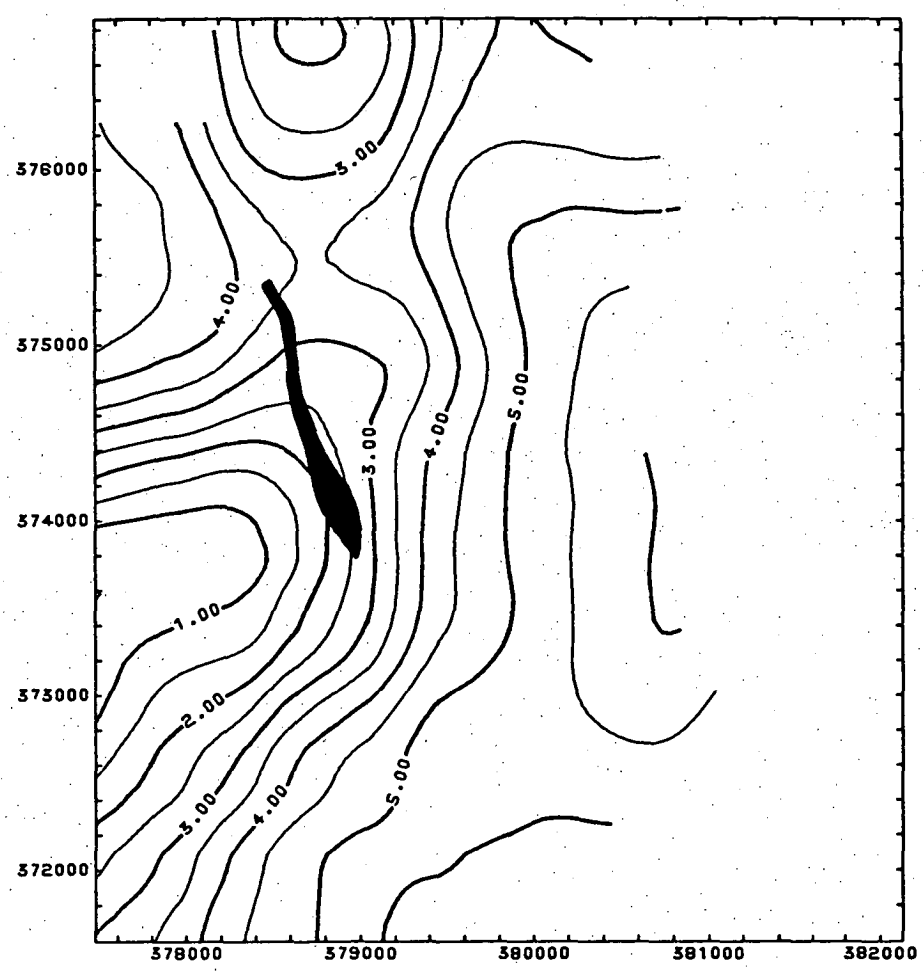

Fig. 35: Smoothed distribution of unstandardized discriminant scores by analogy to element distributions

9. Geology and geochemistry of the mine including underground wall rock alteration.

The aim of this chapter is, in addition to a global description of the mine, to outline the chemical zonation of the orebody. Moreover the footwall alteration pattern in the mine is also described.

9.1. Shape of the ore deposit.

The Rosebery deposit extends over 1650 m along strike and continues down dip at least 800 m (Adams et al., 1976). It is comprised of two tabular orebodies, the southern main orebody and a smaller orebody further north, separated by a barren zone which holds locally some disseminated ore. A longitudinal projection of the mine (fig. 36) outlines the ore. Apart from some possible minor slump structures, the northern orebody is relatively undeformed and includes larger areas of host rock with varying amounts of carbonate, giving it sometimes the appearance of discontinuous and/or stacked ore lenses (fig. 37). According to mine terminology, the northern orebody as a whole unit has been named A and B lens. The southern orebody is a more-or-less continuous sulphide body which was subjected to large scale folding. Based on this structure, the southern orebody has traditionally been subdivided as C to F lens from north to south. The G lens represents a large parasitic fold (fig. 38, 41).

Both sulphide orebodies are emplaced concordantly in the host rock horizon, and overlain by barite-rich bodies (called H lens above the southern orebody). Sulphide and sulphate bodies are usually separated by weakly mineralized host rock. The ore stratum usually varies from <5 m to 20 m thickness and can be wider in the fold hinges.

9.2. Structural geology of the mine.

The summary of the structural geology of the mine is largely based on work carried out by Brathwaite (1969).

The average strike and dip of the bedding in the host rock is 345° - 45° E with very similar orientation for the ore-host rock contact, and banding in the ore. Cleavage is usually subparallel to bedding and has a

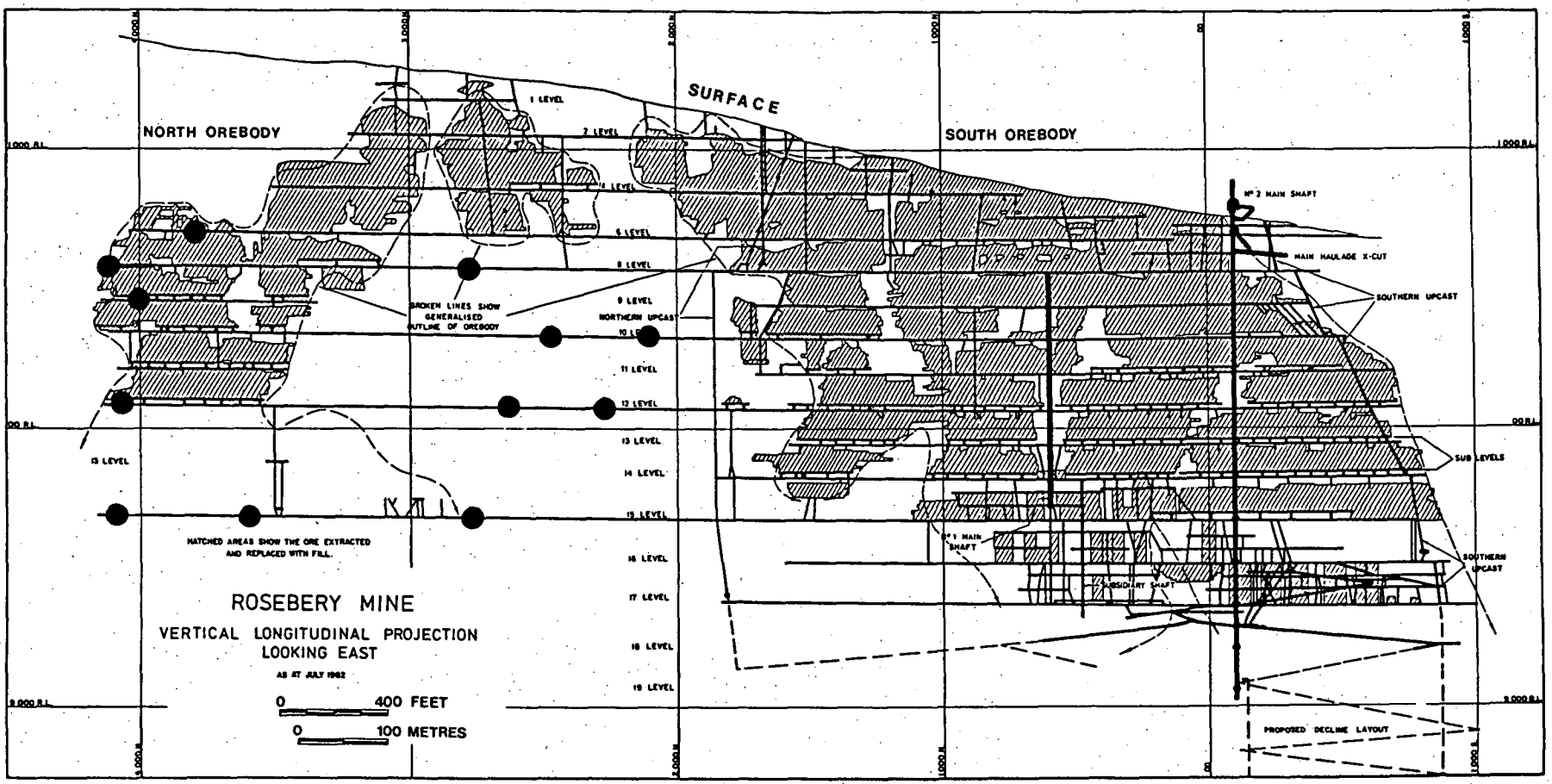

Fig.36: Longitudinal projection of the Rosebery ore deposit, courtesy of Electrolytic Zinc Co. Pty. Ltd., with minor modifications, ● indicate occurrence of feldspars below north orebody and in barren gap below extrapolated ore horizon

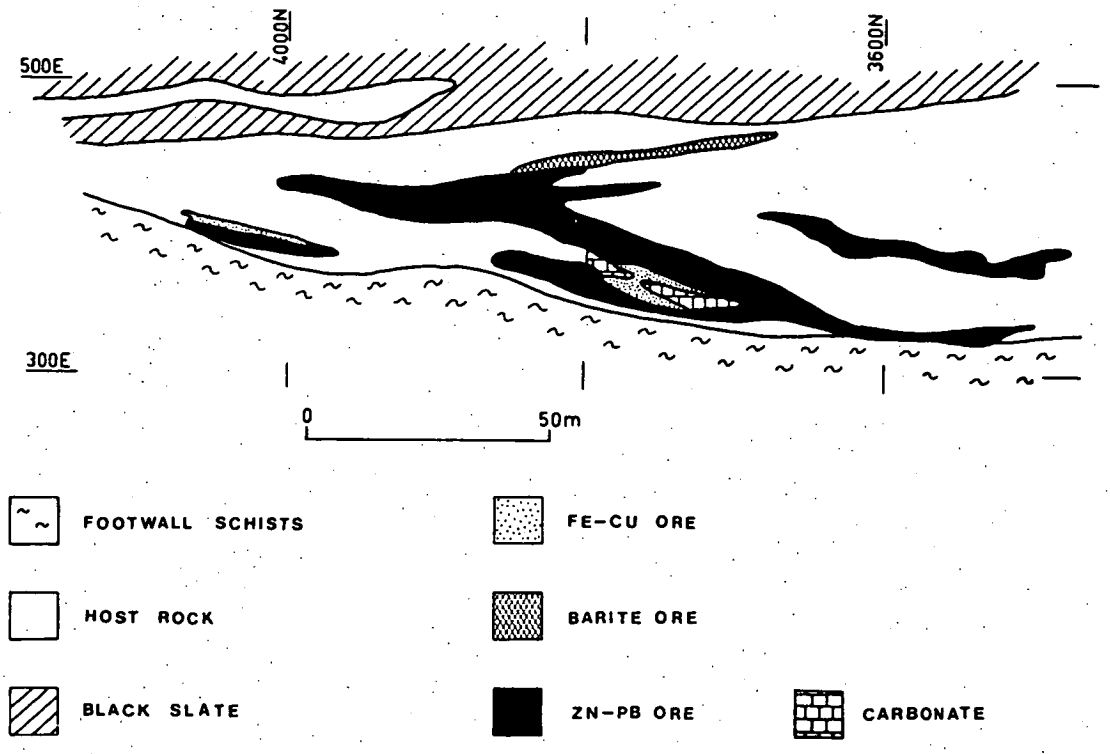

Fig. 37: Longitudinal plan of northern orebody at 11 level, according to mine maps

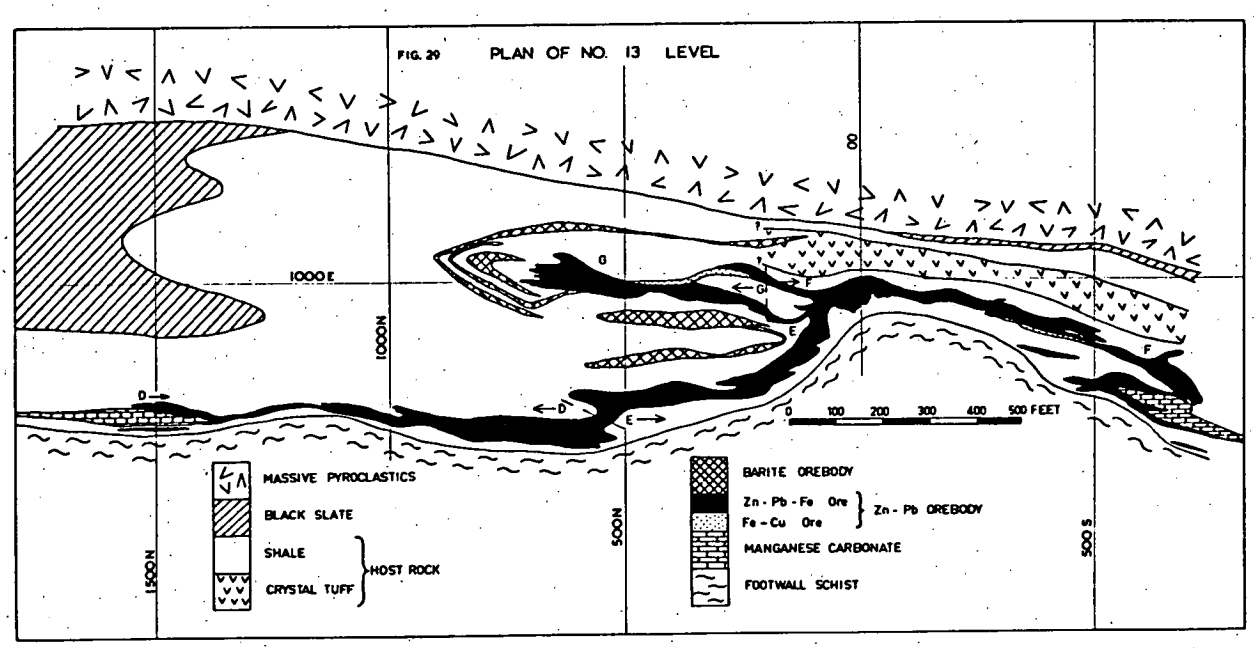

Fig. 38: Longitudinal plan of southern orebody at 13 level after Brathwaite, 1969

uniform strike and dip of 350° - 60° E. Deformation of host rock including ore has resulted in some small to large scale folding. Small scale folding is visible in the banded ore (chap.9.4.1.1, fig.47). Mesoscopic folding has affected host rock and ore. The folds in the host rock are approximately "similar", with cleavage parallel to the inclined axial planes. Folding in the ore is more irregular with similar to concentric style. Kink folding of quartz veins can be seen occasionally (fig.39). Some of the quartz veins contracted coarse remobilized mineralization as demonstrated in fig.40 (see also Brathwaite, 1969). Abundant carbonate veins and less frequently barite veins occur, showing signs of deformation and also including fragments of ore. The southern orebody has undergone large scale folding and this creates the appearance of ore lenses joining in an en echelon pattern as shown in fig.38. The dip of the axial plane shows a range of 55° - 60° E. Among these drag-folds, which are of limited extent, one particularly large fold between 0 N and 700 N in the longitudinal centre of the southern orebody, is the most prominent structural feature of the mine (fig.41).

This large fold is also reflected in the footwall schist-host rock contact and the host rock-black shale contact. The hinges of the drag folds plunge south at the southern end and reverse to mainly northerly plunges towards the north end of the southern orebody.

Brathwaite (1969), although aware of a possibly synsedimentary origin explained the large scale folds as being caused by drag shear during the formation of the anticlinal structure (fig.7, chap.6) at Rosebery. He described the relatively mobile ore embedded on the east dipping limb of the anticlinal structure as more subjected to deformation and subsequent parasitic folding than the more competently behaving silicates. Adams et al. (1976) preferred as deformational mechanism a post-black slate gravitational slump, on the grounds that only two complete ore sequences are present, as opposed to three required for a drag fold.

9.3. Footwall schists in the mine, underground.

The footwall schists immediately below the northern orebody are comparable to those described from the field, which outline the alteration below the southern orebody according to this study. They include siliceous augen schists, Brathwaite's chert, and fine schists. Their main difference

Fig.39: Kinkfolded quartz vein, amplitude about 1 m, at 16 level, southern orebody

Fig.40: Coarse grained mineralization (pyrite, chalcopyrite and galena) in quartz vein, at 17 level, southern orebody

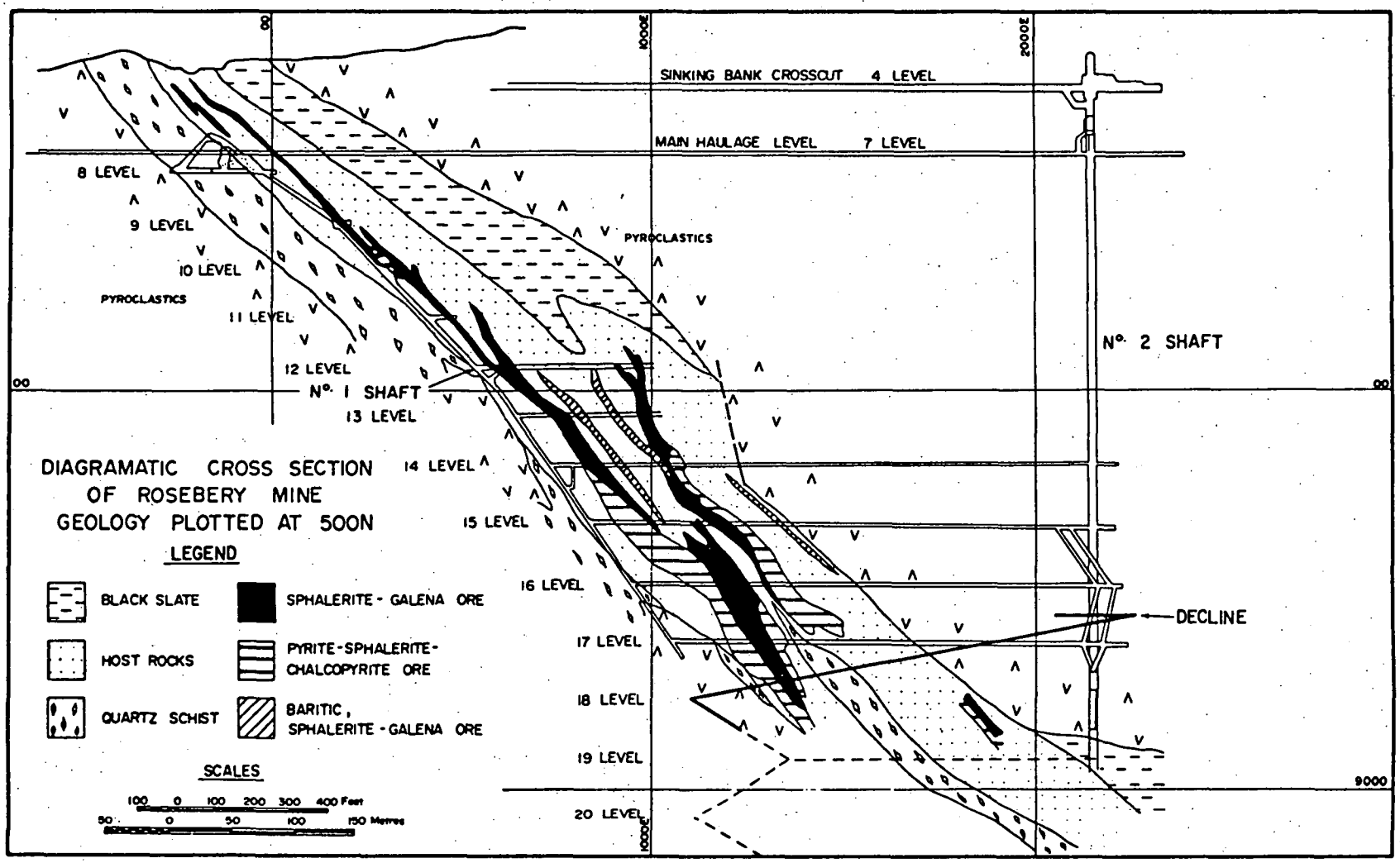

Fig.41: Cross section of southern orebody normal to strike, courtesy of Electrolytic Zinc Co. Pty. Ltd.

is a generally larger proportion of disseminated ore, carbonate and chlorite. Chlorite averages 5 - 10 % (volume) and can locally reach up to 20% (e.g. 68018). A carbonate content of up to 20% and occasionally higher is not uncommon (e.g. 67973). The texture of the augen schists underground appears to be more pronounced with more clearly defined augen. Disseminated ore, if present, is more abundant in the chlorite-sericite schlieren than in the quartz augen (fig.42).

The footwall schists underlying the southern orebody, as far as studied, are completely devoid of feldspar (Dr. G.R. Green, pers. comm.). In the footwall below the northern orebody, a weak zonation could be established, marked by the presence of feldspar. Slightly to totally decomposed plagioclase is absent from the approximately 300 m wide central hydrothermal channel and immediately below the host rock in the peripheral vent area. This channel is hidden from the surface and exists independently of the larger halo below the southern orebody (fig. 59, chap. 9.5.). Siliceous schists partly with augen texture appear to be more dominant in this central pipe up to 30 m below the host rock horizon. However the pattern is not consistent, and also the lack of long drill cores into the footwall schists makes a more profound examination impossible.

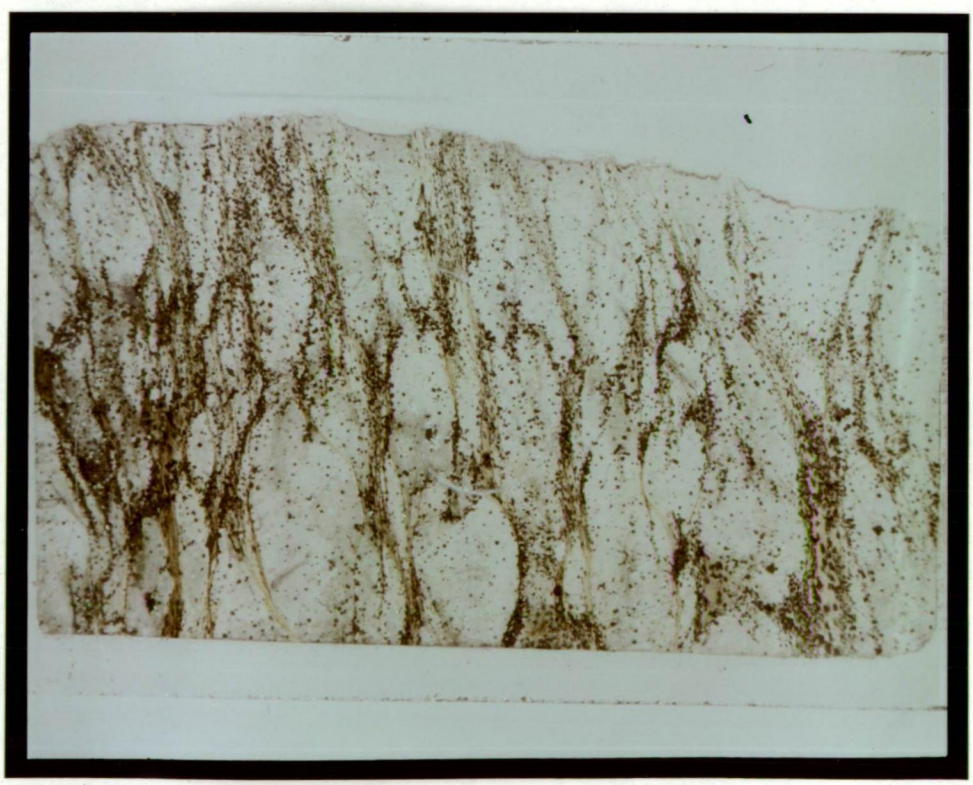

Fig.42: Augen schist (68091) below northern orebody at 15 level, field length = 35 mm

Intensive disseminated mineralization in the footwall schists occurs only sporadically in larger amounts. The central hydrothermal channel below the northern orebody generally contains higher amounts of pyrite, chalcopyrite, sphalerite and galena (py > cpy > sp > ga). This is reflected in the distribution pattern of S, Cu, Zn and Pb respectively as discussed below. Pyrite euhedras are the most abundant sulphide phase in the footwall schists. They are frequently associated with pressure shadows. Fine grained pyrite (0.01 - 0.02 mm) in streaks of sericite and chlorite without traces of disruption are probably of secondary origin (e.g. 67986). Chalcopyrite, sphalerite and galena are less regular in shape.

The chlorite content immediately below the ore is higher than in the surface alteration area. A strict zonation into a chlorite dominated core surrounded by a peripheral sericite alteration as in some of the Canadian Archaean massive sulphide deposits (Riverin & Hodgson, 1980; Spence, 1975) does not exist. The central alteration pipe of the northern orebody at Rosebery can be roughly compared to the combined alteration zone 3 and 4 of the Kuroko-type deposits (Shirozu, 1974).

There is one drill hole available (DDH 1121), which penetrates 420 m into the footwall from the south end of the northern orebody. The first approximately 20 m intersected are host rock with a high proportion of chlorite, followed by 32 m of footwall schists. Over the next 300 m, slightly sheared footwall pyroclastics with relatively fresh plagioclase alternate with schists containing altered feldspars or relics only. Possibly faint textures of deformed glass have been preserved where alteration was less active (e.g. 67931). Feldspars up to 3 mm, and sparse quartz grains ($\leq$ 1.5 mm) with signs of deformation and resorption are present. The bottom part is formed by rocks which resemble the massive siliceous rock in hand specimen (e.g. 67941). They contain coarse fractured and embayed quartz grains, but their sericite and carbonate content is significantly higher. Clear albitic plagioclase is a constant minor constituent. An interpretation of the intersected rock pile is presented in fig.43.

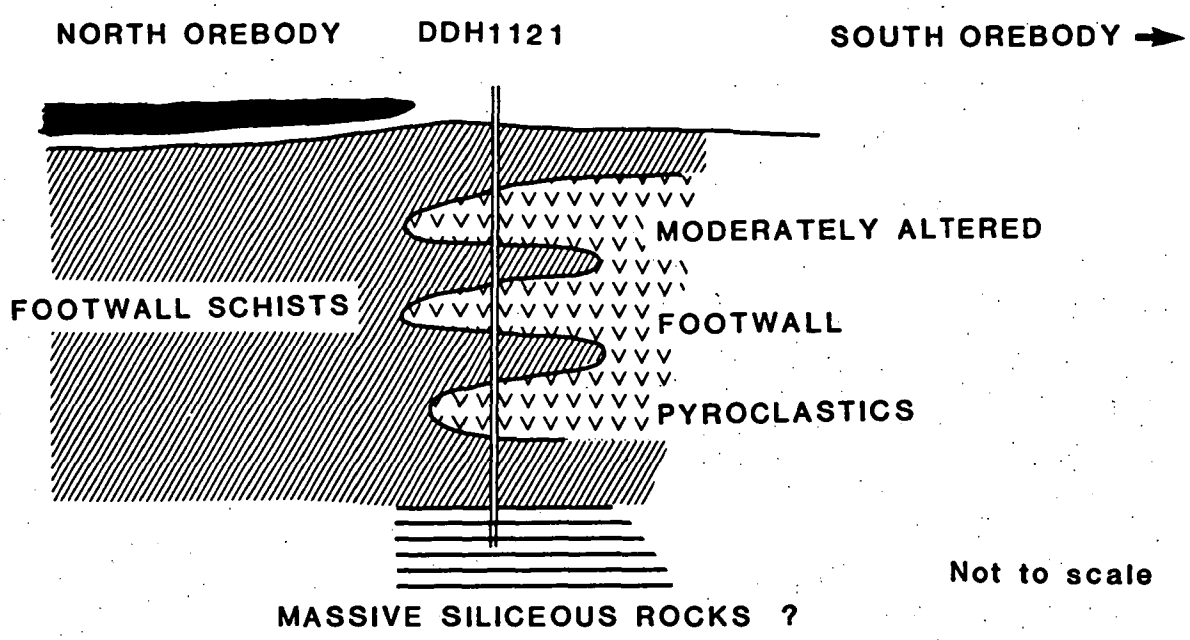

Fig.43: Interpretation of marginal aleration zone underground, below northern orebody, intersected by DDH 1121

9.3.1. Chemical zonation of the footwall, underground.

The presence of minor disseminated mineralization in the footwall schists helps to demonstrate an enrichment pattern for the major ore forming elements and also several other trace elements. The chemistry of the ore forming elements proved to be more regular than the chemistry of the major rock forming elements due to varying amounts of carbonate and in particular, silica.

Sampling in the footwall schists was based approximately on four cross sections (fig.44). In order to produce a horizontal sample distribution as shown in fig 44, the whole data set was rotated. This procedure is explained in chap.9.4.5. . Depending on the availability of drill cores, samples were collected from each, at different levels, to overcome strong variations in the metal content. The samples are listed in appendix 2. Samples from the host rock were not included. Due to the lack of long drill holes, core sampling was restricted to a shallow footwall zone of $\leq$ 80 m depth below the ore body. In most cases, the drill core extension was much more limited. In order to test for a bias introduced by

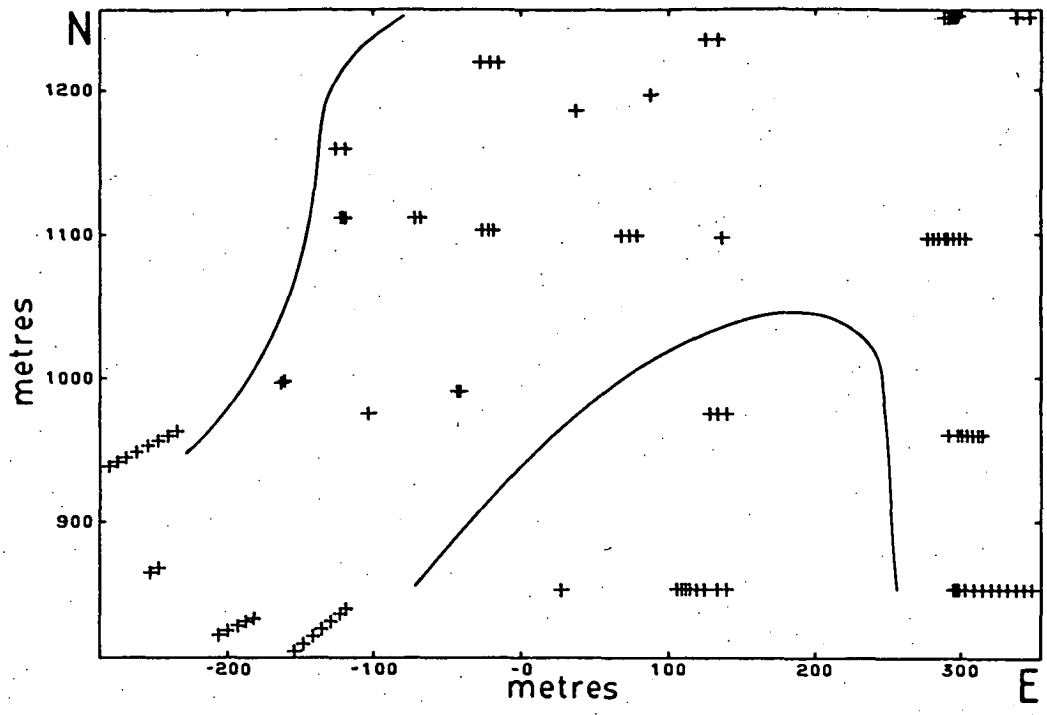

Fig. 44: Sample distribution (n = 96) in footwall schists underground below northern orebody rotated in horizontal position. Lines delineate boundary of overlying orebody

a fluctuating sampling depth, a vertically more restricted footwall section, which was essentially confined to the siliceous schists was also chosen for contouring. The metal zonations of Cu, Pb, Zn and S based on both sets of samples are in good agreement. Contouring was performed by the program package Surface II as discussed in chap. 8.3.1.2.2., and was based on the full set of drill core data.

Essentially two different patterns emerged. One group includes Cu, S and Co (fig. 45a-c), the second is represented by Pb, Zn, and Ni (fig. 45d-f). The outline of the zonation of Cu, Co and S is similar to that of the shape of the overlying orebody, and also to the ore-grade zonation of Cu and Fe, suggesting an instant precipitation of pyrite and chalcopyrite. Pyrite, the most abundant sulphide mineral in the footwall can be equated to the concentration of S. The increase of Co is steeper than that of S which might indicate a higher Co content in pyrite in the area most strongly affected by hot solutions, as recognised by Loftus-Hills & Solomon (1967). Based on this concept, Green et al. (1981) were able to delineate a feeder channel in the footwall of the south orebody. The enrichment of the above mentioned elements in the underground schists is in contrast to

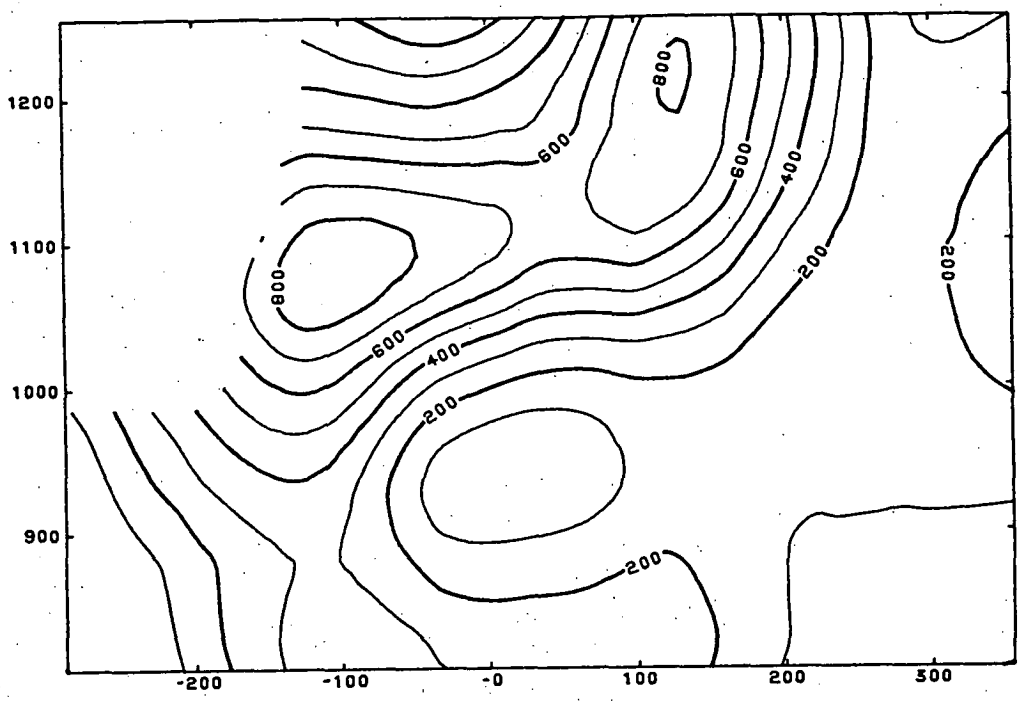

Fig. 45a: Smoothed horizontal distribution of Cu (ppm) in footwall schists (underground) below northern orebody

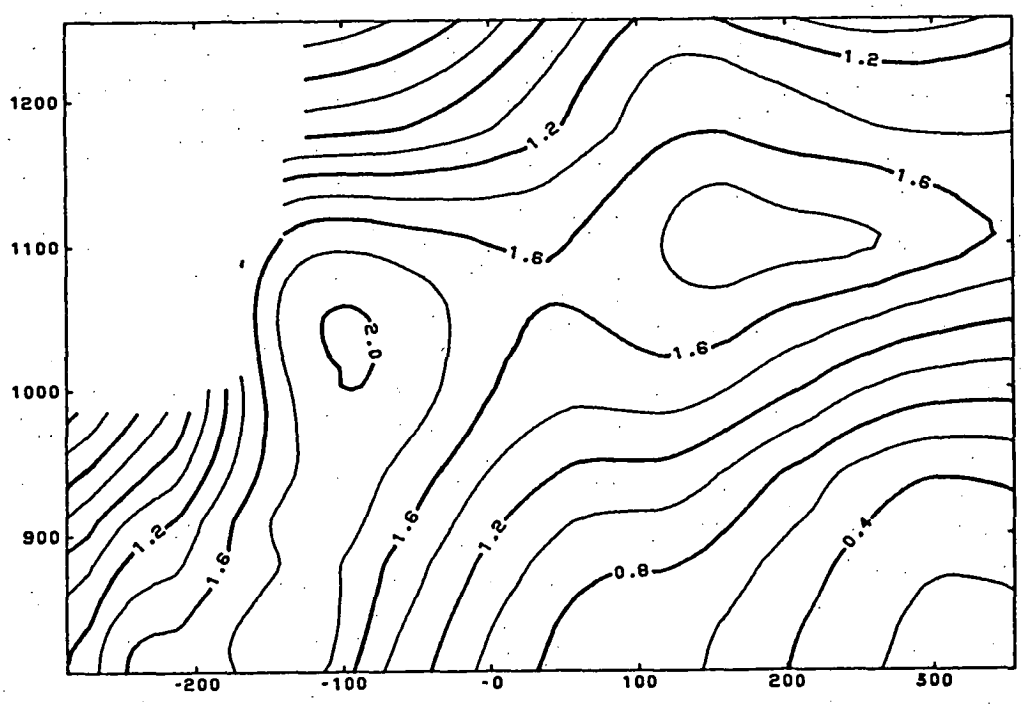

Fig. 45b: Smoothed horizontal distribution of S (%) in footwall schists (underground) below northern orebody

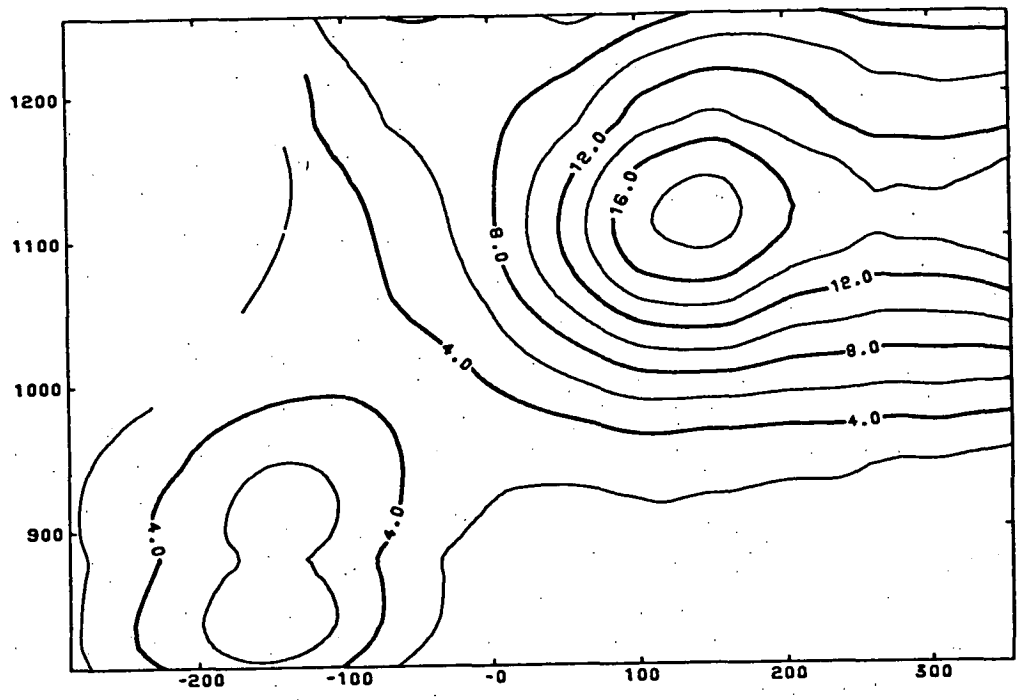

Fig. 45c: Smoothed horizontal distribution of Co (ppm) in footwall schists (underground) below northern orebody

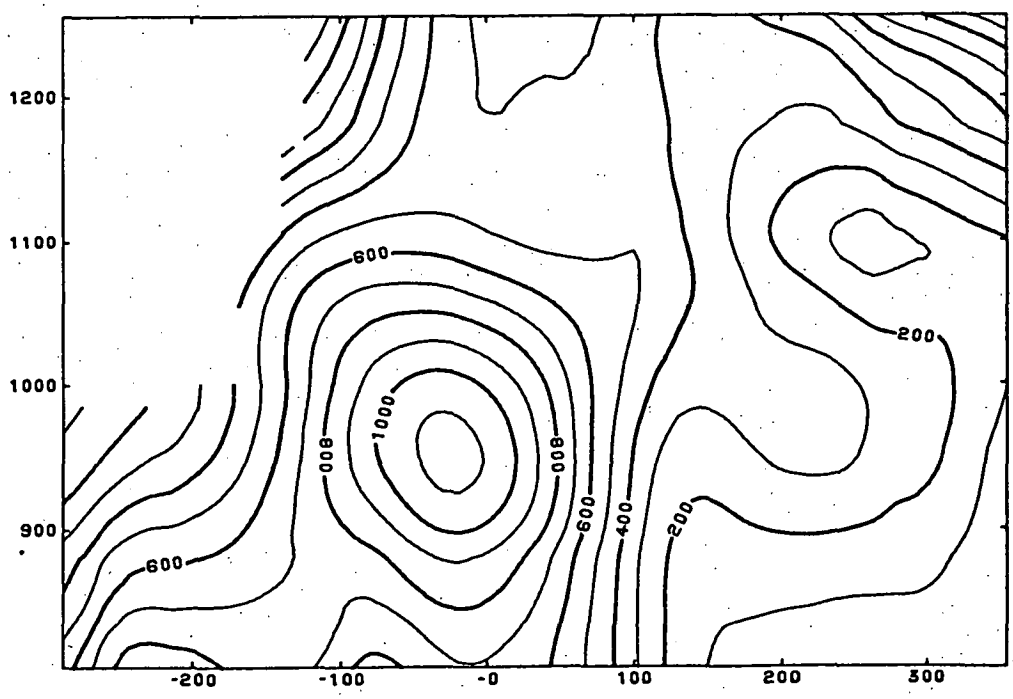

Fig. 45d: Smoothed horizontal distribution of Pb (ppm) in footwall schists (underground) below northern orebody

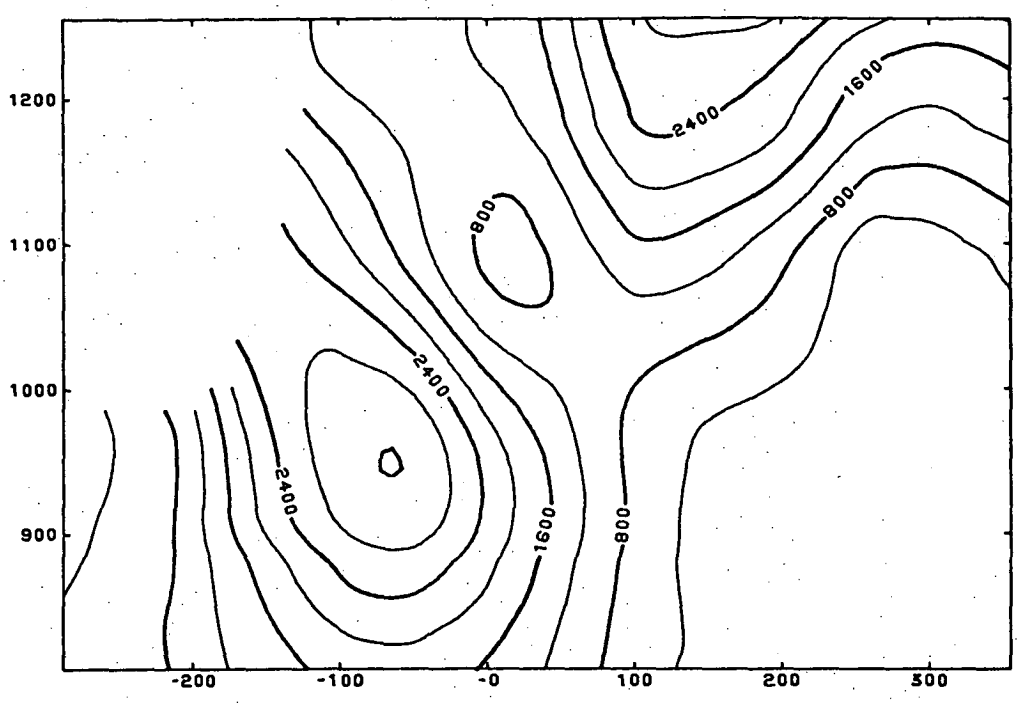

Fig.45e: Smoothed horizontal distribution of Zn (ppm) in footwall schists (underground) below northern orebody

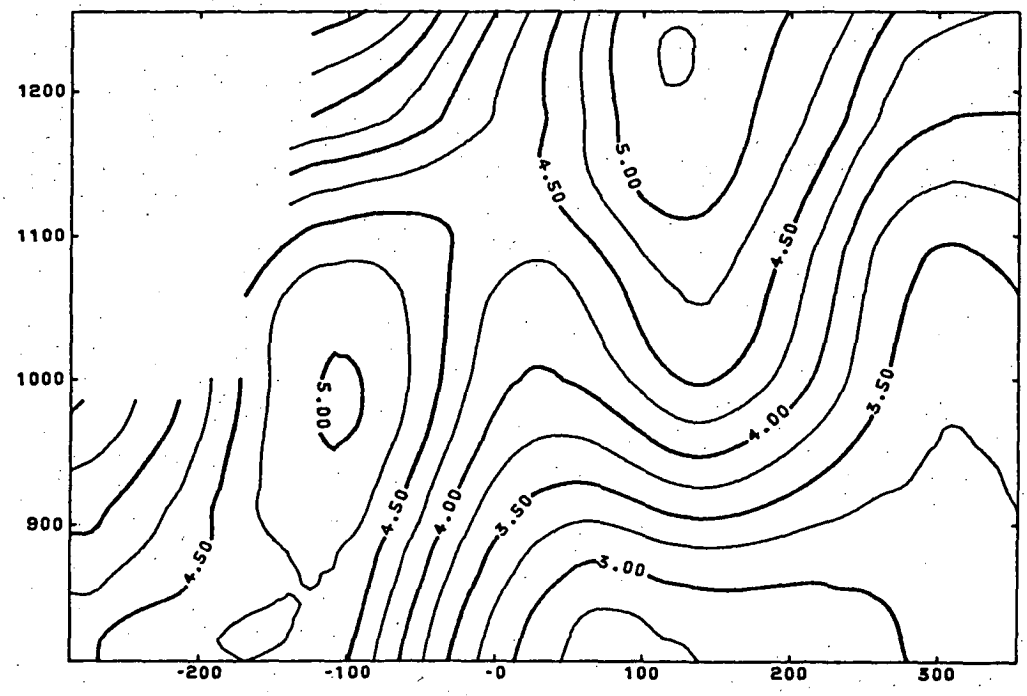

Fig.45f: Smoothed horizontal distribution of Ni (ppm) in footwall schists (underground) below northern orebody

the alteration zone on the surface, which is further away from the central feeder channel below the southern orebody. However, weathering could have affected the surface pattern as well.

Attempts to fit a cubic trend surface through the original data of the ore-forming elements Pb, Zn, Cu and S resulted in poor correlations between fitted surface and data. Except for S this did not change markedly, even after the use of unsmoothed and smoothed ($R_s^2 = 0.58$) grid data derived from program package Surface II as explained in chap. 8.3.1.2.3. Again trend fitting did not achieve any improvements, as already demonstrated in the case of the surface haloes.

9.4. The orebody, including mineralogy and chemical zonation.

The two orebodies forming the Rosebery deposit consist of mainly massive ore with 50 - 90% sulphide and sulphate (Brathwaite, 1969), consisting of 25% sphalerite, 5% galena, 30% pyrite and 3% chalcopyrite on average (West Coast Mines, Description of Activities, E.Z.). The north and south orebodies are typically zoned with a Cu-Fe-rich base and a Pb-Zn-rich upper part (Lusk, 1969). Limited haematite mineralization occurs at the top of the massive sulphide ore, and in conjunction with the overlying barite ore lenses. The barite ore is usually separated from the sulphide ore by weakly mineralized host rock. Carbonate occurs at the strike limits of both orebodies and within the ore.

9.4.1. Massive sulphide ore.

The main sulphide minerals are pyrite, sphalerite, galena and chalcopyrite. Apart from the haematite and magnetite, minor constituents include tetrahedrite-tennantite, arsenopyrite, gold, electrum, ilmenite, rutile, meneghinite, jordanite and bournonite. A detailed description has been given by Brathwaite (1969) followed recently by a brief discussion by Green et al. (1981). Gangue minerals include sericite, chlorite, Mn-rich carbonate, calcite, quartz, barite, sphene and albite.

9.4.1.1 Primary ore textures.

Textures exhibiting clearly synsedimentary features are rare. Fig. 46 shows a sequence of crossbedded pyrite which is graded microscopically in each cycle. Several colloform and framboidal pyrite textures have been interpreted by Brathwaite (1969) as primary.

The most persistent textural feature is the fine banding of the ore due to varying degrees of mineralization or alternation of different sulphide phases. Brathwaite (1969) recognized the conformity between the sulphide layers and the bedding in the host rock and in addition observed post-layer folding. Evidence for a pre-deformation banding has also been found in the north orebody (fig. 47) in this study. Folding and the varying style of layering led Brathwaite to the conclusion of a sedimentary origin.

Based on two sampled cross sections of the northern orebody from drill cores (DDH 3236, 3391) some new ideas about the origin of the fine layers have emerged, which are discussed in chap. 15. Stratigraphically above the frequently uniformly massive Cu-Fe ore (106715), the layering appears to be produced by recurring thin bands, $\leq$ 1 mm across, of mainly very fine disseminated pyrite ($\leq$ 0.01 m) in dominantly Zn-Pb ore (fig. 48). Occasionally the massive ore gives way to the pyrite and gangue minerals or pyrite only. The fine, densely disseminated pyrite can form large xenomorphic pyrite grains of poikiloblastic appearance by joining large numbers of fine crystals (106719). This fine grained idiomorphic to hypidiomorphic pyrite is in stark contrast to the ever present coarser and resorbed pyrite (fig. 49).

Although the majority of examined layers exhibits this pattern, bands of coarser, partly rounded and embayed pyrite exist as well, more loosely distributed over a larger width.

A much more vaguely defined banding or alternation has also been observed for chalcopyrite in gangue minerals (106713) at the base of the ore, and for galena in the Zn-Pb ore (106720). Pyrite is seemingly more abundant in these galena-rich sections. Apart from the above mentioned types of layers, Brathwaite (1969) also recognized banding of magnetite and arsenopyrite in several polished thin sections.

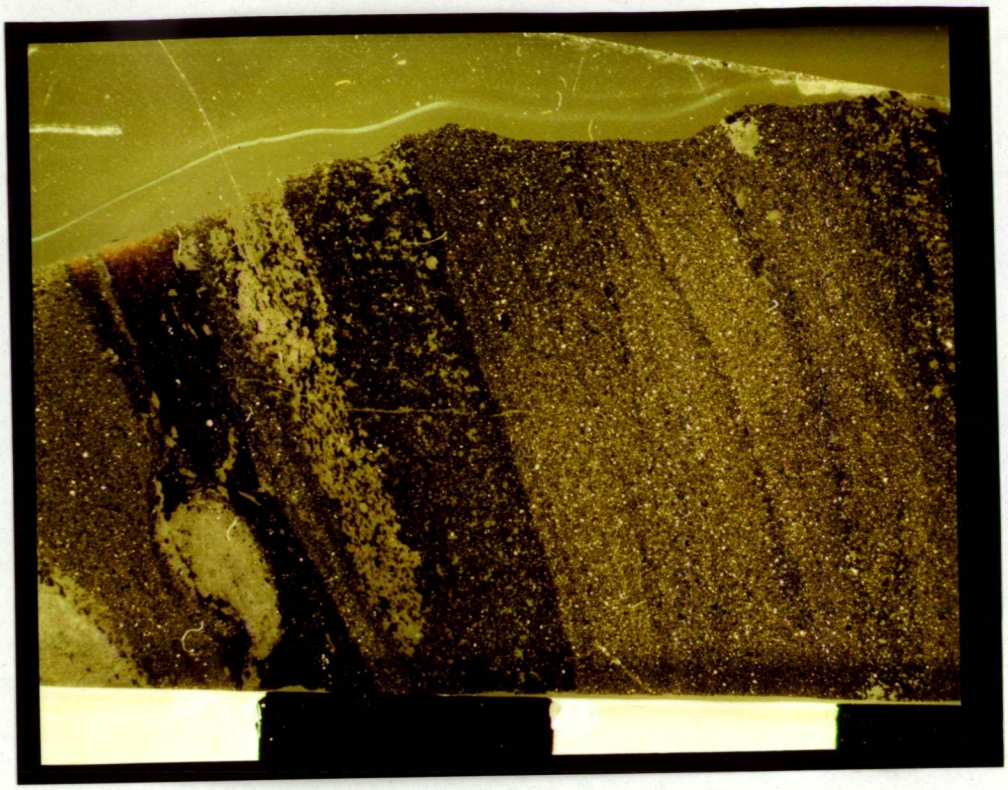

Fig.46: Crossbedded pyrite (106705), scale at bottom in cm

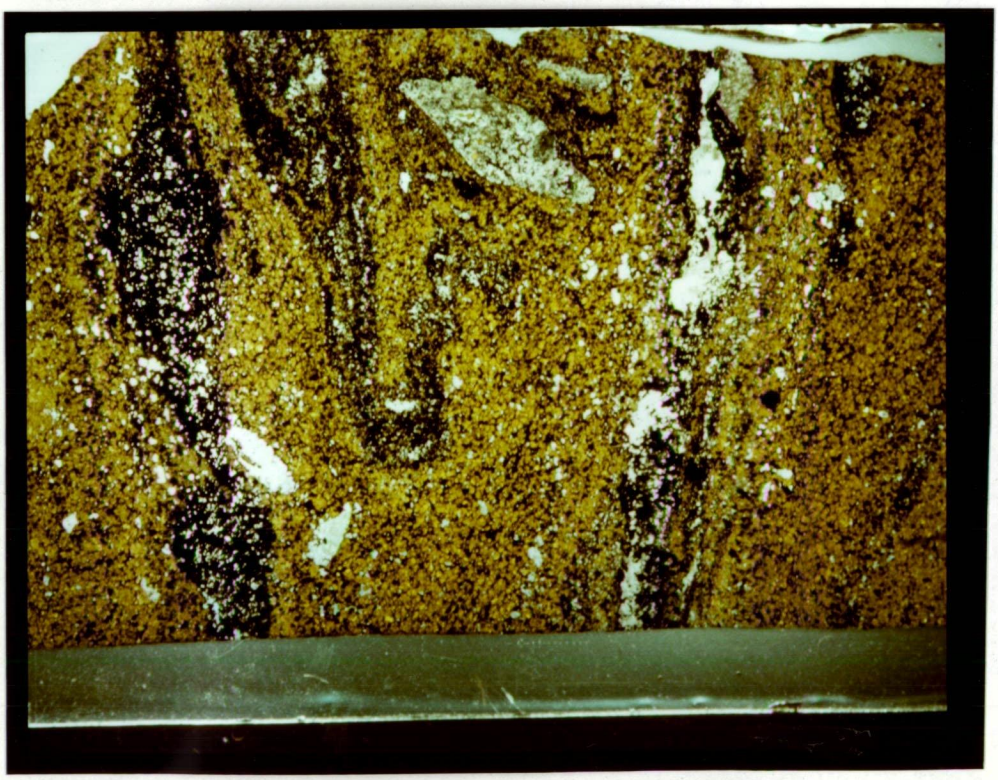

Fig.47: Folded pyrite band in massive sphalerite (106711), field length = 34 mm

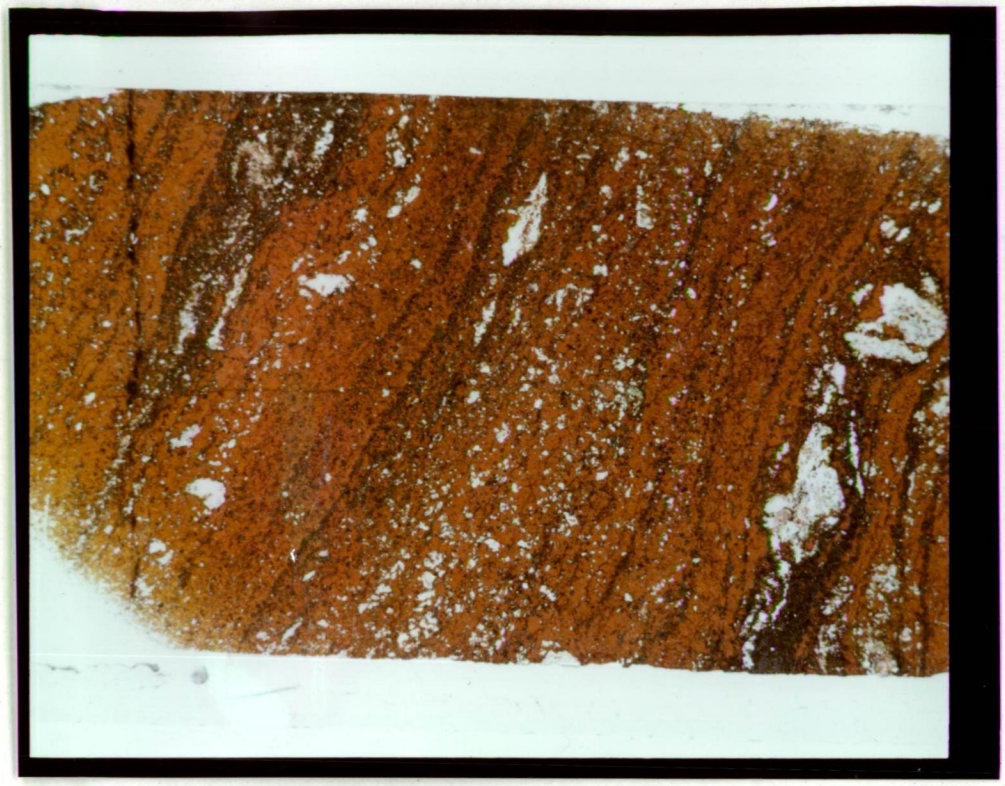

Fig.48: Pyrite bands in massive sphalerite (106704), gangue is mainly carbonate, field length = 35 mm

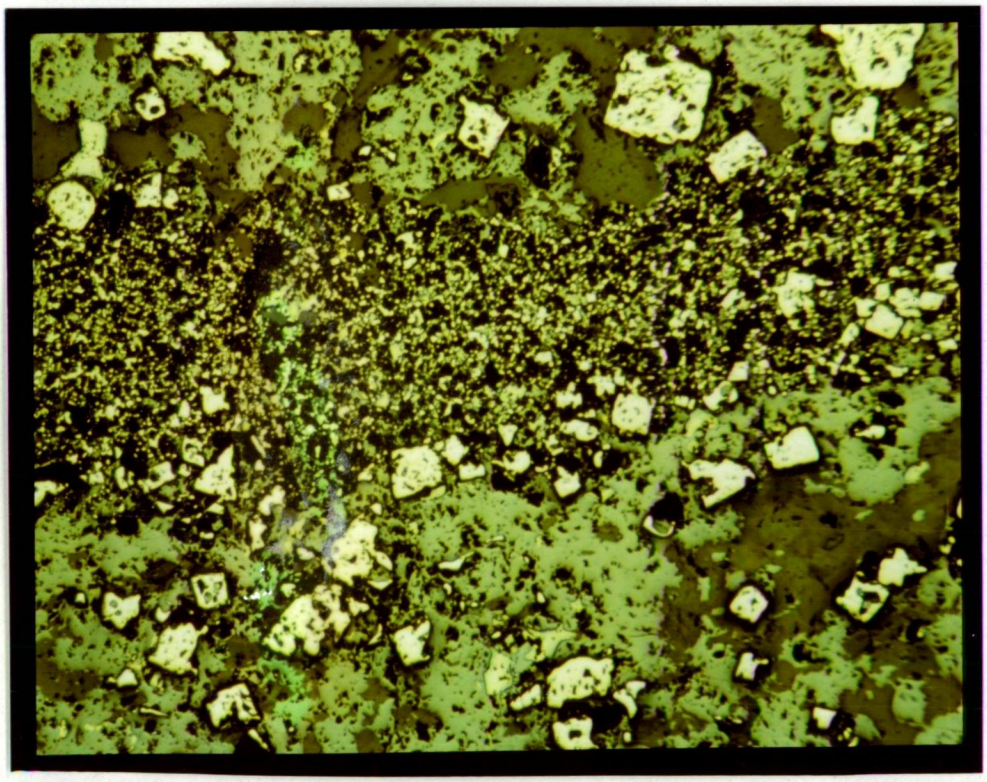

Fig.49: Micrograph (106706) with layer of fine grained pyrite (yellow), coarse resorbed pyrite grains (yellow) in sphalerite (light grey) and gangue (dark grey), field length = 2.3 mm

As well as a sedimentary origin for these textures, generation of the fine grained pyrite bands by supercritically concentrated solutions precipitating a large number of nuclei is considered possible in analogy to Liesegang rings. This leaves little material for the growth of the small crystals ignoring any supply by subsequent solution fronts ascending through the ore. The idea of introducing the main portion of the Cu-Fe ore at a later higher temperature stage into the already deposited Zn-Pb ore (Eldrige et al., 1983) could induce such a mechanism. In addition there is evidence for a post-sphalerite deposition of chalcopyrite in both stratigraphically lower and higher levels of the ore. Chalcopyrite preferably is located in galena fields, occasionally overlapping the boundary between galena and the surrounding sphalerite (fig.50). Even without assuming a replacement, this texture could be regarded as a later stage in filling of open spaces by chalcopyrite, approximately coeval with or later than galena (Dr.H-W. Matzat, pers. comm.). Small amounts of tetrahedrite in comparison to chalcopyrite are also present.

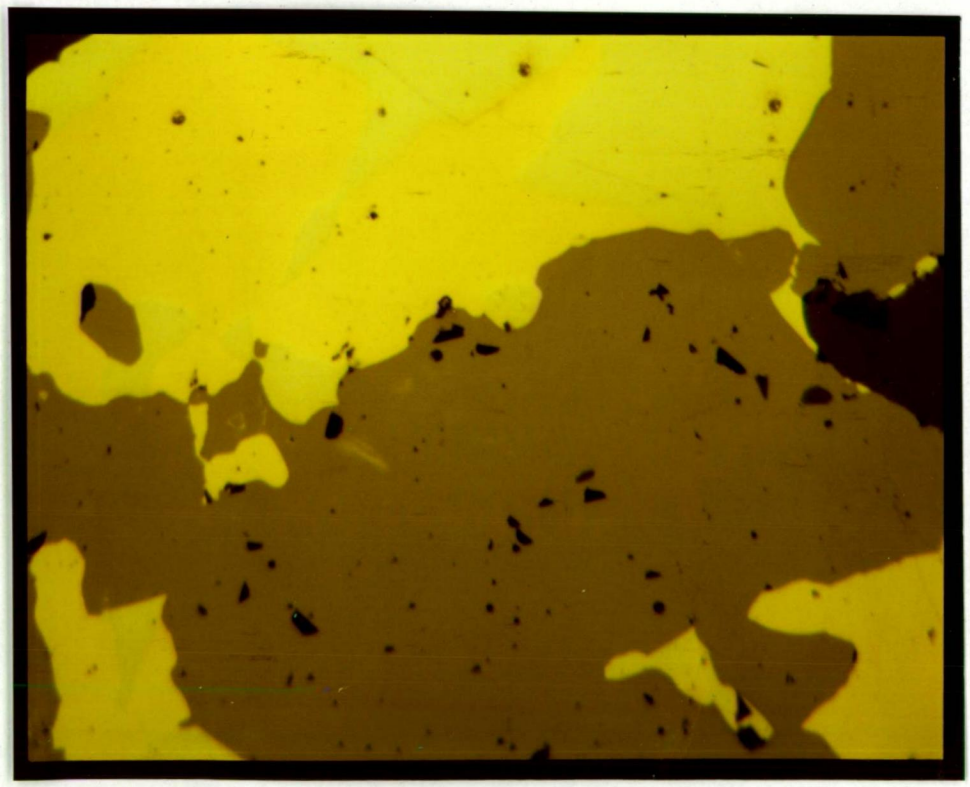

Fig.50: Micrograph (106721) with chalcopyrite (yellow) in galena (light grey), overlapping galena-sphalerite (dark grey) boundary, field length = 0.6 mm

9.4.1.2. Secondary ore textures.

The ore textures have probably been affected by the Devonian metamorphism. Pyrite and magnetite megablasts, deformation twinning and bent twin lamellae in sphalerite and polygonal textures in sphalerite, galena and chalcopyrite with triple junctions approaching 120° angles support this view (Brathwaite, 1969). Similar polygonal textures although less perfectly developed, have been found in gangue minerals like quartz, albite and coarse barite ($\leq$ 1 mm) (e.g. 106693). Larger patches of unoriented or partly spherulitic sericite and chlorite occur in a matrix of aligned sericite particularly in conjunction with elongated sphalerite blebs (106716). Also, large pyrite crystals ($\leq$ 1 mm) occasionally show fillings of sphalerite, galena and chalcopyrite (106702).

9.4.2. Pyrrhotite mineralization.

Pyrrhotite mineralization including hexagonal and monoclinic pyrrhotite exists at the southern end of the F-lens of the south orebody. It has been interpreted as a post-depositional replacement of the Zn-Pb ore because of its crosscutting relationship with the former (Brathwaite, 1969). This view has been confirmed by Vokes (1983).

9.4.3. Haematite mineralization.

Acicular haematite occurs at various locations at the top of the southern sulphide orebody (e.g. 106723) together with magnetite, pyrite and small amounts of chalcopyrite. In one case, banded pyrite-magnetite ore was found in this area (106724). Brathwaite (1969) also recorded this mineral assemblage occasionally within the Zn-Pb ore. In addition he found magnetite sporadically scattered throughout the ore. Textural evidence (106723) points to a post-pyrite formation for haematite. Green et al. (1981) reported haematite from the footwall at the southern end of the F lens at 16 level. They suggested a possible metamorphic origin similar to the finding at Mt. Lyell (Walshe & Solomon, 1981), another massive sulphide deposit south of Rosebery. However they pointed out that the formation conditions of haematite differ markedly from those of pyrrhotite, which is also considered a product of the Devonian Tabberabberan Orogeny. Haematite is also present in the ferruginous chert of the Kuroko type deposits as a

late stage exhalite (Shimazaki, 1974) suggesting a primary origin. The evidence available may suggest a dual origin of haematite.

9.4.4. Barite ore.

The barite orebody as described by Brathwaite (1969) consists of semi-massive to massive barite, and smaller amounts of sulphides, creating a fine to coarse layering. The sulphides include sphalerite, galena, tetrahedrite, chalcopyrite and pyrite, with galena and tetrahedrite enriched and pyrite depleted in contrast to the Zn-Pb orebody. At the strike limits, the barite ore grades into haematite-pyrite ore, which can also succeed barite ore stratigraphically as small concordant lenses. Gangue minerals are carbonate, sericite, albite, quartz and tourmaline. In this study barite was also found at the bottom part of the north orebody. Textural evidence (106693) suggests a late stage introduction.

9.4.5. Large scale zonation.

In this chapter, the vertical and horizontal zonation of the northern orebody is discussed. Virtually all available assay data for Pb, Zn, Cu, Fe, Ag and Au from the north orebody, which is less deformed than the south orebody were stored on a computer file, including the sample locations which had to be calculated from the drill core surveys. The large number of 3600 individual assay values prevented a listing within this thesis. The records are stored on a magnetic tape and kept in the Geology Department, University of Tasmania.

Testing the dip of the sheetlike orebody at subsequent cross sections along the north axis revealed a slightly undulated shape with a small flexure between 1067 m N and 1093 m N (3500′ N - 3600′ N).

In order to iron out some of these "wrinkles", the orebody was rotated stepwise into a horizontal position in intervals of 30 m (100′) and between 1067 - 1098 m N in intervals of 15 m (50′). This computer operation was based on the matrix equation:

$$\begin{pmatrix} E \\ L \end{pmatrix} = \begin{pmatrix} \cos\alpha & \sin\alpha \\ -\sin\alpha & \cos\alpha \end{pmatrix} \begin{pmatrix} E-I \\ L-0 \end{pmatrix} + \begin{pmatrix} I \\ 0 \end{pmatrix}$$

E = east coordinate, L = level coordinate

It interpolated the angle of dip (α) and the E-intercept (I) for each sample point according to its location along the N-axis between the measured points as indicated in fig.51.

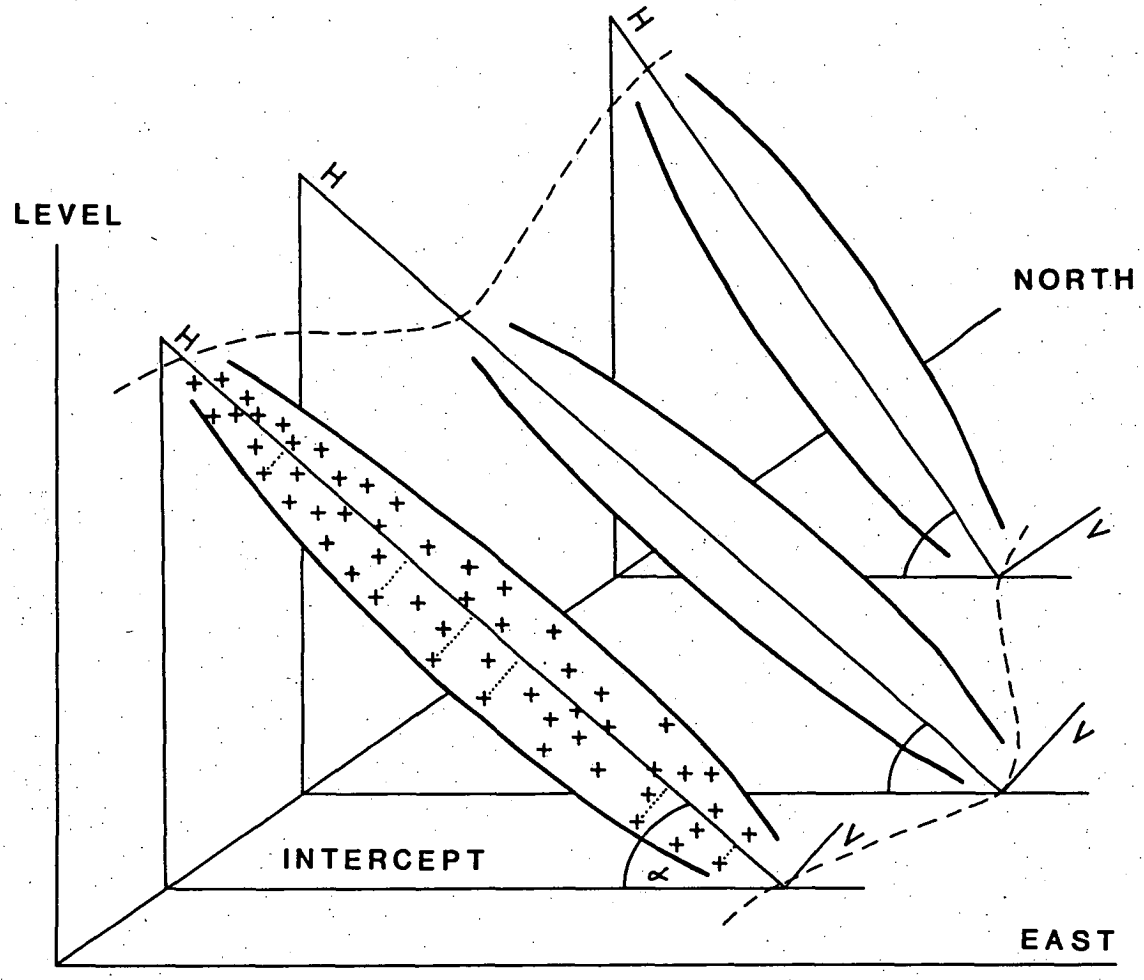

Fig.51: Schematic rotation of northern orebody: after stepwise rotation of slices according to angle of dip and east intercept along north (N), lines "H" and "V" are horizontal and vertical respectively. The H-N plane is used for horizontal metal zonation by projecting samples of bottom part of ore onto this plane. Plane V-N represents longitudinal cross section at 15 level defined by drill holes intersecting the ore at right angles

9.4.5.1. Horizontal chemical zonation.

The distribution of the above listed elements was examined within several horizontal slices. The element distributions for the bottom layer are presented in fig. 53a-f. The samples within this bottom section of approximately 3 m thickness, projected onto a plane (fig. 51, 52), were read by the program package Surface II to calculate the grid nodes by a moving average algorithm as explained in chap. 8.3.1.2.2.. Choosing a thin bottom layer offered a less disturbed metal zonation by reducing the variation of a superimposed vertical zonation. This lower zone of the orebody also uses the distribution of Fe and Cu to indicate the discharge area. Pyrite and chalcopyrite, the main Fe and Cu sulphide minerals are assumed to precipitate instantly when hydrothermal solutions are quenched on entering the sea floor (chap. 15). In addition, it enables a comparison with the metal and sulphur zonation in the immediately underlying footwall schists. The spatial correlation between the distribution patterns of footwall schists and ore base as depicted by the ore-forming elements mentioned above suggests a proximal deposition at the seafloor. The zonation for Cu (fig. 53a) and Fe (fig. 53b) reflects the distribution pattern of Cu and S

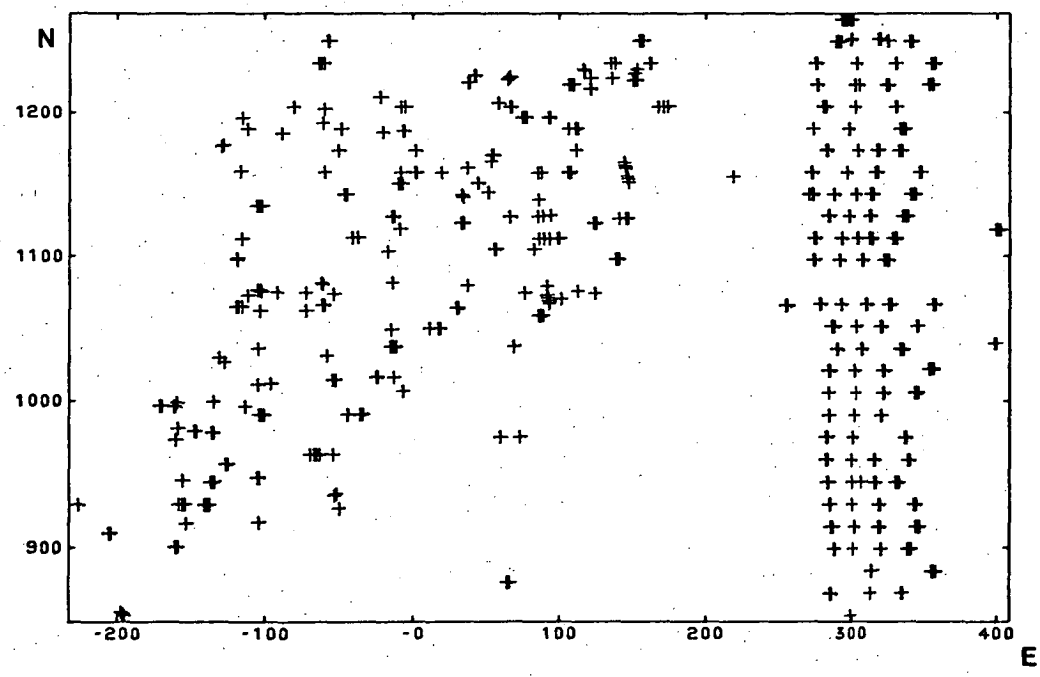

Fig. 52: Sample distribution (n = 601) within bottom layer of northern orebody rotated in horizontal position, coordinates (E, N) in metres are based on mine grid (feet), sample locations define the orebody and apply to fig. 53a-f

in the footwall schists below the orebody. This can be explained by instant precipitation of chalcopyrite and pyrite on the seafloor, or by a blocked vent system, covered by overlying sphalerite-galena ore. The wider and more uniform zonation of Zn (fig.53c) and Pb (fig.53d) above one or two areas of enrichment (vents) may indicate an unimpeded distribution of sphalerite and galena away from the rising metal-bearing solutions above the seafloor. Very similar zonations exist for Ag (fig.53e) and Au (fig. 53f). The implications of these results are discussed in chap.15. The zonations from subsequent layers (centre and top) indicate a shift to the west for the maximum ore grade.

A cubic trend surface analysis carried out on the original data after their transformation to a normal distribution (appendix 3) failed to detect a significant fit ($R^2 \leq 0.2$). The explained surface variation was greatly improved for several elements, by feeding the gridded data created by program package Surface II into the SPSS regression program. The trend surface for Pb almost achieved a perfect correlation when the smoothed grid data were used instead. Tab.8 lists the squared correlation coefficients

	R^2(unsmoothed)	R^2(smoothed)
Pb	0.70	0.92
Zn	0.47	0.81
Cu	0.19	0.40
Ag	0.60	0.89
Au	0.30	0.79
Fe	0.41	0.68

Tab.8: Goodness of fit (R^2) for cubic regression analysis based on unsmoothed and smoothed gridded data

The main reason for a poorer correlation between the fitted surface and the data of Cu and Fe, lies in their more complex distribution pattern which requires a higher order of regression than cubic. Contouring by local fitting is in this case considered more suitable than a global fit, because trend surface analysis adds an extra smoothing process to the already treated raw data.

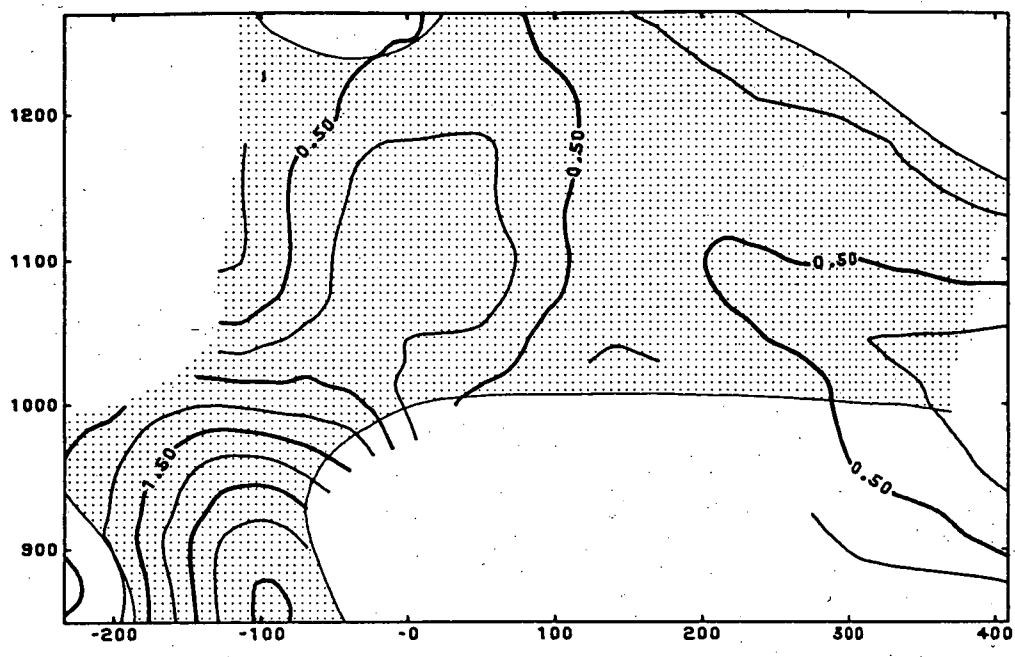

Fig. 53a: Smoothed horizontal distribution of Cu (%) in bottom layer of northern orebody. Shaded area represents $\geq$ 200ppm Cu zone in immediate footwall schists

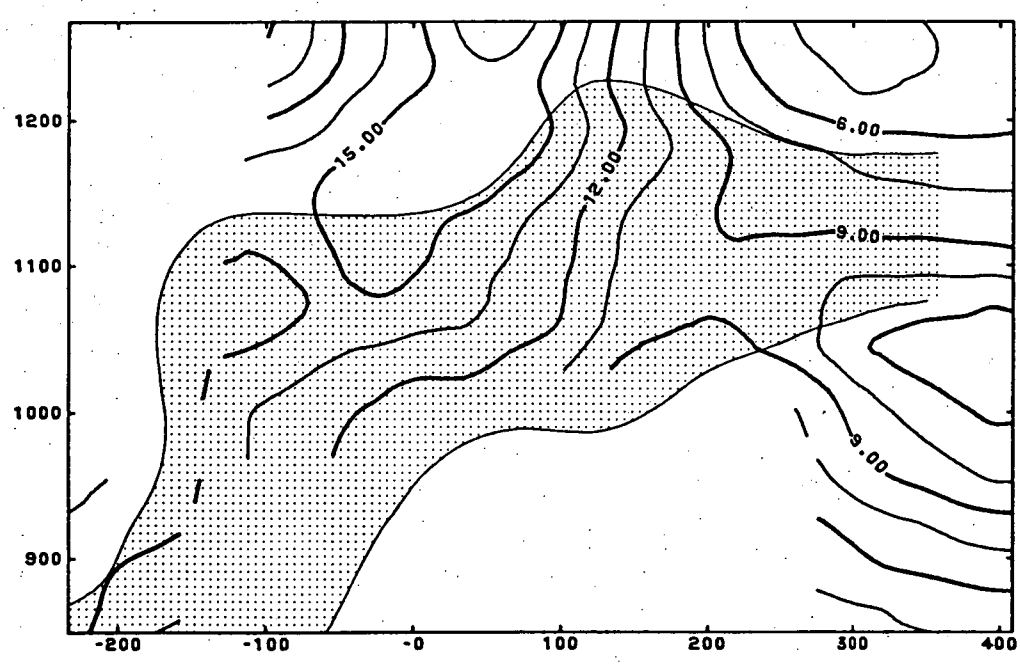

Fig. 53b: Smoothed horizontal distribution of Fe (%) in bottom layer of northern orebody. Shaded area represents $\geq$ 1.4% S zone in immediate footwall schists

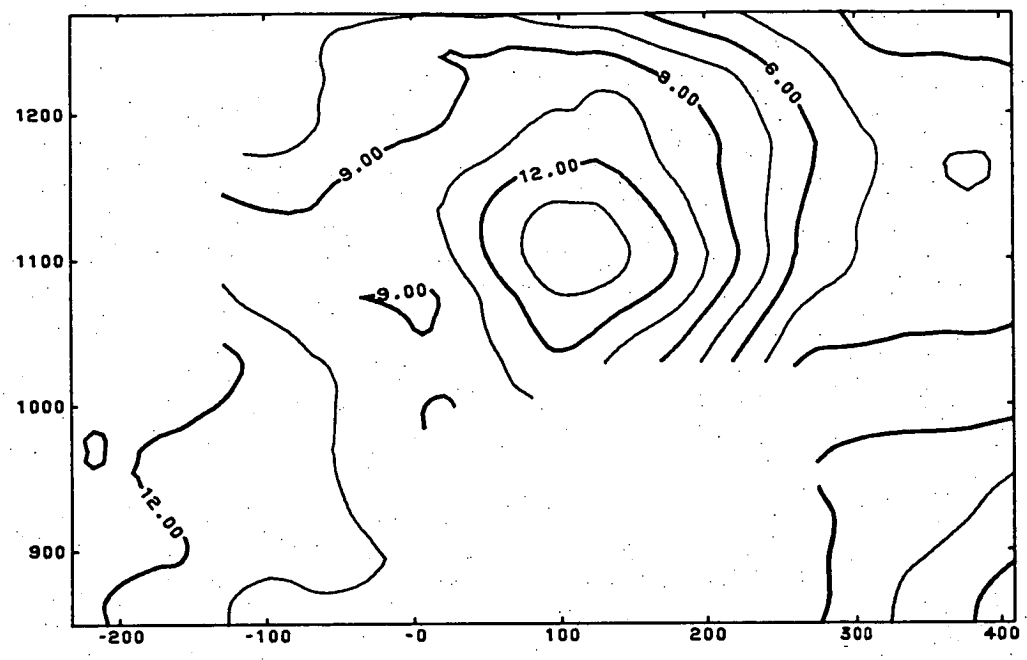

Fig.53c: Smoothed horizontal distribution of Zn (%) in bottom layer of northern orebody

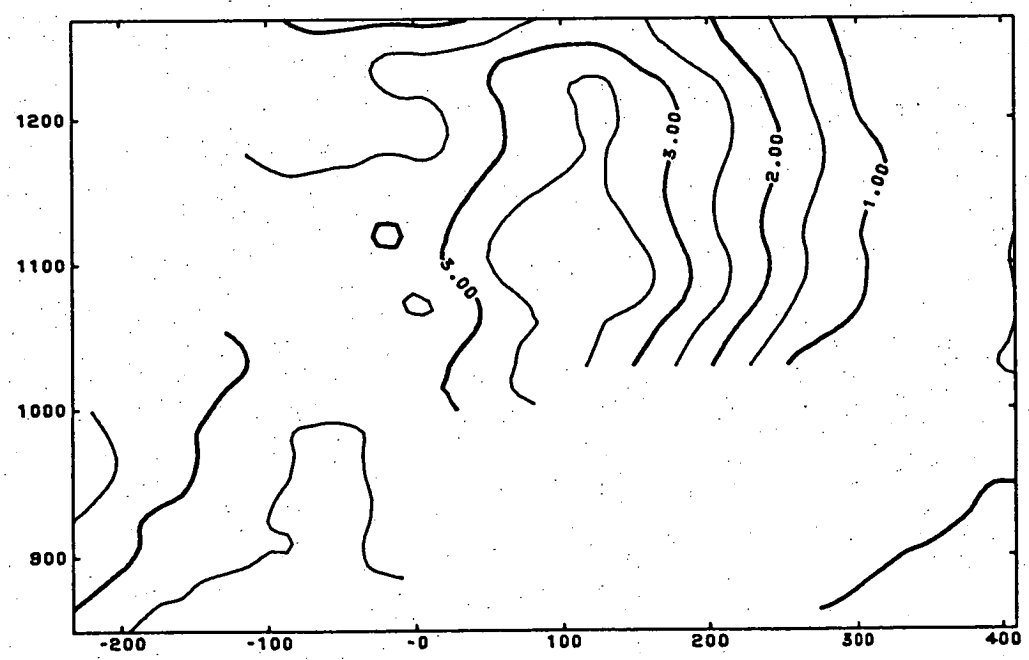

Fig.53d: Smoothed horizontal distribution of Pb (%) in bottom layer of northern orebody

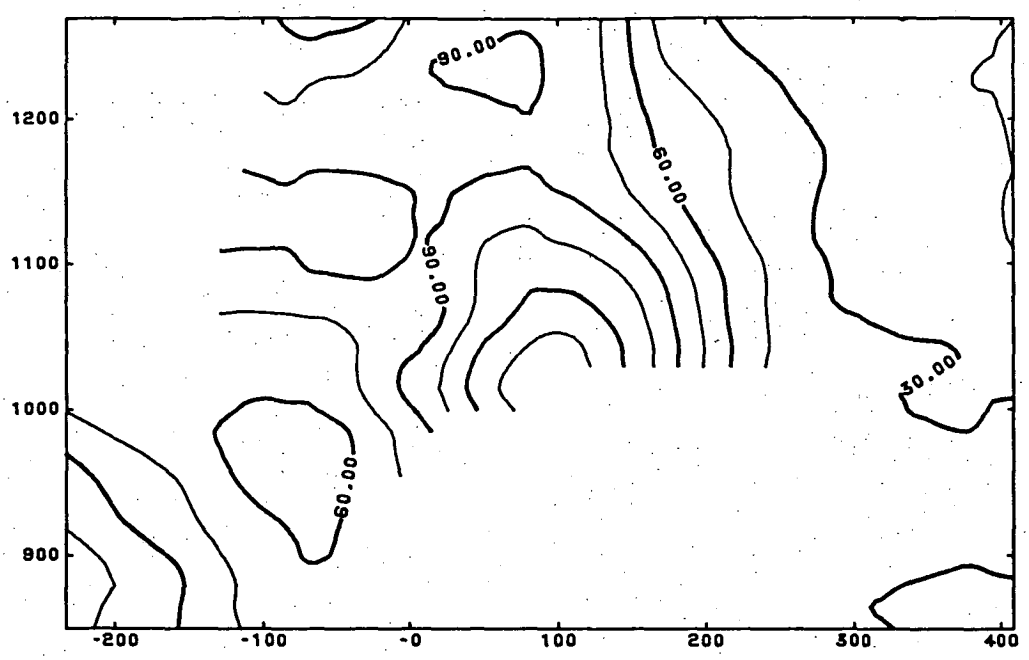

Fig. 53e: Smoothed horizontal distribution of Ag (ppm) in bottom layer of northern orebody

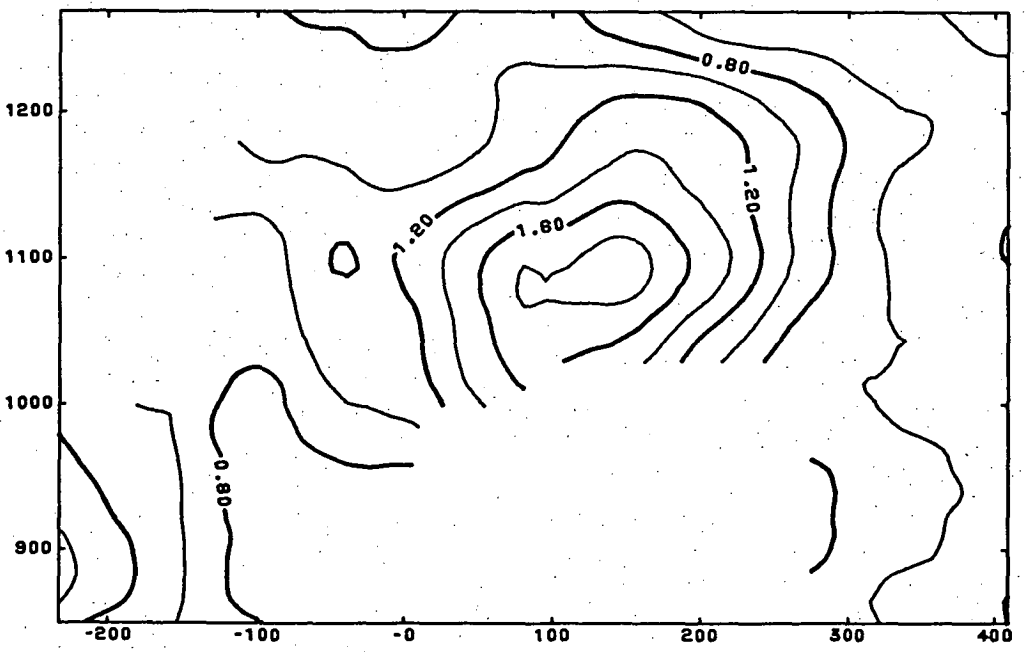

Fig. 53f: Smoothed horizontal distribution of Au (ppm) in bottom layer of northern orebody

The zonation of the southern orebody was examined by Green et al. (1981). The resulting trend surfaces essentially indicated low values for Zn, Pb and Ag in the central southern orebody, increasing towards the margin, and the opposite trend for Cu, Fe and Au.

9.4.5.2. Vertical zonation in longitudinal cross section.

The mineralogical and chemical zonation of the northern orebody has also been studied in a longitudinal cross section at 15 level. The choice of this location rather than through the maximum of the metal concentrations as indicated in the previous chapter, was determined by the availability of a densely and uniformly sampled cross section as part of a fan drilling program. This program covered the entire length of the northern orebody along strike with drilling intervals of 15m (50').

9.4.5.2.1. Mineralogical zonation.

The mineralogical zonation is based on a number of logged drill cores from 15 level intersecting the ore at right angles. From fig.54 (in back pocket), a general two fold zonation into a Cu-Fe rich base and a Zn-Pb rich top part becomes apparent similar to the southern orebody (Brathwaite, 1969; Green et al., 1981). This simple zonation is complicated by smaller sections of Zn-Pb rich ore occurring persistently throughout the bottom half of the northern orebody. This pattern is also reflected in the distribution of Pb, Zn, Fe, Cu, Ag and Au along a transverse section based on the assay data of a single drill core (see below). Post-depositional minor deformation of the northern orebody could be responsible for an inconsistent stratigraphical correlation of the lower Zn-Pb rich zone (see next chapter). On a mesoscopic (< 1 m) scale, a periodic change in the Fe and Cu content of the massive Zn-Pb ore occurs. This variation probably depends on the spacing of the fine layers as discussed above.

9.4.5.2.2. Chemical zonation.

The study of the vertical chemical zonation in longitudinal cross section was based on the same data pool as described in chap. 9.4.5. . Only rotated assay data from drill cores at 15 level that intersected the

orebody at right angles, were used, as demonstrated in fig.51. This sampling pattern provided a nearly two dimensional cross section in the N-axis-level plane without the need of a projection of stacked data. This is particularly important for a thin tabular orebody with an average thickness to lateral extension ratio of less than 0.05.

As in the case of the horizontal zonation, Cu and Fe behave in a different way compared to the remaining four elements. The relatively narrow zone of highest concentration for Zn, Pb, Ag and Au runs generally from a central bottom part of the orebody to the upper half, and proceeds from there to the southern end of the ore (fig.55a-d). The high concentration at the base could be regarded as the site of a vent releasing hydrothermal solutions onto the sea floor. Fe and Cu delineate a wider discharge area extending further south. Their maximum concentration remains in the central part ascending vertically to the top of the ore (fig. 55e, f). These patterns could lend support to the idea of a later stage introduction of the Fe-Cu ore as indicated in the previous chapter. The implications will be discussed further in chap.15.

Despite the flattening process, the rotated ore samples lack an even spread over the contoured area (fig.56a). A more regular sample grid can be achieved by using relative sample location along each drill core in percent of total length (fig.56b). This means correlating all top samples as coeval. This assumption can be accepted considering the ore forming process (chap.15) but is questionable for the bottom part. However, a slight continuous thinning for the southern half of the North orebody is still visible when considering the position of the bottom sample and the sample just below the top. If the two zones of high Pb-Zn concentration are in a wider sense regarded as marker beds (fig.54), some support for a roughly coeval base could be obtained. Also from the point of the gridding process this sample relocation is preferable in order to avoid the inclusion of top and bottom samples together in the calculation of one grid node (fig.56a, southern end). The new metal zonations in fig.57a-b portray the ascending nature of Fe and Cu more clearly. The change to the remaining elements Pb, Zn, Ag and Au due to sample relocation is negligible.

Fig.58 is presented to overcome the resolution problem due to the extreme thickness to length ratio of the orebody. This transverse section which represents most clearly a fairly common chemical cross section along

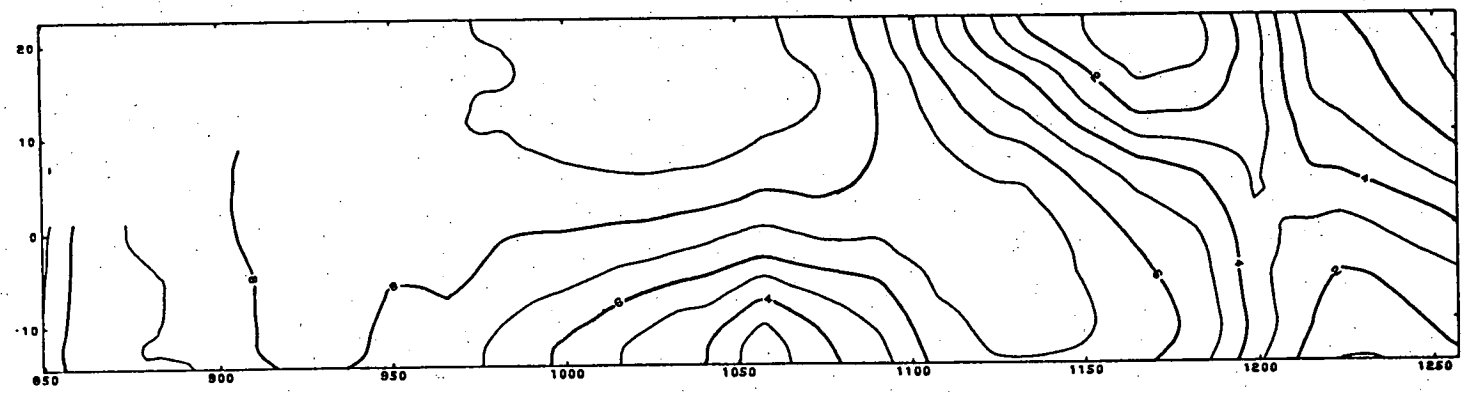

Fig.55a: Smoothed vertical distribution of Zn (%) in longitudinal cross section of northern orebody at 15 level, ore thickness (V) 2.74x enhanced, based on original sample distribution

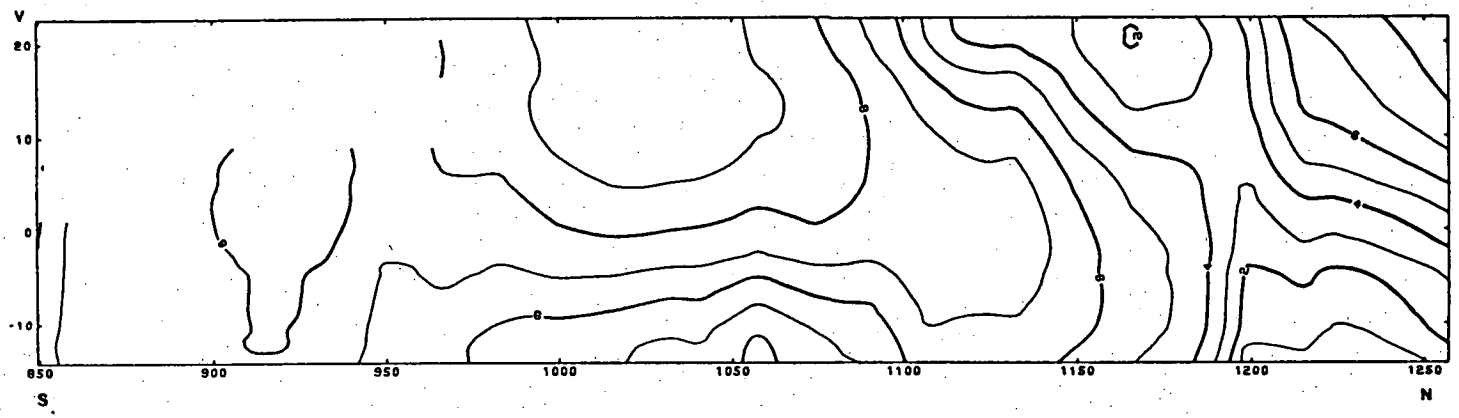

Fig.55b: Smoothed vertical distribution of Pb (%) in longitudinal cross section of northern orebody at 15 level, ore thickness (V) 2.74 enhanced, based on original sample distribution, contour lines in LOG 10 linearly spread over range of 1 - 10 to overcome large variation

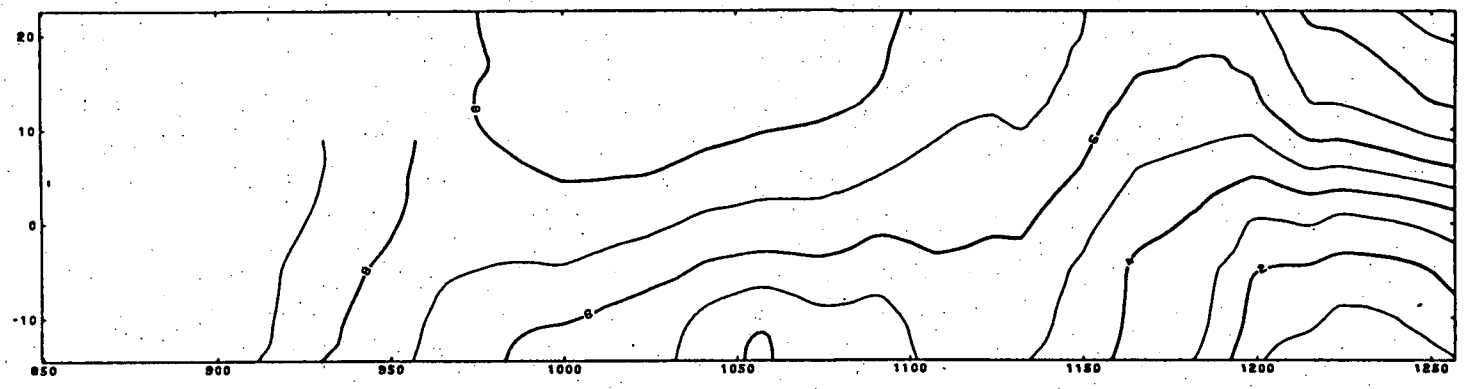

Fig.55c: Smoothed vertical distribution of Ag (ppm) in longitudinal cross section of northern orebody at 15 level, ore thickness (V) 2.74x enhanced, based on original sample distribution

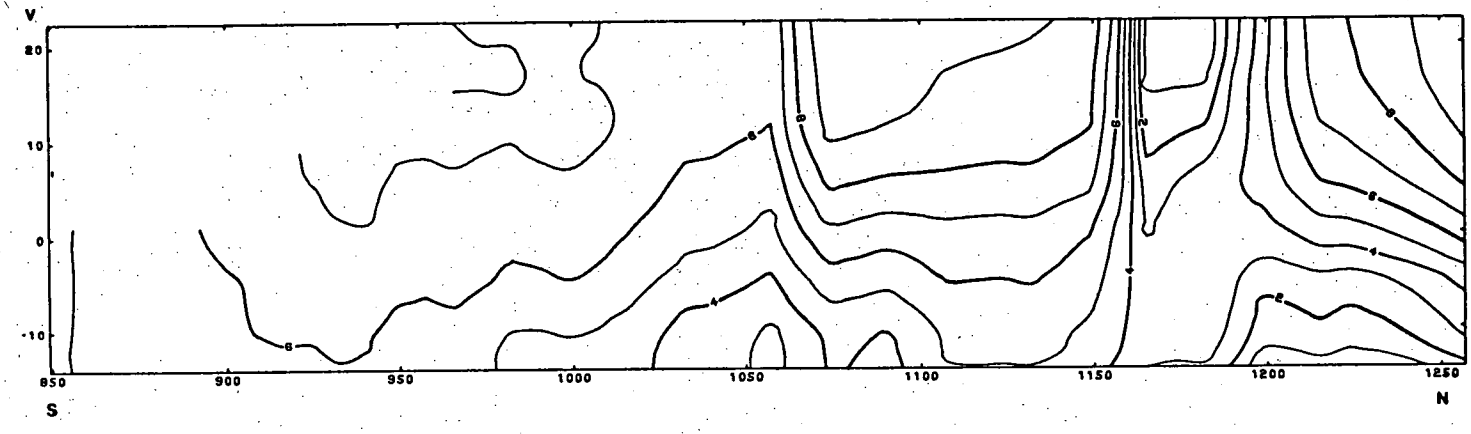

Fig.55d: Smoothed vertical distribution of Au (ppm) in longitudinal cross section of northern orebody at 15 level, ore thickness (V) 2.74x enhanced, based on original sample distribution

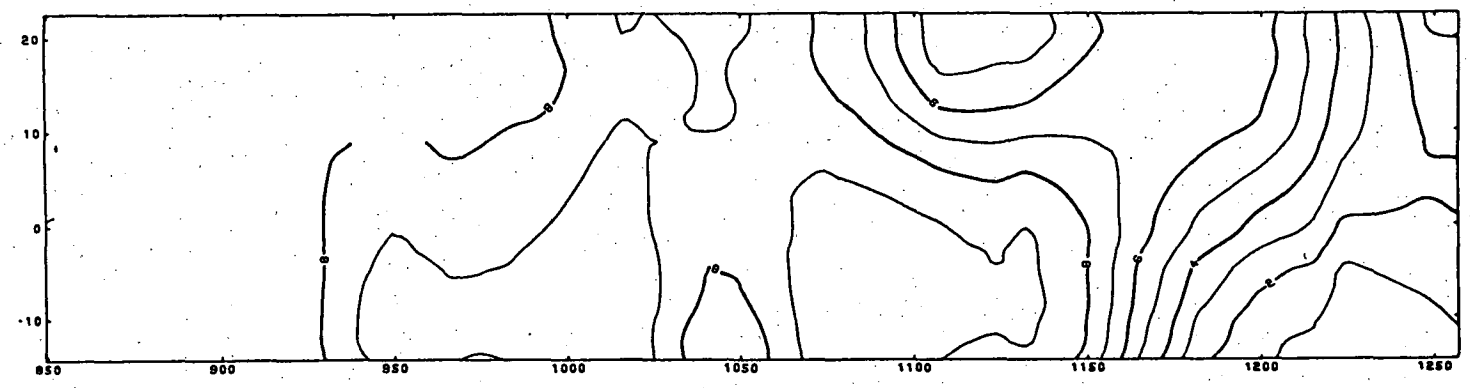

Fig.55e: Smoothed vertical distribution of Fe (%) in longitudinal cross section of northern orebody at 15 level, ore thickness (V) 2.74x enhanced, based on original sample distribution

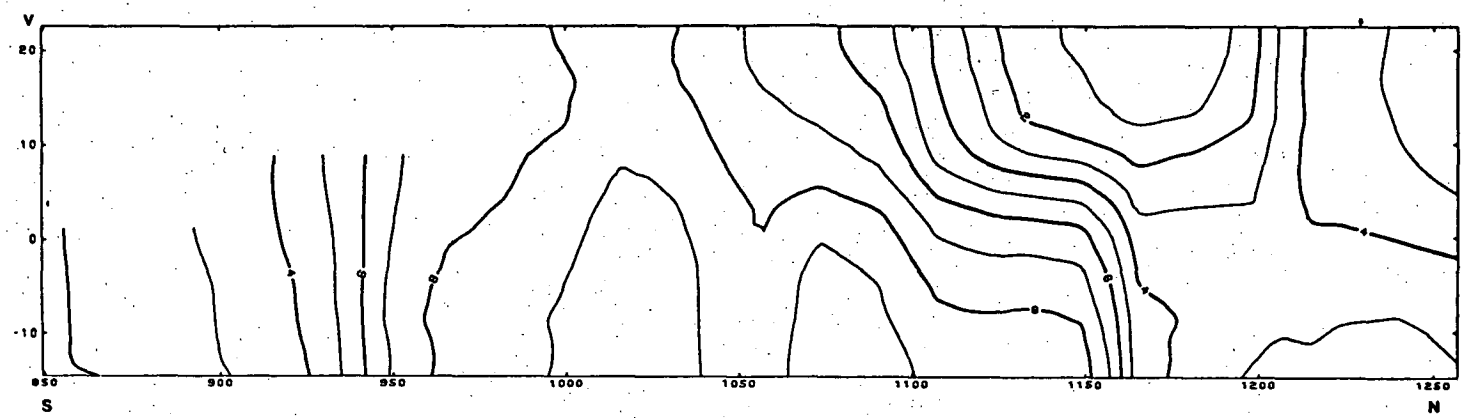

Fig.55f: Smoothed vertical distribution of Cu (%) in longitudinal cross section of northern orebody at 15 level, ore thickness (V) 2.74x enhanced, based on original sample distribution

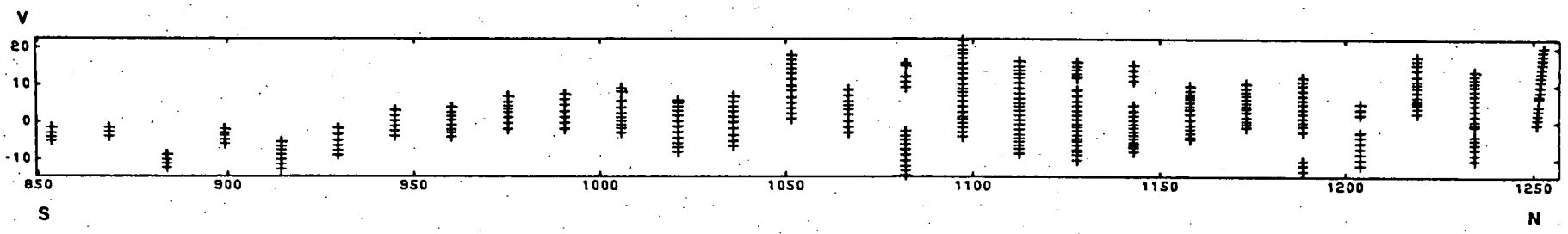

Fig.56a: Original sample distribution (n = 321) in vertical longitudinal cross section of northern orebody at 15 level, coordinates (N, V) in metres based on mine grid (feet), true thickness, sample locations apply to fig.55a-f

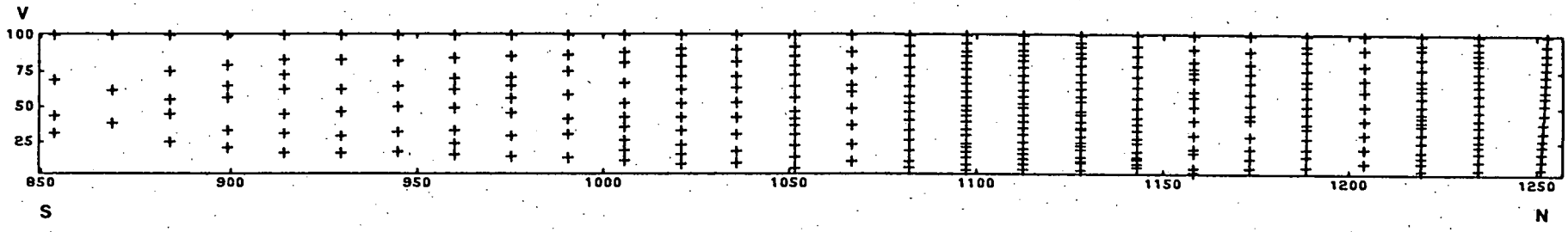

Fig.56b: Relocated sample distribution locations in each drill core are calculated as percent of ore thickness and are used in fig.57a, b

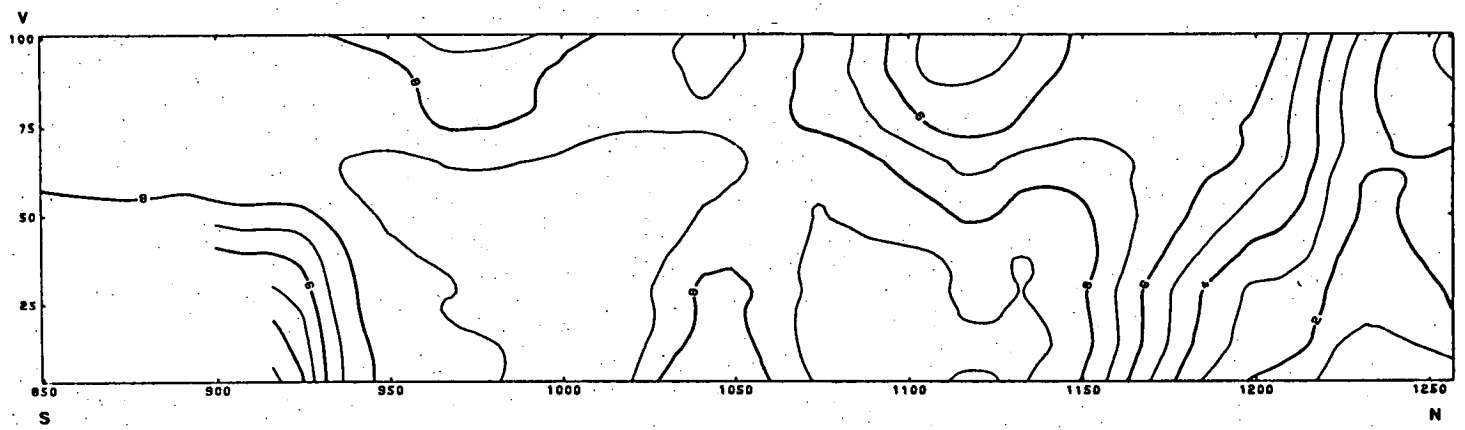

Fig.57a: Smoothed vertical distribution of Fe (%) in longitudinal cross section of northern orebody at 15 level, ore thickness (V) 2.74x enhanced, based on relocated sample distribution

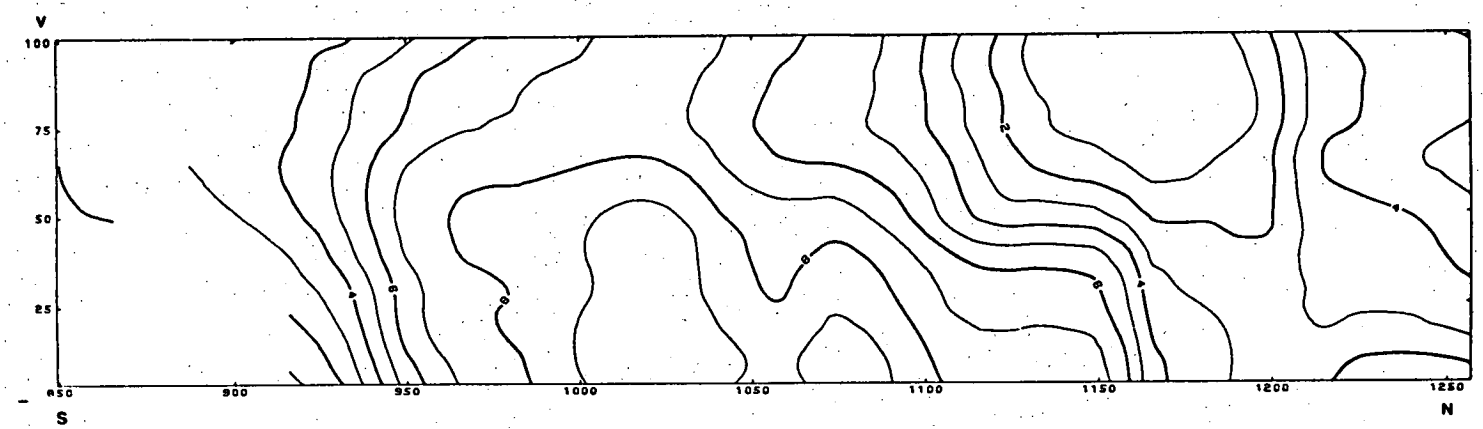

Fig.57b: Smoothed vertical distribution of Cu (%) in longitudinal cross section of northern orebody at 15 level, ore thickness (V) 2.74x enhanced, based on relocated sample distribution

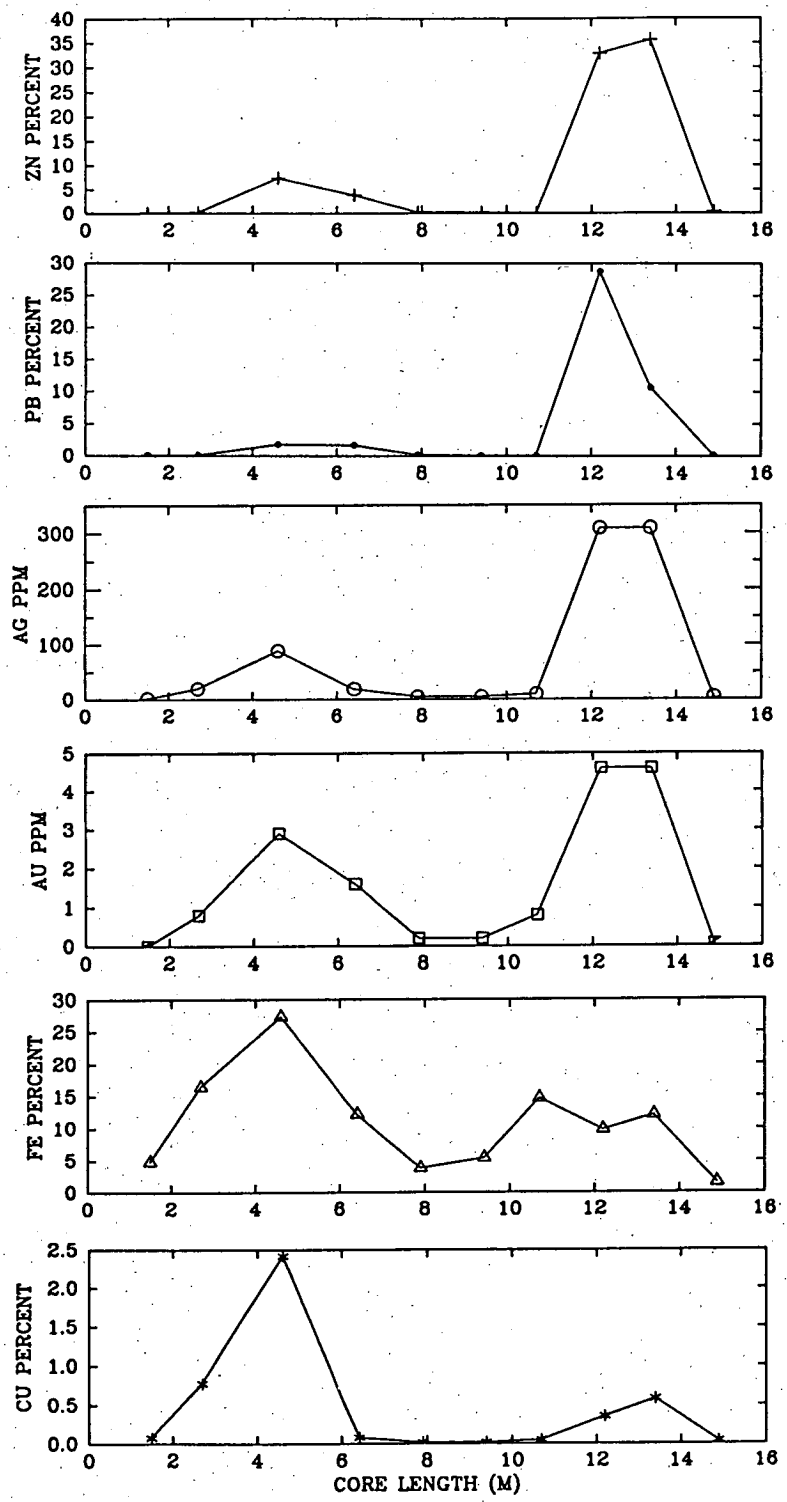

Fig.58: Metal distribution in transverse section along DDH 3169 (1036 m N /3400' N) through northern orebody at 15 level, from bottom (left) to top (right) of ore

drill cores of the southern two thirds of the northern orebody underscores the assumption of two different marker horizons as in fig.54. Two peaks exist for Cu-Fe and Pb-Zn with opposite trends for the maximum grades. Metal ratios such as Pb/Zn, Cu/Fe and Cu/Pb+Zn tend to follow a similar pattern with higher values at the base and top part of the ore.

To test the metal correlation on 15 level, the normally distributed (log 10) metals were used to calculate Pearson's correlation coefficients (tab.9a). In addition, Spearman's rank order correlation (Nie et al., 1975) was also performed on the original data as a double check. These coefficients based on a nonparametric procedure generally agree quite well (tab.9b) with the above mentioned correlation coefficients. The important feature which is apparent from both correlation matrices is the positive correlation between all metal elements. A partial correlation was performed on the normally distributed metals to correct for the influences of the remaining elements on the variable pair under examination. As a result, the correlation between most elements was significantly reduced except for the Pb-Zn pair (tab.9c). This method also failed to come up with a significant negative correlation between the element groups Pb-Zn and Cu-Fe, which would be expected if the orebody had a clear cut zonation of a Cu-Fe-rich base and a Pb-Zn-rich top. As sulphide and gangue combined form a closed system, the positive correlation can be expected to be better than shown. The large pool of assay data of the northern orebody will certainly provide further insight into the zonation and mechanism of ore deposition.

9.5. Host rock shale of the mine.

The hydrothermal alteration has largely obliterated the contact between footwall schists and host rock shale. If present it can be recognized by the slaty cleavage of the shale. The difference between host rock shale from the field and the main alteration underground is the same as explained for the footwall schists. Carbonate frequently occurs as nodules draped by sericite and with quartz pressure shadows as shown in fig.59, and the chlorite content is less uniform.

Brathwaite (1969) reported slightly sheared crystal tuff from the north and south end of the mine above the ore horizon and around 2500 N on 12 level which is in the barren gap (fig.60). In this study moderately to

Pearson's correlation coefficients

	Pb	Zn	Cu	Ag	Au	Fe
Pb						
Zn	0.87					
Cu	0.58	0.66				
Ag	0.77	0.68	0.52			
Au	0.69	0.63	0.52	0.70		
Fe	0.42	0.42	0.51	0.34	0.36	

Spearman's correlation coefficients

	Pb	Zn	Cu	Ag	Au	Fe
Pb						
Zn	0.87					
Cu	0.60	0.70				
Ag	0.76	0.69	0.56			
Au	0.70	0.65	0.54	0.72		
Fe	0.43	0.43	0.49	0.36	0.39	

Partial correlation coefficient

	Pb	Zn	Cu	Ag	Au	Fe
Pb						
Zn	0.70					
Cu	-0.14	0.38				
Ag	0.40	-0.05	0.10			
Au	0.17	0.01	0.13	0.36		
Fe	0.10	-0.01	0.33	-0.04	0.04	

Tab. 9: Correlation of ore forming element

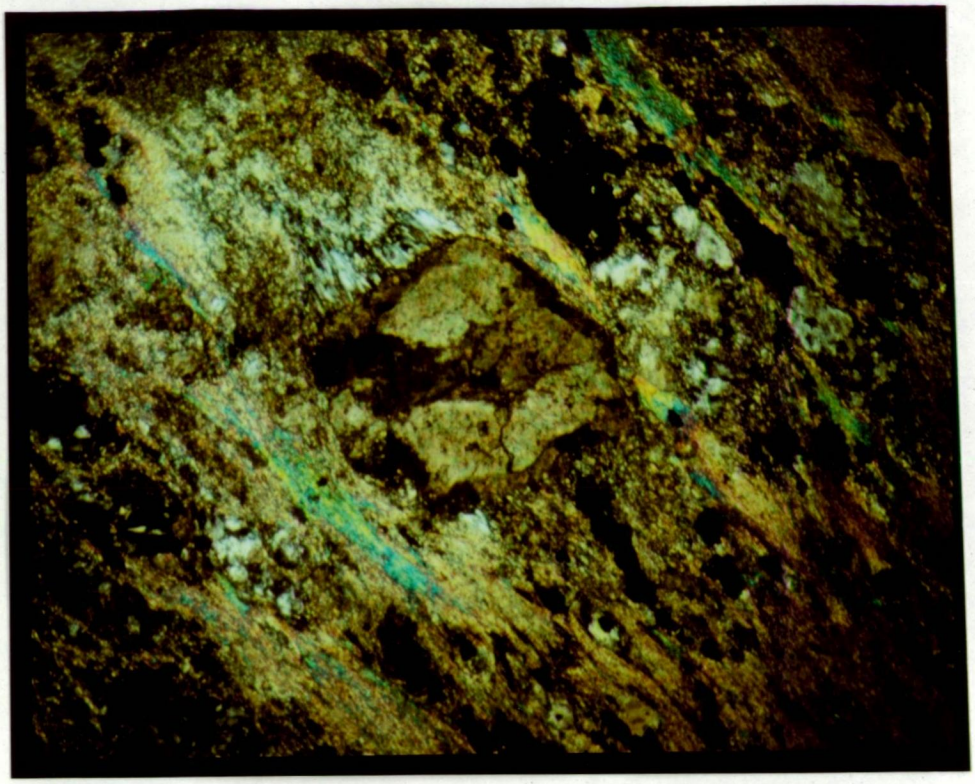

Fig.59: Carbonate nodule with quartz pressure shadow in sericitic host rock shale, (68043), field length = 4.6mm

strongly sheared crystal tuff were also found below the ore horizon between 2100 N and 2600N (e.g. 68085, 68034). Green et al. (1981) in their model for the generation of two separate orebodies suggested an elevation representing the barren gap at the time of deposition. Mine maps however show a continuation of host rock shale and black slate between the two orebodies. It is now obvious from the alteration zone below the northern orebody (as discussed above), that two hydrothermal vents separated by a few hundred metres must have existed, leaving a small area less affected by hydrothermal fluids in between (fig.60).

Crystal tuff is also widespread above the northern orebody. The crystal component can dominate completely to the point that very little or no matrix remains. The feldspar phenocrysts ($\leq$ 3 mm), are frequently fractured and occasionally rounded. Their state of alteration ranges from relatively fresh to advanced altered. Quartz grains ($\leq$ 1.5 mm), fractured and embayed, form the dominant crystal component in a few cases. The crystal tuffs probably represent primary and reworked pyroclastics. In particular, those with little ash sized matrix remaining have undergone epiclastic processes (e.g. 68033). This problem has been discussed by Eastoe (1973).

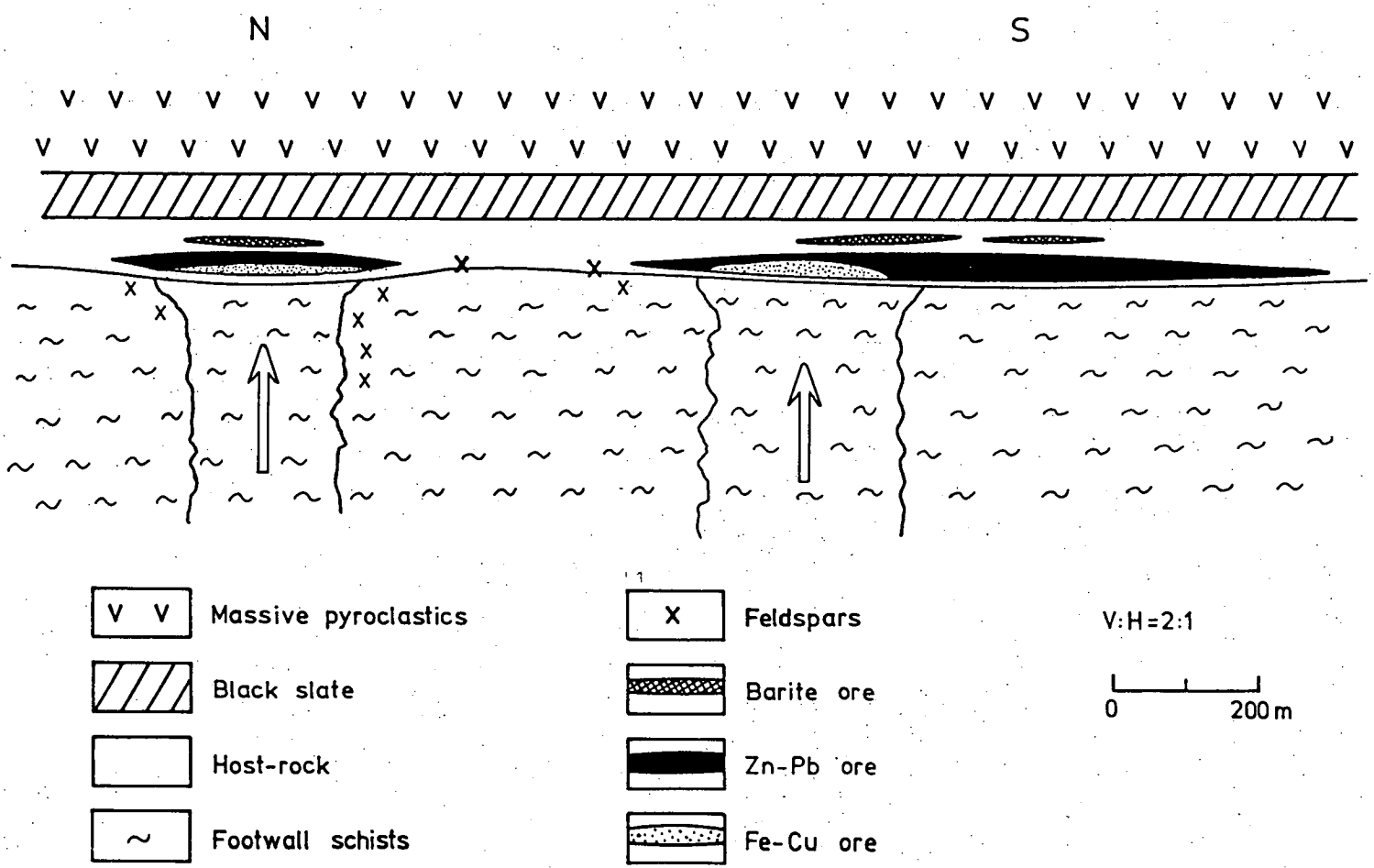

Fig.60: Reconstruction of the Rosebery ore deposit with two orebodies capping two independent hydrothermal vents, longitudinal cross section. Vent below southern orebody, according to Green (1983)

9.6. Black slate in the mine.

The host rock is succeeded at a sharp contact by black slate (fig.61), which can be used as a marker horizon.

Black slate is partly missing above the southern orebody. In the gap, fragments of black slate in the order of tens of centimetres are present in the massive pyroclastics which indicates a scour. Brathwaite (1969) recognised the disconformity as evidence for the east-facing of the mine sequence.

Coarse grained sandstone beds exist locally near the top of the black slate. They have been interpreted as detritus transported from the Tyennan Nucleus (Brathwaite, 1969; Green et al.,1981). Above the northern orebody, black slate is occasionally interbedded with host rock shale and crystal-lithic tuff reflecting changes in the geological environment (e.g. DDH 46R, DDH 3268).

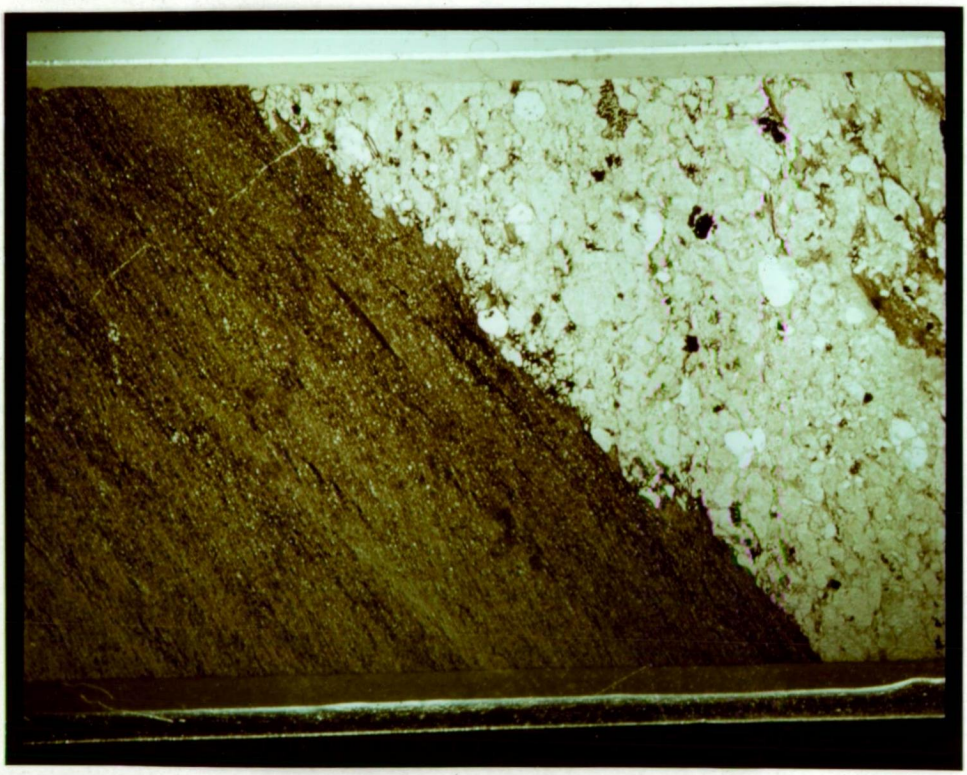

Fig.61: Contact host rock-black slate, host rock consists of altered reworked tuff, cleavage in black slate is oblique to bedding, (68028), field length = 36mm

9.7. Massive pyroclastics in the mine.

Hydrothermal alteration has probably influenced the massive pyroclastics immediately above the black slate to various degrees. This is demonstrated in fig. 62 by decreasing Na_2O content and increasing K_2O content. Plagioclase can be in an advanced stage of alteration, and more important, the alignment of matrix sericite is at least partly due to shearing and is similar to that of the footwall schists. Feldspar phenocrysts and coarse fractured quartz grains are abundant (e.g. 67955). From roughly 70 m above the northern orebody, moderately altered plagioclase is the dominant crystal component. Pumice ($\leq$ 1 cm) and streaky glass shards can be identified in the less altered tuffs (DDH 46R). According to Brathwaite (1969) a bottom layer of about 75 m crystal-lithic tuff is overlain by 300 m of predominantly vitric tuff above the central part of the southern orebody. This is also reflected in the field along the Murchison Highway.

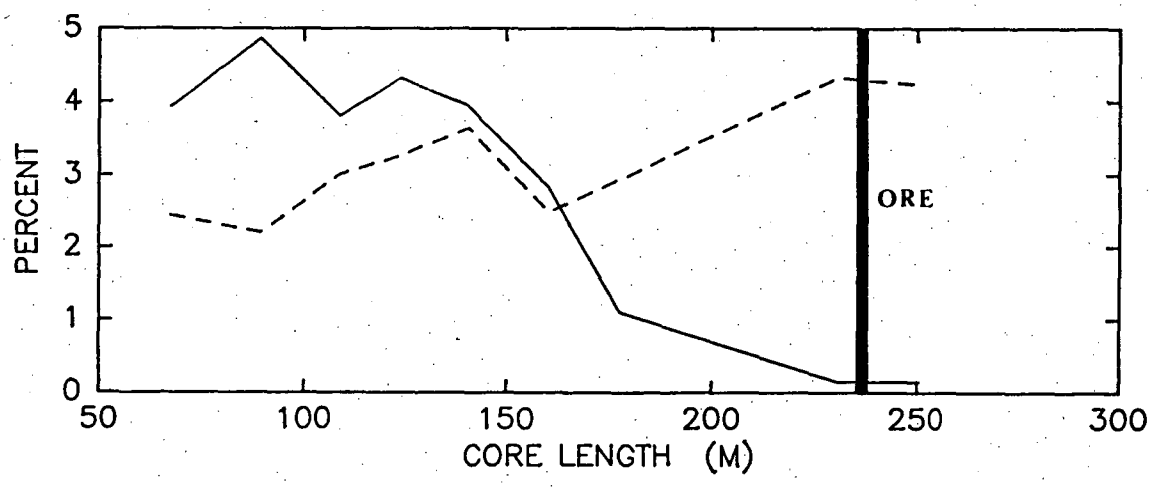

Fig. 62: Increasing alteration in massive pyroclastics (DDH 46R) moving down towards ore, Na_2O: continuous line, K_2O: dashed line

9.8. Underground and surface alteration combined.

Both alteration patterns, in the field and underground, have been discussed separately above. In a three-dimensional picture it is possible to combine the most altered zone immediately below the two 45° east dipping orebodies underground with the alteration in the field.

On the surface, east of Karlson's Knob (fig.6b, 7), the host rock containing the northern orebody is underlain by relatively fresh footwall pyroclastics. This is in agreement with the underground geology where the northern orebody is capping a $\geq$ 300 m wide zone of intensive alteration surrounded by feldspar-bearing schists. The feldspars vary from relics to moderately altered plagioclase. Over a distance of roughly 300 m from the centre of the northern feeder pipe to the surface, the alteration peters out completely as demonstrated in fig.63.

Further south, the host rock containing the larger southern orebody is underlain by siliceous augen schists which in turn are succeeded stratigraphically downwards by schists including K-feldspars and relics. Thus the whole surface alteration can be attributed to the southern orebody. Fig.63 illustrates the alteration surrounding the southern orebody.

The footwall schists at the top of the mine office car park seem to be less sheared, and are probably not far away from the alteration boundary of the southern orebody. The larger alteration zone below the southern orebody can be explained by a more extensive infiltration of the wall rock by hydrothermal fluids. The surface morphology along the western flank of Mt. Black helps to expose the footwall alteration at the southern orebody. In fig.63 there is a drop of 100 m in altitude from the northern surface to the surface of the southern cross-section. The position of the mine on the west flank of Mt. Black means that the unaltered footwall pyroclastics have been eroded.

In summary, the alteration aureole below the northern orebody has a diameter of roughly 300 m. For the southern orebody, the diameter exceeds 800 m normal to strike, using Green's et al. (1981) model for the feeder channel. These estimates were calculated for a flat lying ore deposit. By comparison, the width of the alteration on the surface below the southern

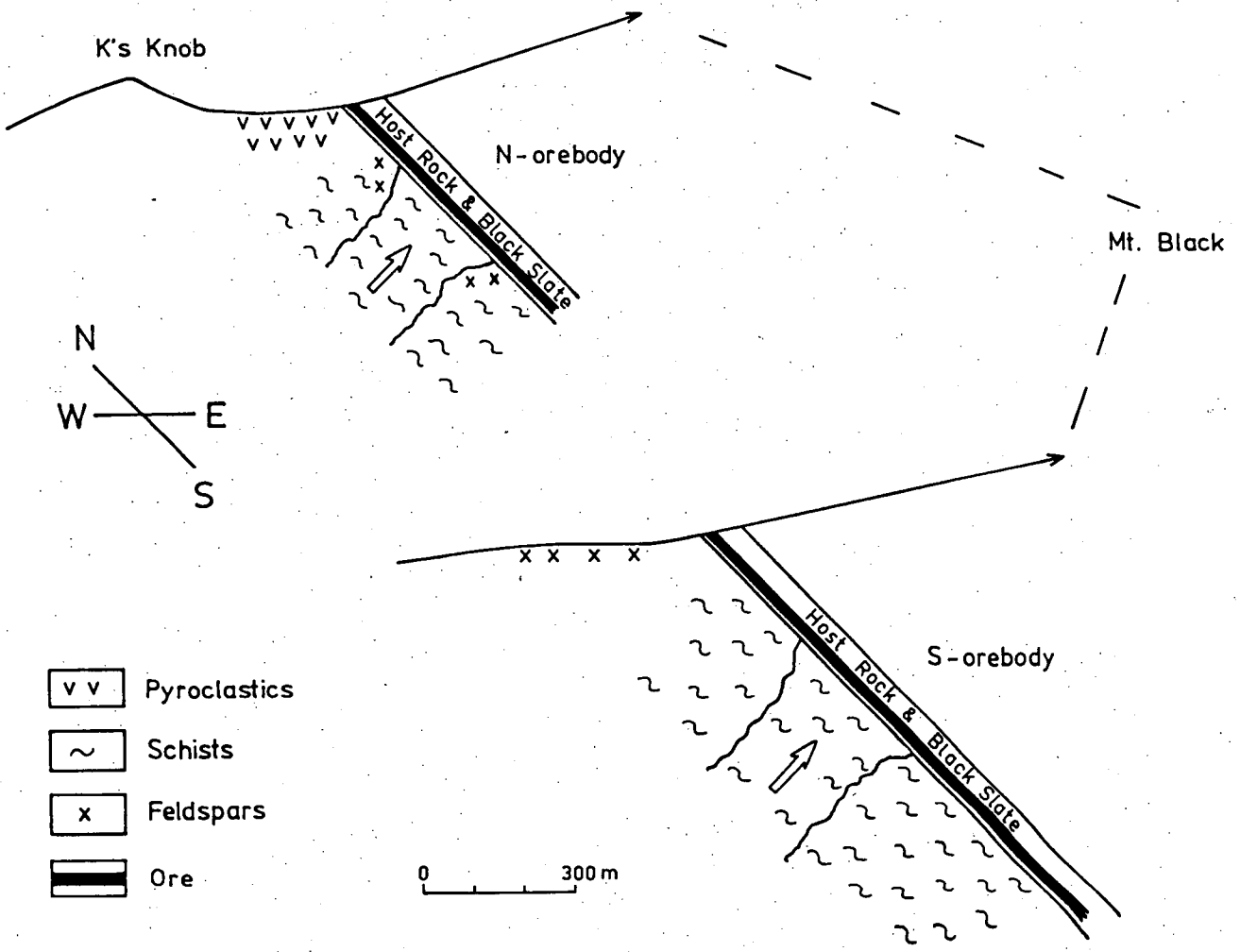

Fig.63: Surface and underground alteration combined based on two E-W cross sections, through southern and northern orebody

orebody extends in NNW direction for about 1400 m - 1500 m, extending considerably beyond the surface limits of the southern orebody. If, however, the maximum length of the orebody in this direction at lower levels (underground) is taken into account, a good spatial match between size of the orebody and the footwall alteration can be demonstrated. This estimate is not to be confused with the maximal extension of the surface alteration of about 2 km, due to a northerly strike. In east-west direction, the exposed schistose alteration area stratigraphically below the southern orebody extends over 700 m (fig.6a, b, 7, chap.6).

The restriction of the wall rock alteration, geochemically and geologically, to the lateral limits of the ore puts the Rosebery deposit in line with the majority of the Canadian Archaean deposits (Spence & de Rosen-Spence, 1975). A similar case exists south of Rosebery at Mt. Lyell. According to Cox (1981) the Na-depleted altered volcanics extend over 8 km within the mine field. However, Goodfellow (1975) described the chemical halo at the Brunswick No. 12 deposit as extending 500 m laterally away from the ore. Marcotte and David (1981) were able to trace the geochemical alteration of deposits in the Abitibi belt as far as 2.3 km based on discriminant analysis. According to Date et al. (1979, 1983) the Na-poor dacite underlying the Fukazawa deposits stretches over a 1.5 x 3 km area exceeding well beyond the deposits.

10. Mineralogy.

A number of polished thin sections were used to investigate the chemical composition of the most common rock-forming minerals in altered and unaltered rocks by micro-probe analysis. Point and area scans were carried out, and both achieved the same results. The K-feldspars were also examined by XRD-analysis to determine their temperature state. This study excludes a detailed examination of the ore mineralogy.

10.1. Feldspars.

The feldspars in the vicinity of the Rosebery deposit display variable chemistry and appearance. They may contain small amounts of Mg, and particularly Fe and Ti. P and Cr are present infrequently, and Mn is rare. Small quantities of these elements can be incorporated in the crystal lattice (Deer, Howie & Zussman, 1966), larger amounts however are presumably caused by chlorite and mica inclusions. The composition of the feldspars examined (appendix 4) does not reflect any zonation with respect to the hydrothermal alteration, although their abundance and nature does as discussed below.

As pointed out in chap.6.4.-6.5., the coarse grained plagioclase and alkali-feldspar phenocrysts are primary, of volcanogenic origin, some of which could have been albitized during the hydrothermal and/or metamorphic event. The mottled, partly altered K-feldspar phenocrysts in the surface alteration zone probably are also igneous feldspars with a secondary overprint. In one case (67824), coarse microperthite was found in the unaltered massive pyroclastics.

Apart from these igneous feldspars, there exist other types which may be of metamorphic origin, such as the fine to medium sized albite and microcline crystals, and feldspars of hydrothermal origin, as in the case of albite subhedra associated with the ore. Fig.64 shows the chemical distribution of averaged primary feldspar compositions. Secondary feldspars plot in the K-feldspar and albite corner. The feldspars were grouped according to their composition (Deer, Howie & Zussman, 1966) and mode of occurrence.

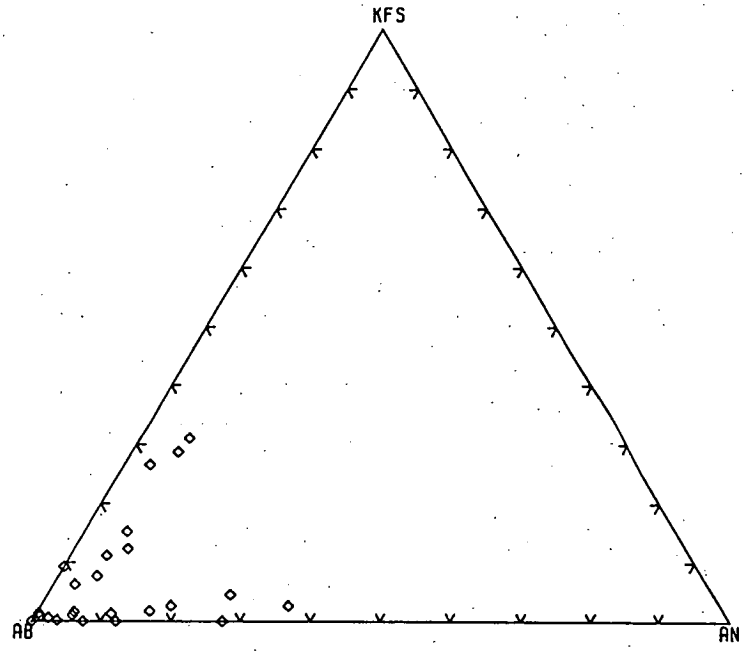

Fig.64: Composition of coarse grained primary feldspars, according to the method of Deer Howie & Zussman (1966), secondary feldspars plot in Kfs and Ab corner

10.1.1. Coarse grained feldspars.

The coarse and frequently fractured feldspars represent the main crystal component in the volcanic rocks. They are usually sericitized to various degrees. Solomon (1964) reported 2V-readings, of what he called albite, which indicated both high and low temperatures of formation. He therefore concluded a possible "secondary" origin derived from earlier crystals of different composition. Hall (1967), using the same method, and Brathwaite (1969), employing measurement of extinction angles and XRD-analysis, regarded the coarse feldspars as low temperature albite.

Microprobe analyses of coarse felsdspar from this study are plotted in fig.64. According to their composition, the feldspars exhibit two trends, alkali-feldspar ($\leq Kfs_{31}$) and plagioclase ($\leq An_{36}$), which converge in the albite corner. They probably represent the original composition of volcanogenic feldspars. The plagioclase do not reflect the peristerite gap (An_5 - An_{20}) which should become effective below 350°C (Trøger, 1969). The alkali branch has an An content of less than An_8. The amount of Kfs in the plagioclase does not exceed Kfs_5. The majority of examined thin sections plot in the albite corner which, together with the unstable compositions at

low temperatures perhaps indicates an incomplete albitization in the post-eruptive period. This assumption is further supported by the existence of coarse grained micro-antiperthite (Kerr, 1977), which was recognised in one section. Metamorphic albite of the greenschist facies should be essentially free of K_2O and also should not exceed An_8 (Turner,1981).

10.1.2. Coarse grained K-feldspar.

Coarse grained, partly altered and mottled K-feldspar is the only remaining species in the altered schists in the field, except for unidentifiable relic grains. Infrequently the mottled K-feldspars exhibit polysynthetic microcline twinning. This is the consequence of a transition from a higher temperature configuration with random Al distribution in a monoclinic crystal lattice, to a low temperature state with a more ordered Al distribution in a triclinic crystal lattice (Tröger, 1969). The XRD-method of Wright (1968) was used to determine the temperature configuration of four samples. Although they did not plot in his 2θ (060-$\bar{2}01$-$\bar{2}04$) diagram, the determined X-ray pattern compared best with that of Wright's (1968) intermediate microcline. This structural configuration could have been achieved either by re-equilibration of volcanogenic sanidine or by changes in the lattice of metamorphic microcline after reaching peak temperatures of $400^{o}C$.

The partial sericitization of the microcline, and the lack of any preserved plagioclase can be explained by the stability fields of K-feldspar and albite in the log $a_{Na}+/a_{H}+$ vs. log $a_{K}+/a_{H}+$ diagram as discussed in chap.13. According to Eastoe (1981), the mottled K-feldspar is also associated with massive sulphide deposits at Hercules, Red Hills and Mt. Sedgewick (fig.4, chap.5), defining a large aureole around the deposits. A K-metasomatism replacing feldspars of different composition cannot be excluded for this reason, and probably played a part in forming the "secondary" K-feldspars.

10.1.3. Clear feldspar rims.

Coarse grained albitic feldspar phenocrysts with a clear to mottled rim of fresh feldspar (fig.65), in the majority of cases K-feldspar, exist in the massive pyroclastics within a few hundred metres above the host

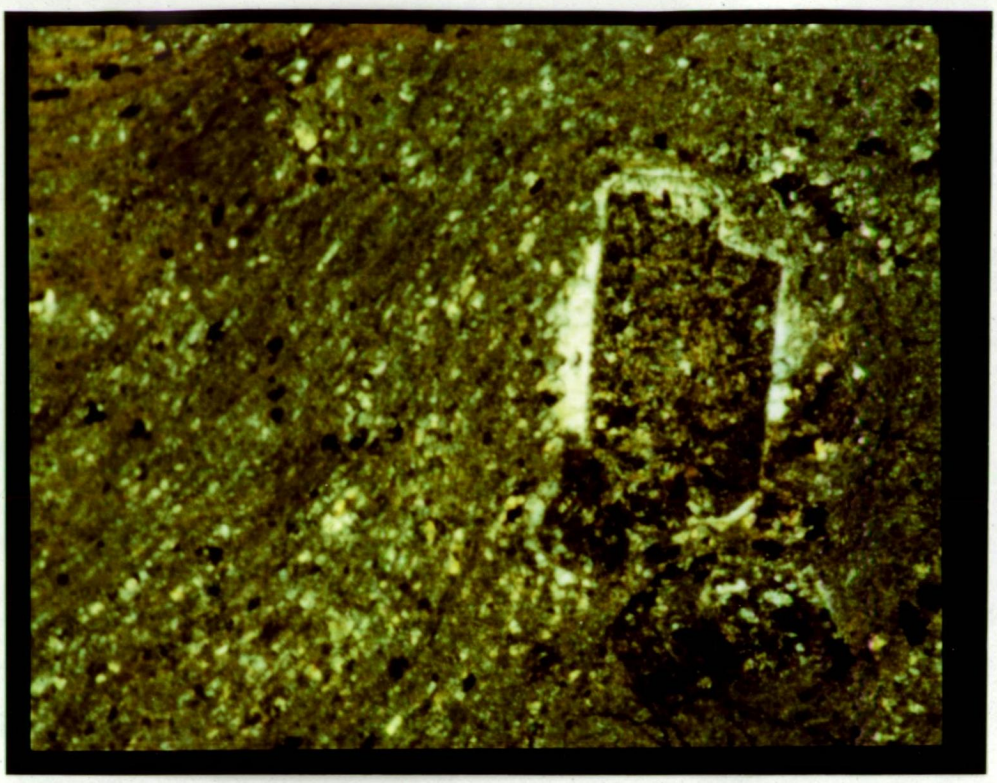

Fig.65: Altered feldspar with clear K-feldspar rim (67857)
field length = 6mm

rock, and in the footwall pyroclastics. Apart from the rims, fresh veinlets inside the coarse grained sericitized albites can also be present in the same crystal (67847).

Solomon (1964) explained the K-feldspar rims surrounding a plagioclase core as a late volcanic product. Hall (1967) produced evidence of albite froth rims which would substantiate Solomon's explanation, ignoring the difference in composition. Weak signs of froth rimming are also present in the examined sections. The rims, which are frequently discontinuous, show a high degree of inhomogeneity under polarized light. They are closely associated with aggregates of fine to medium grained fresh feldspar and quartz. These properties, including the absence of polysynthetic twinning are regarded as evidence for secondary processes affecting the primary feldspar rims. Also clusters of altered feldspars can be seen to be surrounded by one common clear rim (67878).

10.1.4. Fine to medium grained feldspars.

The fine to medium grained metamorphic alkali-feldspars have a fresh appearance and occur mostly in aggregates of interlocking crystals. They are comprised of K-feldspar and albite. Brathwaite (1969) also described medium grained unaltered plagioclase with simple albite or chess-board twinning as a second generation of feldspars believed to have been formed under low grade metamorphic conditions.

10.2. Phyllosilicate.

Chlorite, mica and clay minerals from different locations in respect to the hydrothermal alteration were analyzed, and multiple analyses of various grains were averaged. They cover the ore-bearing host rock, the footwall schists and partly altered pyroclastics immediately below and above the host rock horizon (underground), and samples from the surface alteration and hydrothermally unaltered volcanics. Their compositions are listed in appendix 4.

10.2.1. Chlorite.

The chlorite compositions show a large variation between different locations, but are fairly uniform within the same sample. This feature has also been noticed from Prince Lyell (Hendry,1981) south of Rosebery.

Small amounts of K_2O, Na_2O, CaO and TiO_2 are common. The sum of the alkali cations never exceeds 0.19 units per 28 oxygens or 0.71 wt % oxide, and are usually considerably lower. Following Foster (1962), the alkalis were ignored in the computation of the structural formula, and Ti was assigned to the octahedral position. Traces of Cl and S are rare. The calculation of the structural formula was based on 28 oxygens per unit cell and neutrality of charge. This allows an estimate for the number of ferric ions. Only 7 out of 31 samples exhibit a slightly positive total charge ($\leq$ 0.04), which indicates a reasonable estimate for the structural formula. More Al^{3+} cations occupy the octahedral than the tetrahedral position, explaining the negigible ferric ion contents so that virtually all iron is calculated as ferrous ions. Additionally, a small deficiency in the octahedral position is required to maintain neutrality of charge.

Compositions of chlorite associated with carbonate, feldspar and pyrite, dispersed in the matrix or as vein chlorite of the same section are essentially identical. However, samples as little as 4 m apart in the same geological environment can have significantly different FeO and MgO contents. Green (1983) in his attempt to determine the thermodynamical conditions of the ore deposition, using the six component chlorite model of Walshe & Solomon (1981), came to the conclusion that the chlorites produced during hydrothermal alteration were subjected to re-equilibration during the metamorphic event. This has been confirmed in this study as discussed further below.

All chlorite grains examined appear to overgrow mica, quartz and feldspar minerals. In the case of chlorite-carbonate contact the textural relationship is not clear, although chlorite seems to overlap carbonate more often than vice-versa. The only time chlorite appears to be replaced is in association with epidote.

Chlorites from four different geological environments were analysed. Their Mg/Mg+Fe ratios (Mg ratios) and Fe/Fe+Mg+Mn ratios (Fe ratios) do not suggest significant differences with respect to their sample location. The latter are plotted against Si (Foster, 1962) in fig.66.

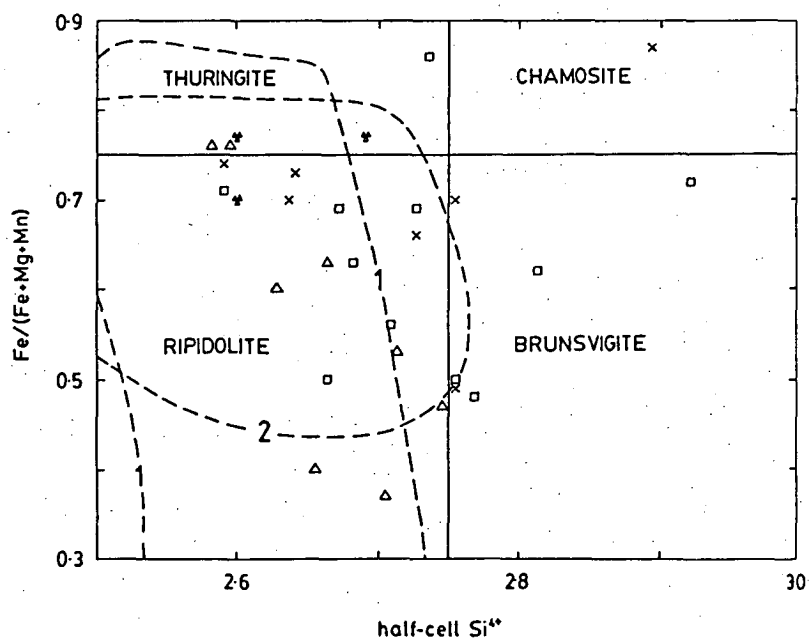

Fig.66: Chlorite compositions according to the method of Foster (1962), $Fe^{2+}/Fe^{2+}+Mg^{2+}+Mn^{2+}$ vs. Si atoms per half cell, chlorite compositions of Green (1983) (1) and Hendry (1981) (2) marked by dashed lines. Symbols - (△): host rock, (✱): footwall, underground, (×): surface alteration, (□): unaltered volcanics

a. Host rock, including samples from mineralized parts:
The Mg ratios from samples of the host rock vary considerably and spread evenly across the whole range from 0.21 to 0.61 (0.37 - 0.76). The numbers in brackets represent the Fe ratios as used by Green (1983).

b. Immediate footwall, underground:
Chlorite compositions from the footwall of the north orebody immediately below the host rock horizon are more limited in their variation, with Mg ratios from 0.19 to 0.26 (0.70 - 0.77). The range of Green's (1983) Fe ratios from the footwall of the F lens of the south orebody is 0.4 to 0.6 .

c. Altered hanging wall and surface alteration:
This group includes drill core samples from the hanging wall, as well as samples from the altered surface area. Their Mg ratios fall into a range from 0.13 to 0.49 (0.49 - 0.87).

d. Unaltered volcanics:
The range of the Mg ratios of the unaltered volcanic rocks is similar to that of the host rock. The Mg ratios vary from 0.13 to 0.51 (0.47 - 0.86).

Based on the Fe ratios, Green (1983) distinguished three groups of chlorites (>0.6, <0.35 and 0.4 - 0.6) within and below the south orebody. The Mg ratios from drill hole 434 at Prince Lyell which intersects the host rock (Hendry, 1981) range from about 0.20 to 0.55, being almost identical to that of the Rosebery host rock (fig.66).

The distribution of chlorite compositions from fig.66 does not suggest a strong influence on their composition by the hydrothermal alteration. A trend to lower Mg ratios (higher Fe ratios) towards the ore is not conclusive due to large variations within groups. Their variation rather is controlled by the bulk rock composition. The large spread in chlorite composition from unaltered volcanics and host rock, and the more limited variation of altered rocks from the uniform footwall pyroclastics (chap.6) within a small area, confirms this view. Conversely, Gannicott et al. (1979) recorded an increase in the Fe content of chlorite away from the Seneca prospect, British Columbia.

It is therefore questionable in the case of Rosebery to use chlorite composition models as mentioned above to study the conditions of ore formation. Also, exploration based on Mg ratios cannot be recommended in general. There may be some indication of higher Mn contents in chlorites from the immediate footwall and host rock. This trend has also been reported from the footwall of the Hercules mine (Eastoe,1981), a deposit very similar to that in Rosebery.

10.2.2. Phengite.

The abundant "sericite" is in fact a phengite with a deficiency in the 12-fold co-ordinate position. This is common in the illite group where illite and phengite can be regarded as end members (Deer, Howie & Zussman, 1972).

The phengite compositions show a wider variation within samples than chlorite. This is best reflected in the Mg ratio (appendix 4). Within this variation, the unoriented and frequently larger phengite grains replacing feldspar, match the composition of the fine grained matrix phengite from the same section. Na_2O occurs irregularly and can exceed the K_2O content, forming sodic phengite (McNamara, 1965). TiO_2 is consistently present, and smaller amounts of CaO and MnO occur less regularly. Cr_2O_3 , P_2O_5 ,Cl and S are rare constituents.

The computation of the structural formula followed the same principle (Foster, 1960) as for chlorites but was based on 22 oxygens per unit cell. The sum of cations in the octahedral position with the exception of Al (Fe^{3+}, Fe^{2+}, Mg, Mn, Ti, Cr) range from 0.04 to 1.76 units. Sodic phengite only contains between 0.04 and 0.26 non-Al cations. These results may have been caused by albite inclusions in phengite. Since the sum of the alkali cations is usually larger than the number of Al^{VI} cations, the positive charge has to be balanced in the octahedral position. As in the case of the chlorites, the estimated structural formula appears to be reasonable, with one positive charge of +0.10 the largest deviation. The Mg ratios vary from 19 to 87, compared with 30 to 70 at Prince Lyell (Hendry, 1981). They show a weak correlation (r = 0.5) with the Mg ratios of the co-existing chlorites. This trend has also been observed by Eastoe (1981) and Hendry (1981). In addition, the Al/Al+Si ratios are also weakly correlated (r = 0.5).

The positive correlation of the above mentioned ratios between co-existing chlorite and phengite minerals, in conjunction with improved correlations (both r = 0.7) of phengites and chlorites with the bulk chemistry, suggests that their composition depended on the original rock chemistry. This view has also been expressed by Hendry (1981) .

10.2.3. Biotite-Phlogopite.

The composition of three biotites and one phlogopite are plotted in fig.67. Their variation does not allow any firm conclusions as to whether the origin of the minerals is magmatic or metamorphic. The sum of their cations lies between 15.33 and 15.68 units, in contrast to the phengites with a cation sum of usually slightly less than 14. The number of Al^{VI} cations in phlogopite is almost nil and ranges from 0.41 to 0.81 for biotite. The total amount of octahedral cations is 5.84 and 5.38 - 5.88 respectively.

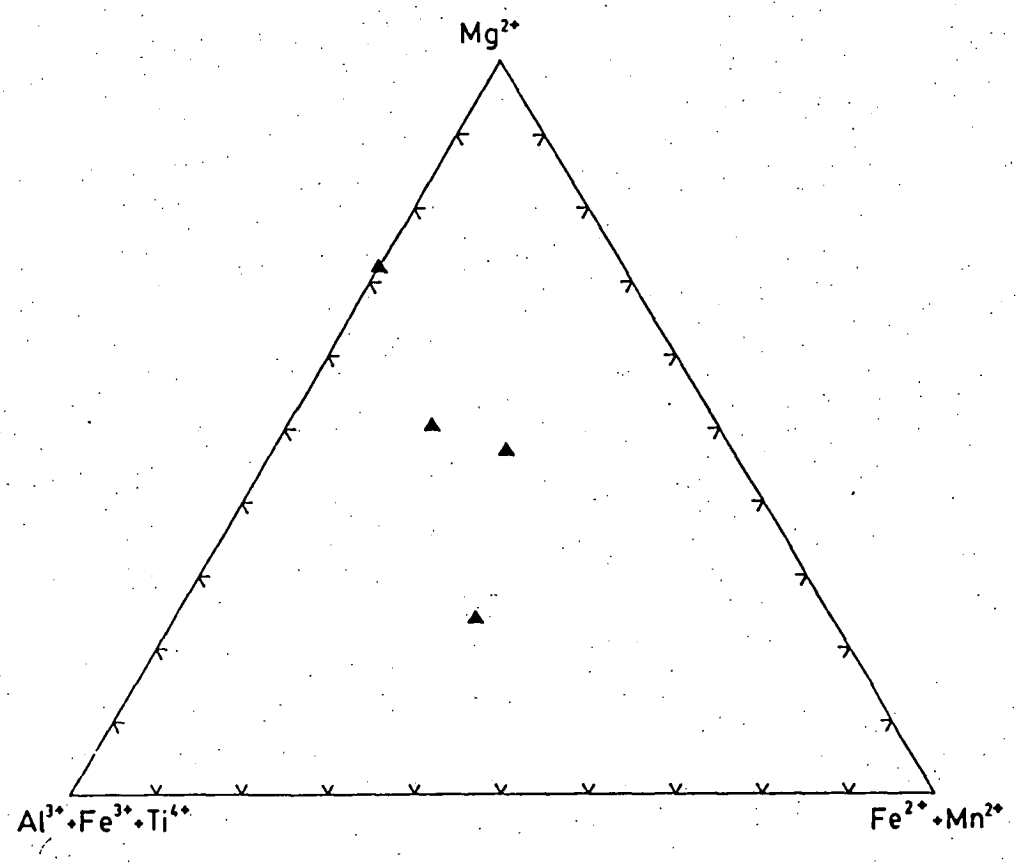

Fig.67: Biotite compositions according to the method of Foster (1960)

10.2.4. Clay or mixed clay-mica minerals.

Another small group of phyllosilicates with 14.12 to 15.19 cations per unit cell is represented by five additional analyses. One of these minerals is in composition very similar to nontronite. The cation sum is the lowest (14.11), and the number of alkali cations (0.55) stays within the limits of 0.66 units. It occurs in one section as yellow-green-brown aggregates of tiny grains, and as rhombic crystals with a granular texture. The other four minerals were optically indistinguishable from white micas. They contain between 0.44 and 0.96 K-cations, and the composition of their octahedral cations resembles that of biotite except for the greater number of Al^{VI} cations. Their composition could be the result of a mixed layer of clay and mica.

10.3. Epidote group.

Epidote and clinozoisite are present and can be easily distinguished by their appearance. The clear subhedral epidote grains mainly replacing feldspar are slightly enriched in CaO and Al_2O_3, and have somewhat lower FeO and MnO contents relative to clinozoisite. The latter occurs as light grey-brown spherulitic clusters containing REE, which are detectable on the energy dispersive spectrum. The average compositions of epidote and clinozoisite are listed in appendix 4. Both minerals contain spurious quantities of P_2O_5, TiO_2, MgO, Cr_2O_3 and alkali cations.

10.4. Carbonates.

The carbonates basically fall into two groups:
a. calcite, and b. carbonates of various compositions which occur more frequently in the host rock.

a. Calcite generally contains small amounts of Fe down to nil, and slightly higher quantities of Mn. Mg is usually absent. The range in composition is shown below, in mol %, normalized to 100 mol %:

Ca	Mn	Fe
92.3 - 99.3	0.7 - 7.7	0 - 1.8

Calcite occurs in veins, as grains dispersed in the matrix, and as feldspar replacement. It is the dominant species away from the immediate vicinity of the ore, although it can be found associated with mineralization. In all cases examined, calcite appears to overgrow quartz, feldspar, mica and also barite.

b. The second group includes a wide range in composition. The dominant component in nodules is Mn with varying contents of Fe. Their composition within occasionally concentric shell structures is uniform, and was determined by Brathwaite as that of rhodochrosite to ferroan rhodochrosite. Textural evidence suggests their origin is pre-cleavage (fig.59, chap.9.5.).

The carbonates from the second group are considered to be genetically related to the volcanic-exhalative ore. They have been discussed in more detail by Brathwaite (1969), Eastoe (1973) and Dixon (1980). At a few locations in the field, in schists and in massive pyroclastics immediately above the host rock horizon, carbonate veins and grains of the second type were found. The distribution of all examined carbonate compositions is shown in fig.68 and listed in appendix 4.

10.5. Sulphide minerals

The sulphide minerals in footwall schists and ore of the north orebody overall contain generally similar amounts of trace elements which can vary to a large extent within each environment (appendix 4). Testing of the Co and Ni content in pyrite by wavelength dispersive microprobe analysis did not reveal any conclusive zonation in respect of the hydrothermal activity due to large variations. The Co and Ni contents as determined range from 350 ppm to 950 ppm Co and from 171 ppm to 1340 ppm Ni. Similar values have been reported by Green et al. (1981). The wide range of As contents in pyrite is expressed in the whole rock As content as confirmed by a preliminary examination. The Fe content in sphalerite is in agreement with results by Green et al. (1981). As and Zn contents in pyrite and Fe contents in sphalerite are listed in appendix 4.

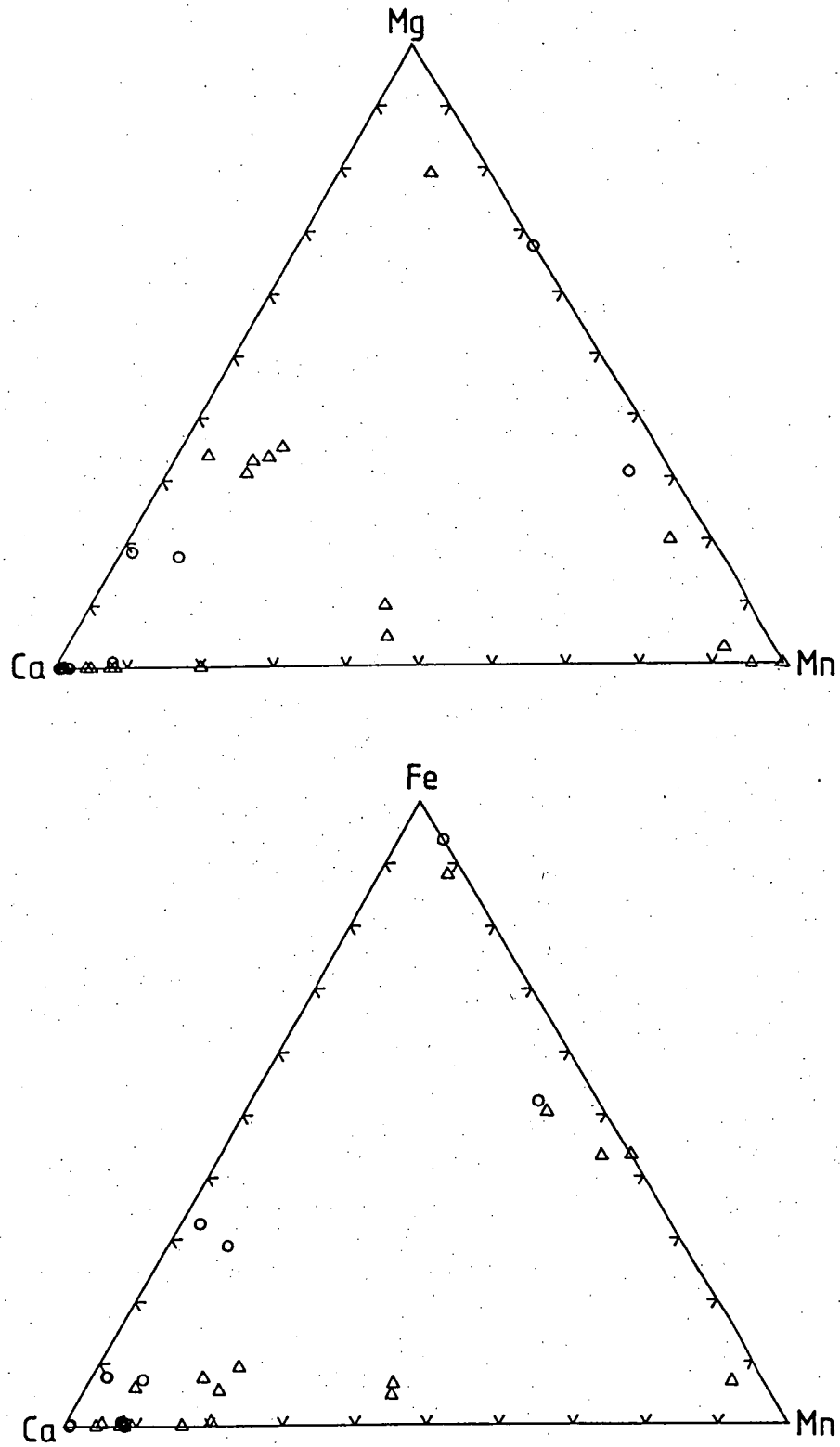

Fig.68: Carbonate composition in mol % normalized to 100% in host rock (△) and altered and unaltered volcanics (o)

11. Additional exploration methods.

11.1. Rare earth chemistry.

The rare earth elements (REE) study of the Rosebery rocks had two aims: Firstly to test whether the primary magmatic REE chemistry in the unaltered volcanics indicates a potential host (Campbell et. al, 1982) for massive sulphide deposits (regional target), and secondly, to examine the influence of hydrothermal fluids on the original REE pattern (local target).

11.1.1. Rare earth chemistry in ore-associated volcanics (regional target).

According to Campbell et al. (1982), the magmatic processes producing volcanics associated with massive sulphide deposits are responsible for a specific REE pattern. Exploration for rocks having such patterns could assist in pin-pointing promising regional target areas. Their study of barren and mineralized felsic volcanics from several parts of the world indicated that the latter were more enriched in heavy REE (HREE). The mineralized felsic volcanics also exhibited a negative anomaly of varying proportions (fig.69). Similar flat REE trends were recorded by Thurston (1981) in the third cycle of mineralized calc-alkaline rhyolites from the Confederation Lake area, northwest Ontario. In contrast the rhyolites from cycle I and II are more fractionated with relatively increased abundances of light REE (LREE) over HREE. In the same study calc-alkaline rhyolites from the mineralized Lower Supergroup in the Abitibi Belt were found to have a flat REE pattern but mostly lack the negative Eu anomaly. Campbell et al. and Thurston disagree on the mechanism that produced the "mineralized" REE trend. The former proposed a magmatic process for the relative enrichment in HREE while the latter preferred a hydrothermal cause.

11.1.1.1. Rare earth chemistry in unaltered Rosebery volcanics.

To test the idea of a genetic relationship between volcanism, and the formation of massive sulphide ore and accompanying hydrothermal alteration at Rosebery, a large set of samples was analysed for La, Ce, Nd and Y by

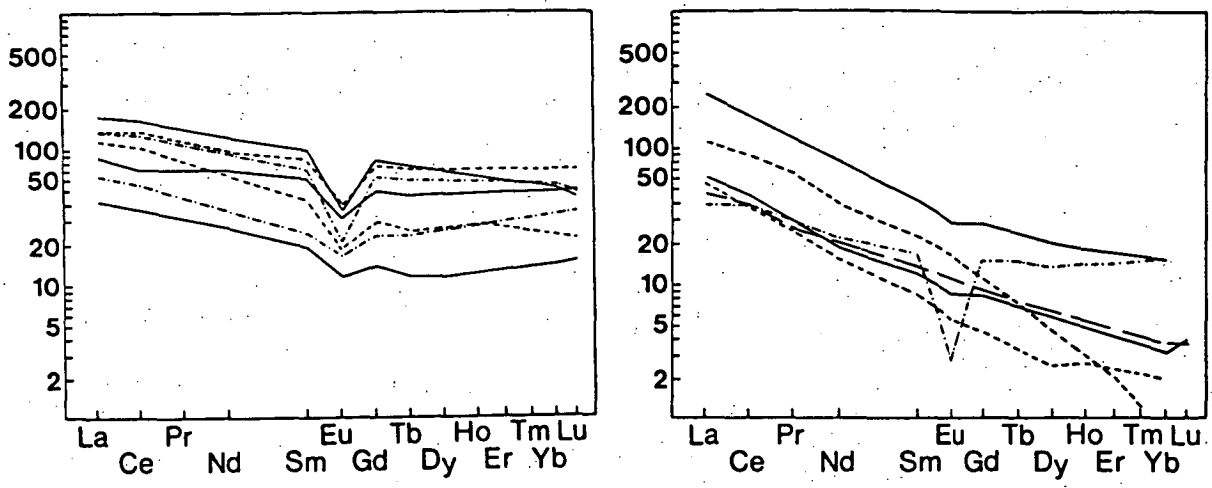

Fig.69: REE pattern from mineralized (left) and barren (right) felsic volcanics after Campbell et al. (1982), chondrite-normalized

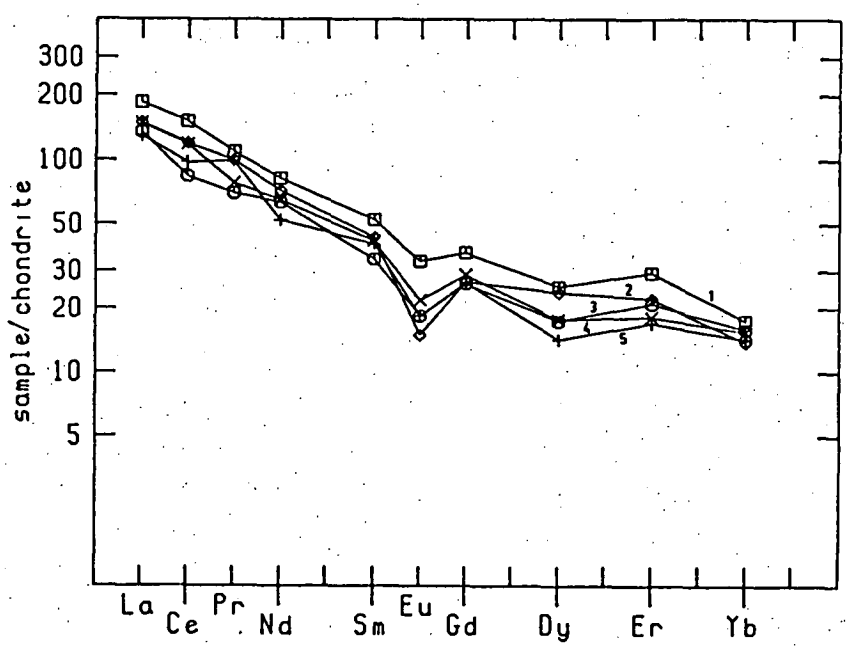

Fig.70: REE pattern from rhyolitic volcanics at Rosebery
1: (67848), 2: (67811), 3: (67891), 4: (67829), 5: (67802)

XRF in the form of pressed powder pills. A smaller batch of samples was analysed also for an extended range of REE with the addition of Pr, Sm, Eu, Dy, Er and Yb, by an ion-exchange method (Higgins et al., 1983; see also appendix 7). The chondrite normalization in the figures referred to is based on McLennan & Taylor (1980).

The REE trend of the unaltered felsic volcanics at Rosebery (fig.70) is rather steep when compared to those from mineralized rock units mentioned above. The fractionation between LREE and HREE resembles that of unmineralized rhyolitic volcanics (fig.69). However the negative Eu anomaly is present in the Rosebery volcanics. Whitford & Wallace (1984) reported a more strongly fractionated REE distribution for dacites from the Mt. Read volcanics at Que River, some 20 km north of Rosebery.

The REE abundances of dacitic-andesitic volcanics at Rosebery (fig.71) follow the same pattern at a slightly lower level of chondride normalized enrichment. However they still are within the range of felsic volcanics, considering the larger sample number of the reduced set of LREE and Y (fig.72). Compared to the calc-alkaline andesites ($Eu/Eu^* \approx 0.97$) from Viti Levu, Fiji (Gill, 1970), both andesites from Rosebery have a higher REE content and larger negative Eu anomaly ($Eu/Eu^* \approx 0.86 - 0.67$) which is similar to those in andesites from Que River ($Eu/Eu^* \approx 0.7$) (Whitford & Wallace, 1984). However it is not the purpose of this study to speculate about magmatic processes. As this study has demonstrated, the Mt. Read Volcanics at Rosebery are essentially not enriched in HREE and the existence of at least three different REE trends associated with massive sulphide mineralization does not support the idea of a simple relationship.

11.1.2. Hydrothermal influences on REE distribution at Rosebery (local target).

The REE in the surface schists are somewhat depleted. Their distribution (fig.73) follows the same pattern as in the unaltered volcanics, at a slightly lower level of chondrite enrichment (fig.74). A more obvious depletion trend affecting LREE and HREE likewise was recognized from the hanging wall alteration on the surface (fig.75) and in drill core DDH 46R (fig.76). Post-ore magmatic processes can be excluded as the fractionation between LREE and HREE does not change systematically. The Eu/Eu^* ratios for unaltered to moderately altered feldspar-bearing

volcanics and for feldspar free schists are conflicting, and do not suggest a clear pattern in respect to the removal of this mineral, although Eu depletion associated with destruction of feldspar was recognized (fig. 77). Clearly more data is required, to come to a firm conclusion. According to Whitford & Wallace (1984), Eu is the only REE that has been mobilized in the intensely hydrothermally altered rocks at Que River.

Apart from the REE depletion in the surface schists, and two systematic trends for decreasing REE abundance towards the ore deposit in the altered hanging wall pyroclastics, mentioned above, the hydrothermal influence is weak. The LREE + Y contents in mine schists taken from drill core below the north orebody and from the barren gap are essentially identical (fig. 78), and both fall within the variation of the unaltered volcanics (fig. 72), although slightly below the average content. Similar REE abundances exist for the feldspar free massive siliceous rocks (fig. 74) with a Eu/Eu^{*} ratio $\simeq$ 0.47 . The close similarity between the REE pattern of host rock shale (fig. 77) and volcanics confirms the latter as a source for the shale (Gee, 1970).

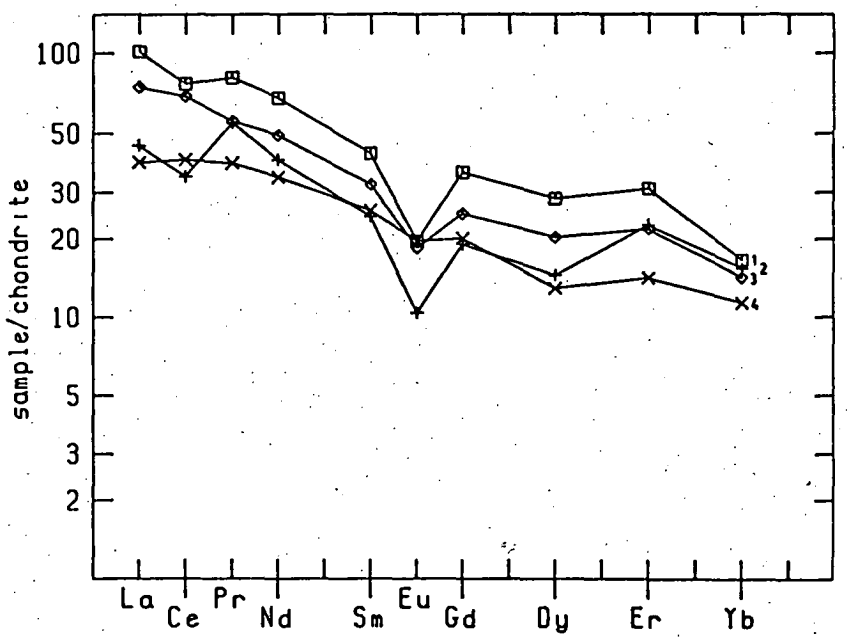

Fig. 71: REE pattern from andesitic-dacitic volcanics.
1: (67818), 2: (67827), 3: (67856), 4: (67874)

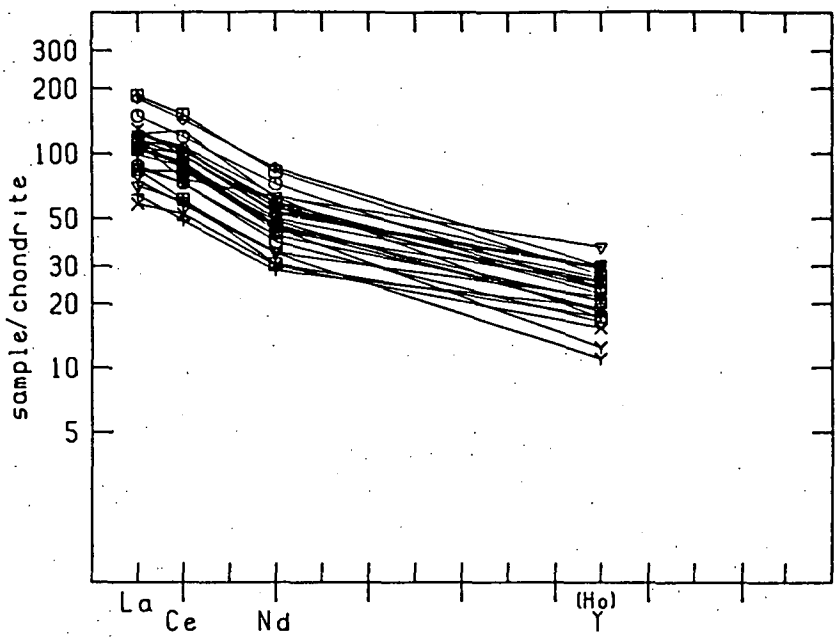

Fig.72: LREE + Y pattern for felsic volcanics (see appendix 2)

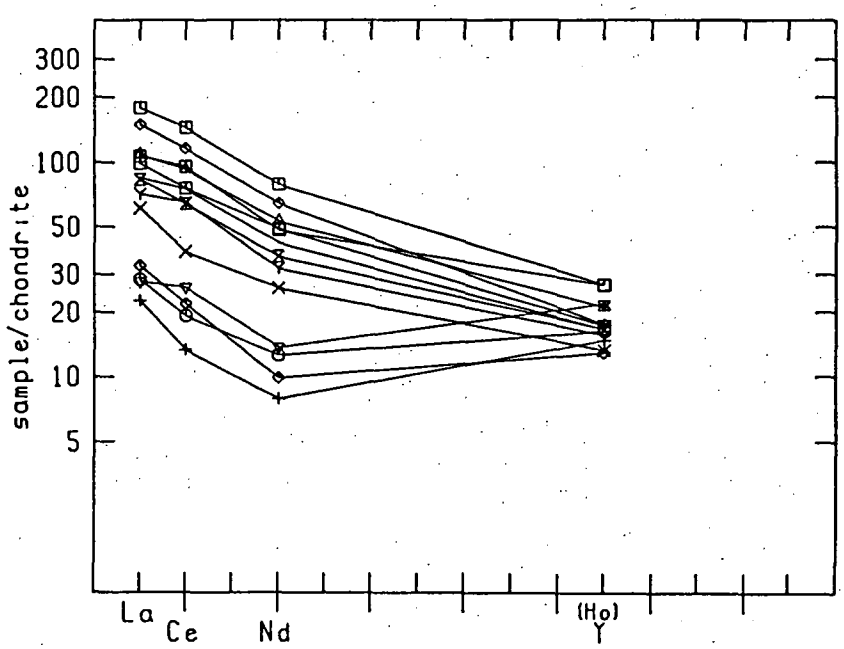

Fig.73: LREE + Y pattern from altered footwall rocks (see appendix 2)

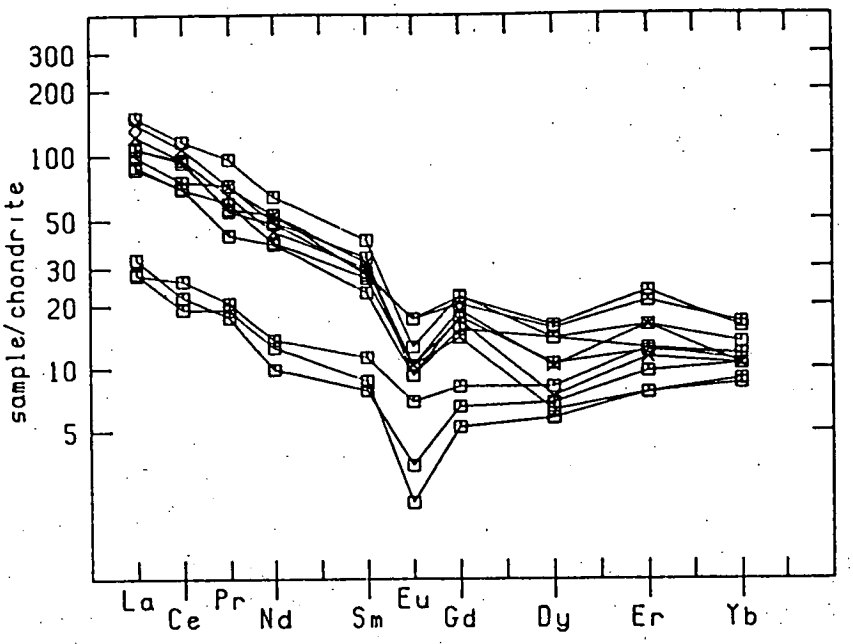

Fig.74: REE pattern of altered footwall rocks (see appendix 2, REE analyses). Two massive siliceous rock samples are within the more LREE enriched trend

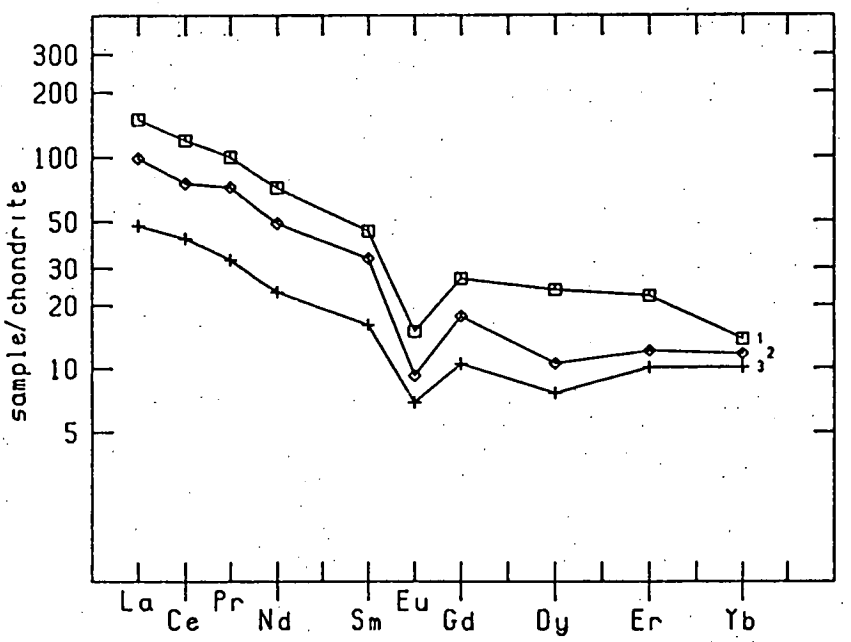

Fig.75: Increasing depletion of REE in surface rock of hanging wall approaching ore horizon. 1: (67811), 2: (67813), 3: (67816)

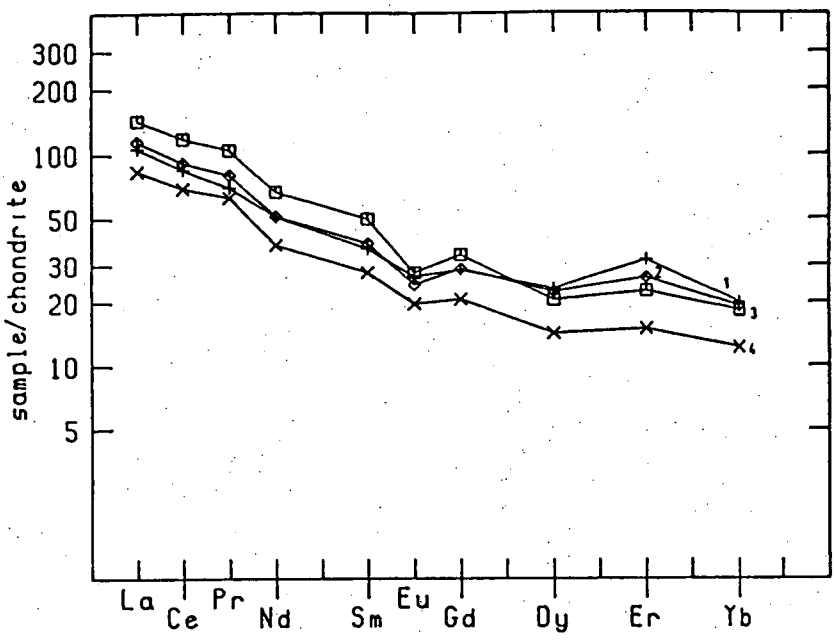

Fig.76: Increasing depletion of REE in DDH 46R (hanging wall) approaching ore horizon. 1: (67912), 2: (67916), 3: (67917), 4: (67918)

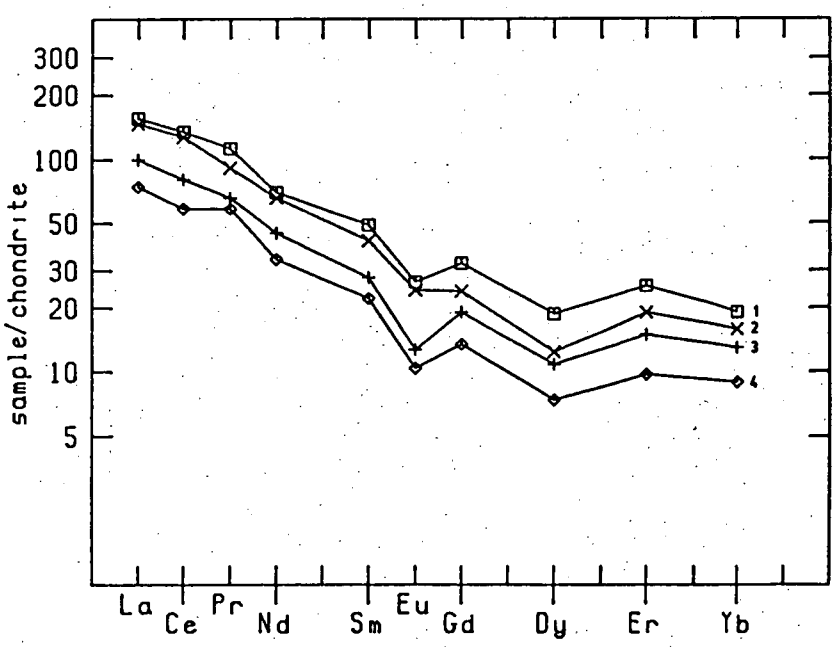

Fig.77: REE pattern in DDH 1121. 1: host rock (67923), 2: moderately altered footwall pyroclastic (67929), 3: footwall schist (67927), 4: host rock (67921)

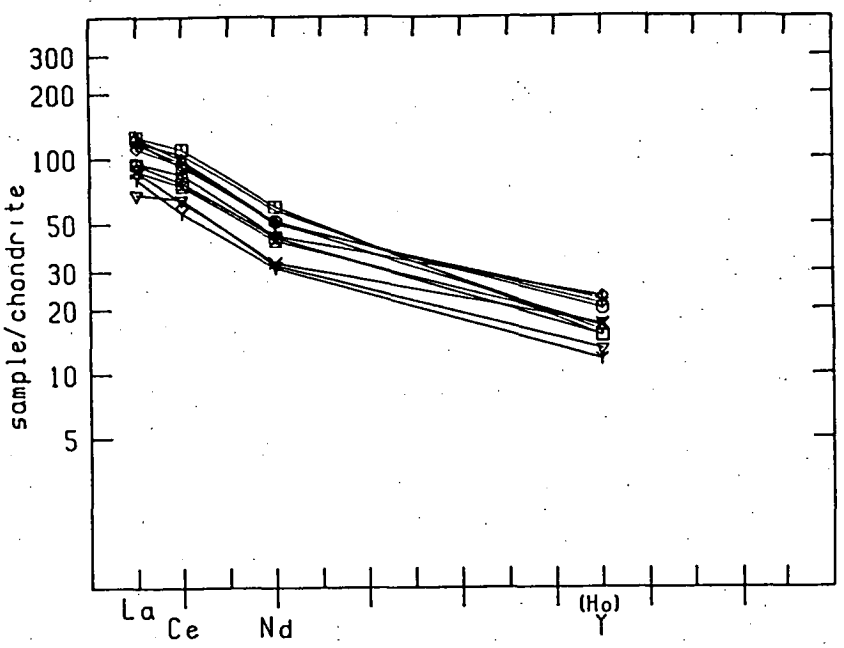

Fig.78: LREE + Y pattern of footwall immediately below the host rock horizon, underground

The general hydrothermal REE pattern at Rosebery does not agree with Graf's model (1977). He envisaged a hydrothermal solution enriched in Eu and HREE which may have been precipitated on the seafloor together with sulphide minerals. It is more likely that low pH conditions and high water/rock ratios such as are present during massive sulphide formation, caused a small decrease in the REE content as suggested by Taylor & Fryer (1980, 1982) for the REE behaviour in the phyllic alteration assemblage of a porphyry ore system.

Remobilization of the REE during the Tabberabberan Orogeny by remaining hydrothermal solutions (chap.13) cannot be excluded. Hellman et al. (1979) showed the REE to be locally mobile under the conditions of burial metamorphism. Furthermore, weathering could have contributed to the large variation of the REE content in the surface rocks (Nesbitt, 1979).

Zircon, apatite (Hanson, 1978), sphene and allanite (Gromet & Silver, 1983) are the most likely host minerals for REE in felsic igneous rocks. In two cases, detectable amounts of REE (with EDAX, microprobe) in clinozoisite (chap.10.3) were not reflected in the bulk REE analysis. The LREE and Y correlate positively with Ti, Al, Na and in particular with Zr (tab.15, chap.12.3.). Based on a partial correlation which controlled for the influence of Ti, Si, Zr and S in subsequent trials, only a good correlation (> 0.5) between Zr and LREE including Y remained. However zircon, the major Zr-bearing mineral is a HREE acceptor and can only incorporate small amounts of LREE (Hanson, 1978). The poor correlation between P, representing apatite, and the LREE including Y, may be caused by low concentrations of P_2O_5 close to or below the detection limit. Most of the REE content has probably been contained in the volcanic magma at the time of eruption. As a consequence the REE may be expected to be incorporated in the phyllosilicates forming the matrix of the present volcanics.

In summary, the REE distribution at Rosebery is not suited for regional or local target exploration. No host mineral could be identified, unless the REE are assumed to be distributed in the matrix sericite and chlorite.

11.2. Oxygen isotope chemistry.

Whole rock oxygen isotope studies are being increasingly used to delineate alteration haloes around massive sulphide deposits, and also to examine the history of the hydrothermal fluids. Results compiled by Beaty & Taylor (1982) indicate a decrease of $\delta^{18}O$ values in the alteration zones relative to the surrounding unaltered volcanics, except for the Kidd Creek deposit, Canada. The process causing this pattern is mainly thought to be a temperature dependent isotope fractionation between circulating seawater ($\delta^{18}O \simeq 0$) and felsic volcanic tuff ($\delta^{18}O \simeq 6 - 10$).

The fractionation (Δ_{SF}) between different phases such as hydrothermal fluids (F) and silicates (S) can be described by the equation:

$$10^3 \ln\alpha_{SF} \simeq \delta_S - \delta_F = \Delta_{SF}$$

α = fractionation coefficient, temperature dependent

$$\delta = 10^3 \left(\frac{R_{sample}}{R_{standard}} - 1\right) \text{ in per mil, } R = {}^{18}O/{}^{16}O$$

(Ohmoto & Rye, 1974; Taylor, 1974; Sheppard 1977; Heaton & Sheppard, 1977)

11.2.1 Oxygen isotope distribution at Rosebery.

In a preliminary study, a small set of 21 samples (including two duplicates) covering a wide area of geochemical environments were commercially analysed for whole rock ^{18}O. The results are listed in tab. 10.

In contrast to the massive sulphide deposits listed by Beaty & Taylor (1982) and deposits in the Fukazawa-Kosaka area, Japan (Green et al., 1983), the $\delta^{18}O$ values from Rosebery do not indicate a systematic trend. With the exception of one sample, the $\delta^{18}O^f$ values lie at the upper end, or above the recorded range for felsic pyroclastics (Taylor, 1974). The slightly higher $\delta^{18}O$ values of the massive siliceous rocks (67840, 67846) are either caused by fractionation of ^{18}O into larger amounts of quartz or by a somewhat different hydrothermal history (chap.12). Sample 67995 from the immediate footwall below the ore, is dominated by sericite and

Sample	$\delta^{18}O$ value	Description
67800	+12.4	unaltered volcanic rock
67802	+11.5	" " "
67811	+10.7	" " "
67848	+11.8	" " "
67855	+11.4	" " "
67867	+ 9.1	" " "
67912 (DDH 46R)	+10.9	" " "
67918 (DDH 46R)	+12.0	moderately altered rock
67927 (DDH 1121)	+10.8	altered schist
67929 (DDH 1121)	+11.1	moderately altered volcanic
67866	+12.0	altered volcanic
67816	+ 7.4	chloritic schist
67835	+12.0	schist
67881	+10.1	"
67884	+11.2	"
67958 (DDH 1222)	+10.9	"
67995 (DDH 3376)	+ 9.3	sericite rich schist
67840	+14.2	massive siliceous rock
67846	+13.2	" " "

Tab.10: $\delta^{18}O$ values from Rosebery rocks

shows a low $\delta^{18}O$ value. Sample 67816 from the altered hanging wall with 30 - 40 vol % chlorite has the lowest ^{18}O enrichment when compared to SMOW. This pattern is in agreement with the fractionation behaviour of ^{18}O between H_2O and the silicate minerals dominating the hydrothermal assemblage at Rosebery. The fractionation (Δ_{SF}) decreases from quartz over muscovite to chlorite (Taylor, 1974).

The consistency of the $\delta^{18}O$ values not only extends into the hanging wall where hydrothermal activity had occurred (chap.8.3.1.3.1), but also laterally away from the centre of the surface alteration for at least 3 km,

far beyond the geological and geochemical halo. Possibly a re-equilibration and homogenization (Garlick & Epstein, 1967) of the $^{18}O/^{16}O$ ratios took place during the Tabberabberan Orogeny. The large number of abandoned mines and prospects surrounding Rosebery are evidence for a wider spread of fluid circulation. Furthermore, a second period of mineralization during this orogeny might have introduced additional magmatic fluids ($\delta^{18}O \approx 6 - 9$ per mil, Taylor, 1974). According to Green (1983), the massive siliceous rocks have resulted from this process. The slightly higher $\delta^{18}O$ values in both samples mentioned above could indicate a magmatic component. More data are required to come to a firm conclusion.

11.2.2 Source of the hydrothermal fluids.

In the light of the above, and the lack of δD values at Rosebery, any attempt to determine the source of the hydrothermal fluids must remain speculative. The fractionation coefficients are based on equilibrium conditions which may not have been achieved in a circulatory system. In addition, the influence of high salt concentrations in the ore-bearing brine on the ^{18}O activity (Truesdell, 1974) are not accounted for.

However boundary conditions may be estimated by using the combined formula by Ohmoto & Rye (1974) and Taylor (1979):

$$\delta\,^{18}O_R^f = \frac{8 + 2r(\Delta_{RF} + \delta^{18}O_F^i)}{1 + 2r}$$

As the oxygen content of the felsic unaltered volcanics lies in a narrow range of 49 - 51% (weight), the multiplication of the rock/water ratio (r) by a factor of 2 is a good approximation to compensate for the difference between atomic oxygen and weight oxygen ratios.

Five assumptions are necessary to solve this problem:

a. The total amount of ^{18}O in fluids (F) and wall rock (R) combined, did not change between ore deposition and metamorphic event. This means that the second event is basically a replay of the first event at perhaps different temperatures and improved equilibrium conditions.

b. The initial $\delta^{18}O_R^i$ values of the unaltered volcanics are around 8 per mil (between 6 per mil and 10 per mil).

c. The rock/water ratio (r) lies between $r_1 = 0.04$ and $r_2 = 0.08$, implying a porosity of the original volcanics of 10 volume % (Ohmoto & Rye, 1974) and at the most 20 volume % (this study, chap. 12).

d. The initial fluid was mainly Cambrian seawater ($\delta^{18}O_F^i \approx 0$), as suggested by Green et al. (1981) (chap.15), or derived from seawater.

e. Rock-fluid fractionation is represented by the feldspar-H_2O fractionation $\Delta_{RF} \approx 2.68\ (10^6/T^2) - 3.53$ by O'Neil & Taylor (1967) as suggested by Taylor (1979). The feldspar-H_2O fractionation lies between quartz-H_2O and muscovite-H_2O fractionation.

The results in tab.11 suggest that the ^{18}O contents in seawater cannot account for the final $\delta^{18}O_R^f$ values in altered and unaltered volcanics, unless equilibration occurred at a very low temperature.

T (°C)	0		50		100		200		350	
	r_1 0.04	r_2 0.08	r_1 0.04	r_2 0.08	r_1 0.04	r_2 0.08	r_1 0.04	r_2 0.08	r_1 0.04	r_2 0.08
$\delta^{18}O_F^i \approx 0$	9.8	11.4	9.0	10.0	8.6	9.1	8.0	8.1	7.7	7.4
$\delta^{18}O_F^i \approx 7$	10.32	12.3	9.6	10.9	9.1	10.0	8.6	9.0	8.2	8.3

Tab.11: Calculated $\delta^{18}O_R^f$ values for Rosebery volcanics based on seawater ($\delta^{18}O_F^i = 0$) and modified seawater ($\delta^{18}O_F^i = 7$) at water/rock ratios of $r_1 = 0.04$ and $r_2 = 0.08$

At temperatures < 150°C, reactions are extremely slow (Cole et al., 1983). Ripley & Ohmoto (1979) explained the similarly high $\delta^{18}O$ values from the alteration zone at the Raul mine, Peru, by fractionation with modified seawater. An increase in $\delta^{18}O$ of approximately 7 per mil (see tab. 11) is thought to be possible by evaporation of 20% of seawater. Craig et al. (1963) demonstrated a strong enrichment of ^{18}O during evaporation of 50% of water under various conditions of humidity. The envisaged lagoonal environment around Rosebery at the time of ore deposition (chap.7) would permit such a model. Additional ^{18}O enrichment could have occurred by shale ultrafiltration, which increases the ^{18}O content in the migrating fluids (Coplen & Hanshaw, 1973), and by fractionation between the ore-depositing fluids and shales. Smecite in Gulf Coast clay has $\delta^{18}O$ values ranging from 18 to 23 per mil (Land, 1983). Solomon (1981) suggested a convection of the hydrothermal fluids through sediments at Rosebery, based on the existence of arsenopyrite, which requires relatively reduced solutions. He also proposed membrane filtration and evaporation of seawater to increase the salt content. Dixon (1980) also inferred a modified seawater as the source of the metal-bearing solutions, based on carbon and oxygen isotope chemistry of carbonates at Rosebery.

Conversely, magmatic water may have been introduced during the hydrothermal event and subsequently during the Tabberabberan Orogeny as mentioned above. This simple model also ignores the fact that the water/rock ratio in the surrounding "unaltered" volcanics was probably lower than in the schists. It also fails to identify the influence of repeated migration of fluid units (Ohmoto & Rye, 1974) on the $\delta^{18}O$ values of the altered wall rock during the lifetime of a continuously flowing hydrothermal system. If the hydrothermal schists had originally been depleted in ^{18}O due to large amounts of circulating hot seawater as in other massive sulphide deposits, the process of post-ore homogenization and the nature of the fluids involved would be open to much wider speculations. Based on a total amount of 18 million metric tons of ore at Rosebery with 0.7% Cu, 5.2% Pb and 16.6% Zn (Reid & Meares, 1981) and 1 - 2 km^3 of altered volcanics (radius = 0.8 km, depth = 0.5 - 1 km) the total water/rock ratio should have been in the order of 100 if metal solubilities of 0.3 ppm Cu, 3 ppm Pb and 10 ppm Zn are assumed (Dickson, 1977; Pisutha-Arnond & Ohmoto, 1983; Ohmoto et al., 1983). During the metamorphic event, circulation of fluids was probably much more limited due to the lack of large temperature gradients. This model satisfies the condition of a static rock-fluid system required for the equation employed, in contrast to

the continuous migration of hydrothermal solutions, as during ore deposition.

In summary, it is possible to explain the Rosebery hydrothermal solutions as modified seawater, although the addition of a magmatic component cannot be excluded. The $\delta^{18}O$ values cannot be used as a guide to the alteration halo unless these values change at a further distance away from the ore deposit.

12. Element exchange.

In chap. 8.3.1.3.3., the enrichment and depletion of certain elements has been discussed from a statistical view point, in order to explain the geochemical alteration patterns contoured by the program package Surface II. In this chapter the alteration chemistry is discussed in the context of real element exchange.

12.1. Immobile elements.

The elements Y, Sc, Nb, Ga, Ce, Al and in particular Zr and Ti have been considered to remain immobile during hydrothermal alteration (Seyfried & Bischoff, 1977; Winchester & Floyd, 1977; Humphries & Thompson, 1978; Finlow-Bates & Stumpfl, 1981). Enrichment or depletion in these elements is therefore regarded as a relative change due to addition or removal of mobile elements or phases such as sulphides, sulphates, carbonates and silica, the latter being the most important factor in the altered volcanics at Rosebery. The addition of SiO_2 to the siliceous schists immediately below the ore deposit appears to markedly decrease the abundance of Y, Nb, Ti, Zr and Al.

Conversely MacGeehan & MacLean (1980) proposed an addition of SiO_2 and Zr and a depletion of Ti based on a constant Al_2O_3 content and constant volume during alteration of basalt. Roberts & Reardon (1978) noticed addition and removal of Ti at different stages of the alteration halo at Mattagami (Quebec).

Bulk rock analyses from unaltered dacitic-rhyolitic volcanics, massive siliceous rocks, surface schists and mine schists (underground) from the immediate footwall below the ore deposit at Rosebery were used to study the influences of the SiO_2 content on the variation of TiO_2 and Zr. Relationships between SiO_2 and Y and Nb show a similar pattern, except for more scatter in the data. In fig. 79 , TiO_2 versus SiO_2, three trends are apparent: The magmatic differentiation trend in the unaltered volcanics, and two trends with a smaller gradient for the mine schists and the massive siliceous rocks. The variation in the TiO_2 content of the surface schists appears to be merely an extension of the primary differentiation to lower values. The intercept of the SiO_2 axis is 100% and 90% for the mine schist and the massive siliceous rocks respectively. Their gradients are

approximately parallel. When extrapolated, the unaltered volcanics intercept the SiO_2 axis at 87%.

The variation pattern is less clear in fig.80, Zr versus SiO_2. Post-magmatic processes presumably blurred the fractionation curve of Zr, which should increase from dacites to rhyolites (Winchester & Floyd, 1977). Zr and TiO_2 can be mobilized by weathering as reported by Butt (1983) for granites of the Yilgarn Block. Weathering may have also contributed to the scatter of Zr and TiO_2 of the surface schists. Again, the mine schists and the massive siliceous rocks exhibit a similar gradient which leads to an intercept on the SiO_2 axis at 103% and 114% respectively.

In fig.81, Al_2O_3 versus SiO_2, the Al_2O_3 distribution of the mine schists runs parallel to the primary trend at a decreased level indicating depletion of Al_2O_3 at the silica-rich end, and dilution due to the addition of small amounts of carbonate at the opposite end (chap.12.2., 12.3.).

Apart from the pattern shown in fig.81, the two dilution trends represented by Zr and TiO_2, intercepting the SiO_2 axis at about 100% could be ascribed to the addition and removal of silica only. Several reasons however speak against such a simple mechanism:

a. The Zr and TiO_2 trends of the mine schists only pass through the bottom end of the primary fractionation curve, which is best demonstrated in fig.79. Assuming silica addition as the only factor, the dilution trend should form a fan which converges at 100% SiO_2, as shown in fig.82.

b. Although the dilution trend of the massive siliceous rocks points approximately towards 100 % SiO_2, it occurs at a lower TiO_2 content when compared to the mine schists. As both rock types are regarded as alteration products of the pyroclastic wall rock, the difference can only be explained in terms of active removal.

c. The correlation of R = -0.4 between TiO_2 and SiO_2, based on a selected set of drill core samples (chap.12.3) becomes positive (R = 0.3) if corrected for the influence of other variables. By the same method (see chap.9.4.5.2.2.) the correlation between Zr and SiO_2 is reduced from R = -0.5 to R = -0.3.

d. The samples of all groups do not project through the origin if Zr is plotted against TiO_2 (fig. 83) as suggested by Finlow-Bates & Stumpfl (1981). This might be expected if enrichment and depletion of the immobile elements only depends on the variation of silica. Fig. 83 also confirms that "unaltered" volcanics must have undergone chemical alteration to some degree. Conversely fig. 83 could also be interpreted as a mobilization of both Zr and Ti. Similar trends exist when Zr is plotted against Al_2O_3, and the latter versus TiO_2.

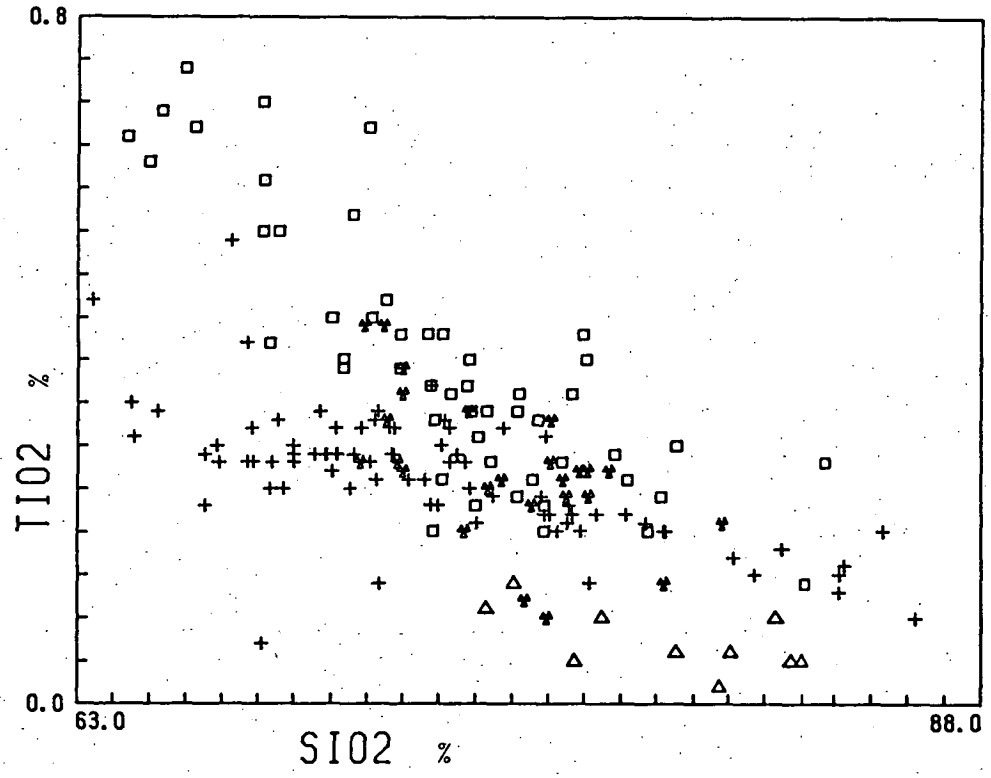

Fig.79: Diagram: TiO_2 contents of unaltered volcanics (□), surface schists (✱), massive siliceous rocks (△), and mineschists (+), underground, plotted against SiO_2 content

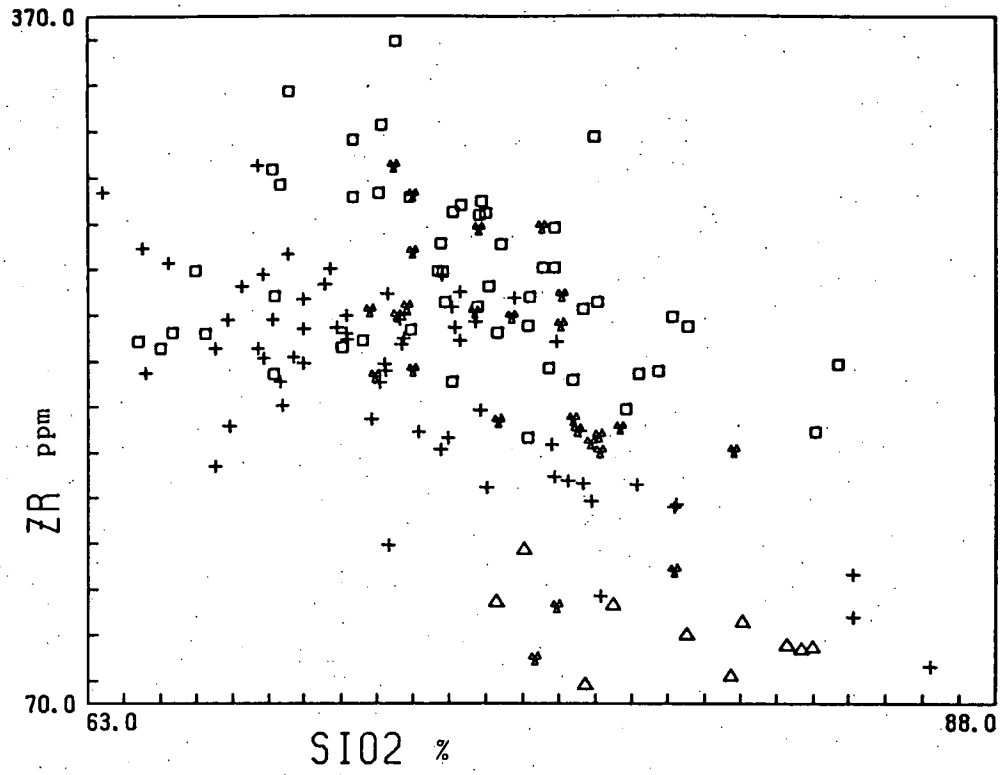

Fig.80: Diagram: Zr content of unaltered volcanics (□), surface schists (✱), massive siliceous rocks (△), and mineschists (+), underground, plotted against SiO_2 content

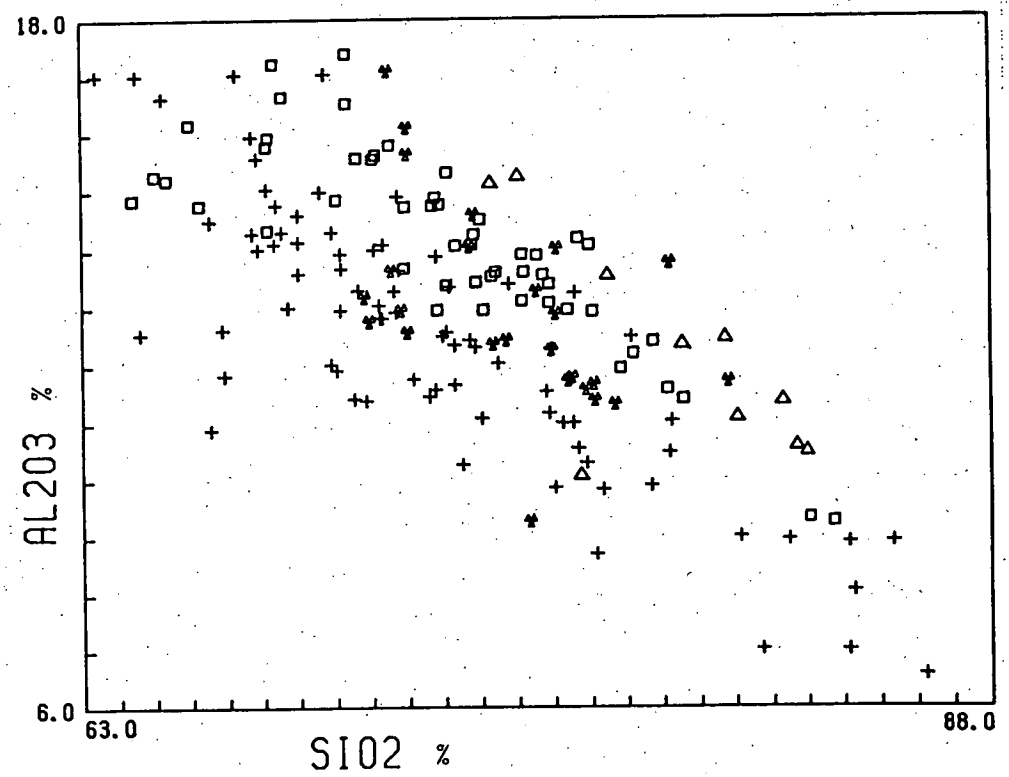

Fig.81: Diagram: Al_2O_3 content of unaltered volcanics (□), surface schists (✱), massive siliceous rocks (△), and mineschists (+), underground, plotted against SiO_2 content

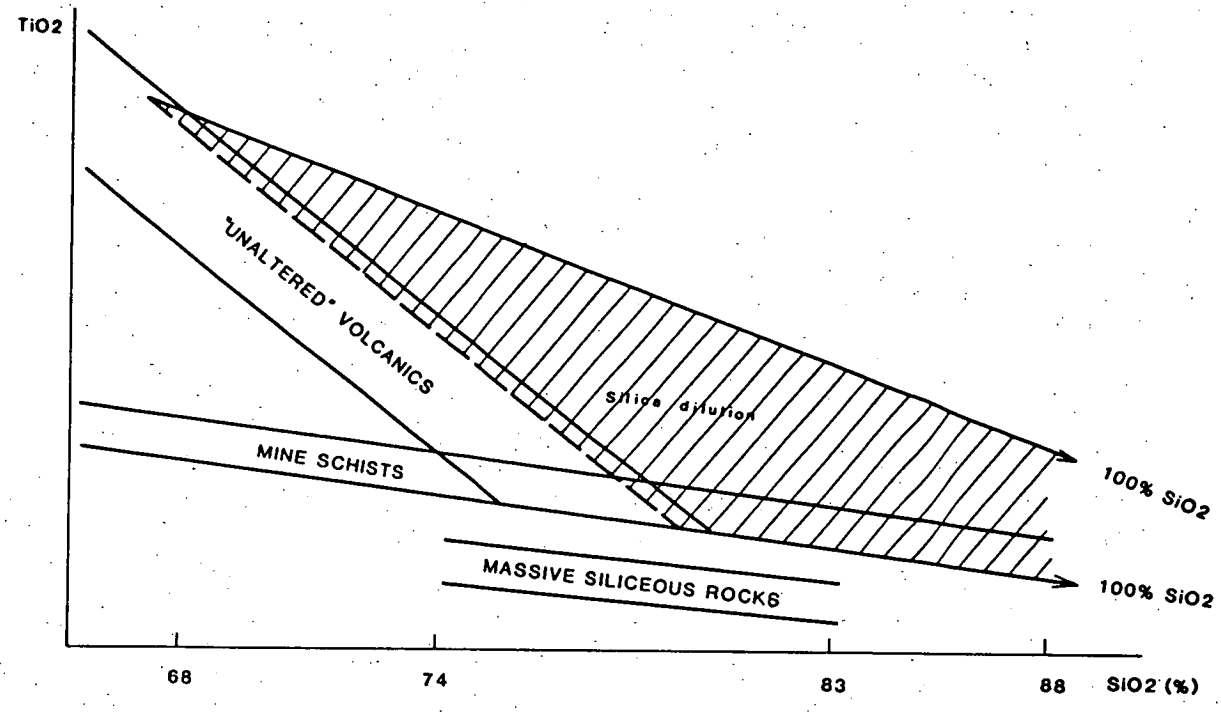

Fig.82: Schematic dilution diagram TiO_2 vs. SiO_2

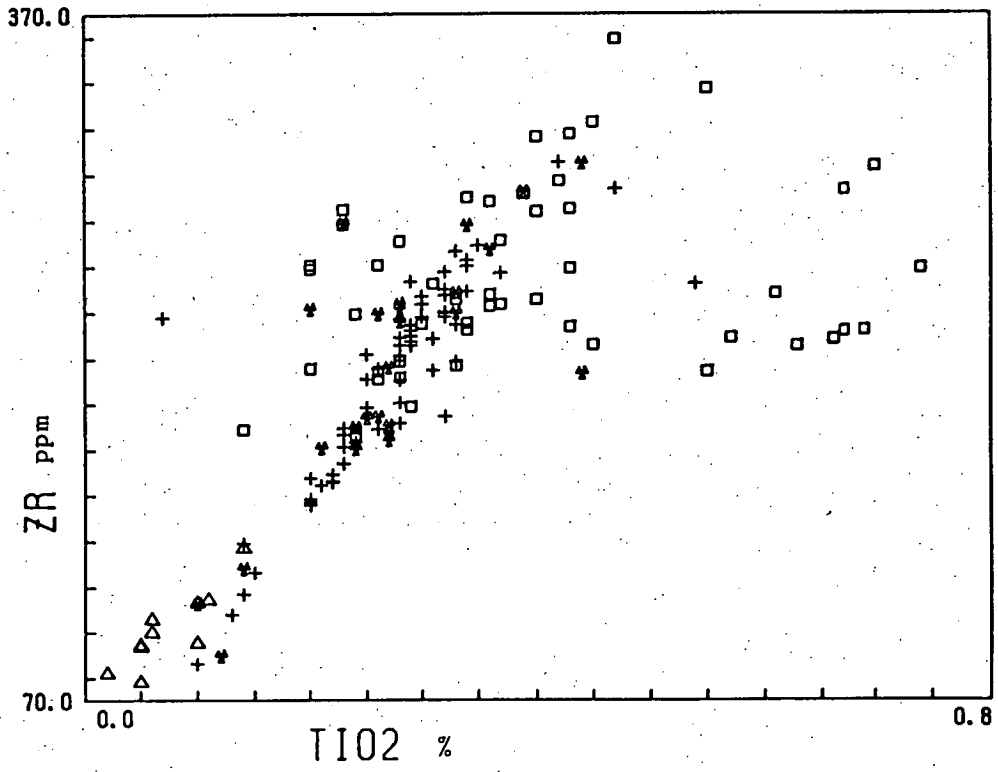

Fig.83: Diagram: Zr contents of unaltered volcanics (□), surface schists (✱), massive siliceous rocks (△), and mineschists (+), underground, plotted against TiO_2 content

e. Within the mine schists, the extension from approximately 75% SiO_2 and 0.25% TiO_2 to 86% SiO_2 and 0.1% TiO_2 requires a volume increase of more than 100% by silica dilution. The relative decrease of an immobile element demands increasingly larger addition of the diluting element or component, assuming no changes for the remaining constituents. This can be demonstrated:

$$100 = Y + X + R$$

$$Y^* = \pm Y \mp \frac{100\ Y}{100 \pm X^*} = \frac{Y\ X^*}{100 \pm X^*}$$

$$\frac{dY^*}{dX^*} = \frac{100\ Y}{(100 \pm X^*)^2}$$

Y = immobile component
Y^* = change in concentration of immobile component
X = diluting component
X^* = additional diluting component.
R = remaining components

Even if the remaining components were completely removed, the volume increase would be still too large to be ignored, and in addition, more silica would have to be added to compensate for the relative enrichment of the immobile element.

f. Mass balance calculations, discussed below, demonstrate the mobility of "immobile" elements under extreme hydrothermal conditions.

In summary, a dilution effect and probably an enrichment effect as well, exists by addition and removal of silica, but it is clearly not the only cause of depletion and enrichment of "immobile" elements such as Ti and Zr. A second process is responsible for the active removal of these elements. Dilution by other phases such as sulphides, and more frequently carbonates, can occur to some extent in the mine schists, and is extremely rare in the massive siliceous rocks.

Because of their proven mobility, Ti, Zr and Al were not used as reference elements in this study.

12.2. Constant volume.

In the absence of immobile elements, a constant mass or volume unit is needed to compare metasomatic processes at different stages of alteration. Several attempts have been made to convert the relative analysis data into absolute numbers by relating them to a constant volume or a mineralogical-structural unit.

Barth (1948) recommended a standard cell of 160 oxygen atoms as a reference unit. This model cannot be supported any longer in the light of modern oxygen isotope chemistry (Babcock, 1973). Poldervaart (1953) proposed a metasomatic calculation based on a constant sum of $(Si, Al)O_4$-tetrahedra assuming changes only between Si^{4+} and Al^{3+}. This method also ignores the mobility of oxygen. Bogolepov (1962) devised an algorithm that requires the normalization of the anions to a volume of 10,000 Å, but lacks a reference value. The method used in this study was developed by Gresens (1967). Not only does it account for differences in rock density as most of the calculations mentioned above, but also for changes in volume:

$$100 \quad f_v \, (d_B/d_A) C_n^B - C_n^A = X_n$$

f_v = volume factor
d = density
C_n^B = concentration of component n in sample B
C_n^A = concentration of component n in sample A
X_n = exchange in component n

Five different metasomatical processes were examined:

a. The element exchange between unaltered pyroclastics (density = 2.63g/cm^3) and surface schists (density = 2.67 g/cm^3) (fig.84a-c).

b. The element exchange between unaltered pyroclastics and siliceous mine schists (density = 2.78 g/cm^3) (fig.85a-c).

c. The element exchange between unaltered pyroclastics and sericitic mine schists (density = 2.78 g/cm^3).

d. The element exchange between unaltered pyroclastics and carbonaceous mine schist (density = 2.74 g/cm^3).

e. The element exchange between unaltered pyroclastics and massive siliceous rocks (density = 2.67 g/cm^3) (fig.86 a-c).

Surface schists, unaltered pyroclastics and massive siliceous rocks have been defined in chap. 8. The siliceous mine schists consist of underground samples taken from the central feeder channel immediately below the northern orebody. The sericitic and carbonaceous mine schists occur more frequently in the marginal zone of this channel.

The average rock densities (see appendix 2) were determined using a pycnometer from random samples of the involved rock groups. All average values, rock densities and chemical analyses are expressed by the median which is less sensitive to extreme values than the mean. All but one variable, the volume factor, are known.

12.2.1. Volume factor.

The volume factor (f_v) accounts for volume changes to the pyroclastic rocks incurred after their deposition, particularly during hydrothermal activity. At this stage presumably two mechanisms were working concurrently:

a. Plagioclase was replaced by sericite. This process could have reduced the volume of the altered schist by maximally 2-3% assuming a plagioclase content of up to 30% (volume).

b. Pore spaces in the original pyroclastics acted as channels for the hydrothermal fluids and became clogged during and/or at the end of the hydrothermal activity.

Part of the pore space may have continued to be filled with solutions into the Devonian, thus helping to produce the schists. The partial to dense welding of the footwall schists would indicate a porosity between < 10% to 20% (Smith, 1960; Sheridan, 1970; Peterson, 1979).

Diagenetic processes in the lagoonal environment of the pre-ore stage (chap. 7) could have further reduced the pore space.

The shearing of the altered tuffs in contrast to the unaltered pyroclastics probably had very little effect on the volume. This view is supported by the equality of rock density for schists and massive siliceous rocks, assuming the latter had a similar porosity. Tab.12 displays the processes that could have influenced the volume of the pyroclastic rocks.

	Unaltered Pyroclastics	Altered Pyroclastics
deposition of welded tuffs	<10-20% porosity	<10-20% porosity
diagenesis	decrease in porosity	decrease in porosity
hydrothermal activity		filling of pore space with deposits and fluids
Tabberabberan Orogeny	compaction	compaction and shearing

Tab.12: Volume changing processes in pyroclastic rocks

In summary, the increase in rock volume remained below 25% ($f_v \leq 1.25$) if the original porosity is considered to be at maximum 20%.

Prior to comparison, the major elements (oxide-%) and the trace elements (ppm) were normalized by converting them to mols and later recalculated to facilitate visual examination. Also included in this calculation were ignition loss and the trace elements Pb, Zn, Cu and Ba which can occur in larger quantities. This was done in order to account for most of the components contributing to the rock density. The element exchange is graphically demonstrated in fig.84a-c - fig.86a-c. The behaviour of Pb, Zn, Cu and Ba is only listed in appendix 5, as they are not part of the silicate alteration.

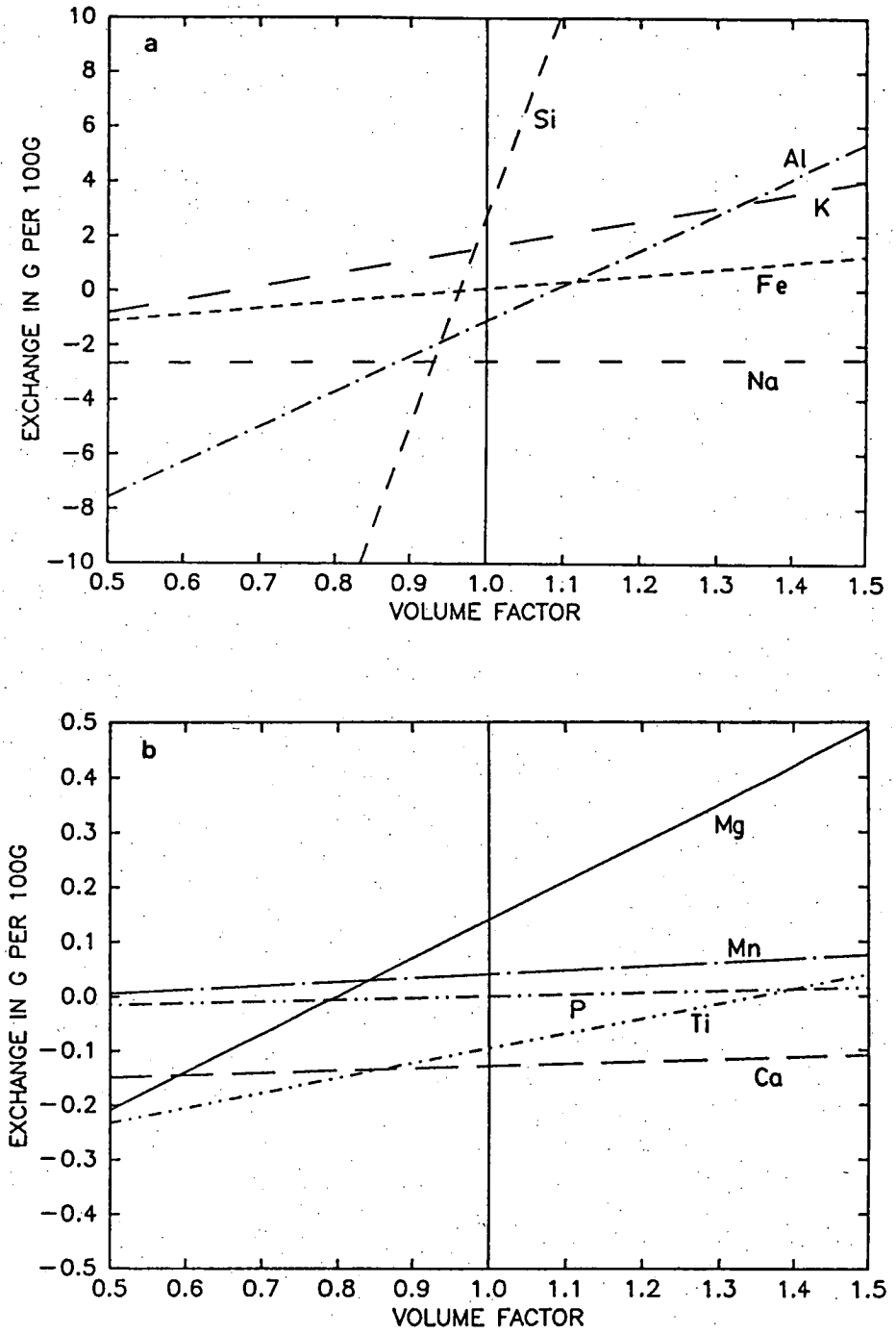

Fig. 84a-c: Element exchange from unaltered pyroclastics to surface schist plotted against volume factor (f_v). Area left/right of constant volume $f_v = 1$ represents volume decrease/increase in altered rocks. Exchange in major elements (a, b) is calculated in gram oxide per 100 gram rock. Trace element exchange (c) is expressed in 10^{-4} gram per 100 gram rock

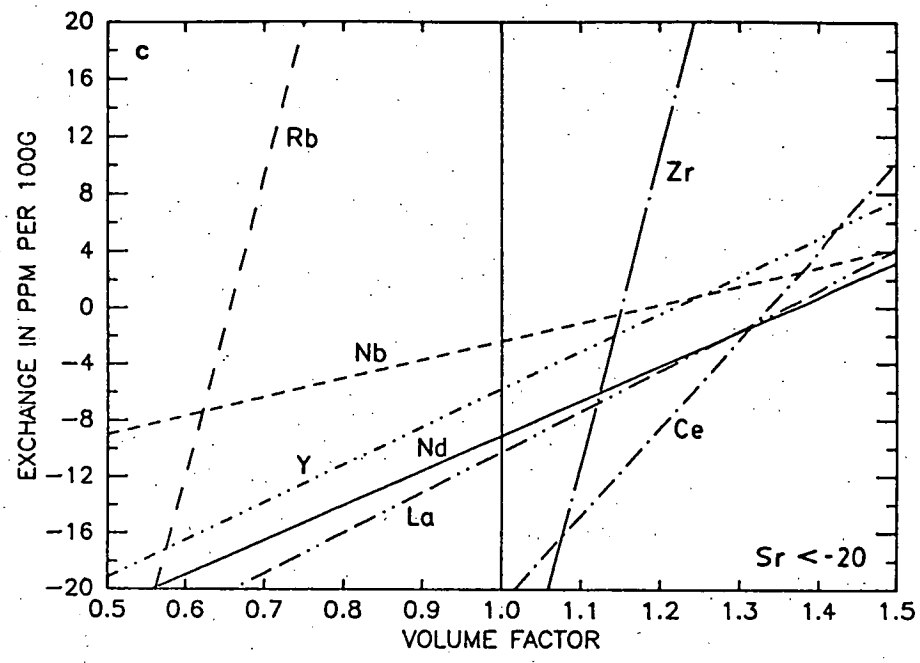
c
Rb
Zr
Nb
Y
Nd
La
Ce
Sr <-20
EXCHANGE IN PPM PER 100G
VOLUME FACTOR
20
16
12
8
4
0
-4
-8
-12
-16
-20
0.5
0.6
0.7
0.8
0.9
1.0
1.1
1.2
1.3
1.4
1.5

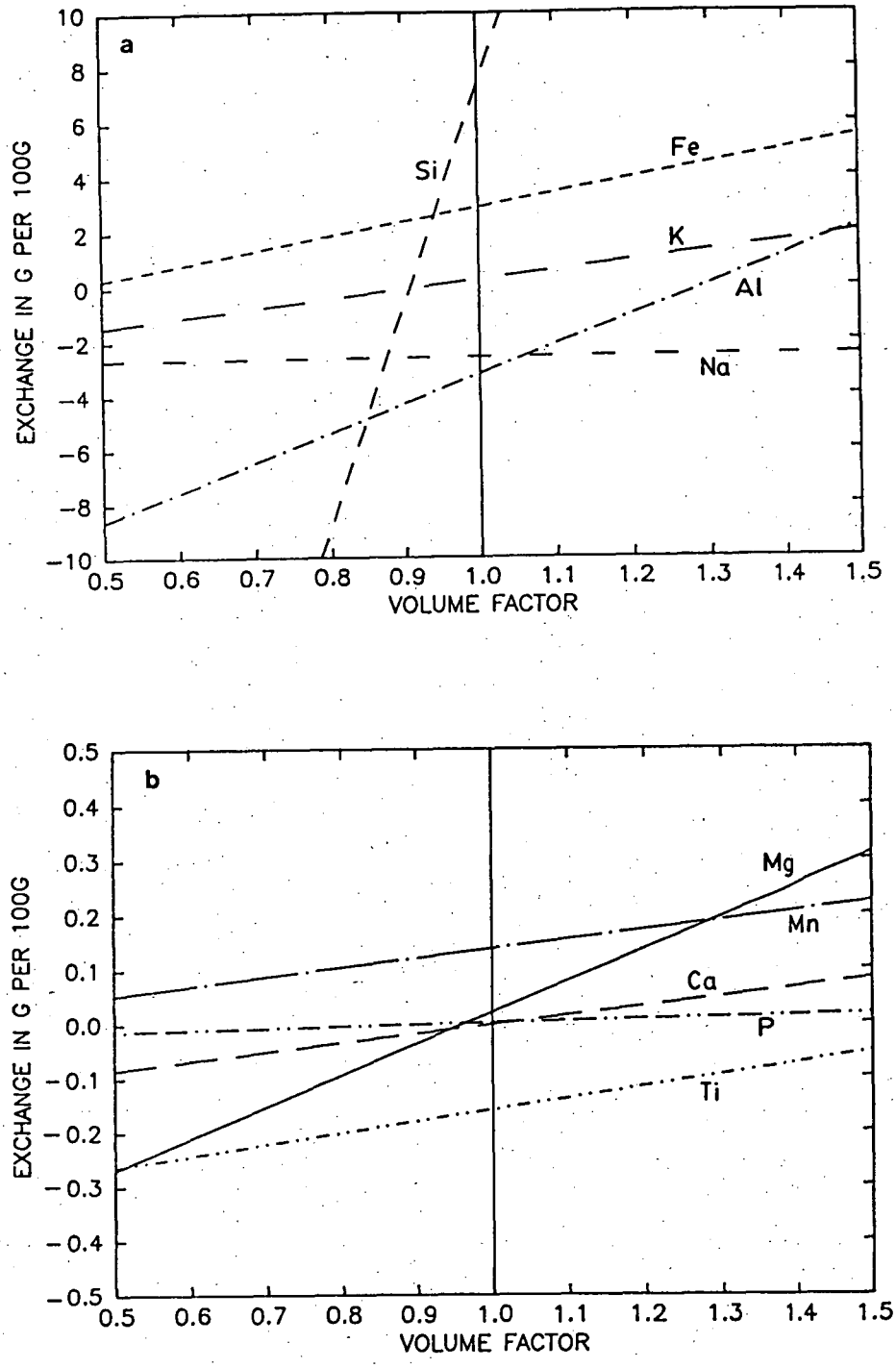

Fig.85a-c: Element exchange from unaltered pyroclastics to siliceous mine schists, underground

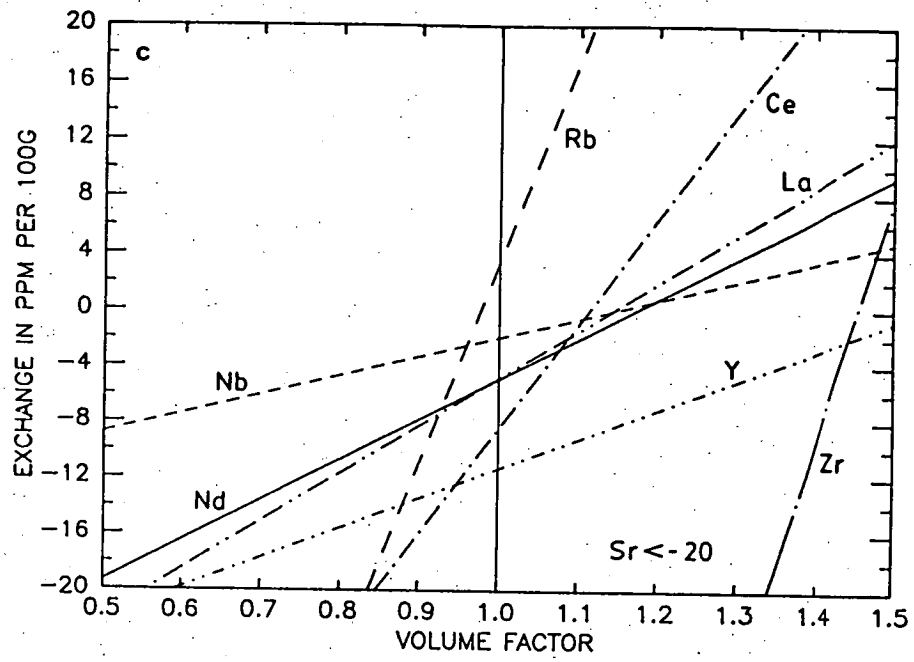
c
Rb
Ce
La
Nb
Y
Nd
Zr
Sr<-20
EXCHANGE IN PPM PER 100G
VOLUME FACTOR
20
16
12
8
4
0
-4
-8
-12
-16
-20
0.5
0.6
0.7
0.8
0.9
1.0
1.1
1.2
1.3
1.4
1.5

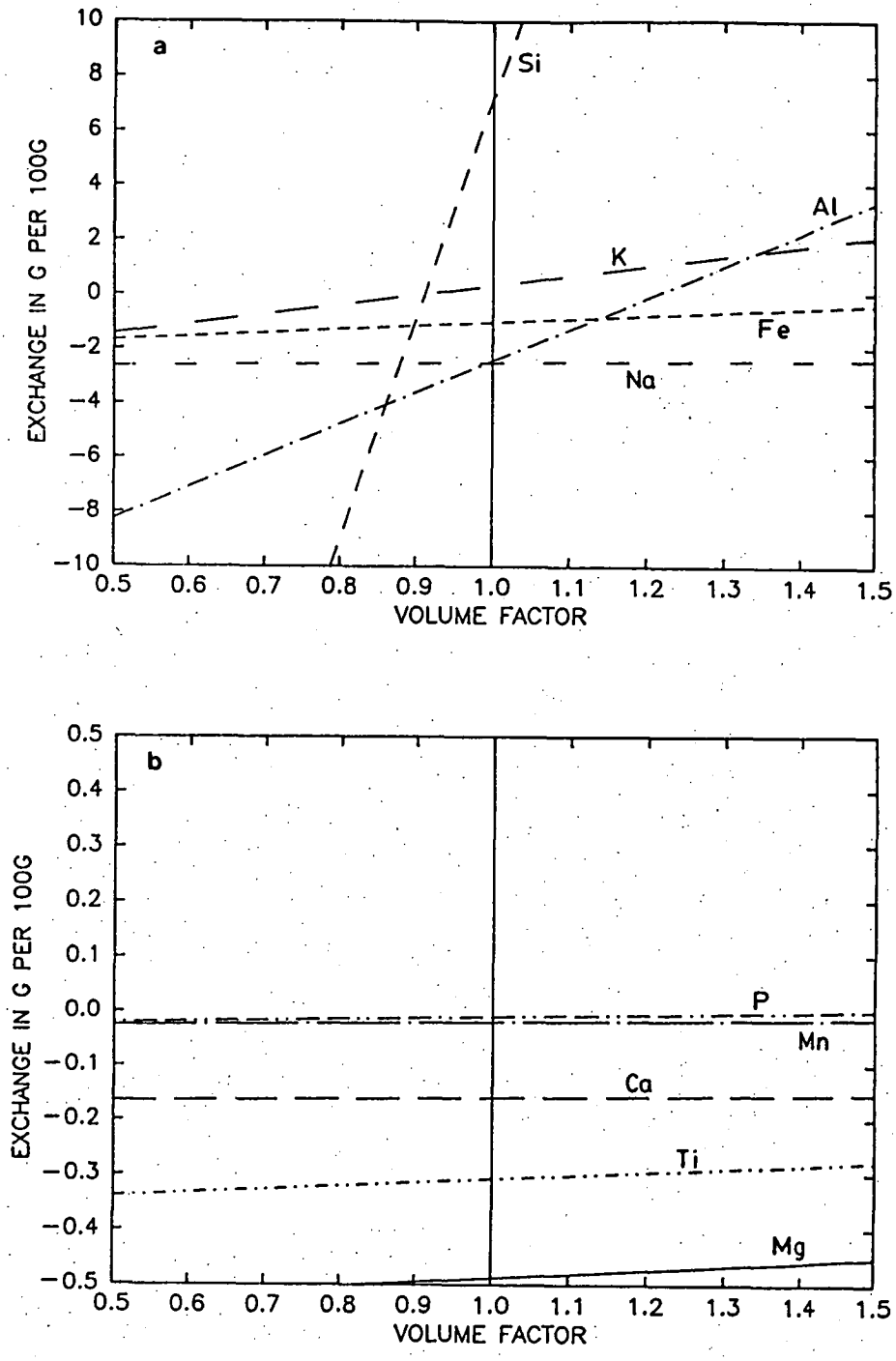

Fig.86a-c: Element exchange from unaltered pyroclastics to massive siliceous rocks

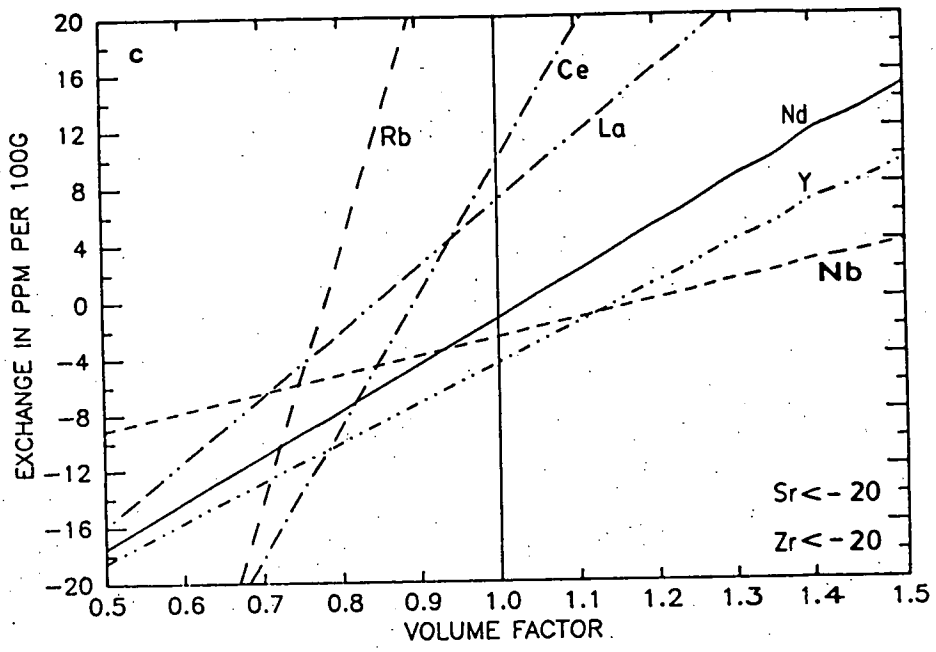
c
Rb
Ce
La
Nd
Y
Nb
Sr<-20
Zr<-20
EXCHANGE IN PPM PER 100G
VOLUME FACTOR
20
16
12
8
4
0
-4
-8
-12
-16
-20
0.5
0.6
0.7
0.8
0.9
1.0
1.1
1.2
1.3
1.4
1.5

Gresens (1967) suggested determining the volume factor (f_v) as the point on the gain-loss zero line where several components cross simultaneously. In the case of Rosebery, no such crossing point exists. Note, however that Nb, one of the elements considered immobile, invariably crosses the gain-loss zero line around f_v = 1.15 - 1.2, which falls into the estimated range of volume increase.

12.2.2. Results.

As expected, the element concentrations that changed statistically, (chap. 8.3.1.3.3.) exhibit a more pronounced depletion or enrichment. The element behaviour is listed in tab. 13. During the transformation from unaltered pyroclastics to massive siliceous rocks Al, Nb and Y may have remained immobile. Si and the LREE were enriched while the remaining elements were depleted. A general increase in the content of Fe, Mn, K and Rb and a decrease in the content of Ti, Na, Ca, Sr and the LREE occurred in the schists during alteration. Al, Y and Zr were only removed from the central vent immediately below the ore (see also below), where the LREE appear to have remained relatively immobile. As the contents of Ca and LREE were only reduced in the surface schists, this pattern could be explained by surface weathering or may be interpreted as an enrichment in these elements from the peripheral alteration zone of the surface schists to the central zone immediately below the ore. Other elements that reveal the same trend are Fe, Mn, Sr and Si. The enrichment of Fe is not correlated with S (see below). Fe is incorporated in sericite and chlorite. Mn, Ca and Sr are contained in carbonate, and Si represents silicification. The behaviour of the LREE - relative immobility in the mine schists in contrast to intensive depletion of Zr - leaves zircon to be an unlikely host mineral as discussed in chap. 11.1.2. However the interpretation of the LREE requires caution due to the small sample size for the mine schists (n = 4) and the massive siliceous rocks (n = 6). P_2O_5 concentrations were usually close to or below the detection limit and are therefore not considered in this discussion. Apart from Al, Zr and Ti, the mobility pattern agrees with findings by Green (1983). The amount of exchanged material in oxide% and in percentage (in respect to unaltered pyroclastics) are listed for volume factor (f_v) 1.0 - 1.2 in appendix 5.

The element behaviour in process c. and d. (see above) indicates immobility of Zr, immobility to minor depletion of Ti and Si, immobility to

	surface schists	siliceous mine schists (underground)	massive siliceous (surface)
SiO_2	+	+	+
TiO_2	-	-	-
Al_2O_3	±	-	(±), -
Fe_2O_3	+	+	-
MnO	+	+	-
MgO	+	+	-
CaO	-	±, +	-
Na_2O	-	-	-
K_2O	+	+	+
P_2O_5	±	(±), +	-
Nb	±, -	±, -	(±), -
Zr	±, -	-	-
Y	±, -	-	±, -
Sr	-	-	-
Rb	+	+	+
La	-	±, -	+
Ce	-	±	+
Nd	-	±, -	±, (+)

Tab. 13: Summary of element enrichment (+) and depletion (-) during alteration

minor enrichment of Al and enrichment of Ca. The complete results are also listed in appendix 5. As no clear zonation of sericitic and carbonaceous footwall schists could be established, below the northern orebody, no detailed discussion for the element mobility in these two facies is given.

12.2.3. Comparison with other massive sulphide deposits.

The removal of Na, Ca and Sr, and the addition of Mg, Fe, Mn K, Rb and Si at Rosebery, with a quartz-sericite-chlorite-(carbonate) assemblage is a common process which has affected the wall rock of many massive sulphide deposits. Some of the better known deposits and their alteration characteristics are listed in tab.14. They have partly been compiled by Goodfellow (1975), McConnell (1976) and Govett & Nichols (1979).

Apart from the "immobile" elements, the geochemical pattern at Rosebery is remarkably similar to that at Que River, Woodlawn and the Kuroko deposits.

12.3. Correlation

A correlation analysis was conducted, based on drill core samples from the transition zone in the footwall schists, with plagioclase alternatively present and removed, including DDH 1121, and from the massive pyroclastics in the hanging wall, including DDH 46R, with decreasing alteration (see appendix 1, 2). This sample selection ensures a wide range, from unaltered to altered volcanics. Also, influences due to weathering could be avoided as could spurious correlations resulting from two clusters, having the practical effect of correlating two points. Apart from Pearson's correlation, the non-parametric Spearman correlation was also calculated to check for the transformation to normally distributed data. The results of both methods are in good agreement. Pearson's correlation coefficients are listed in tab.15. Partial correlation coefficients for major elements (except for P_2O_5) including Zr and S adjusted for the same set of elements are presented in tab.16. Both figures have been referred to in previous discussions. The correlation coefficients in tab.15 essentially reflect the element behaviour during hydrothermal alteration. The general lack of strong correlation is due to the large variation in the collected data. The relatively strong

Tab.14: Alteration around massive sulphide deposits

Deposit	Alteration mineralogy	Elements added	Elements removed	Elements unchanged	Age
Mattabi, Canada Franklin et al. (1975)	qz, cb, ser, chld, chl, andal, gar, kyan	Fe,Mg	Na, Ca	-	archaean
Millenbach, Canada Simmons et al. (1973)	cord, antoph, chl ser, qz	Mg,Fe	Na, Ca, Si	-	archaean
Riverin & Hodgson (1980)	"	Mg, Fe, K, Al, Si	K, Al, Ti, Si		
Lake Dufault, Canada Sakrison (1966)	chl, ser	Mg, Fe, Mn	Na, Ca	Al, Ti, K, Si	archaean
Abitibi volcanic belt, Canada Descarreaux (1973)	chl, ser,qz	Mg, K	Na, Ca	Si	archaean
East Waite, Mobrun, Joutel, Poirier, Agnico-Eagle, Mattabi, Sturgeon Lake, South Bay, Canada McConnell (1976)	qz, ser, chl, sauss, epi	Mg, Fe	Na, Ca	Si,Al	archaean
Mattagami, Canada Roberts & Reardon, (1978)	talc,chl, act, stilp	Ti, Al, Mn, Mg, Ca, K, Na	Ti, Al, Ca, K, Na	-	archaean
Boliden, Sweden Nilsson, (1968)	qz, andal, chl, ser	Mg, K, Al	Na, Ca	-	proterozoic
Buchans, Canada Thurlow et al. (1975)	chl, ser, qz	Mg, Fe, Si	Na, Ca, K	Al	palaeozoic
Heath Steele, Canada Wahl et al. (1975)	chl, ser	Mg	Na, Ca	-	palaeozoic
Brunswick No. 12, Canada Goodfellow (1975)	chl, ser, qz	Mg, Fe, Mn, K	Na, Ca	Al	palaeozoic

Deposit	Alteration mineralogy	Elements added	Elements removed	Elements unchanged	Age
Killingdale, Norway Rui (1973)	chl, bio, qz	Mg, K, Mn	Na, Ca, Si	Al, Ti, Fe_{tot}	palaeozoic
Skorovass, Norway Gjelsvik (1968)	chl, ser	Mg	Na, Ca	-	palaeozoic
Woodlawn, Australia Peterson & Lambert (1979)	qz, ser, chl	Fe, H_2O, Mg, S, Si,	Ca, Na, Sr	-	palaeozoic
Mt. Lyell, Australia Walshe & Solomon (1981)	qz, ser, chl	H_2O, Ba, P	Na, Ca, Rb, Sr, Al	-	palaeozoic
Que River, Australia Whitford et al. (1984) Wallace, (1984)	qz, ser, chl,cb	MgO, FeO, MnO	Na, Ca, Sr, LREE, Al, Ti	_	palaeozoic
Kuroko, Japan Tatsumi & Clark (1972)	ser, qz, cal	K, Mg	Na, Ca, Fe	Al	cenozoic
Kuroko, Japan Lambert & Sato (1974)	mon, ser, chl, kaol	Mg, K, Fe, Si	Ca	-	cenozoic
Fukazawa-Kosaka, Japan Green et al. (1985)	zeol-mont mont-ser, chl	Mg, Na Mg, K	K, Ca Na , Ca, Sr	- -	cenozoic

	Si	Ti	Al	Fe	Mn	Mg	Ca	Na	K	P	Nb	Zr	Y	Sr	Rb	S	La	Ce	Nd
Si																			
Ti	-0.4																		
Al	-0.6	0.5																	
Fe	-0.5	0.5	0.4																
Mn	-0.2	-0.2	-0.1	0.2															
Mg	-0.2	0.0	0.3	0.1	0.2														
Ca	-0.5	0.2	0.0	-0.2	-0.1	-0.2													
Na	-0.2	0.3	0.0	-0.1	-0.5	-0.4	0.4												
K	-0.3	-0.1	0.4	0.2	0.5	0.1	-0.2	-0.4											
P	-0.1	0.3	0.2	0.0	-0.1	0.3	0.1	0.1	-0.2										
Nb	-0.3	0.1	0.5	0.0	0.2	0.5	-0.2	-0.2	0.3	0.2									
Zr	-0.5	0.5	0.7	0.4	0.1	0.2	-0.1	0.1	0.4	0.1	0.6								
Y	-0.5	0.5	0.4	0.4	-0.1	-0.2	0.2	0.3	0.1	-0.1	0.2	0.7							
Sr	-0.3	0.3	0.3	-0.1	-0.6	-0.2	0.5	0.7	-0.4	0.2	-0.1	0.1	0.4						
Rb	0.0	-0.1	0.2	0.1	0.6	0.1	-0.3	-0.6	0.8	-0.3	0.3	0.3	-0.1	-0.7					
S	0.3	-0.3	-0.4	0.1	0.4	-0.2	-0.4	-0.3	0.0	-0.1	-0.2	-0.3	-0.3	-0.5	0.3				
La	-0.1	0.4	0.5	0.0	-0.3	0.0	-0.2	0.4	-0.2	0.1	0.4	0.6	0.6	0.3	-0.2	-0.2			
Ce	-0.1	0.4	0.5	0.0	-0.3	0.0	-0.2	0.3	-0.1	0.2	0.4	0.7	0.6	0.3	-0.2	-0.2	0.9		
Nd	-0.1	0.5	0.4	-0.1	-0.4	-0.1	-0.1	0.4	-0.2	0.2	0.4	0.7	0.7	0.3	-0.2	-0.3	0.9	0.9	

Tab.15: Major and trace element correlation from core samples

correlation betwen Si and Ti and Zr is reduced or reversed in tab.16. The strong negative correlation between Ca and Si (tab.16) is caused by a replacement process (process d., e.) which also includes to a certain degree Fe and Mg.

	Si	Ti	Al	Fe	Mn	Mg	Ca	Na	K	Zr	S
Si											
Ti	0.3										
Al	-0.6	0.2									
Fe	-0.7	0.5	-0.2								
Mn	0.0	-0.2	-0.2	0.2							
Mg	-0.5	0.1	-0.1	-0.4	0.1						
Ca	-0.9	0.4	-0.5	-0.6	0.2	-0.4					
Na	-0.3	0.1	-0.1	-0.2	-0.2	-0.5	-0.1				
K	-0.2	-0.2	0.2	-0.2	0.4	-0.4	-0.2	-0.4			
Zr	-0.3	0.5	0.2	-0.3	0.2	-0.1	-0.4	0.2	0.2		
S	-0.4	0.1	-0.4	-0.1	0.3	-0.2	-0.5	-0.2	-0.3	-0.1	

Tab.16: Partial correlation of major and trace elements from core samples

13. Stability of silicate phases under hydrothermal conditions.

In addition to the exchange reactions of elements, further information about the hydrothermal environment can be obtained by comparing the mineral assemblage to its possible thermodynamic stability under certain assumed conditions.

The calculations of the phase diagrams given in (fig.87-89, 91) have been based on the equilibrium equation ($\Delta G = 0$):

$$\Delta G^{o} = -RT \ln \frac{\pi a_i}{\pi a_j} = -RT \ln K$$

The equilibrium constant (K) can be calculated if the standard free energy of each component (G^{o}) involved in the reaction is known. In the case of the reaction

$$3Kfs + 2H^{+} \leftrightarrow musc + 6qz + 2K^{+}$$

the equation $$K = \frac{a_{musc}\ a_{qz}^{6}\ a_{K^+}^{2}}{a_{Kfs}^{3}\ a_{H^+}^{2}}$$

can be reduced to $$K = \frac{a_{K^+}^{2}}{a_{H^+}}$$ if the activity (a) of the solid phases Kfs, musc and qz are taken as unity. The equilibrium constants of all reactions involved are listed in appendix 6. Their calculation was based on thermodynamic data by Helgeson (1969) and Helgeson et al. (1978)

In fig. 87-89, the stability fields of kaolinite (kaol), albite (ab), muscovite (musc), K-feldspar (Kfs), illite (ill), zoisite (zoi) and Mg-chlorite (Mg-chl) are shown at temperatures from 200°C to 300°C, which is considered to be the maximum temperature during ore deposition at Rosebery (Green et al., 1981). Similar or slightly higher temperatures of 350°C to 400°C (Green, 1983) existed during the Tabberabberan Orogeny in the Devonian. These temperatures and also increased pressure (see below) should not have shifted the stability fields greatly. Based on the estimated thickness of overlying Cambrian volcanics, and late Cambrian to early Devonian sediments, Green (1983) derived a lithostatic pressure of 1.6 - 2.1 kbar during the Tabberabberan Orogeny. This pressure increase for example would mean a shift of the muscovite-K-feldspar boundary from

log K^+/H^+ = 3.8 to log K^+/H^+ = 4.0 for 1 kbar and to log K^+/H^+ = 4.2 for 2 kbar at 300°C. According to Helgeson et al. (1978) the phase boundaries remain relatively unchanged up to 400°C and 4kbar. These variations probably lie within the accuracy of the experimentally determined thermodynamic data, as evident in fig. 87 and fig 88 for the kaolinite-muscovite boundary based on Helgeson (1969) and Helgeson et al. (1978). Apart from this inherent inaccuracy, the assumption of unit activity of the silicate phase and also the requirement of chemical equilibrium, further reduces the value of these diagrams as a quantitative tool. The large variation in mineral composition, particularly for chlorite and sericite (chap. 10.2.) speaks against equilibrium conditions (see also Green, 1983).

Keeping in mind the restrictions of these diagrams, fig.87 allows a qualitative explanation of the existence of feldspars under various hydrothermal conditions. K-feldspar in the peripheral alteration zone on the surface can presumably co-exist with sericite in a regime of reduced H^+ activity and/or increased K^+ activity as indicated by the potassium gain in the surface schists (chap. 12.2.2.). The partial survival of albite around the central feeder channel immediately below the ore requires a higher Na^+

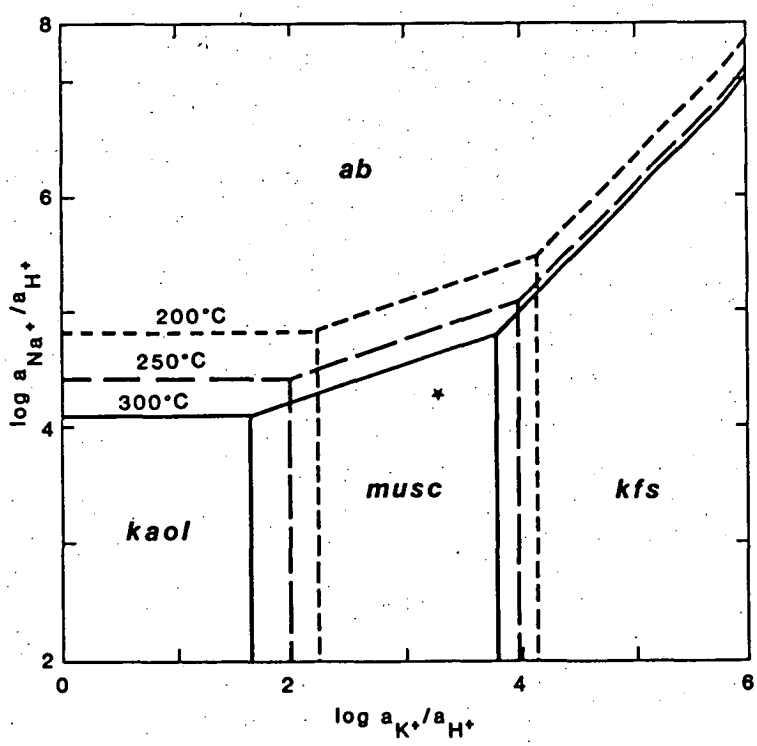

Fig. 87: Phase diagram log $a_{Na^+}/a^2_{H^+}$ vs. log a_{K^+}/a_{H^+} at 1 bar, qz-saturated , symbol * indicates estimated conditions. Paragonite field is omitted due to conflicting thermodynamic data

activity to balance the more acid conditions. The formation of albite in the host rock, below and within the ore, occurred after mixing of hydrothermal fluids with seawater. The occurrence of these feldspars places some constraint on the hydrothermal solution in respect to the activity of Na^+, K^+ and H^+. An estimate is indicated by the symbol (*). The log $a_{Na}+/a_H+$ must have been close to the albite-muscovite boundary to enable the formation of albite in the host rock due to local fluctuations in temperature, acidity and Na^+ activity. The existence of moderately to advanced altered albite surrounding the central alteration zone, in contrast to its absence on the surface schist is a further indication that the condition could have been close to albite-muscovite stability. If mixing of 10% seawater ($T \simeq 0^oC$) with the hydrothermal solution ($T \simeq 300^oC$) would lead to the precipitation of the ore as proposed by Ohmoto et al. (1983), the temperature of the hot fluids would be reduced to 270^oC, further increasing the stability field of muscovite. In order to form albite under these conditions, local boiling as suggested by Green (1983) may be necessary to decrease the acidity.

Conversely a secondary origin of albite could possibly be conceived. Albite is present as fresh euhedra in a polygonal matrix which could be indicative of metamorphic growth. At 350^oC and 1 - 2 kbar pressure, the albite stability field extends to slightly lower log $a_{Na}+/a_H+$ ratios, thus providing the conditions for an albite-muscovite-quartz assemblage. This idea is based on the assumption that the hydrothermal conditions in respect to the proportion of Na^+ and H^+ prevailed into the Devonian. The close association between schist and chemical alteration lends support to the existence of fluid in the wall rock during the Tabberabberan Orogeny.

Furthermore, estimates can also be made about the Ca^{2+} and Mg^{2+} content of the hydrothermal solutions. Clinozoisite and epidote, minerals of the greenschist facies occur only in unaltered and weakly altered volcanics. Allowing again for metamorphic peak temperatures of approximately 350^oC, the extrapolated zoisite-muscovite boundary at this temperature would indicate a log $a_{Ca}2+/a_H^2+$ close to 6, marked by (*) in fig. 88. No estimates are provide for influence of Fe on the thermochemical stability of zoisite. Textural evidence - epidote and clinozoisite overgrowing chlorite and sericite - probably excludes retrograde growth.

The sericite at Rosebery is similar in its composition to the Mg-illite in Helgeson (1969) except for its Fe-contents. The Mg/Mg+Fe ratio

of the examined chlorite never exceeds 0.6. Based on these mineralogical constraints, the stability field of illite gives a very general indication of the Mg concentration under hydrothermal conditions, assuming they persisted into the Devonian. At temperatures of 300° or 350°C the log $a_{Mg}2+/a_{H}+^{2}$ should have been at or above a value of 4.5 to stay within the illite field. A more exact delineation, represented by (*) in fig.89, in respect of the Mg^{2+} and H^{+} proportion is not possible, as the addition of Fe to these phyllosilicates certainly has a strong influence on the position of their respective phase stabilities. Because of the lack of reliable thermodynamic data, no evaluation for Fe-bearing silicate phase could be made.

The overprint of the metamorphic conditions on the hydrothermally affected volcanics makes a clear definition of this hydrothermal environment virtually impossible, unless it is regarded as having persisted essentially unchanged into the Devonian Orogeny. During the metamorphic event, slightly different conditions for temperature and pressure existed apart from the remaining fluids in the pore space of the volcanics.

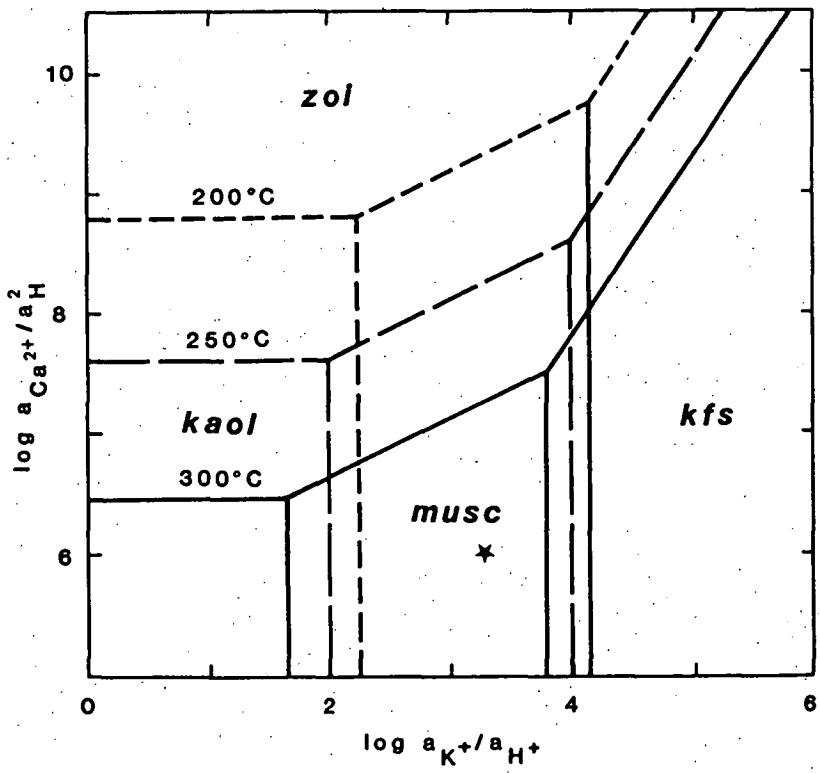

Fig.88: Phase diagram log $a_{Ca}2+/a^{2}_{H}+$ vs. log $a_{K}+/a_{H}+$ at 1 bar, qz-saturated. Symbol * indicates estimated conditions. Wairakite field omitted due to conflicting thermodynamic data

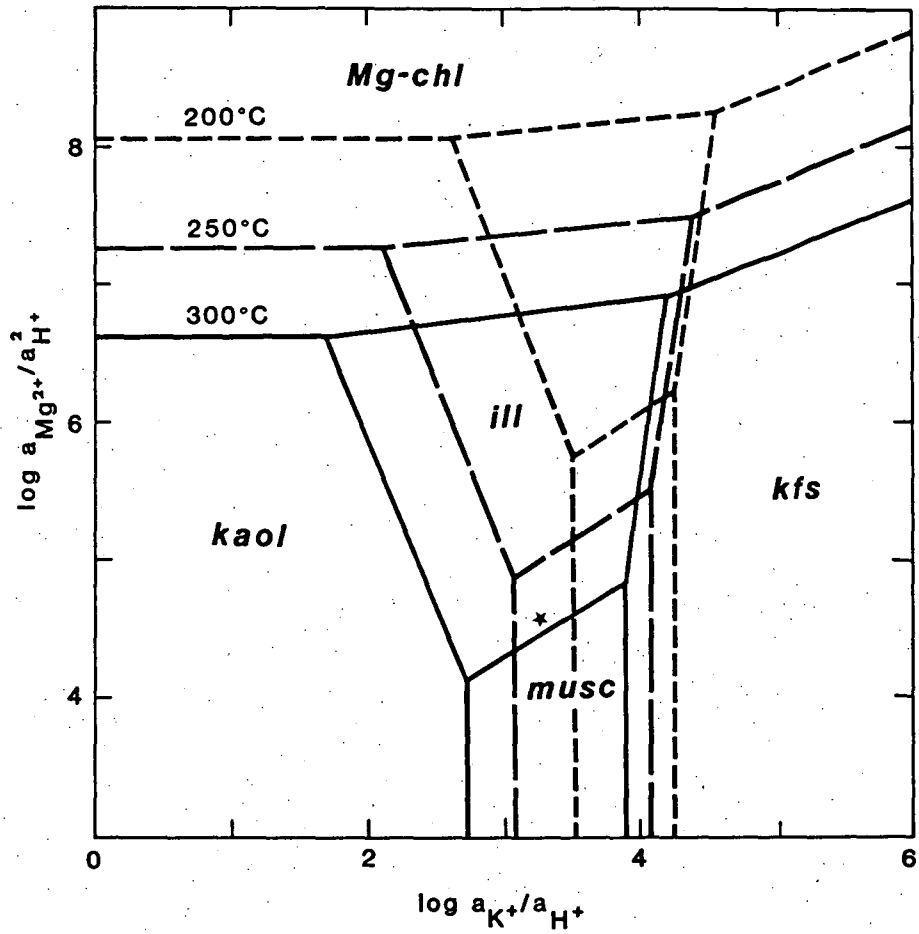

Fig.89: Phase diagram log $a_{Mg}2+/a^2_{H}+$ vs. log $a_{K}+/a_{H}+$ at 1 bar, qz-saturated. Symbol * indicates estimated conditions.

14. Solution conditions.

Temperature estimates of approximately 300°C for the hydrothermal environment at Rosebery are based on sulphur isotope fractionation between co-existing sulphides and sulphide-barite (Green et al., 1981). They also assumed an acidity of 1 unit below neutral for their solution model. Further evaluation of the solution conditions including solute concentrations for massive sulphide deposits and modern hydrothermal systems are listed in tab.17 for comparison.

For the purpose of this study, a maximum temperature of 300°C and an acidity of one unit below neutral (pH ≃ 4.5) was also chosen. From the estimated ion activities it was possible to calculate the ionic strength,

$$I = 1/2 \sum_{i=1}^{n} m_i z_i^2$$

m = mol of solute

z = electric charge of solute

the activity coefficients (γ), and subsequently the ion concentrations in weight solute per 1000 grams of water (m) using the Debye-Hückel equation.

$$-\log \gamma = \frac{A z^2 I^{1/2}}{1 + \mathring{a} B I^{1/2}} \qquad m = a/\gamma$$

The values for A, B and $\mathring{a}$ were taken from Henley et al. (1984). The concentrations were calculated by reducing the original set of five variables (Na^+, K^+, Mg^{2+}, Ca^{2+} and Cl^-) with five equations to the two main variables Na^+ and K^+. The activities of Mg^{2+} and Ca^{2+} were negligibly small when compared to the first two ion activities. The concentration of Cl^-, a major component in hydrothermal fluids, can be taken as the sum of the concentrations of Na^+ and K^+ (Henley et al., 1984). As a result, the concentrations for Na^+ and K^+ were found to be 2.2m and 0.1m respectively. Based on an ionic strength of 2.3 (2.2 + 0.1), the concentrations for Ca^{2+} and Mg^{2+} were calculated to be 0.04m and 0.002m. Except for Na^+, the concentrations are basically in agreement with other quoted estimates (tab.17). The concentrations calculated above are used in the following chapter (fig.91) to model the ore deposition.

	T °C	pH	log fO_2 atm	log ∑S m	Na m	K m	Mg m	Ca m	Ba m	Zn	Pb	Cu	Fe	References
A														
Kuroko deposits[1]	250	≥2.5**	-35 to -32	-3 to -1	0.9	0.1			0.001m					a
"	235	3.6-4.4		-3 to -2.5	3	1						0.0001m		b
				-1.7 to -0.9										c
"	≤300													d
Archaean deposits[2]	250-300	5.0	-36	-3	1									e
Cyprus deposits[3]	300	0.5**	-1 to 0*	-2	0.5	0.04						1ppm		f
Mt Lyell deposits[4]	300	1**	-2 to 0*	-2.8	0.9	0.1	0.025	0.001						g
Rosebery deposit[4]	300	1**	-8 to -4*	-2.7	0.9	0.1	0.001	0.001	0.001m					h
"		1**	-7 to -4*	-2.7	3.5									i
Kuroko deposit[1]	350±50				0.6	0.08	0.013	0.06		≤3ppm	≤3ppm	≤5ppm	≤6ppm	j
"	≤350	4.5±0.3			0.6	0.06	0.01	0.05		10ppm	<--few ppm-->		100ppm	
B														
East Pacific Rise[5]	380±80													k
"	350	3.6(25°C, 1 atm)												l
Atlantis II deep[6]	200-250 (>334)	4.5	-42 to -37	-3 to -2										m
Salton Sea[5]	≤325		≥-27		52000		10-50	28000		650	82	5	2050	n
Taupo, N.Z.[7]	275				740		<0.1	1.5		0.007	0.002	0.15	0.25	o

Key:

1: Japan
2: Canada
3: Cyprus
4: Tasmania
5: California (Salton Sea: mean, no. 1 and 2 I.I.D well)
6: Red Sea
7: N.Z. (no. 2 well, Broadlands)
**: unit acid
*: $\log \sum SO_4 / H_2S$
A: Massive sulphide deposits
B: Modern hydrothermal systems

References:

a: Kajiwara, 1971
b: Sato, 1971
c: Kajiwara, 1973
d: Tokunga & Honma, 1974
e: Large, 1977
f: Solomon & Walshe, 1979
g: Walshe & Solomon, 1981
h: Green et al., 1981
i: Green, 1983
j: Pisutha-Arnond & Ohmoto, 1983
k: Spiess et al., 1980
l: Edmond, 1983
m: Pottorf & Barnes, 1983
n: Skinner et al., 1967
o: Ellis, 1968

Tab. 17: Conditions of hydrothermal solutions

In addition to the solutes listed in tab.17, small amounts of silica (quartz) with < 700 ppm (Fournier & Truesdell, 1970) and amorphous silica with > 1000 ppm (Rimstidt & Cole, 1983) at 300°C are carried in solution. These concentrations are strongly temperature dependent and could have caused repeated clogging of the hydrothermal system at the rock-water interface (see next chapter).

The ore-forming metals are mainly transported as soluble chloride complexes (Barnes, 1979). The importance of chloride as a complexing agent that enables the formation of economic ore deposits, is demonstrated when Cl poor hydrothermal springs from Wairakei, Ngawha and Broadlands (Ellis, 1968) as an example are compared to Cl-rich hydrothermal wells in the Salton sea (Skinner et al., 1967), on the Cheleken peninsula (Lebedev, 1967 in Ellis, 1968) and in the Red sea (Miller et al., 1966; Brewer & Spencer, 1969). The difference in the Cl content is in the order of two magnitudes. The amount of ore metals in solution in the latter wells is in the range considered necessary for the generation of ore deposits, and generally exceeds that of low Cl wells by two orders of magnitude or more. In addition Na, Ca, Mg and Mn are present in large amounts. Two representative wells are listed in tab.17.

The interaction of heated seawater and hot brines with basalt, andesite (Seyfried & Bischoff, 1977 & 1981; Mottl & Holland, 1978; Mottl et al., 1979; Hajash, 1975; Bischoff & Dickson, 1975), rhyolite (Dickson, 1977) and graywacke (Bischoff et al., 1981) have been studied experimentally. During the reactions at temperatures above 200°C, seawater became acid due to the incorporation of Mg and OH^- into the altered rock material to form phyllosilicates. Base metals were soluble in the ppm range, particularly in NaCl rich brines. The concentrations of Ca^{2+}, CO_2, SiO_2, K^+, Fe^{2+}, Mn^+, Ba^{2+}, and H^+ were enriched. Only small quantities of Al^{3+} entered the solution. Na^+ was removed from or added to seawater to a small degree, and the amount of SO_4^{2-} decreased, due to formation of anhydrite. Reduced sulphur was released from the rock material into the solution, and was also produced by reduction of seawater sulphate by ferrous iron in the basalt. The slight increase of Cl^- in seawater after reacting with rhyolite cannot explain the required amounts of NaCl in solution. Green (1983) argued that the hydrothermal fluids at some stage must have passed through sediments containing evaporites. The NaCl content may have also been increased by evaporation in a partly closed basin, as suggested in chap. 11.2.2.

The experimental element behaviour is only partly reflected in the altered Rosebery volcanics. Na_2O is removed from surface and mine schists, and CaO is depleted in the surface schists only. SiO_2, K_2O, FeO and MnO are enriched in all schists (chap. 12.2). This indicates that the element behaviour is not only governed by the degree of solution saturation, but also by the thermochemical environment encountered and the total water/rock ratio.

15. Ore genesis.

The model of large convective systems with hot brines leaching the heavy metals from the wall rock and depositing them on the sea floor (White, 1968; Anderson, 1969), has been widely accepted as the mechanism that generates massive sulphide deposits. Green et al. (1981) and Green (1983) inferred from sulphur isotope data, with a range of 8.8 - 15.5 for sulphides and 34.6 - 41.2 for sulphates (Stanton & Rafter, 1966; Solomon et al., 1969; Green et al., 1981), seawater to be the main source of the hydrothermal fluids at Rosebery.

Sato (1972) described the behaviour of metal-bearing hot brines in respect to their density after entering cold seawater (fig.90). He envisaged three different mechanisms describing the buoyancy of the hot solutions on entering the sea floor:

Type I :A low temperature high salinity brine, always denser than seawater, would remain close to the sea floor preferably filling depressions.

Type II :A solution higher in temperature and originally buoyant at the time of discharge, passes through a density maximum greater than that of seawater during continuous mixing, resulting in a plume reversal. This heavier than seawater brine would behave as type I.

Type III:A high temperature, low salinity solution never exceeding the density of seawater, would rise to the seawater surface or rise until diluted infinitely, and thus disperse the suspended sulphide particles over a wide area.

Solomon & Walshe (1979) explained the large scale zonation of a Cu-Fe-rich bottom and a Pb-Zn-rich top part for massive sulphide deposits by a type III mechanism. Precipitation of the less soluble Cu-Fe-sulphides from the solution on entering seawater, would form a mound of chalcopyrite and pyrite around the discharging vent. The more soluble Pb-Zn-sulphides entrained as fine particles in the rising plume could reach the water surface. After lateral spreading, the sinking particles could interact with the precipitation of chalcopyrite and pyrite, to generate the fine

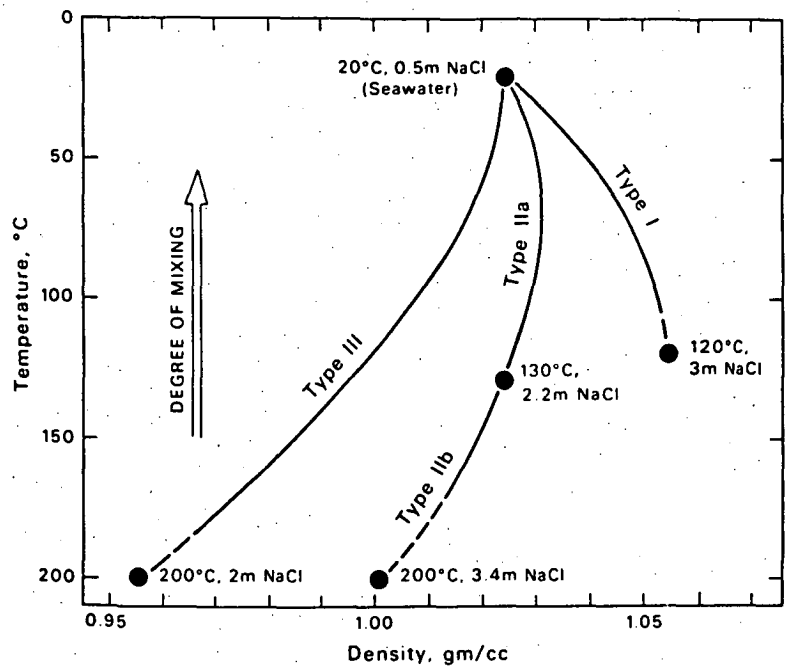

Fig.90: Behaviour of ore solutions after mixing with seawater after Sato (1972)

layering of the ore at Rosebery, and generally envelope the lower part of the ore. This model explains the large scale zonation but has its drawbacks in describing the process of the fine banding. To explain this pattern the model was slightly revised (Green et al., 1981). Instead of a type III plume (3*m* NaCl, 250° - 300°C), they chose a type II plume (3.5*m* NaCl, 250°C) with reversing buoyance. The pulsatory effect generated by the interference of rising and sinking solutions was thought to be able to produce the intermittent fine layering. This model has been further extended to include lateral spreading of the hydrothermal fluids beneath the sulphide mound, and is discussed in Green (1983).

A completely different approach was followed by Large (1977): The banding in the ore is considered due to a distal successive precipitation away from the area of discharge. The transport of the metals occurs in oxygenated ($s_{ox} > s_{red}$, see fig.91), near neutral solutions. Subsequent precipitation of metal sulphides is induced by a reduced environment which could be provided by a depression in graphitic shales trapping the oxidized solutions. Green et al. (1981) and this study however, have demonstrated the existence of a discharge area immediately below the Rosebery deposit. Also, unaerobic shales are only present in the hanging wall of the ore.

A third alternative model could be an early deposition of galena-sphalerite ore followed by dissolution, and replacement by chalcopyrite-pyrite ore. Textural evidence of replacement of black ore (Pb-Zn) by yellow ore (Cu-Fe) in Kuroko deposits accompanied by an upward and outward trend was provided recently by Eldridge et al. (1983). This process is thought to be a function of rising temperatures, which has been confirmed by fluid inclusion studies (Pisatha-Arnond & Ohmoto, 1983). Temperatures initially between 150°C and 250°C passed through a maximum of 250° - 350°C, and finally dropped again towards the end of the hydrothermal activity . A similar model could explain the vertical zonation as found for the north orebody at Rosebery (chap.9.4.5.2.2.). Both a chemical and a mineralogical cross section (fig.54, 55, 57, 58) indicate a Cu-Fe rich bottom layer, with smaller quantities of Pb and Zn, and a Pb-Zn rich top part with a smaller Cu and Fe content, separated by a zone of host rock with a reduced proportion of sulphides and varying amounts of carbonate. The longitudinal chemical cross-section (fig.55, 57) on 15 level clearly demonstrates the tendency of Cu and Fe to extend into the upper part of the ore to which Pb and Zn are essentially confined. In addition, the textural evidence of chalcopyrite either replacing galena and sphalerite, or chalcopyrite filling pore space in galena-sphalerite ore throughout the ore column is further support for this model, assuming these textures are of primary origin. The advance of chalcopyrite was made possible by the rising temperatures and the protecting blanket of the original Pb-Zn ore (Barton, 1978). Self sealing of the discharge area presumably by silica might have occurred (Henley & Thornley, 1979), interrupting the transport of material during the sealing stage, relatively increasing the amount of sedimented shale. At a subsequent higher temperature, the originally deposited galena-sphalerite ore could have been successively dissolved by solutions carrying more Cu and Fe, and deposited further upward and outward. The fine banding in the ore, and the general lack of brecciation requires a low power discharge as already mentioned by Green (1983). The rising of the saline solutions at low speed could have provided the conditions for the generation of the very fine grained pyrite layers as Liesegang-rings. This process demands a heavy layer of water saturated sulphide mud, to balance the buoyancy of the rising solution (2.3 m, 300°C), or denser brines than considered in this study.

Except for the occasional pockets of sulphides, the occurrence of disseminated mineralization in the footwall schists is poor. Assuming a shallow water depth, either boiling must be excluded largely as an

unimportant factor, or the solutions were not sufficiently saturated as suggested by Green (1983). According to Haas (1971, 1976) the water depth necessary to prevent boiling of a 2 - 3*m* solution at 300°C ranges from 750 - 1000 m. This estimate ignores the existence of CO_2 in the system, which significantly raises the required water depth (Drummond, 1981 in Green, 1983). If, however, a two-stage ore deposition is considered, with initial temperatures of up to 250°C, a depth of approximately 450 m would be enough to prevent boiling in a CO_2-free solution (Haas, 1971). During the high temperature stage, the sulphide mud would increase the hydrostatic pressure, further limiting the escape of vapour. However the abundance of carbonate in and around the Rosebery ore prevents a firm conclusion, and the values quoted for water depth must be regarded as minimum values. The formation of carbonate may have occured in the final stages of ore generation with hydrothermal conditions of $\leq$ 300°C and pH = 4.5 (Pisutha-Arnond & Ohmoto, 1983).

The conditions of ore formation are qualitatively shown in fig. 91 which is based on a computer model developed by Ripley and Ohmoto (1977, 1980) and modified by J. L. Walshe, D. J. Patterson, M. Ahmad, A. Bush and G.R. Green. As in the case of the silicate phase diagrams, the ore

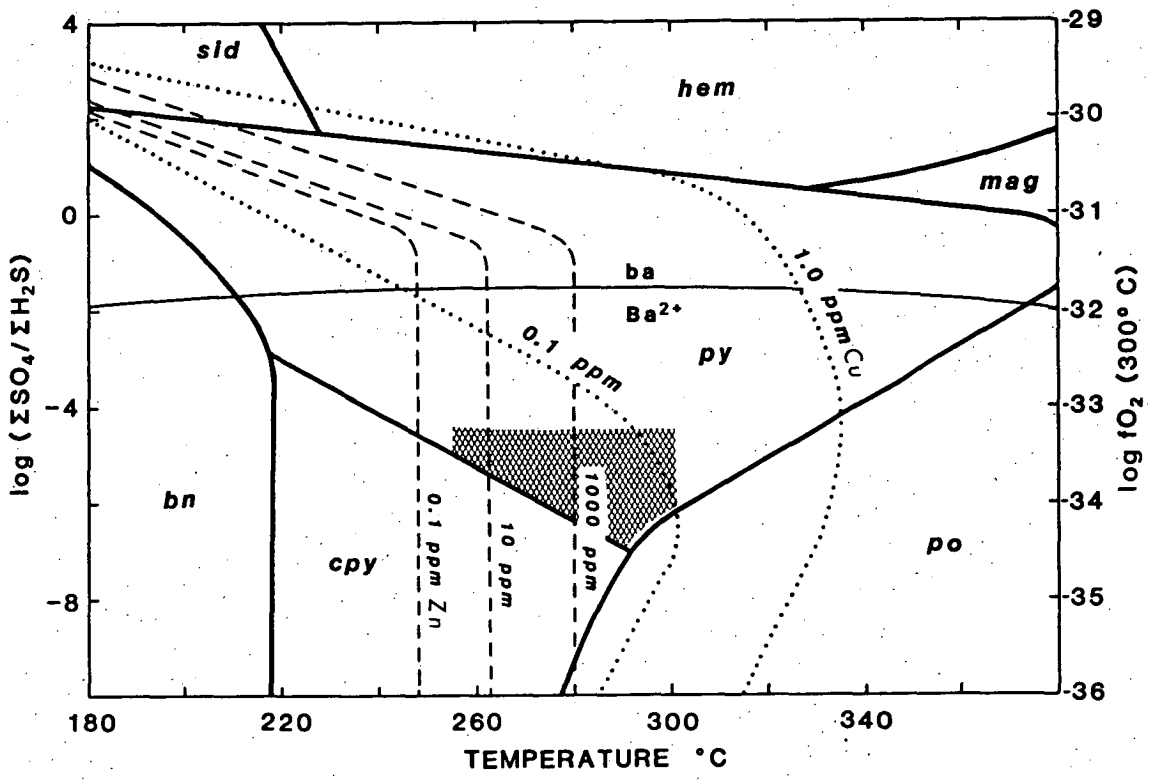

Fig. 91: Conditions of ore formation as estimated for the Rosebery deposit indicated by shaded area. Solution conditions: 2.2*m** Na^+, 0.1*m* K^+, 0.04*m* Ca^{2+}, 0.02*m* Mg^{2+}, 0.001*m* Ba^{2+}, 0.003*m* ΣS, $-6.1 \log m\ \Sigma Cu$, 1 unit acid. * = molal

minerals are assumed to have unit activity, and to co-exist in equilibrium. The existence of small amounts of trace elements in pyrite and chalcopyrite (chap. 10.5.) are in contrast to the first assumption. Equilibrium conditions were certainly not maintained during rapid cooling and precipitation, on mixing hot fluids with cold seawater (Green, 1983; Ohmoto et al., 1983). The thermodynamic data used to calculate the solubilities and phase boundaries in fig. 91 are listed in appendix 6. The range of the composition of the solutions discharging onto the seafloor is indicated by the shaded area. The possible conditions are confined by the co-existence of chalcopyrite and pyrite, and the absence of primary pyrrhotite (chap. 9.4.2.). Further restrictions are imposed by the capability of the hot brines to carry sufficient quantities of base metals in solution. During mixing with seawater the solutions became more oxidised, the temperature decreased, and the pH rose. According to Ohmoto et al. (1983), the decrease in temperature due to mixing with cold seawater is the single most important factor in precipitating the ore. The formation of barite requires a different mixing path, which is discussed in Green (1983) who treated the topic of ore genesis very extensively. His conclusions about the ore-forming conditions differ slightly from this study, due to differences in the assumed composition of the hydrothermal fluids, as discussed in chap. 14.

The writer is aware that the model discussed is based on many speculative assumptions. Most probably an interplay of the processes mentioned, and other mechanisms not yet conceived, contribute to the deposition of massive sulphide deposits.

CONCLUSION

The deposition of two adjacent orebodies at Rosebery resulted from discharge of metal-bearing hot brines onto the seafloor from two separate vents. The initial formation of sphalerite-galena layers was followed by the introduction of pyrite-chalcopyrite ore, due to the increased temperatures of the hydrothermal fluids. The occurrence of several small and large sediment lenses throughout the sequence of welded tuffs suggests an unstable tectonic setting, with fluctuating vertical movements. The presence of black shale in the sedimentary horizons indicates a euxinic environment in shallow marine basins.

The high $\delta^{18}O$ whole rock values can be explained by the interaction of felsic volcanic rocks and seawater modified in a lagoonal environment by evaporation and ^{18}O exchange with shale, although a magmatic component cannot be excluded.

Of the two 45^{o} east dipping ore bodies, only the hydrothermal path below the larger southern ore body is exposed (due to erosion) as quartz-sericite schists occasionally containing K-feldspars and minor amounts of chlorite and biotite. This alteration zone extends for $\leq$ 1500 m parallel to the strike of the orebody, and stretches over 700 m into the footwall as indicated on the surface. The hydrothermal vent below the northern orebody is hidden beneath the western flank of Mt. Black. The centre of the latter consists of siliceous quartz-sericite-chlorite schists with slightly increased sulphide mineralization in the immediate footwall. This area of intense alteration is marked by the absence of feldspar and is > 300 m across. Traces of alteration in the hanging wall up to 2 km stratigraphically above the host rock horizon indicate continued hydrothermal activity after ore deposition.

Exploration based on the geochemistry of the major and conventional trace elements is the most efficient method of defining the path of the hydrothermal fluids. The geochemistry reflects the mineral assemblage, in and outside the alteration zone, and is easy and fast to quantify. In order to decrease variance, it is however of importance to select rocks with a comparable origin for chemical analysis. Despite variation of the data, meaningful trends and patterns can be obtained using univariate and multivariate statistical methods and smoothing techniques.

REE and oxygen isotope geochemistry did not prove successful in delineating the alteration area at Rosebery. The REE distribution on the surface has probably suffered from the influences of weathering and from the redistribution during the Devonian greenschist metamorphism which presumably affected the oxygen isotope chemistry as well. Also, the REE behaviour as a guide to regional targets does not agree with the model of flat distribution curves (HREE enriched) for massive sulphide hosting felsic volcanics.

REFERENCES

Adamides, N.G., 1975: Geological history of the Limni concession, Cyprus, in the light of the plate tectonics hypothesis, Trans. Inst. Min. Metall., 84, B17-B23

Adams, R.L., Burton, C.C.J., Druett, J.G., Hanson, N.H. & McNaught, J.S., 1976: The Rosebery and Hercules zinc-lead deposits, 25th Internat. Geol. Congr., Sydney 1976, Excursion Guide No. 31AC, Ore Deposits Of Western Tasmania, 31-36

Agterberg, F.P., 1974: Geomathematics, Elsevier Scientific Pub. Co., Amsterdam, 596p

Anderson, C.A., 1969: Massive sulfide deposits and volcanism, Econ. Geol., 64, 129-146

Anderson, C.A. & Nash, J.T., 1972: Geology of the masive sulfide deposits at Jerome, Arizona - A reinterpretion, Econ. Geol., 67, 845-863

Anderson. W.B., 1972: The Mt. Read volcanics in the Rosebery-Tullah area, unpub. B.Sc. Hons. Thesis, Univ. of Tasmania, 107p

Appel, R.W.U., 1980: Strata-bound copper sulphides in a banded iron-formation and in basaltic tuffs in the Early Precambrian supracrustal belt, West Greenland, Econ. Geol., 74, 45-52

Amor, S.D. & Nichol, I., 1983: Identification of diagnostic geochemical alteration in the wallrocks of Archaean volcanic-exhalative massive sulphide deposits, Jour. Geochem. Expl., 19, 543-562

Babcock, R.S., 1973: Computational models of metasomatic processes, Lithos, 6, 279-290

Bachinski, D.J., 1977: Sulfur isotopic composition of ophiolitic cupriferous iron sulfide deposits, Notre Dame Bay, Newfoundland, Econ. Geol., 72, 243-257

Banks, M.R. & Solomom, M., 1961: Cambrian succession in West Tasmania, Australian Jour. Sci., 23, 337

Banks, P.O. & Robello, D.P., 1969: Zircon age of a Precambrian rhyolite, northwestern Wisconsin, Geol. Soc. America, 80, 907-910

Barnes, H.L., 1979: Solubilities of ore minerals, in: Barnes, H.L., ed. Geochemistry of hydrothermal ore deposits, 2nd ed., John Wiley & Sons, New York, 404-460

Barth, T.F.W., 1948: Oxygen in rocks: A basis for petrographic calculations, Jour. Geol., 56, 50-60

Barton Jr, P.B., 1978: Some ore textures involving sphalerite from the Futurobe mine, Akita prefecture, Japan, Mining Geol., 28, 293-300

Beaty, D.W. & Taylor Jr., H.P., 1982: Some petrologic and oxygen isotopic relationships in the Amulet Mine, Noranda, Quebec, and their bearing on the origin of Archaean massive sulphide deposits, Econ. Geol., 77, 95-108

Beus, A.A. & Grigorian, S.V., 1977: Geochemical exploration methods for mineral deposits, Applied Publishing Ltd, Wilmette, 287p

Bischoff, J.L. & Dickson, F.W., 1975: Seawater-basalt interaction at 200°C and 500 bars: Implications for origin of sea-floor heavy-metal deposits and regulation of seawater chemistry, Earth Planet. Sci., 25, 385-397

Bischoff, J.L., Radtke, A.S. & Rosenbauer, R.J., 1981: Hydrothermal alteration of graywacke by brine and seawater: Roles of alteration and chloride complexing on metal solubilization at 200°C and 350°C, Econ. Geol., 76, 659-676

Black, L.P. & Adams, C.J., 1980: Radiometric dating studies bearing on the late Proterozoic - early Palaeozoic evolution of western Tasmania (abstract), 4th Australian Geol. Conv., Hobart, 1980, Programmes and abstracts, 24

Blount, C.W., 1977: Barite solubilitties and thermodynamic quantities up to 300°C and 1400 bars, American Mineralogist, 62, 942-957

Bogolepov, V.G., 1962: The recomputation of the chemical analysis of rocks in studying metasomatic precesses, Intern. Geol. Rev., 5, 1585-1592

Brathwaite, R.L., 1969: Geology of the Rosebery ore deposit, unpub. Ph.D. thesis, Univ. of Tasmania, 218p

Brathwaite, R.L., 1972: The structure of the Rosebery ore deposit, Tasmania, Proc. Australasian Inst. Min. Metall., 241, 1-13

Brathwaite, R.L., 1974: The geology and origin of the Rosebery ore deposit, Tasmania, Econ. Geol., 69, 1086-1101

Brewer P.G. & Spencer, D.W., 1969: A note on the chemical composition of the Red Sea brines, in: Degens, E.T. & Ross, R.A., eds., Hot brines and recent heavy metal deposits in the Red Sea- A geochemical and geophysical account, Springer Verlag, Berlin, 174-179

Brown, A.V., 1980: Early deposits in a lower Palaeozoic trough of western Tasmania (abstract), 4th Australian Geol. Conv., Hobart, Jan. 1980, Programmes and abstracts, 23

Brown, B.M., 1982: Robustness against inequality of variances, Australian Jour. Statist., 24, 283-295

Burton, C.C.J., 1975, Hercules and Farrell orebodies, Rosebery district in: Knight, C.L., ed., Economic Geology of Australia and Papua New Guinea, 1. Metals, Monogr. 5, Australasian Inst. Min. Metall., 626-628

Butt, C.R.M., 1983: Granite weathering and silcrete formation on the Yilgarn Block, western Australia (abstract), 6th Australian Geol. Conv., Canberra, 1983, Abstracts, 213

Cagatay, M.N. & Boyle, D.R., 1980: Geology, geochemistry and hydrothermal alteration of the Madenkoy massive sulfide deposit, eastern Vlack Sea region, Turkey, in: Ridge, J.D., ed., 5th IAGOD Symp., Schweizerbart'sche Verlagsbuchhdlg., 653-678

Campana, B., Dickinson, S.B., King, D. & Matheson, R.S., 1958: The mineralized rift valleys of Tasmania, in: Stillwell, F.L., ed., Anniversary vol., Melbourne, Australasian Inst. Mining Metallurgy, 41-60

Campana, B. & King, D., 1963: Palaeozoic tectonism sedimentation and mineralization in West Tasmania, Jour. Geol. Soc. Australia, 10, 1-53

Campbell, I.H., Coad, P., Franklin, J.M., Sowa, J. & Thurston, P.C., 1982: Rare earth elements in volcanic rocks associated with Cu-Zn massive sulphide mineralization: A preliminary report, Canadian Jour. Earth Sci., 19, 619-623

Carey, S.N. & Sigurdson, H., 1980: The Roseau ash: Deep-sea tephra deposits from a major eruption on Domenica Lesser Antilles arc, Jour. Volc. Geoth. Res., 7, 67-86

Cas, R.A.F. & Wright, J.V., 1983: Modern and ancient volcanic successions - an approach to analysis of facies, environments of deposition and tectonic setting, Course Notes, Dept. of Earth Scis., Monash Univ., Melbourne

Chatfield, C. & Collins, A., 1980: Introduction to multivariate analysis, Chapman & Hall, London, 246p

Cole, D.R., Ohmoto, H. & Lasaga, A.C., 1983: Isotopic exchange in mineral-fluid systems, I. Theoretical evaluation of oxygen isotopic exchange accompanying surface reactions and diffusion, Geoch. Cosmoch. Acta, 47, 1681-1693

Cole, J.W., 1979: Structure, petrology and genesis of Cenozoic volcanism, Taupo Volcanic Zone, New Zealand - a review, N.Z. Jour. Geol. Geophys. 22, 631-657

Colley, H. & Rice, C.M., 1975: A Kuroko-type ore deposit in Fiji, Econ. Geol., 70, 1373-1386

Collins, P.L.F., 1981: Economic Geology - metallic minerals, Mackintosh, Tasmania Geol. Surv., Expl. Rept., 69-116

Constantinou, G. & Govett, G.J.S., 1972: Genesis of sulphide deposits, ochre and umber of Cyprus, Trans., Inst. Mining Metallurgy, 81, B34-B46

Constantinou, G. & Govett, G.J.S., 1973: Geology, geochemistry and genesis of Cyprus sulphide deposits, Econ. Geol., 68, 843-858

Coplen, T.B. & Hanshaw, B.D., 1973: Ultrafiltration by a compacted clay membrane - I. Oxygen and hydrogen isotope fractionation, Geoch. Cosmoch. Acta, 37, 2295-2310

Corbett, K.D., 1981: Stratigraphy and mineralization in the Mt. Read volcanics, western Tasmania, Econ. Geol., 76, 209-230

Corbett, K.D., Banks, M.R. & Jago, J.B., 1972: Plate tectonics and the Lower Paleaozoic of Tasmania, Nature Phys. Sci., 240, 9-11

Cox, S.F., 1981: The stratigraphic and structural setting of the Mt. Lyell volcanic-hosted sulfide deposits, Econ. Geol, 76, 231-245

Craig, H., Gordon, L.J. & Horibe, Y., 1963: Isotopic exchange affects in the evaporation of water, Jour. Geophys. Res., 63, 5079-5087

Crook, K.A.W., 1979: Tectonic implications of some field relations of the Adelaidean Cooec Dolerite, Tasmania, Jour. Geol. Soc. Australia, 26, 353-361

Date, J. & Tanimura, S., 1974: Dacite and rhyolite associated with the Kuroko mineralization, Mining Geol. Spec. Issue, 6, 261-265

Date, J., Watanabe, Y., Iwaya, Sh. & Horiuchi, M., 1979: A consideration on the alteration of dacite below the Fukazawa ore deposits, Fukazawa Mine Akita Prefecture, Mining Geol., 29, 187-196 (Japanese with English abstract)

Date, J., Watanabe, Y. & Saeki, Y., 1983: Zonal alteration around the Fukazawa Kuroko deposits, Akita Prefecture, northern Japan, Econ. Geol. Monogr. 5, 365-386

Davis, J.C., 1973: Statistics and data analysis in geology, John Wiley & Sons, New York, 550p

Davis, L.W., 1975: Captains Flat lead-zinc orebody, in: Knight, C.L., ed., Economic geology of Australia & Papua New Guinea, 1. Metals, Monogr. 5, Australasian Inst. Min. Metall., 694-700

Deer, W.A., Howie, R.A. & Zussman, J., 1966: An introduction to the rock-forming minerals, Longman, London, 528p

Deer, W.A., Howie, R.A. & Zussman, J., 1972: Rock forming minerals, vol.3, 2nd ed., Longman, London, 270p

Derkmann, K. & Klemm, D.D., 1977: Strata-bound kies-ore deposits in: Klemm, D.D. & Schneider, ed., ophiolitic rocks of the "Tauernfenster" (Eastern Alps, Austria/Italy) in time- and strata-bound ore deposits, H.J., Springer Verlag, Berlin, 305-313

Descarreaux, J., 1973: A petrochemical study of the Abitibi volcanic belt and its bearing on the occurrence of massive sulphide ores, CIM Bull., 66, 61-69

Dickson, F.W., 1977: The role of rhyolite-seawater reaction in the genesis of Kuroko ore deposits, Intern. Symp. on Water Rock Interaction, 2nd Proc., Strasbourg, France, IAGC/IV, 181-190

Dixon, G.H., 1980: The carbonates of Rosebery, geology, geochemistry, stable isotopes, unpub B.Sc. Hons. thesis, Univ. of Tasmania, 173p

Drummond Jr., S.E., 1981: Boiling and mixing of hydrothermal fluids: chemical effects on mineral precipitation, unpub. Ph.D thesis, Pennsylvania State Univ., 380p

Duke, N.A. & Hutchinson, R.W., 1974: Geological relationships between massive sulfide bodies and ophiolitic volcanic rocks near York Harbour, Newfoundland, Canadian Jour. Earth Sci., 11, 53-69

Duncan, D.B., 1955: Multiple range and multiple F tests Biometrics, 11, 1-42

Easterbrook, B.E., 1962: History and development of the Read-Rosebery mining district, Mining Chem. Eng. Rev., 54, 36-40

Eastoe, C.J., 1973: The Rosebery host rock horizon, unpub. B.Sc. Hons. thesis, Univ. of Tasmania, 148p

Eastoe, C.J., 1981: Alteration and mineralisation in the Mt. Read volcanics, western Tasmania, internal rep., Univ. of Tasmania, 63p

Edmond, J.M., 1983: Chemistry of the 350°C hot springs on the crest of the East Pacific rise at 21°N (abstract), Jour. Geochem. Expl., 19, 491-492

Eldridge, C.S., Barton Jr., P.B. & Ohhmoto, H., 1983: Mineral textures and their bearing on formation of the Kuroko orebodies, Econ. Geol., Monogr. 5, 241-281

Ellis, A.J., 1968: Natural hydrothermal systems and experimental hot-water/rock interaction: Reactions with NaCl solutions and trace metal extraction, Geoch. Cosmoch. Acta, 32, 1356-1363

Ewart, A., Taylor, S.R. & Capp, A.C., 1968: Trace and minor element geochemistry of the rhyolitic volcanic rocks, central North Island, New Zealand, Contr. Mineral Petrol., 18, 76-104

Fedikow, M.A.F. & Turek, A., 1983: The appliction of stepwise discriminant analysis to geochemical data from the host rocks of the Sullivan Pb-Zn-Ag deposit, Kimberley, B.C., Canada, Jour. Geochem. Expl., 18, 231-244

Finlow-Bates, T. & Stumpfl, E.F., 1981: The behaviour of so-called immobile elements in hydrothermally altered rocks associated with volcanogenic submarine-exhalative ore deposits, Mineralium Deposita, 16, 319-328

Finucane, K.J., 1932a: Preliminary report on geological survey of the Rosebery district, Tasmania, part 1, Chem. Eng. Mining Rev., 25, 5-7

Finucane, K.J., 1932b: Preliminary report on geological survey of the Rosebery district, Tasmania, part 2, Chem. Eng. Mining Rev., 25, 43-46

Fiske, R.S., 1969: Recognition and significance of pumice in marine pyroclastic rocks, Geol. Soc. America Bull., 80, 1-8

Fitzgerald, F.G., 1974: The Primrose pyroclastics in the Hercules-White Spur area, Western Tasmania, unpub. B.Sc. Hons. thesis, Univ. of Tasmania, 188p

Foster, M.D., 1960: Interpretation of the composition of trioctahedral micas, U.S. Geol. Surv. Prof. Pap., 354B, 11-49

Foster, M.D., 1962: Interpretation of the composition and classification of the chlorites, U.S. Geol. Surv. Prof. Papl, 414A, 1-33

Fournier, R.O. & Truesdell, A.H., 1970: Chemical indicators of subsurface temperature applied to hot spring waters of Yellowstone national park, Wyoming, USA, Geothermics, Spec. Issue 2, 529-535

Francis, E.H. & Howells, M.F., 1973: Transgressive welded ash-flow tuffs among the Ordivician sediments of NE Snowdonia, N. Wales, Jour. Geol. Soc. London, 129, 621-641

Franklin, J.M., Kasarda, J., Paulsen, K.H., 1975: Petrology and chemistry of the alteration zone of the Mattabi massive sulphide deposit, Econ. Geol. 70, 63-79

Franklin, J.M., Lyden, J.W. & Sangster, D.F., 1981: Volcanic-associated massive sulphide deposits, Econ. Geol. 75th Anniversary Vol., 485-627

Frietsch, R., Papunen, H. & Vokes, F.M., 1979: The ore deposits in Finland, Norway, and Sweden - A review, Econ. Geol., 74, 975-1001

Gannicott, R.A., Armbrust, G.A. & Agterberg, F.P., 1979: Use of trend surface analysis to delimit hydrothermal alteration patterns, CIM Bull., 82-89

Garlick, D.G., & Epstein, S., 1967: Oxygen isotope ratios in coexisting minerals of regionally metamorphosed rocks, Geoch. Cosmoch. Acta, 31, 181-214

Garrett, R.A., 1983: Sampling methodology in: Govett, G.J.C., ed., Handbook of exploration geochemistry, vol. 2: Statistics and data analysis in geochemical prospecting, Elsevier Pub. Co., Amsterdam, 83-110

Gee, C.E., 1970: The geochemistry of some black shales in relation to the origin of certain stratiform orebodies in Tasmania, unpub. Ph.D. thesis, Univ. of Tasmania, 153p

Gee, C.E., Jago, J.B. & Quilty, P.G., 1970: The age of the Mt. Read volcanics on the Que River area, western Tasmania, Jour. Geol. Soc. Australia, 16, 761-763

Gill, J.B., 1970: Geochemistry of Viti Levu, Fiji, and its evolution as an island arc, Contrib. Mineral. Petrol., 27, 199-203

Gjelsvik T., 1968: Distribution of major elements in the wall rocks and the silicate fraction of the Skorovass pyrite deposit, Grong area, Norway, Econ. Geol., 63, 217-231

Goldfarb, M.S., Converse, D.R., Holland, H.D. & Edmond, J.M., 1983: The genesis of hot spring deposits on the East Pacific rise, 21°N, Econ. Geol., Monogr. 5, 184-197

Goodfellow, W.D., 1975: Major and minor element halos in volcanic rocks at Brunswick no. 12 sulphide deposit, N.B., Canada, in: Elliott, I.L. & Fletcher, W.K., eds., Geochemical exploration 1974, Elsevier Scientific Pub. Co., Amsterdam, 279-295

Govett, G.J.S., 1972: Interpretation of a rock geochemical exploration survey in Cyprus - statistical and graphical techniques, Jour. Geochem. Expl., 1, 77-102

Govett, G.J.S., 1983: Handbook of exploration geochemistry, III: Rock geochemistry in mineral exploration, Elsevier Scientific Pub. Co., Amsterdam, 269-303

Govett, G.J.S. & Nichols, I., 1979: Lithogeochemistry in mineral exploration, in: Hood, P.J., ed., Geophysics and geochemistry in the search of metallic ores, Geol. Surv. Canada Econ. Geol. Rept., 31, 339-362

Graf Jr., J.L., 1977: Rare earth elements as hydrothermal tracers during the formation of massive sulfide deposits in volcanic rocks, Econ. Geol. 72, 527-548

Green, G.R., 1975: Sundry mineralization in Tasmania, in: Knight, C.L., ed., Economic geology of Australia & Papua New Guinea, 1.Metals, Monogr.5, Australasian Inst. Min. Metall., 632-635

Green, G.R., 1983: Rosebery ore deposit, unpub. Ph.D. thesis, Univ. of Tasmania

Green, G.R, Solomon, M., Walshe J.C., 1981: The formation of the volcanic-hosted massive sulphide ore deposit at Rosebery, Tasmania, Econ. Geol., 76, 304-338

Green, G.R., Ohmoto, H., Date, J. & Takahashi, T., 1983: Whole-rock oxygen isotope distribution in the Fukazawa-Kosaka area, Hokuroku district, Japan, and its potential application to mineral exploration, Econ. Geol. Monogr. 5, 395-411

Gresens, R.L., 1967: Composition-volume relationships of metasomatism, Chem. Geol., 2, 47-65

Griffiths, J.R., 1971: Reconstruction of south-west Pacific margin of Gondwanaland, Nature, 234, 203-207

Gromet, L.P. & Silver, L.T., 1983: Rare earth element distributions among minerals in a granodiorite and their petrogenetic implications, Geoch. Cosmoch. Acta, 47, 925-939

Haas Jr., J.L., 1976: Thermodynamic properties of the coexisting phases and thermochemical properties of the NaCl component in boiling NaCl solutions, U.S. Geol. Surv. Bull., 1421B, 71p

Haas Jr., J.L., 1971: The effect of salinity on the maximum thermal gradient of a hydrothermal system at hydrostatic pressure, Econ. Geol., 66, 940-966

Hajash, A., 1975: Hydrothermal processes along mid-ocean ridges: An experimental investigation, Contrib. Mineral. Petrol., 53, 205-226

Hall, D., Cottle, V.M., Rosenheim, P.B. & McGhie, R.R., 1953: The lead-zinc deposits of Read-Rosebery and Mount Farrell, in: Edwards, A.B., ed., Geology of the Australian ore deposits, 1st ed., 5th Emp. Min. Metall. Congr., Melbourne, 1145-1159

Hall, G. & Solomon, M., 1962: Metallic mineral deposits, Jour. Geol. Soc. Australia, 9, 285-309

Hall, R.J., 1967: The geology of the Hercules mine area, Williamsford, unpub. B.Sc. Hons. thesis, Univ. of Tasmania, 227p

Hallberg, J.A., Johnston, C. & Bye, S.M., 1976:The Archaean Marda igneous complex, Western Australia, Precamb. Res., 3, 111-136

Hanson, G.H., 1978: The applications of trace elements to the petrogenesis of igneous rocks of granitic composition, Earth Planet. Sci. Let., 38, 26-43

Harcourt Smith, J., 1898: Report on the mineral fields in the neighbourhood of Mt. Black, Ringville, Mt. Read, and Lake Dora, Tasmania, Mines Dept. Annual Rept. no. 51, 24p

Harley, D.N., 1979: A mineralized Ordivician resurgent caldera complexion the Bathurst-Newcastle mining district, New Brunswick, Canada, Econ. Geol., 74, 786-796

Hassan, M.A., Al-Sulaimi, J.S., 1979: Copper mineralization in the northern part of Oman Mountains near AL Fujairah, United Arab Emirates, Econ. Geol., 74, 919-924

Hayman, R.M., 1983: Hydrothermal deposition on the East Pacific at 21°N (abstract), Jour. Geochem. Expl., 19, 493-495

Heaton, T.H.E. & Sheppard, S.M.F., 1977: Hydrogen and oxygen isotope evidence for seawater-hydrothermal alteration and ore deposition, Troodos complex, Cyprus, in: Volcanic processes in ore genesis, Geol. Soc. London, Spec. Pub, 7, 42-57

Helgeson, H.C., 1969: Thermodynamics of hydrothermal systems at elevated temperatures and pressures, American Jour. Sci., 267, 729-804

Helgeson, H.C., Delaney, J.M., Nesbitt, H.W. & Bird, D.K., 1978: Summary and critique of the thermodynamic properties of rock forming minerals, American Jour. Sci., 278A, 1-229

Hellman, P.L., Smith, R.E. & Henderson, P., 1979: The mobility of the rare earth elements: Evidence and implications from selected terrains affected by burial metamorphism, Contrib. Mineral. Petrol., 71, 23-44

Helovuori, O, 1979: Geology of the Pyhäsalmi ore deposit, Finland, Econ. Geol., 74, 1084-1101

Hendry, D.A.F., 1981: Chlorites, phengites, and siderites from the Prince Lyell ore deposit, Tasmania, and the origin of the deposit, Econ. Geol., 76, 285-303

Henley, R.W. & Thornley, P., 1979: Some geothermal aspects of polymetallic massive sulfide formation, Econ. Geol., 74, 1600-1612

Henley, R.W., Truesdell, A.H. & Barton Jr., P.B., 1984: Fluid-mineral equilibria in hydrothermal systems, Rev. Econ. Geol., 1, Soc. Econ. Geol., 267p

Higgins, N.C., Robinson, P. & Jenner, G., 1983: Procedure for the determination of REE by ion-exchange x-ray fluorescence method, Tech. Rept. 1983-1, Geol. Dept., Univ. of Tasmania

Hills, C.L., 1915a: The zinc-lead sulphide deposits of the Read-Rosebery district, part 1, Geol. Surv., Tasmania Bull., 19

Hills, C.L., 1915b: The zinc-lead sulphide deposits of the Read-Rosebery district, part 2, Geol. Surv., Tasmania Bull., 23

Hoel, P.G., 1976: Elementary statistics, 4th ed., John Wiley & Sons, New York, 361p

Horikoshi, E & Sato, T, 1970: Volcanic activity and ore deposition in the Kasaka mine in: Tatsumi, T., ed., Volcanism and ore genesis, Univ. of Tokyo Press, Tokyo, 181-195

Huhtala, T., 1979: The geology and zinc-copper deposits of the Pyhäsalmi-Pielavesi district, Finland, Econ. Geol., 74, 1069- 1083

Humphries, S.E. & Thompson, G., 1978: Trace element mobility during hydrothermal alteration of oceanic basalts, Geoch. Cosmoch. Acta, 42, 127-136

Hutchinson, R.W., 1973: Volcanogenic sulfide deposits and their metallogenic significance, Econ. Geol., 68, 1223- 1246

Hutchinson, R.W., 1980: Massive base metal sulphide deposits as guides to tectonic evolution in the continental crust and its mineral deposits, in: Strangway, D.W., ed., The continental crust and its mineral deposits, Geol. Assoc. Canada. Spec. Pap., 20, 659-684

Hutchinson, R.W & Searle, D.L., 1971: Stratabound pyrite deposits in Cyprus and relations to other sulphide ores, Soc. Mining Geol. Japan Spec. Issue, 3, 198-205

Irvine, T.N. & Baragar, U.R.A., 1971: A guide to the chemical classification of the common volcanic rocks, Canadian. Jour. Earth Sci., 8, 523-548

Ishikawa, Y., Sawaguchi, T., Iwaya, S. & Horiuchi, M., 1976: delineation of prospecting targets for Kuroko deposits based on models of volcanism of underlying dacite and alteration halos, Mining Geol., 26, 105-117 (Japanese with English abstract)

Jago, J.B., 1979: Tasmanian Cambrian biostratigraphy - a preliminary report, Jour. Geol. Soc. Australia, 26, 223-230

Jago, J.B., Reid, K.O., Quilty, P.G., Green, G.R. & Dailey, B., 1972: Fossiliferous Cambrian limestone from within the Mt. Read Volcanics, Mt. Lyell mine area, Tasmania, Geol. Soc. Australia Jour., 19, 379-382

Johnson, J.R. & Klingner G.D., 1975: Broken Hill ore deposit and its environment in: Knight, C.L., ed., Economic Geology of Australia and Papua New Guinea 1. Metals, Monogr. 5, 476-401

Kajiwara, Y., 1971: Sulfur isotope study of the Kuroko-ores of the Shakanai no. 1 deposits, Akita Prefecture, Japan, Geochem. Jour., 4, 157-181

Kajiwara, Y., 1973a: Chemical composition of ore-forming solutions responsible for the Kuroko type mineralization in Japan, Geochem. Jour., 6, 141-149

Kajiwara, Y., 1973b: A simulation of the Kuroko type mineralization in Japan, Geochem. Jour., 6, 193-209

Kanasewich, E.R., 1968: Precambrian Rift: Genesis of strata-bound ore deposits, Science, 161, 1002-1005

Kanehira, K., 1970: Conformable copper-pyrite deposits in the Iimori mining district, in: Tatsumi, T., ed., Volcanism and ore genesis, Univ. of Tokyo Press, 93-104

Kanehira, K. & Tatsumi T., 1970: Bedded cupriferous iron sulphide deposits in Japan, a review in: Tatsumi, T.,ed., Volcanism and ore genesis, Univ. of Tokyo Press, 51-76

Kerr, P.F., 1977: Optical mineralogy 4th ed., McGraw-Hill Book Co., New York, 492p

Klau, W. & Large, D.E., 1980: Submarine exhalitive Cu-Pb-Zn deposits - A discussion of their classification and metallogenesis, Geol. Jahrb., D40, 13-58

Koch, G.S. & Link, R.F., 1971: Statistical analysis of geological data, vol. 2, John Wiley & Sons, New York

Koo, J & Mossman, D.J., 1975: Origin and metamorphism of the Flin Flon strata-bound Cu-Zn sulfide deposit, Saskatchewan and Manitoba, Econ. Geol., 70, 48-62

Krumbein, W.C. & Graybill, F.A., 1965: An introduction to statistical models in geology, McGraw-Hill Book Co., New York, 475p

Lambert, I.B. & Sato, T., 1974: The Kuroko and associated ore deposits of Japan: A review of their features and Metallogenesis, Econ. Geol., 69, 1215-1236

Land, L.S., 1983: The application of stable isotopes to studies of the origin of dolomite and to problems of diagenesis of clastic sediments 4-1 - 4-22, in: Arthur, M.A., Anderson, T.F., Kaplan, I.R., Veizer, J. & Land, L.S., eds., Stable isotope in sedimentary Geology, SEPM short course no. 10, Dallas, 1983, 439p

Large, R.R., 1977: Chemical evolution and zonation of massive sulfide deposits in volcanic terrains, Econ. Geol., 72, 549-572

Latvalahti, U., 1979: Cu-Zn-Pb ore in the Aijala-Orijärvi area, Southwest Finland, Econ. Geol., 74, 1035-1059

Lebedev, L.M., 1967: Recent deposition of native lead from Cheleken thermal springs, Dokl. Akad. Nauk SSSR, 174, 197-200 (in Russian)

Leblanc, M. & Billaud, P., 1978: A volcano-sedimentary copper deposit on a continental margin of Upper Proterozoic age: Bleida (Anti-Atlas, Morocco), Econ. Geol., 73, 1101-1111

Legge, P.J., Haslam, C.O. & Taylor, S., 1984: Lead-zinc-silver exploration and development in Australia, Proc. Australasian Inst. Min. Metall., 289, 119-135

Levinson, A.A., 1980: Introduction to exploration geochemistry, Applied Publishing Ltd, Calgary, p761-778

Le Maitre, R.W., 1982: Numerical petrology - Statistical interpretation of geochemical data, Elsevier Scientific Pub. Co., Amsterdam, 281p

Loftus-Hills, G. & Solomon, M., 1967: Cobalt, Nickel and Selenium in sulphides as indicators of ore genesis, Mineralium Deposita, 2, 228-242

Loftus-Hills, G., Solomon, M. & Hall, R.J., 1967: The structure of the bedded rocks west of Rosebery, Tasmania, Jour. Geol. Soc. Australia 14, 333-337

Lusk, J., 1969: Base metal zoning in the Heath Steele B-1 orebody, New Brunswick, Canada, Econ. Geol., 64, 509-518

McConnell, J.W., 1976: Geochemical dispersion in wall rocks of Archaean massive sulfide deposits, unpub. M. Sc. thesis, Queens Univ., Kingston, Ontario, 230p

McDougall, I., Leggo, P.J., 1965: Isotopic age determinations on granite rocks from Tasmania, Jour. Geol. Soc. Australia, 12, 295-332

MacGeehan, P.J. & MacLean, W.H., 1980: An Archaean sub-seafloor geothermal system, "calc-alkali" trends, and massive sulphide genesis, Nature, 286, 767-771

McLennan, S.M. & Taylor, S.R., 1980: Geochemical standards for sedimentary rocks: Trace-element data for U.S.G.C. standards SCo-1, MAG-1 and SGR-1, Chem. Geol., 29, 333-343

McNamara, M., 1965: The lower greenschist facies in the Scottish highlands, Geol. För. Stockholm Förh., 87, 347-389

Malone, E.J., 1979: Nature, distribution and relationships of the mineralization at Woodlawn, New South Wales, Jour. Geol. Soc. Australia, 26, 141-153

Malone, E.J., Olgers, F., Cucchi, F.G., Nicholas, T. & McKay, E.J., 1975: Woodlawn copper-lead-zinc deposit, in: Knight, C.L., ed., Economic geology of Australia and Papua New Guinea, 1. Metals, Monogr.5, Australasian Inst. Min. Metall., 701-710

Marcotte, D. & David, M., 1981: Target-defination of Kuroko-type deposits in Abitibi by discriminant analysis of geochemical data, CIM Bull., 74 (828), 102-108

Marriott, F.H.C., 1974: The interpretation of multiple observations, Academic Press, London, 117p

Massart, D.L. & Kaufmann, L., 1983: The interpretation of analytical chemical data by the use of cluster analysis, John Wiley & Sons, 237p

Mendenhall, W., Scheaffer, R.L. & Wackerly, D.D., 1981: Mathematical statistics with applications, 2nd ed., Duxbury Press, Boston, 686p

Miller, A.R., Densmore, C.D., Degens, E.T., Hathaway, J.C., Manheim, F.T, McFarlin, P.F., Pocklington, R. & Jokela, A., 1966: Hot brines and recent iron deposits in deeps of the Red Sea, Geochim. Cosmochim. Acta, 30, 341-359

Miller, L.J. & Gair, H.S., 1975: Mons cupri copper-lead-zinc-silver deposits in: Knight, C.L., ed., Economic geology of Australia and Papua New Guinea, 1. Metals, Monogr. 5, Australasian Inst. Min. Metall., 195-202

Mitchell, A.H. & Bell, J.D., 1973: Island-arc evolution and related mineral deposits, Jour. Geol., 81, 381-405

Miyashiro, A., 1975: Volcanic rock series and tectonic setting, Annual Rev. Earth & Planet. Sci., 3, 251-269

Mottl, M.J. & Holland, H.D., 1978: Chemical exchange during hydrothermal alteration of basalt by seawater -I. Experimental results for major and minor components of seawater, Geoch. Cosmoch. Acta, 42, 1103-1115

Mottl, M.J., Holland, H.D. & Corr, R.F., 1979: Chemical exchange during hydrothermal alteration of basalt by seawater - II. Experimental results for Fe, Mn, and sulfur species, Geoch. Cosmoch. acta, 43, 869-884

Nie, N.H., Hull, C.H., Jenkins, J.G., Steinbrenner, K. & Bent, D.H., 1975: SPSS - Statistical package for the social sciences, 2nd ed., 675p

Nilsson, C.A., 1968: Wall rock alteration at the Boliden deposit, Sweden, Econ. Geol., 63, 472-494

Nesbitt, H.W., 1979: Mobility and fractionation of rare earth elements during weathering of a granodiorite, Nature, 279, 206-210

Norrish K. & Hutton, J., 1969: An accurate X-ray spectrographic method for the analysis of a wide range of geologica samples, Geoch. Cosmoch. Acta, 33, 431-453

Norrish K. & Chappell, B.W., 1977: X-ray fluorescence spectrometry in: Zussman, J., ed., Physical methods in determinative mineralogy, 2nd ed., Academic Press, London, 201-272

Ohmoto, H. & Rye, R.O., 1974: Hydrogen and oxygen isotopic compositions of fluid inclusions in the Kuroko deposits, Japan, Econ. Geol., 69, 947-953

Ohmoto, H., Mizukami, M., Drummond, S.E., Eldridge, C.S.,Pisutha-Arnond, V. & Lenagh, T.C., 1983: Chemical processes of Kuroko formation, Econ. Geol., Monogr. 5, 570-604

O'Neil, J.R. & Taylor Jr., H.P., 1967: The oxygen isotope and cation exchange chemistry of feldspars, American Mineralogist, 52, 1414-1437

Packham, G.H. & Falvey, D.A., 1971: An hypothesis for the formation of marginal seas in the western Pacific, Tectonophys., 11, 79-109

Papula, L., 1975: Mathematik für Chemiker - Ein Lehrbuch für Studenten der Chemie und anderer Naturwissenschaften, Ferdinand Enke Verlag Stuttgart, 342p

Peccerillio, A. & Taylor, S.R., 1976: Geochemistry of Eocene calc-alkaline volcanic rocks from the Kastamonu area, Northern Turkey, Contrib. Mineral. Petrol,. 58, 63-81

Peterson, D.W., 1979: Significance of the flattening of pumice fragments in ash-flow tuffs, Geol. Soc. America Spec. Pap., 180, 195-204

Peterson, M.S. & Lambert I.B., 1979: Mineralogical and chemical zonation around the Woodlawn Cu-Pb-Zn ore deposit, southeastern New South Wales, Jour. Geol. Soc. Australia, 26, 169-186

Pichler, H. & Zeil, W., 1970: The Cenozoic rhyolite-andesite association of the Chilean Andes, Bull. Volc., 35, 424-452

Pisutha-Arnond, V. & Ohmoto, H., 1983: Thermal history, and chemical and isotopic compositions of the ore forming fluids responsible for the Kuroko massive sulfide deposits in the Hokuroku district of Japan, Econ. Geol., Monogr. 5, 523-558

Platt, J. W., 1977: Volcanogenic mineralization at Avoca, Co. Wicklow, Ireland, and its regional implications, in: Volcanogenic processes in ore genesis, Geol. Soc. London Spec. Pub., 7, 163-174

Poldevaart, A., 1953: Petrological calculations in metasomatic processes, American Jour. Sci., 251, 481-504

Pottorf, R.J. & Barnes, H.L., 1983: Mineralogy, geochemistry, and ore genesis of hydrothermal sediments from the Atlantis II deep, Red Sea, Econ. Geol., Monogr. 5, 198-223

Reid, K.O., 1975: Mount Lyell copper deposits, in: Knight, C.L., ed., Economic Geology of Australia & Papua New Guinea, 1.Metals, Monogr.5, Australasian Inst. Min. Metall., 604-619

Reid, K.O. & Meares, R.M.D., 1981: Exploration for volcanic-hosted massive sulfide deposits in western Tasmania, Econ. Geol., 76, 350-364

Reynolds, D.G., Brook, W.A., Marshall, A.E. & Allchurch, P.D., 1975: Volcanogenic copper-zinc deposits in the Pilbara and Yilgarn Archaean Blocks, in: Knight, C.L., ed., Economic geology of Australia and Papua New Guinea, 1. Metals, Monogr. 5, Australasian Inst. Min. Metall., 185-195

Reynolds M.A. & Best, J.G., 1976: Summary of the 1953-57 eruption of Tuluman volcano, Papua New Guinea, in: Johnson, R.W., ed., Volcanism in Australasia, 287-296

Rickard, D.T. & Zweifel, H., 1975: Genesis of Precambrian sulfide ores, Skellefte district. Sweden, Econ. Geol., 70, 255-274

Rickard, D.T., Zweifel, H. & Donnelly, T.H., 1979: Sulfur isotope systematics in the Åsen pyrite-barite deposits, Skellefte district, Sweden, Econ. Geol., 74, 1060-1068

Rimstidt, J.D. & Cole, D.R., 1983: Geothermal mineralization I: The mechanism of formation of the Beowawe, Nevada, siliceous sinter deposit, American Jour. Sci., 283, 861-875

Ripley E.M. & Ohmoto, H., 1977: Mineralogy, sulfur isotope, and fluid inclusion studies of the stratabound copper deposits at the Raul mine, Peru, Econ. Geol. 72, 1017-1041

Ripley, E.M. & Ohmoto, H., 1979: Oxygen and hydrogen isotopic studies of ore deposition and metamorphism at the Raul Mine, Peru, Geoch. Cosmoch. Acta, 43, 1633-1643

Ripley E.M. & Ohmoto, H., 1980: A FORTRAN program for plotting mineral stabilities on the Fe-Cu-S-O system in terms of log (SO_4/ H_2S) or log f O_2vs. pH or T, Computers Geosci., 5, 289-300

Riverin, G. & Hodgson, C.J., 1980: Wall-rock alteration at the Millenbach Cu-Zn mine, Noranda, Quebec, Econ. Geol., 75, 424-444

Roberts, R.G. & Reardon, E.J., 1978: Alteration and ore-forming processes at Mattagami lake mine, Quebec, Canadian Jour. Earth Sci., 15, 1-21

Saeki, Y. & Date, J., 1980: Computer application to the alteration data of the footwall dacite lava at the Ezuri Kuroko deposits, Akita-prefecture, Mining Geol., 30, 241-250 (Japanese with English abstract)

Sakrison, H.C., 1966: Chemical studies of the host rocks of the Lake Dufault mines, Quebec, unpub. Ph.D. thesis, McGill Univ., Montreal

Sampson, R.J., 1978: Surface II graphics system (rev. 1), Computer Services Sect., Kansas Geol. Surv., Lawrence, Kansas, 240p

Sangster D.F., 1972: Precambrian volcanogenic massive sulphide deposits in Canada: A review, Canadian Geol. Surv. Pap., 72 (22), 44p

Sangster D.F., 1980: Distribution and origin of Precambrian massive sulphide deposits of North America, in: Strangway, D.W., ed., The continental crust and its mineral deposits, Geol. Assoc. Canada Spec. Pap., 20, 723-739

Sangster, D.F. & Scott, S.D., 1976: Precambrian, strata-bound, massive Cu-Zn- Pb sulphide ores of North America in: Wolf, K.H., Handbook of strata-bound and stratiform ore deposits, Elsevier Scientific Publishing Co., Amsterdam, 129- 222

Sato, T., 1971: Physicochemical environments of Kuroko mineralization at Uchinotai deposit of Kosaka mine, Akita Prefecture, in: Takeuchi, Y., Takeuchi, T., Sasaki, A. & Sakamake, Y., Geochemistry and crystallography of sulphide minerals in hydrothermal deposits, Proc. IMA-IAGOD meetings '70, soc. Mining Geol. Japan, Spec. Issue, 2, 137-144

Sato, T., 1972: Behaviours of ore-forming solutions in seawater, Mining Geol., 22, 31-42

Sato, T., 1974,: Distribution and geological setting of the Kuroko deposits, Mining Geol. Spec. Issue, 6, 1-9

Sato, T., 1977: Kuroko deposits: their geology, geochemistry and origin, in: Volcanic processes in ore genesis, Geol. Soc. London Spec. Pub., 7, 153-161

Sawkins, F.J., 1972: Sulphide ore deposits in relation to plate tectonics, Jour. Geol., 80,377-397

Sawkins, F.J., 1976: Massive Sulfide deposits in relation to geotectonics in: Strong, D.F., ed., Metallogeny and plate tectonics, Geol. Assoc. Canada Spec. Pap., 14, 221-240

Scheibner, E. & Markham, N.L., 1976: Tectonic setting of some strata-bound massive sulphide deposits in New South Wales, Australia in: Wolf, K.H., Handbook of strata-bound and stratiform ore deposits, Elsevier Scientific Pub. Co., Amsterdam, 55-77

Schermerhorn, L.J.G., 1970: The deposition of volcanics and pyrite in the Iberian pyrite belt, Mineralium Deposita, 5, 273-279

Schneeberg, E.P., 1973: Sulfur fugacity measurements with the electrochemical cell $Ag|AgI|Ag_{2+x}S$, fS_2, Econ. Geol., 68, 507-517

Scott, S.D., 1978: Structural control of the Kuroko deposits of the Hokuroko district, Japan, Mining Geology, 28, 301-311

Seal, H.L., 1968: Multivariate statistical analysis for biologists, Methuen and Co Ltd., London, 209p

Seyfried, W. & Bischoff, J.L., 1977: Hydrothermal transport of heavy metals by seawater: The role of seawater/basalt ratio, Earth Planet. Sci. Let., 34, 71-77

Seyfried,W.E. & Bischoff, J.L., 1981: Experimental seawater-basalt interaction at 300°C, 500 bars, chemical exchange, secondary mineral formation and implications for the transport of heavy mitals, Geoch. Cosmoch. Acta, 45, 135-147

Sheppard, S.M.E., 1977: Identification of the origin of ore-forming solutions by the use of stable isotopes, in: Volcanic processis in ore genesis, Geol. Soc. London, Spec. Pub., 7, 25-41

Sheridan, M.F., 1970: Fumarolic mounds and ridges of the Bishop tuff, California, Geol. Soc. America Bull., 81, 851-867

Shirozu, H., 1974: Clay minerals in altered wall rocks of the Kuroko-type deposits in: Ishihara, S., ed., Geology of Kuroko deposits, Mining Geol. Spec. Issue, 6, Soc. Mining Geol. Japan, 303-310

Sillitoe, R.H., 1972: Formation of certain massive sulphide deposits at sites of sea-floor spreading, Trans., Inst. Mining Metallurgy, 81, B141-B148

Sise J.R. & Jack, D.J., 1984: Exploration case history of the Hellyer deposit, in: Baillie, P.W. & Collins, P.L.F., eds., Mineral exploration and tectonic processis in Tasmania, abstract volume and excursion guide, 48-49

Skey, E.H., 1984: Dualism in the discovery of the Que River and Hellyer polymetallic sulphide deposits in western Tasmania, 7th Australian Geol. conv., Sydney, 1984, Geol. soc. Australia, 489-490

Skinner, B.J., White, D.E., Rose, H.J. & Mays, R.E., 1967: Sulphides associated with the Salton Sea geothermal brine, Econ. Geol. 62, 316-330

Skinner, R., 1974: Geology of the Tetagouche lakes, Bathurst and Nepesiquit falls map-areas, New Brunswick, Canada Geol. Surv. mem., 377, 133p

Smith, R.L., 1960: Zones and zonal variations in welded ash flows, U.S. Geol. Surv. Prof. Pap., 354-F, 149-159

Smith, R.N., 1975: Precious and volatile metal distributions in the ores and host rocks of the Rosebery sulphide deposit, Tasmania, unpub. M.Sc. thesis, Univ. of Melbourne, 171p

Solomon, M., 1960: The Dundas group in the Queenstown area, Pap. Roy. Soc. Tasmania, 94, 33-50

Solomon, M., 1964: The spilite-keratophyre association of West Tasmania and the ore deposits at Mt. Lyell, Rosebery and Hercules, unpub. Ph.D. Thesis, Univ of Tasmania, 419p

Solomon, M., 1965: Lead-silver-zinc ore deposits at Mt. Farrell, in: McAndrew, J., ed. Geology of Australian ore deposits, 2nd ed., 8th Commonw. Min. Metall. Congr., Melbourne, 490

Solomon, M., 1976: "Volcanic" massive sulphide deposits and their host rocks - A review and explanation in: Wolf, K.H., ed., Handbook of strata- bound and stratiform ore deposits, Elsevier Scientific Pub. Co., Amsterdam, 21-54

Solomon, M., 1981: An introduction to the geology and metallic ore deposits of Tasmania, Econ. Geol., 76, 194-208

Solomon. M. & Elms, R.G., 1965: Copper ore deposits of Mt. Lyell in: McAndrew, J., ed., Geology of Australian ore deposits, 2nd ed., 8th Commonw. Min. Metall. Congr., Melbourne, 478-484

Solomon, M., Rafter, T.A. & Jenson, M.L, 1969: Isotope studies on the Rosebery, Mount Farrell and Mount Lyell areas, Tasmania, MIneralium Deposita, 4, 172-199

Solomon, M. & Griffiths, J.R., 1972: Tectonic evolution of the Tasman orogenic zone, Eastern Australia, Nature Phys. Sci., 237, 3-6

Solomon, M. & Griffiths, J.R., 1974: Aspects of the early history of the southern part of the Tasman orogenic zone, in: Denmead, A.K., Tweedale, G.W. & Wilson, A.F., eds., The Tasmanian geosyncline - a symposium, Brisbane, Geol. Soc. Australia, Queensland Div., 19-44

Solomon, M., Green, G.R. & Reid, K.O., 1976: Geological history of western Tasmania, 25th Internat. Geol. Congr., Sydney 1976, Excursion Guide No. 31AC, Ore Deposits Of Western Tasmania, 1-12

Solomon, M. & Walshe, J. L., 1979: The formation of massive sulfide deposits on the sea floor, Econ. Geol., 74, 797-813

Sparks, R.S.J., Wilson, L., Hulme, G., 1978: Theoretical modelling of the generation, movement , and emplacement of pyroclastic flows by column collapse, Jour. Geophys. Res. 83 (34), 1727-1739

Sparks R.S.J., Sigurdson, H. & Carey, S.N., 1980: The entrance of pyroclastic flows into the sea, I. Oceanographic and Geologic evidence from Domenica, Lesser Antilles, Jour. Volc. Geoth. Res. 7, 87-96

Spence, C.D., 1975: Volcanogenic features of the Vauze sulfide deposit, Noranda, Quebec, Econ. Geol., 70, 102-114

Spence, C.D. & de Rosen-Spence, A.F., 1975: The place of sulfide mineralization in the volcanic sequence of Noranda, Quebec, Econ. Geol., 70, 90-101

Spiess F.N., MacDonald, K.C., Atwater, T., Ballard, R., Carranza, A., Cordoba, D., Cox, C., Diaz Garcia, V.M., Francheteau, J., Guerrero, J., Hawkins, J., Haymon,R., Hessler, R., Juteau, T., Kastner, M., Larson, R., Luyendyk, B., MacDougall, J.D., Miller, S., Normak, W., Orcutt, J., Rangin, C., 1980: East Pacific Rise: Hot springs and geophysical environments, Science, 270, 1421-1433

Spry, A.H., 1962: Igneous activity, Jour. Geol. Soc. Australia, 9, 255-284

Stanton, R.L. & Rafter, T.A., 1966: The isotopic composition of sulphur in some stratiform lead-zinc sulphide ores, Mineralium Deposita, 1, 16-29

Strauss, G.K. & Madel, J., 1974: Geology of massive sulphide deposits in the Spanish-Portuguese pyrite belt, Geol. Rundsch., 63, 191-211

Strauss, G.K., Madel, J., Alonso, F.F., 1977; Exploration practice for strata-bound volcanogenic sulphide deposits in the Spanish-Portuguese pyrite-belt: Geology geophysics, and geochemistry, in: Klemm, D.D. & Schneider, H.J., Time- and strata-bound ore deposits, Springer Verlag, Berlin, 55-93

Suffel, F.G. & Hutchinson, R.W., 1973: Massive cupriferous pyrite deposits at Küre, Turkey, Econ. Geol., 68, 140-141 (abstract)

Takahashi, T. & Suga, K., 1974: Geology and ore deposits of the Hanaola Kuroko belt, Akita Prefecture, in: Ishihare, S., ed., Geology of Kuroko deposits, Mining Geol. Spec. Issue, 6, 101-113

Tatsumi, T. & Clark L.A, 1972: Chemical composition of acid volcanic rocks genetically related to formation of the Kuroko deposits, Jour. Geol. Soc. Japan, 78, 191-201, 1972

Tatsuoka, M.M., 1970: Selected topics in advanced statistics - an elementary approach, no. 6, Discriminant analysis - The study of group differences, Institute for Personality and Ability Testing, Champaign, Illinois, 57p

Tatsuoka, M.M., 1974: Selected topics in advanced statistics - an elementary approach, no. 3, Classification procedures - Profile similarity, Institute for Personality and Ability Testing, Champaign, Illinois, 47p

Taylor Jr., H.P., 1974: The application of oxygen and hydrogen isotope studies to problems of hydrothermal alteration and ore deposition, Econ. Geol., 69, 843-883

Taylor Jr., H.P., 1979: Oxygen and hydrogen isotope relationships in hydrothermal mineral deposits, in: Barnes, H.L., ed., Geochemistry of hydrothermal ore deposits, 2nd ed., John Wiley & Sons, New York, 236-277

Taylor, R.P. & Fryer, B.J., 1980: Multi-stage hydrothermal alteration in porphyry copper systems in northern Turkey: The temporal interplay of potassic, propylitic, and phyllitic fluids, Canadian Jour. Earth Sci., 17, 901-926

Taylor, R.P. & Fryer, B.J., 1982: Rare earth element geochemistry as an aid to interpreting hydrothermal ore deposits in: Evans, A.M., ed., Metallization associated with acid magmatism, John Wiley & Sons, New York, 385p

Taylor, S.R., 1969: Trace element chemistry of andesites and associated calc-alkaline rocks, in: McBirney, A.R., ed., Proc. of The Andesite Conference, Portland, 43-63

Thurlow, J.G., Swanson, E.A. & Strong, D.F., 1975: Geology and lithogeochemistry of the Buchans polymetallic sulfide deposits, Newfoundland, Econ. Geol., 70, 130-144

Thurston, P.C., 1981: Economic evaluation of Archaean volcanic rocks using REE geochemistry, in: Glover, J.E. & Groves, D.I., eds., Archaean Geology, 2nd Intern. symp., Perth, 1980, Geol. Soc. Australia, Spec. Pub., 7, 439-450

Tokunga, M. & Honma, H., 1974: Fluid inclusions in the minerals from some Kuroko deposits, in: Ishihara, S., ed., Geology of Kuroko deposits, Mining Geol. Spec. Issue, 6, 1974, Soc. Mining Geol. Japan, 385-388

Tröger, W.E., 1969: Optische Bestimmung der gesteinsbildenden Minerale, Teil 2 Textband, 2. Auflage, Herausgeber (eds.), Bambauer, H.U.,Taborszky, F. & Trochim, H.D., Schweizerbart'sche Verlagsbuchhdlg., Stuttgart, 822p

Truesdell, A.H., 1974: Oxygen isotope activities and concentrations in aqueous salt solutions at elevated temperatures, Earth Planet. Sci. Let., 23, 387-396

Turnbull, K.R., 1980: Analytical Geochemistry report 7/74, The Leco automatic sulphur determinator, Analytical Geochemistry - a compilation of reports 1973-1979, Centre for Precambrian Research, Res. Rept., 3, 41-46

Turner, F.J., 1981: Metamorphic petrology - Mineralogical, field, and tectonic aspects, 2nd ed., McGraw-Hill Book Co., New york, 524p

Twelvetrees, W.H. & Petterd, W.F., 1899: On the felsites and associated rocks of Mount Read and vicinity, Proc. Roy. Soc. Tasmania, 33-46

Urabe, T., 1974: Mineralogical aspects of the Kuroko deposits in Japan and their implications, Mineralium Deposita, 9, 309-324

Van den Boom, G., Rehder, S. & Kottrup, G. 1980: Geochemical patterns in the rocks surrounding the Woodlawn volcanogenic ore deposit, New South Wales, Australia, Geol. Jahrb., D40, 169-200

Van Moort, J.C., 1982: Exploration for base metals in the cool and wet climate of Western Tasmania (Australia), Congreso Geologico Chileno, Actas-Tomo II, E327-E348

Vokes, F.M., 1976: Caledonian massive sulphide deposits in Scandinavia: A comparative review in: Wolf, K.H., Handbook of strata-bound and stratiform ore deposits, Elsevier Scientific Pub. Co.,Amsterdam, 79-127

Vokes, F.M., 1983: Paragenetical and textural relations in the south end of F-lens (16 level), Rosebery mine, Tasmania, preliminary report

Vokes, F.M. & Gale. G.H., 1976: Metallogeny relatable to global tectonics in southern Scandinavia, Geol. Assoc. Canada. Spec. Pap., 14, 413-441

Wahl, J.L., Govett, G.J.S. & Goodfellow, W.D., 1975: Anomalous element distribution in volcanic rocks around Key Anacon, Heath Steele, B-zone and Brunswick no.12 sulphide deposits (abstract), CIM Bull., 68, 49

Wallace, D.B., 1984: Developments in the geological understanding of the Que River deposit, in: Baillie, P.W. & Collins, P.L.F., eds., Mineral exploration and tectonic processes in Tasmania, abstract volume and excursion guide, Burnie 1984, Geol. Soc. Australia, 55-56

Wallace, D.B. & Green, G.R., 1982: Que River mine and aspects of the Mt. Read volcanics in the Pieman River area in: Green, D.C., ed. Geology, Mineralisation, Exploration: Western Tasmania, 52-63

Wallace, R., Griffiths, W.R., Albers, J.P. & Öner, Ö., 1972: Massive sulfide copper deposits of the Ergani-Maden area, south-eastern Turkey, Econ. Geol., 67, 701-716

Walshe, J.L. & Solomon, M., 1981: An investigation into the environment of formation of the volcanic-hosted Mt. Lyell copper deposits using geology, mineralogy, stable isotopes, and a six-component chlorite solid solution model, Econ. Geol.,76, 246-284

Watson, J., 1973: Influence of crustal evolution on ore deposition, Transcr. Inst. Min. Metall., 82, B107-B113

White, D.E., 1968: Environments of generation of some base-metal ore deposits, Econ. Geol., 63, 301-335

White, N.C., 1975: Cambrian volcanism and mineralization in south-west Tasmania, unpub. Ph.D. thesis, Univ. of Tasmania, 264p

Whitford, D.J., 1984: Geochemistry of alteration around the que River orebodies in: Baillie, P. W. & Collins, P.L.F., eds., Mineral exploration and tectonic processes in Tasmania, abstract volume and excursion guide, Burnie, 1984, Geol. Coc. Australia, 57-58

Whitford, D.J. & Wallace, D.B., 1984: The Mt. Read volcanics at Que River: Primary geochemical affinities and REE geochemistry (abstract), 7th Australian Geol. Conv., Sydney, 1984, Abstracts Geol. Soc. Australia, 547-548

Williams, E., Solomon, M. & Green, G.R., 1975: The geological setting of metalliferous ore deposits in Tasmania, in: Knight, C.L., ed., Economic geology of Australia & Papua New Guinea, 1.Metal, Monogr. 5, Australasian Inst. Min. Metall., 567-581

Wilson, J.B., 1978: Teddybear, statistical program, tech. rep. T5, ed. 2.4, Univ. of Otago, Dunedin, New Zealand, 89p

Winchester, J.A. & Floyd, P.E., 1977: Geochemical discrimination of different magma series and their differentiation products using immobile elements, Chem. Geol., 20, 325-343

Wishart, D., 1978: CLUSTAN, user manual, 3rd ed., Inter-University/Res. Councils Ser., 47, 174p

Wright J.V. & Coward, M.P, 1977: Rootless vents in welded ash-flow tuffs from northern Snowdonia, North Wales, indicating deposition in a shallow water environment, Geol. Mag., 114, 133-140

Wright, J.V. & Mutti, E., 1981: The Dali ash, island of Rhodos, Greece : A problem in interpreting submarine volcanogenic sediments, Bull. Volc., 44 (2), 153-167

Wright, T.L., 1968: X-ray and optical study of alkali feldspar: II. An X-ray method for determining the composition and structural state from measurement of 20 values for three refections, American Mineralogist, 53, 88-104

Zielinski, R.A., Lipmann, P.W. & Hugh Jr., T.M., 1977: Minor-element abundancies in obsidian, perlite, and felsite of calc-alkalic rhyolites, American Mineralogist, 62, 426-437

Zurffardi, P., 1977: Ore/mineral deposits related to the Mesozoic ophiolites in Italy, in: Klemm, D.D. & Schneider, ed., Time- and Strata-bound ore deposits, H.J., Springer Verlag, Berlin, 314-323

APPENDIX I

Specimen catalogue

Specimens referred to by five-digit catalogue numbers indicate silicate rock. Specimens referred to by six-digit catalogue numbers indicate mineralized host rock and ore.

Field numbers with up to four characters (e.g. 122A) indicate surface samples. Field numbers e.g. 3268/9 indicate "drill hole number/sample location in feet" and refer to underground drill holes. Samples with field numbers e.g. 46R/220 have been collected from drill holes started at the surface.

Preparation codes for specimen are:

CA: crushed rock, chemical analysis and hand specimen
T: hand specimen and thin section
PT: hand specimen and polished thin section
PE: hand specimen and Probe analysis

Locations for surface samples are given in metres and are based on the Australian Map Grid (AMG). Locations of drill core samples apart from north (N) and east (E) coordinates, which are given in feet, are presented with level (L), direction (D) and angle of dip (A) for the collar of each drill hole.

Catalogue Number	Field Number	Rock type	Preparation	Location
67795	1	footwall pyroclastic	CA, T	378 400E 371 645N
67796	10	massive siliceous rock	CA, T	377 750E 372 240N
67797	14	footwall pyroclastic, with coarse grained quartz	CA, PE	378 320E 372 710N
67798	15	transition footwall pyroclastics to schist	CA, T	378 400E 372 765N
67799	16	" " " " "	CA, T	378 455E 372 813N
67800	18	footwall pyroclastic	CA, T	378 460E 373 005N
67801	25	footwall schist	CA, T	378 625E 373 135N
67802	30	footwall or massive pyroclastic	CA, T	377 975E 375 715N
67803	31	massive pyroclastic	CA, T	378 290E 376 130N
67804	32A	massive pyroclastic	CA, PE	378 800E 376 280N
67805	32B	" "	CA, PE	378 800E 376 280N
67806	34	footwall pyroclastic	CA, T	377 670E 376 290N
67807	36	" "	CA, T	377 805E 376 120N
67808	39	" "	CA, T	377 520E 376 810N
67809	40	" "	CA	378 190E 375 095N
67810	41R/215	altered? massive pyroclastic	CA, T	379 090E 374 450N
67811	42	massive pyroclastic	CA, T	379 280E 375 550N
67812	42R/402	altered? massive pyroclastic	CA, T	379 140E 374 160N
67813	43A	transition hanging wall schist to massive pyroclastic	CA	378 990E 375 370N
67814	43B	hanging wall schist	CA, T	378 900E 375 110N
67815	44B	footwall schists	CA	378 610E 373 600N
67816	45	hanging wall schist	CA, PE	378 810E 375 120N
67817	46	footwall pyroclastic	CA, P	378 520E 375 025N
67818	50	footwall or massive pyroclastic	CA, PE	377 590E 374 690N
67819	51	footwall schist	CA, T	378 230E 374 215N
67820	52	" "	CA, T	378 200E 374 260N
67821	53	transition	CA, T	378 140E 374 350N
67822	54	massive pyroclastic	CA, PE	379 230E 373 410N
67823	55	" "	CA, T	379 060E 373 760N
67824	56	altered? massive pyroclastic	CA, PE	379 590E 373 530N
67825	57	Mt. Black volcanic	CA, T	379 975E 373 520N
67826	58	" "	CA, PE	381 520E 372 895N
67827	59	" "	CA, PE	382 080E 373 370N
67828	60	altered? massive pyroclastic	CA, T	379 190E 373 740N
67829	61	massive pyroclastic	CA, PT	379 095E 372 670N
67830	62A	massive siliceous rock	CA, T	377 780E 372 360N
67831	62B	massive pyroclastic	CA, T	378 890E 372 140N
67832	63	" "	CA, PE	378 480E 372 540N
67833	64	footwall schist	CA, PE	378 570E 372 975N
67834	66A	" "	CA, PT	378 560E 373 800N
67835	66B	" "	CA, T	378 560E 373 800N
67836	68	massive siliceous rock	CA, T	377 975E 373 040N
67837	69	" "	CA, PE	378 320E 372 890N
67838	69R/423	massive pyroclastic	CA, T	379 580E 374 140N
67839	71	transition footwall schist to pyroclstic	CA, T	378 060E 373 105N
67840	72	massive siliceous rock	CA, T	378 050E 373 370N
67841	73	" " "	CA, T	377 915E 313 430N
67842	74	massive siliceous rock with feldspars	CA, T	377 955E 373 695N
67843	75	massive siliceous rock	CA, PT	378 110E 373 905N
67844	78	" " "	CA, T	378 140E 374 350N
67845	79	transition footwall schist to pyroclastic	CA, T	378 310E 373 135N
67846	81	massive siliceous rock	CA, T	377 990E 373 235N
67847	82	massive pyroclastic	CA, PE	379 075E 372 480N
67848	83	" "	CA, PT	379 215E 372 180N
67849	84	footwall pyroclastic	CA, T	378 675E 372 265N
67850	86	" "	CA, T	378 845E 372 240N
67851	87	" "	CA, T	378 590E 372 430N

Catalogue Number	Field Number	Rock type	Preparation	Location
67852	89	massive pyroclastic	CA, T	379 760E 372 910N
67853	90	Mt. Black volcanic	CA, T	379 740E 372 930N
67854	91	massive pyroclastic	CA, T	379 285E 373 035N
67855	92	" "	CA, T	379 690E 372 530N
67856	93	Mt. Black volcanic	CA	380 140E 372 515N
67857	95	footwall or massive pyroclastic	CA, PT	378 930E 372 590N
67858	96	massive pyroclastic?	CA, T	379 280E 375 700N
67859	97	Mt. Black volcanic?	CA, T	379 310E 375 760N
67860	98	massive pyroclastic	CA, T	379 425E 375 785N
67861	99	" "	CA	379 960E 376 240N
67862	100	Mt. Black volcanic	CA, T	379 960E 376 240N
67863	102	massive pyroclastic	CA, T	379 790E 376 260N
67864	103	Mt. Black volcanic?	CA, T	379 785E 376 250N
67865	104	Mt. Black volcanic?	CA, T	380 015E 376 240N
67866	105	altered? Mt. Black volcanic	CA, T	380 660E 376 460N
67867	106	Mt. Black volcanic	CA, P	380 730E 376 240N
67868	107	altered? massive pyroclastic	CA, T	379 550E 376 260N
67869	108	footwall pyroclastic	CA	378 250E 374 955N
67870	109	footwall schist	CA, T	378 340E 374 510N
67871	110	Mt. Black volcanic	CA, PT	381 020E 374 755N
67872	111	" "	CA	381 365E 374 060N
67873	112	" "	CA	380 860E 372 860N
67874	113	" "	CA, P	380 400E 373 255N
67875	114	massive pyroclastic	CA, T	379 370E 373 690N
67876	115	footwall schist	CA, T	378 400E 373 310N
67877	116	" "	CA, T	378 260E 373 910N
67878	117	massive pyroclastic	CA, PE	379 200E 372 950N
67879	118	footwall schist	CA, T	378 725E 372 880N
67880	119	" "	CA, PE	378 760E 373 925N
67881	120	" "	CA, PE	378 600E 374 075N
67882	121	footwall schist	CA, T	378 895E 373 670N
67883	122A	footwall schist with K-feldspar	CA, PE	378 780E 373 300N
67884	122B	footwall schist	CA	378 780E 373 300N
67885	123	footwall schist with feldspar	CA, PE	378 620E 373 450N
67886	124	massive pyroclastic	CA,T	379 110E 373 360N
67887	125	massive siliceous rock	CA	378 365E 373 720N
67888	126	footwall pyroclastic	CA	378 990E 373 110N
67889	127	footwall schist	CA	378 820E 373 430N
67890	47	host rock, shale	CA, T	378 560E 374 970N
67891	2	footwall pyroclastic	CA, PE	377 780E 370 000N
67892	13	shale with feldspar relics	R, PT	378 040E 372 460N
67893	17	massive siliceous rock with feldspar	R, T	378 160E 372 550N
67894	19	footwall schist	R, T	378 350E 372 900N
67895	21	" "	R, T	378 030E 373 080N
67896	22	black shale	R, T	378 050E 373 080N
67897	24	footwall schist with K-feldspar	R, PE	378 610E 373 100N
67898	26	transition footwall pyroclastic to schist	R, T	378 460E 373 300N
67899	27	footwall schist with K-feldspar	R, T	378 410E 373 300N
67900	29	massive pyroclastic	R, T	377 750E 377 330N
67901	33	" "	R, PE	378 960E 376 200N
67902	41	" "	R, T	379 050E 375 420N
67903	49	shale (Rosebery Group)	R, T	377 640E 374 640N

Catalogue Number	Field Number	Rock type	Preparation	Location
67904	128	altered lava? (3 m block) in footwall schist	R, PE	378 780E 373 920N
67905	129	footwall schists with K-feldspar	R, PT	378 580E 373 880N
67906	130	footwall pyroclastic	R, T	378 540E 373 150N
67907	V	chlorite vein in massive siliceous rocks	R, PE	378 000E 373 070N
67908	131	massive pyroclastic	R, PT	379 100E 373 000N
67909	132	" "	R	379 000E 372 970N
67910	133	" "	R	379 160E 373 000N
67911	12	massive siliceous rock with augentexture	R	377 840E 372 420N
67912	46R/220	hanging wall pyroclastics from drill core DDH 46R	CA, PE	67E 3888N surface-
67913	46R/293		CA, PE	270°D -87°A
67914	46R/357		CA, T	
67915	46R/407		CA, T	
67916	46R/461	increasing alteration	CA, PE	
67917	46R/526		CA, PE	
67918	46R/582		CA, T	
67919	46R/757	host rock (reworked) altered tuff in black slate	CA, PE	
67920	46R/811	footwall schist	CA, T	
67921	1121/1	host rock, shale	CA, T	138'E 2780'N 8L-
67922	1121/24	" "	CA, PE	269°D -7°A
67923	1121/48	" " ?	CA, PT	
67924	1121/79	" " ?	CA, T	
67925	1121/108	footwall schist?	CA, PT	
67926	1121/138	footwall schist?	CA< T	138'E 2780'N 8L-
67927	1121/168	" " ?	CA, T	269°D -7°A
67928	1121/198	footwall schits with feldspar relics	CA, T	
67929	1121/250	sheared footwall pyroclastic with fresh feldspar	CA, T	
67930	1121/300	footwall schist with feldspar relics	CA, T	
67931	1121/348	sheared footwall pyroclastic withfresh feldspar	CA, PE	
67932	1121/400	sheared footwall pyroclastic with altered feldspar	CA, T	
67933	1121/449	footwall schist with altered feldspar	CA, PE	
67934	1121/500	footwall schist with moderately altered feldspar	CA, T	
67935	1121/550	footwall schist with moderately altered feldspar	CA, T	
67936	1121/648	footwall schist with altered feldspar	CA, PT	
67937	1121/749	footwall schist with feldspar relics	CA, T	
67938	1121/844	" " " " "	CA, T	
67939	1121/943	footwall schist	CA, T	
67940	1121/1053	footwall schist with fresh feldspar	CA, PE	
67941	1121/1155	footwall schist	CA, PT	
67942	1121/1255	footwall schist, fragmented	CA, T	
67943	1121/1355	massive siliceous rock?	CA, T	
67944	936/15	footwall schist	CA, PT	132'E 3620'N 9L-
67945	936/30	" "	CA, T	270°D 0°A
67946	936/50	" "	CA, T	
67947	1079/65	footwall schist with fresh feldspar	CA, T	525'E 2801'N 12L-
67948	1079/95	footwall schist	CA, T	270°D 0°A
67949	1079/145	" "	CA, T	
67950	1079/175	" "	CA,T	
67951	1079/205	" "	CA, T	
67952	1079/230	" "	CA, PT	
67953	1079/255	" "	CA, T	
67954	1079/287	footwall schist	CA, PE	
67955	1080/120	massive pyroclastic	CA, PE	536'E 2801'N 12L-
67956	1080/135	" "	CA, PE	90°D 0°A

Catalogue Number	Field Number	Rock type	Preparation	Location
67957	1222/0	footwall schist,	CA, T	328'E 3607'N 11L-
67958	1222/24	" "	CA, T	270°D 0°A
67959	1222/50	" "	CA, T	
67960	3265/191	" "	CA, T	771'E 4100'N 15L-
67961	3265/229	" "	CA< T	90°D -10°A
67962	3267/17	footwall schist with feldspar relics,	CA, T	782'E 2800'N 15L-
67963	3267/41	" " " " "	CA, P	90°D +35°A
67964	3267/66	" " " " "	CA, P	
67965	3267/90	" " " " "	CA, T	
67966	3267/138	host rock (reworked), altered tuff	CA, T	
67967	3267/163	host rock shale	CA, P	
37968	3267/182	black slate	CA, P	
67969	3268/9	footwall schist	CA< T	782'E 2800'N 15L-
67970	3268/33	footwall schist with feldspar relics	CA, T	90°D -8°A
67971	3268/57	" " " " "	CA, T	
67972	3268/81	" " " " "	CA, T	
67973	3268/105	footwall schist	CA, T	
67974	3268/129	footwall schist with feldspar relics	CA, T	
67975	3268/154	" " " " "	CA, P	
67976	3268/179	" " " " "	CA, P	
67977	3268/202	footwall schist	CA, T	
67978	3268/226	" "	CA, T	
67979	3268/297	host rock (reworked), sheared tuff	CA, T	
67980	3268/345	" " " " "	CA, T	
67981	3268/563	tuff within black slate	CA, T	
67982	3268/610	host rock shale within black slate	CA, T	
67983	3268/667	massive pyroclastic, altered	CA, T	
67984	3368/0	footwall schist	CA, T	783'E 3600'N 15L-
67985	3368/23	" "	CA, T	90°D +12°A
67986	3368/47	footwall schists with feldspar relics?	CA, T	
67987	3368/71	footwall schists	CA, T	
67988	3368/141	host rock, dark shale	CA, PE	
67989	3368/192	host rock, shale	CA, T	
67990	3368/217	host rock, altered tuff	CA, P	
67991	3368/241	host rock (reworked) tuff	CA, P	783'E 3600'N 15L-
67992	3368/263	host rock, shale	CA, T	90°D +12°A
67993	3375/40	footwall schist	CA, T	786'E 3150'N 15L- 90°D 71°A
67994	3376/3	footwall schist	CA< T	782'E 3600'N 15L-
67995	3376/31	" "	CA, T	90°D +76°A
67996	3376/53	" "	CA, T	
67997	3376/78	" "	CA, T	
67998	3376/175	host rock, shale	CA, T	
67999	3376/199	host rock, (reworked) altered tuff	CA, T	
68000	12/1	host rock; mineralized shale	R, CA, PE	96'W 2769'N 6L-
68001	12/25	footwall schist, mineralized shale	CA, T	238°D 0°A
68002	12/46	footwall schist	CA	
68003	12/78	footwall schist	CA	
68004	12/111	" "	CA, T	
68005	12/142	" "	CA	
68006	12/176	" "	CA	
68007	12/206	" "	CA	
68008	1036/120	massive pyroclastic,	CA	537'E 2599'N 12L- 90°D 0°A
68009	42/9	host rock, mineralized shale	R, CA, PE	344'W 2856'N 2L-
68010	42/25	footwall schist	CA	250°D 0°A

Catalogue Number	Field Number	Rock type	Preparation	Location
68011	42/55	footwall schist	CA	344'W 2856'N 2L- 250°D 0°A
68012	93/44	" "	CA	207'W 2751'N 4L-
68013	93/70	" "	CA	250°D 0°A
68014	93/97	" "	CA	
68015	93/130	footwall schist with feldspar relics	CA, T	
68016	93/161	footwall schist with faint feldspar relics	CA, T	
68017	609/24	host rock shale?	CA, P	44E 3648N 8L-
68018	609/40	footwall schist	CA, PE	270°D 0°A
68019	609/58	" "	CA, PE	
68020	717/4	" "	CA, PT	106'W 3649'N 6L-
68021	717/12	" "	CA, T	269°D 0°A
68022	717/19	" "	CA, PT	
68023	1136/10	host rock, shale	R, CA, PT	505'E 3602'N 12L-
68024	1136/40	footwall schist	CA, T	270°D 0°A
68025	42R/235	massive pyroclastic, drill core DDH 42R	R, T	998'E 270'S surface-
68026	42R/705	altered? massive pyroclastic, drill core DDH 42R	R, T	70°D -75°A
68027	41R/462	altered? massive pyroclastic, drill core DDH 41R	R, T	1038'E 593'S surface- 250°D -88°A
68028	760/38	contact host rock (reworked altered tuff)-black slate	R, T	70'W 3803'N 6L-
68029	1015/18	host rock, altered (reworked tuff)	CA, T	541'E 2193'N 12L-
68030	1015/146	altered massive pyroclastic	CA, T	90°D 0°A
68031	1015/213	" " "	CA, PE	
68032	879/14	host rock, carbonaceous shale	R, PE, CA	250'E 3600'N 10L-
68033	879/97	host rock, reworked tuff	R, T	90°D 0°A
68034	1034/29	host rock, altered tuff	CA, Pe	525'E 2599'N 12L-
68035	1034/37	host rock, altered (reworked) tuff	CA, PE	270°D 0°A
68036	1034/240	footwall schist	CA, T	
68037	1034/270	" "	CA, PE	
68038	3265/114	footwall schists with altered feldspar	R	
68039	C1	footwall schists, shale, with altered feldspar	R, PE	1240'E 175'S 16L
68040	2963/49	footwall schists, carbonaceous, mineralized shale	R, PE, CA	275'E 3520'N 10L 270°D -32°A
68041	741/52	footwall schist with altered feldspar?	CA	211'E 2100'N 10L- 270°D 0°A
68042	3474/179	footwall schist, carbonaceous shale	R, PE	
68043	3474/187	" " " "	R, PE	
68044	3474/207	" " " "	R, PE	
68045	G	" " " "	R, PE	1550'E 733'N 16L-
68046	740/3	host rock	R, CA	229'E 1999'N 10L-
68047	142/43	footwall schist, carbonaceous shale	CA	273'W 3175'N 2L-
68048	142/74	" " " "	CA	250°D 0°A
68049	142/107	" " " "	CA	
68050	142/143	" " " "	CA	
68051	142/183	" " " "	CA	
68052	142/220	" " " "	CA	
68053	142/250	" " " "	CA	
68054	142/280	" " " "	CA	
68055	206/8	" " " "	CA	183'W 3278'N 4L-
68056	206/21	" " " "	CA	250°D 0°A
68057	289/37	" " " "	CA	22'W 3214'N 6L- 250°D 0°A
68058	3173/32	" " " "	CA	78'E 3252'N 8L
68059	3173/48	" " " "	CA	270°D -68°A
68060	750/78	footwall schist with altered feldspar	R, T	47'E 4101'N 8L- 270°D 0°A

Catalogue Number	Field Number	Rock type	Preparation	Location
68061	572/85	footwall schist with moderately altered feldspars	R, T	713'W 3901'N surface 90°A
68062	1103/73	footwall schist	CA	525'E 3200'N 12L-
68063	1103/103	" "	CA	270°D 0°A
68064	1103/128	" "	CA	
68065	3367/0	footwall schist	CA	1786'E 3150'N 15L-
68066	3367/17	" "	CA	90°D +15°A
68067	3367/41	" "	CA	
68068	3367/65	" "	CA	
68069	3367/90	" "	CA	
68070	3367/113	" "	CA	
68071	761/37	" "	CA, T	76'W 3803'N 6L-
68072	761/68	footwall schists with feldspar relics	CA, T	270°D 0°A
68073	1055/75	" " " " "	CA, T	188'E 4000'N 6L-
68074	1055/101	footwall schists with altered feldspar	CA, T	270°D 0°A
68075	1055/130	footwall schists with altered feldspar relics	CA, T	
68076	967/66	" " " " " "	CA	309'E 3891'N 10L- 270°D 0°A
68079	1429/42	" " " " " "	CA, T	397'E 3926'N 11L- 270°D 0°A
68078	1682/100	footwall schist with feldspar relics?	CA, T	566'E 4050'N 12L-
68079	1682/130	" " " " "	CA, T	270°D +26°A
68080	3286/19	" " " " "	CA	771'E 4100'N 15L-
68081	3286/59	" " " " "	CA	90°D +38°A
68082	3286/98	" " " " "	CA	
68083	3286/135	footwall schist	CA, T	
68084	3286/159	" "	CA	
68085	1016/17	host rock, altered (reworked) tuff	CA, T	529'E 2199'N 12L-
68086	1016/44	" " " " "	CA, T	270°D 0°A
68087	1016/226	footwall schist, altered (reworked) tuff	CA, T	
68088	773/44	host rock, altered sheared tuff	CA, T	219'E 2500'N 10L- 90°D 0°A
68089	772/1	host rock shale	CA, PT	228'E 2799'N 10L-
68090	772/37	footwall schist	CA, T	270°D 0°A
68091	3195/88	footwall schist	R, P	783'E 3300'N 15L- 90°D +35°A
106693	42/1	pyrite barite mineralization, fresh albite	PE	344'W 2856'N 2L-
106694	A1	disseminated pyrite in quartz-sericite host rock	PT	783'E 3100'N 90°D +38°A 121.3'

Catalogue Number	Field Number	Rock type	Preparation	Location
106695	A2	disseminated banded/sheared pyrite in sericitic host rock	PT	122.5′
10696	A3	disseminated banded/sheared sphalerite-pyrite in sericitic host rock	PT	124.2′
106697	A18	disseminated banded/sheared sphalerite-pyrite in sericitic host rock	PT	124.6′
106698	A17	banded sheared semimassive sphalerite-pyrite ore	PT	127.3′
106699	A4	disseminated banded/sheared sphalerite-pyrite in sericitic host rock	PT	127.7′
106700	A5	semimassive banded/sheared sphalerite-pyrite-	PT	128.2′
106701	A7	semimassive banded sphalerite-pyrite ore	PT	128.6′
106702	A16	" " " " "	PT	129.0′
106703	A15	patches of sphalerite and chalcopyrite in vein, chalcopyrite along cracks in sphalerite	PT	130.3′
106704	A6	massive banded sphalerite-pyrite ore	PT	132.0′
106705	A19	folded pyrite band in massive sphalerite	PT	132.3′
106706	A8	massive sphalerite-galena with band of fine grained pyrite	PT	133.0′
106707	A10	semimassive sphalerite-galena-pyrite ore, moderately altered feldspar	PE	134′
106708	A11	banded sphalerite-galena-pyrite-chalcopyrite ore	PT	134.0′
106709	A9	crossbedded pyrite	PT	135.0′
106710	A14	deformed mineralized host rock quartz-sericite-carbonate	PT	135.4′
106711	A12	banded sphalerite-galena-pyrite ore	PT	138.7′
106712	A13	sericitic host rock with extremely fine grained pyrite	PT	144.7′
106713	B9	pyrite-chalcopyrite mineralization in carbonaceous host rock	PE	1783′E 3650′N 15L- 90°D +45°A 92.0′
106714	B1	pyrite-chalcopyrite mineralization in host rock	PE	97.0′
106715	B2	massive chalcopyrite	PT	102.0′
106716	B3	sphalerite-galena in sericitic host rock	PE	109.0
106717	B4	banded pyrite-sphalerite-galena ore	PE	109.0′
106718	B5	" " " " "	PE	120.5′
106719	B6	" " " " "	PE	142.0′
106720	B7	" " " " "	PE	144.5′
106721	B8	sphalerite, galena, chalcopyrite,pyrite ore with barite and tetrahedrite	PE	167.0′
106722	1220/45	pyrite-sphalerite-barite mineralization, fresh albite	PE	338′E 3607′N 11L- 90°D 0°A
106723	N	acicular haematite-(magnetite)		500′N 17L
106724	M	banded pyrite magnitite ore		500′N 17L
106725	D	semimassive host rock sericite, chlorite		1200′E 1000′S 16L-
106726	K	coarse tetrahedrite inclusions in sphalerite		650′N 17subL
106727	608/3	sphalerite-galena-pyrite and barite mineralization	PE	53′E 3648′N 8L- 90°D 0°A
106728	771/1	banded pyrite in host rock quartz-carbonate	PE	240′E 2799′N 10L

APPENDIX 2

Chemical rock analyses

	67795	67796	67797	67798	67799	67800	67801	67802	67803	67804	67805	67806	67807	67808
SiO_2	77.23	76.33	72.24	69.97	70.89	74.22	71.58	73.08	71.48	65.78	69.20	77.18	76.63	71.16
TiO_2	0.40	0.05	0.33	0.50	0.31	0.34	0.33	0.43	0.67	0.46	0.51	0.43	0.36	0.39
Al_2O_3	12.95	10.02	14.63	17.60	15.77	13.52	13.63	14.83	15.65	13.69	13.18	14.10	14.18	17.60
Fe_2O_3	1.65	2.06	2.65	2.69	1.84	2.30	5.39	3.73	3.44	11.49	10.26	1.23	1.10	2.04
MnO	0.02	0.15	0.02	0.01	0.02	0.03	0.01	0.02	0.02	0.21	0.25	0.01	0.01	0.02
MgO	0.34	0.58	1.07	0.97	1.82	1.10	1.30	1.16	1.14	1.58	1.12	0.05	0.60	0.70
CaO	0.23	1.79	0.07	0.15	0.01	0.76	0.05	0.08	0.09	0.02	0.01	0.06	0.04	0.15
Na_2O	2.66	1.19	1.53	1.53	0.15	4.08	0.15	2.48	1.51	0.15	0.15	1.83	1.08	2.56
K_2O	3.21	3.36	3.90	4.81	4.63	1.78	5.52	2.46	3.98	3.72	3.72	3.16	3.58	4.02
P_2O_5	0.03	0.00	0.01	0.02	0.00	0.03	0.01	0.05	0.10	0.01	0.01	0.01	0.01	0.01
ign. loss	1.49	3.93	2.67	2.73	3.35	1.71	2.04	2.20	2.49	3.23	2.74	2.17	2.34	2.51
total	100.21	99.46	99.11	100.98	98.77	99.86	100.00	100.52	100.57	100.34	101.16	100.24	99.92	101.17
Nb	14	10	16	17	15	13	13	13	16	9	9	19	16	18
Zr	245	79	246	317	258	232	240	259	293	202	204	317	242	291
Y	33	29	26	43	40	20	21	47	46	23	36	42	30	46
Sr	217	28	96	136	22	285	11	142	94	22	14	116	148	190
Rb	136	176	205	237	242	87	249	103	156	131	142	141	154	200
Pb	7	15	4	3	5	-	10	2	9	2	4	16	5	11
Zn	20	35	29	19	32	-	47	66	55	116	87	28	25	38
Cu	5	3	4	3	8	-	7	18	5	20	14	4	4	26
Ni	3	4	3	2	3	-	4	5	4	8	5	4	3	3
Co	2	-	4	3	1	-	4	5	5	13	14	1	1	3
Ba	1270	426	1249	1504	1221	-	1241	693	1626	958	813	823	1054	797
S	0.01	0.01	0.00	0.01	0.01	-	0.00	0.00	0.00	0.00	0.00	0.00	0.00	0.01
E	378400	377750	378320	378400	378455	378460	378625	377975	378290	378800	378800	377670	377805	377520
N	371645	372240	372710	372765	372813	373005	373135	375715	376130	376280	376280	376290	376120	376810
rock dens.	2.64		2.64				2.73	2.65	2.62			2.58	2.63	2.62
	SC	SC	SC	SC	SC	SC	SC	SC	SC	SC	SC	SC	SC	SC
	UA	SIL	UA			UA	SCH	UA	UA			UA	UA	UA
	D	D	D			D	D	D	D			D	D	D

	67809	67810	67811	67812	67813	67814	67815	67816	67817	67818	67819	67820	67821	67822
SiO_2	77.43	74.35	71.38	71.37	73.29	74.95	76.28	70.82	76.41	64.76	74.75	76.55	74.73	72.51
TiO_2	0.29	0.25	0.45	0.28	0.38	0.26	0.27	0.28	0.28	0.66	0.12	0.10	0.08	0.36
Al_2O_3	11.88	12.37	15.68	12.87	15.00	12.47	11.54	13.17	12.95	14.95	9.21	12.36	7.37	13.90
Fe_2O_3	1.84	4.78	2.56	4.57	2.68	5.60	2.71	8.22	1.94	5.86	7.44	1.70	2.64	2.28
MnO	0.13	0.14	0.01	0.01	0.01	0.08	0.06	0.18	0.05	0.07	0.01	0.07	0.23	0.07
MgO	0.78	0.79	0.59	0.94	0.81	0.63	1.02	1.05	0.69	1.96	0.05	0.64	1.64	0.53
CaO	0.16	0.79	0.06	1.32	0.01	0.01	0.04	0.04	0.18	3.80	0.01	1.45	4.28	0.58
Na_2O	3.22	0.15	4.42	0.85	0.15	0.60	0.15	0.15	6.01	2.81	0.15	0.15	3.40	2.62
K_2O	1.22	3.84	3.13	3.51	5.44	3.48	4.69	3.50	0.60	2.83	2.71	3.85	0.19	3.69
P_2O_5	0.03	0.10	0.06	0.04	0.01	0.01	0.06	0.04	0.01	0.10	0.01	0.01	0.03	0.01
ign. loss	2.49	2.45	1.97	3.58	2.37	2.22	2.14	2.56	0.90	2.75	4.77	3.87	6.26	2.29
total	99.46	100.02	100.31	99.34	100.16	100.31	98.94	100.01	100.03	100.55	99.22	100.77	100.86	98.84
Nb	12	13	21	14	19	16	10	9	12	11	8	9	6	15
Zr	199	194	323	243	306	239	187	242	212	228	90	113	43	288
Y	22	31	37	27	28	21	22	33	34	58	30	19	24	48
Sr	231	8	74	40	6	4	14	5	252	265	14	43	184	188
Rb	66	183	126	160	235	146	215	157	26	99	149	186	12	143
Pb	-	-	4	-	16	2	-	2	23	8	30	2	6	108
Zn	-	-	20	-	28	53	-	80	165	63	30	23	10	316
Cu	-	-	14	-	5	7	-	10	4	9	8	6	5	14
Ni	-	-	4	-	4	3	-	5	6	10	9	5	5	3
Co	-	-	1	-	5	7	-	7	4	13	3	1	1	2
Ba	-	-	919	-	1085	872	-	859	314	769	551	636	83	2307
S	-	-	0.00	-	0.00	0.00	-	0.01	0.07	0.01	4.37	0.04	0.01	0.19
E	378190	379090	379280	379140	378990	378900	378610	378810	378520	377590	378230	378200	378140	379230
N	375095	374450	375550	374160	375370	375110	373600	375120	375025	374690	374215	374260	374350	373410
Rock dens.			2.63			2.72		2.75						2.70
	SC	SC	SC	SC	SC	SC	SC	SC	SC	SC	SC	SC	SC	SC
	UA	SCH	UA	SCH		SCH	SCH	SCH	UA		SCH	SCH		UA
	D	D	D	D		D	D	D	D		D	D		D

	67823	67824	67825	67826	67827	67828	67829	67830	67831	67832	67833	67834	67835	67836
SiO_2	75.63	74.37	74.88	75.08	58.76	73.06	68.70	82.17	70.28	73.66	71.90	76.77	76.90	80.44
TiO_2	0.33	0.23	0.26	0.24	0.74	0.20	0.55	0.05	0.40	0.37	0.27	0.24	0.24	0.06
Al_2O_3	13.53	13.07	13.76	13.10	15.60	13.93	16.68	10.52	16.51	14.05	12.56	11.83	11.36	12.49
Fe_2O_3	1.96	2.13	1.10	2.46	8.33	3.41	3.55	1.07	2.75	2.20	3.85	4.80	3.60	0.95
MnO	0.01	0.01	0.01	0.01	0.18	0.31	0.14	0.01	0.06	0.01	0.09	0.07	0.10	0.01
MgO	0.65	0.43	0.31	0.05	3.15	0.69	0.05	0.26	0.90	0.32	3.95	0.75	0.42	0.05
CaO	0.16	0.05	0.15	0.30	5.33	0.06	0.32	0.01	0.20	0.55	0.01	0.02	0.06	0.01
Na_2O	3.16	1.49	2.99	3.00	3.12	0.15	3.82	0.15	2.58	2.99	0.15	0.15	0.15	0.92
K_2O	3.12	5.29	4.37	4.97	1.57	4.82	4.49	3.62	4.10	4.34	4.09	3.53	3.97	4.33
P_2O_5	0.01	0.01	0.01	0.01	0.08	0.01	0.10	0.01	0.05	0.01	0.01	0.01	0.01	0.01
ign. loss	1.29	1.37	1.25	0.70	3.16	2.49	1.73	1.52	2.07	1.33	2.95	2.18	2.90	1.87
total	99.85	98.44	99.08	99.91	100.03	99.12	100.14	99.39	99.89	99.83	99.84	100.35	99.70	101.14
Nb	12	18	17	11	12	17	16	9	19	14	11	10	11	11
Zr	217	278	261	186	229	241	337	94	316	244	216	190	181	100
Y	40	37	33	22	44	33	44	29	28	28	26	27	20	45
Sr	280	56	114	127	331	12	193	2	196	381	3	3	7	3
Rb	118	208	159	118	32	275	338	171	206	100	205	173	193	192
Pb	27	7	11	7	7	12	9	2	7	10	2	36	12	66
Zn	79	31	17	30	128	87	43	5	42	25	113	69	393	14
Cu	2	6	4	5	5	8	14	3	3	6	5	10	20	45
Ni	5	4	3	6	14	4	6	4	3	3	3	3	4	5
Co	1	1	1	3	18	3	5	2	3	4	4	1	4	3
Ba	1493	1206	1111	1127	657	1394	1604	538	1241	1306	585	380	539	572
S	0.00	0.00	0.01	0.00	0.02	0.01	0.02	0.06	0.00	0.01	0.01	0.02	0.09	0.02
E	379060	379590	379975	381520	382080	379190	379095	377780	378880	378480	378570	378560	378560	377975
N	373760	373530	373520	372895	373370	373740	372670	372360	372140	372540	372975	373800	373800	373040
rock dens.	2.68	2.64					2.67	2.67	2.62	2.65	2.70	2.72	2.75	2.69
	SC	SC	SC	SC	SC	SC,	SC	SC	SC	SC	SC	SC	SC	SC
	UA	SCH				SCH	UA	SIL	UA	UA	SCH		SCH	SIL
	D	D	D	D		D	D	D	D	D	D	D	D	D

	67837	67838	67839	67840	67841	67842	67843	67844	67845	67846	67847	67848	67849	67850
SiO_2	71.63	72.63	75.35	83.19	77.72	74.70	74.03	81.33	69.53	81.36	73.68	73.78	75.13	73.20
TiO_2	0.44	0.20	0.05	0.05	0.10	0.14	0.11	0.02	0.78	0.06	0.34	0.40	0.36	0.43
Al_2O_3	12.89	12.92	15.27	10.52	13.57	15.18	15.07	12.54	15.77	11.13	13.40	14.24	13.60	15.32
Fe_2O_3	4.12	2.92	1.00	1.22	1.79	1.42	2.11	1.05	3.99	1.97	2.80	2.47	1.90	1.80
MnO	1.35	0.06	0.01	0.01	0.16	0.02	0.33	0.01	0.02	0.01	0.05	0.18	0.02	0.20
MgO	0.70	0.05	0.58	0.05	0.05	0.29	0.05	0.11	0.80	0.05	0.46	0.05	1.15	0.36
CaO	0.29	1.41	0.01	0.01	0.01	0.01	0.01	0.04	0.10	0.01	0.42	0.23	0.64	0.17
Na_2O	0.15	3.78	2.05	0.15	0.15	2.73	0.15	0.15	5.85	0.15	3.46	3.53	2.63	2.72
K_2O	4.79	3.87	3.47	3.42	4.49	3.37	4.85	3.37	0.97	3.68	3.60	3.35	2.57	3.94
P_2O_5	0.03	0.01	0.01	0.01	0.01	0.01	0.01	0.26	0.08	0.01	0.01	0.31	0.01	0.03
ign. loss	4.54	1.84	2.52	1.63	2.27	1.66	2.93	1.85	2.28	1.94	1.50	1.36	1.90	1.91
total	100.94	99.69	100.31	100.26	100.32	99.54	99.65	100.74	100.18	100.36	99.71	99.89	99.90	100.09
Nb	9	20	24	13	14	16	13	18	15	13	16	18	15	17
Zr	213	259	117	95	113	137	114	82	244	106	290	284	248	285
Y	34	41	38	33	28	20	20	88	29	27	48	43	20	38
Sr	18	120	61	2	4	40	8	17	278	3	168	208	342	177
Rb	212	131	221	152	350	192	237	160	62	162	168	140	138	215
Pb	11	5	9	31	42	27	4	5	10	15	13	20	16	9
Zn	38	30	16	13	50	34	21	16	54	20	31	168	22	29
Cu	11	4	5	5	12	4	7	4	6	5	4	5	6	10
Ni	5	5	3	4	6	4	5	6	9	5	4	3	4	4
Co	3	4	1	1	2	4	1	1	6	3	4	4	1	1
Ba	944	1046	548	604	509	601	721	1272	248	516	844	1419	873	1071
S	0.22	0.00	0.01	0.30	0.07	0.01	0.02	0.33	-	0.54	0.01	0.02	0.00	0.00
E	378320	379580	378060	378050	377915	377955	378110	378140	378310	377990	379075	379215	378675	378845
N	372890	374140	373105	373370	373430	373695	373905	374350	373135	373235	372480	372180	372265	372240
rock dens.	2.77	2.64		2.66	2.65	2.64	2.69	2.67		2.71	2.65	2.61	2.57	2.61
	SC	SC	SC	SC	SC	SC	SC	SC	SC	SC	SC	SC	SC	SC
	SCH	UA		SIL	SIL	SIL	SIL	SIL		SIL	SIL	UA	UA	UA
	D	D		D	D	D	D	D		D	D	D	D	D

	67851	67852	67853	67854	67855	67856	67857	67858	67859	67860	67861	67862	67863	67864
SiO_2	77.87	71.55	69.90	67.78	75.82	65.83	72.86	70.55	67.94	74.44	73.79	76.15	78.55	72.77
TiO_2	0.26	0.43	0.45	0.70	0.20	0.74	0.37	0.57	0.55	0.31	0.23	0.23	0.24	0.26
Al_2O_3	12.14	14.66	14.82	15.70	13.37	16.14	14.90	15.56	14.29	13.02	14.47	13.12	11.49	13.32
Fe_2O_3	1.62	3.15	5.40	4.35	2.44	6.49	2.56	3.75	5.84	3.24	2.73	2.41	1.50	2.52
MnO	0.02	0.03	0.03	0.16	0.03	0.06	0.05	0.03	0.66	0.32	0.01	0.01	0.01	0.12
MgO	0.05	0.39	0.53	1.10	0.05	2.00	0.76	0.56	1.12	0.05	0.05	0.66	0.26	0.70
CaO	0.13	0.16	0.14	0.70	0.08	0.16	0.55	0.16	0.31	0.20	0.04	0.03	0.04	1.02
Na_2O	4.13	3.80	1.13	3.78	2.94	1.57	2.75	2.34	2.95	4.96	1.94	1.44	3.14	2.90
K_2O	2.46	3.75	5.11	2.66	3.31	3.57	3.22	3.55	3.18	1.97	4.18	3.98	2.35	3.23
P_2O_5	0.01	0.07	0.09	0.15	0.01	0.09	0.04	0.13	0.13	0.04	0.01	0.01	0.01	0.03
ign. loss	0.88	1.46	2.22	2.42	1.64	3.11	2.02	2.70	2.71	1.92	2.25	2.28	1.67	2.70
total	99.57	99.44	99.82	99.48	99.88	99.76	100.09	99.88	99.67	100.47	99.70	100.33	99.25	99.55
Nb	14	15	16	13	20	17	17	15	14	17	21	22	17	16
Zr	214	233	226	303	260	259	271	229	214	252	285	278	239	211
Y	22	18	33	29	31	30	27	33	37	33	35	39	25	25
Sr	321	113	41	281	70	73	221	76	109	107	57	43	79	115
Rb	79	215	795	204	152	147	158	143	125	89	172	158	81	130
Pb	10	7	3	41	11	12	19	8	5	6	2	4	6	2
Zn	26	46	65	78	24	69	32	39	35	37	25	19	12	19
Cu	6	9	-	11	21	11	6	13	8	4	8	8	7	7
Ni	4	6	5	4	4	8	4	6	6	3	5	4	5	4
Co	4	4	4	4	3	18	3	11	16	7	5	5	2	4
Ba	1606	1209	1260	1345	1215	856	841	903	714	515	1011	994	809	775
S	0.00	0.01	0.02	0.01	0.01	0.00	0.01	0.00	0.01	0.03	0.01	0.02	0.01	0.00
E	378590	379760	379740	379285	379690	380140	378930	379280	379310	379425	379960	379960	379790	379785
N	372430	372910	372930	373035	372530	372515	372590	375700	375760	375785	376240	376240	376260	376250
rock dens.	2.62	2.60		2.63	2.63		2.67	2.58		2.64	2.61		2.57	
	SC	SC	SC	SC	SC	SC	SC	SC	SC	SC	SC	SC	SC	SC
	UA	UA		UA			UA	UA		UA	UA		UA	
	D	D	D	D	D	D	D	D	D	D	D	D	D	D

	67865	67866	67867	67868	67869	67870	67871	67872	67873	67874	67875	67876	67877	67878
SiO_2	68.53	83.00	73.82	83.14	79.49	71.96	64.68	66.20	65.26	60.34	78.58	75.73	79.39	70.89
TiO_2	0.61	0.14	0.28	0.28	0.30	0.36	0.63	0.67	0.69	1.43	0.20	0.33	0.14	0.47
Al_2O_3	16.02	9.33	13.50	9.19	11.40	16.10	15.20	14.75	15.20	13.68	12.38	13.94	13.78	15.64
Fe_2O_3	4.34	2.03	2.63	1.65	1.89	1.61	6.19	5.41	6.03	7.66	1.68	2.00	0.52	2.34
MnO	0.03	0.01	0.02	0.01	0.08	0.06	0.10	0.15	0.11	0.16	0.01	0.04	0.01	0.05
MgO	1.29	0.05	0.33	0.05	0.88	0.94	1.13	1.53	2.25	2.19	0.24	0.24	0.26	0.48
CaO	0.09	0.01	0.15	0.01	0.10	0.01	1.77	2.73	1.12	3.90	0.02	0.04	0.01	0.26
Na_2O	2.28	0.15	2.71	0.15	1.51	0.15	4.40	3.04	3.97	3.23	2.18	0.15	0.15	3.23
K_2O	4.20	3.62	4.73	2.94	1.74	6.23	2.85	3.60	2.32	1.99	2.84	4.90	4.19	3.97
P_2O_5	0.11	0.01	0.01	0.01	0.06	0.01	0.14	0.11	0.12	0.43	0.01	0.04	0.01	0.05
ign. loss	3.01	1.59	1.01	1.88	2.47	2.51	2.40	1.75	2.82	4.95	1.63	2.12	1.76	1.70
total	100.52	99.94	99.18	99.30	99.91	99.93	99.48	99.92	99.88	99.95	99.77	99.52	100.22	99.08
Nb	16	15	21	13	15	19	14	15	14	6	18	17	14	19
Zr	248	189	271	219	235	267	225	232	232	161	216	248	128	359
Y	24	26	43	18	29	37	39	32	25	38	30	35	22	30
Sr	109	20	104	13	143	5	103	193	134	173	43	6	16	264
Rb	156	135	153	124	69	327	142	136	121	84	148	262	210	179
Pb	4	5	9	11	39	2	2	8	14	2	7	36	26	11
Zn	42	17	22	14	46	25	65	57	154	85	24	33	18	36
Cu	8	6	4	4	10	3	9	12	7	12	8	9	5	17
Ni	6	4	4	4	4	4	5	9	8	4	4	2	2	3
Co	14	2	5	1	3	3	12	13	17	17	2	1	1	3
Ba	1001	966	1174	735	442	764	610	1126	694	479	708	953	718	1504
S	0.01	0.00	0.01	0.01	0.01	0.00	0.00	0.00	0.01	0.04	0.01	0.02	0.01	0.01
E	380015	380660	380730	379550	378250	378340	381020	381365	380860	380400	379370	378410	378260	379200
N	376240	376460	376240	376260	374955	374510	374755	374060	372860	373255	373690	373310	373910	372950
rock dens.					2.47	2.66					2.63	2.66	2.60	2.62
	SC	SC	SC	SC	SC	SC	SC	SC	SC	SC	SC	SC	SC	SC
					UA	SCH					UA	SCH	SCH	UA
	D	D	D	D	D	D	D	D	D		D	D	D	D

	67879	67880	67881	67882	67883	67884	67885	67886	67887	67888	67889	67890	67891	67913
SiO_2	72.50	76.19	73.59	80.77	76.76	76.20	77.46	68.53	81.85	75.20	70.76	81.05	74.49	71.89
TiO_2	0.39	0.28	0.34	0.21	0.27	0.26	0.27	0.42	0.10	0.34	0.44	0.17	0.30	0.39
Al_2O_3	15.74	12.91	14.55	11.71	11.56	11.71	11.30	17.27	11.32	13.92	16.93	7.59	13.19	13.66
Fe_2O_3	2.10	2.35	2.04	1.39	2.35	2.34	2.05	2.79	0.44	1.58	1.96	5.73	2.00	2.30
MnO	0.08	0.17	0.06	0.23	0.83	0.85	0.02	0.03	0.01	0.04	0.06	0.01	0.05	0.07
MgO	0.84	2.36	0.88	0.05	0.27	0.18	0.91	1.28	0.33	1.26	0.56	0.24	0.20	0.65
CaO	0.01	0.04	0.03	0.03	0.12	0.14	0.01	0.08	0.01	0.41	0.04	0.01	0.58	2.00
Na_2O	0.82	0.15	0.15	0.15	0.15	0.15	0.15	2.52	0.15	4.12	0.61	0.15	5.41	3.93
K_2O	5.43	2.83	5.89	3.24	6.15	6.51	6.18	4.45	3.44	1.30	4.78	1.77	2.47	2.45
P_2O_5	0.03	0.04	0.04	0.16	0.03	0.04	0.03	0.05	0.01	0.05	0.05	0.01	0.03	0.01
ign. loss	2.73	2.84	2.11	2.00	1.37	1.37	1.34	2.84	1.82	1.84	2.79	3.81	1.05	2.60
total	100.67	100.18	99.69	99.94	99.86	99.75	99.72	100.26	99.48	100.06	98.98	100.54	99.76	99.95
Nb	19	16	17	12	15	14	12	18	9	14	16	8	12	13
Zr	292	236	278	181	184	195	191	297	96	235	305	112	220	291
Y	43	24	34	26	28	27	25	37	11	22	37	22	39	59
Sr	18	36	10	22	40	46	34	95	6	285	55	57	241	284
Rb	289	157	289	175	216	235	284	240	180	81	201	99	69	98
Pb	36	14	31	12	-	-	17	2	-	-	-	109	4	11
Zn	83	123	67	36	-	-	40	47	-	-	-	15	26	34
Cu	15	6	6	4	-	-	6	17	-	-	-	10	2	3
Ni	3	3	2	3	5	5	4	6	-	-	-	5	4	5
Co	2	5	4	3	5	4	1	4	-	-	-	3	3	3
Ba	1300	1435	1603	2144	1189	1283	3513	1249	-	-	-	947	1037	-
S	0.00	0.01	0.00	0.49	0.33	0.31	0.05	0.01	-	-	-	4.13	0.00	0.03
E	378725	378760	378600	378895	378780	378780	378620	379110	378365	378990	378820	378560	377780	378660
N	372880	373925	374075	373670	373300	373300	373450	373360	373720	373110	373430	374970	370000	375350
rock dens.	2.61	2.64	2.67	2.67	2.67	2.70	2.66	2.65						
	SC SCH D	SC SCH D	SC SCH D	SC SCH D	SC SCH D	SC D	SC SCH D	SC UA D	SC SIL D	SC UA D	SC SCH D			SC UA D

	67912	67913	67914	67915	67916	67917	67918	67919	67920	67921	67922	67923	67924	67925
SiO_2	71.90	71.77	70.52	70.52	72.89	62.16	73.30	55.25	74.20	74.70	74.64	56.45	65.90	71.32
TiO_2	0.39	0.44	0.37	0.39	0.35	0.28	0.39	0.65	0.28	0.20	0.24	0.51	0.40	0.33
Al_2O_3	13.66	14.97	14.42	14.92	13.56	11.35	13.38	17.46	12.51	9.78	10.38	20.05	16.18	13.06
Fe_2O_3	2.30	2.94	2.64	2.36	1.94	1.69	3.11	5.12	2.87	7.41	8.49	11.46	3.11	3.13
MnO	0.07	0.09	0.11	0.07	0.06	0.19	0.08	0.24	0.75	0.35	0.50	0.71	1.17	0.35
MgO	0.65	0.64	0.58	0.46	0.45	0.36	0.60	1.68	1.02	0.87	1.10	2.14	1.62	1.07
CaO	2.00	1.53	1.93	1.40	1.65	11.10	2.75	5.60	0.81	0.07	0.06	0.09	1.53	1.02
Na_2O	3.93	4.95	3.81	4.32	3.95	2.88	1.11	0.15	0.15	0.15	0.15	0.15	0.15	0.15
K_2O	2.45	2.25	3.02	3.26	3.65	2.53	2.98	4.30	4.14	2.73	2.55	5.09	5.54	5.00
P_2O_5	0.01	0.04	0.04	0.09	0.04	0.05	0.06	0.14	0.03	0.01	0.01	0.03	0.01	0.01
ign. loss	2.59	2.10	2.64	1.95	1.73	9.06	3.44	8.45	3.88	3.37	2.72	4.38	5.17	4.69
total	99.95	101.71	100.09	99.74	100.28	101.65	101.20	99.04	100.64	99.64	100.85	101.05	100.79	100.13
Nb	13	16	11	13	12	10	8	11	12	10	10	19	16	12
Zr	291	311	260	275	249	187	186	178	237	165	188	371	308	219
Y	59	58	41	45	46	47	29	36	37	25	28	54	46	31
Sr	284	432	303	323	301	340	291	178	45	13	10	19	22	53
Rb	98	82	96	102	96	64	94	153	191	128	119	250	295	228
Pb	11	26	36	67	18	28	21	31	649	300	53	59	65	83
Zn	34	41	207	142	110	82	102	140	330	330	182	251	113	192
Cu	3	2	5	3	6	12	10	36	73	73	17	26	3	12
Ni	5	5	4	5	5	5	5	10	5	5	4	4	3	6
Co	3	2	4	3	1	1	3	12	9	9	7	6	4	1
Ba	-	380	360	380	280	420	430	1200	340	300	120	390	210	360
S	0.03	0.02	0.10	0.04	0.03	0.04	0.03	1.89	1.18	1.70	0.42	0.88	0.28	0.17
E	16	12	8	4	0	-5	-10	-33	-43	42	35	28	18	9
N	1185	1185	1185	1185	1185	1185	1185	1185	1185	847	847	847	847	847
rock dens.									2.74					D
	C	C	C	C	C	C	C		SIMS C					C

	67926	67927	67928	67929	67930	67931	67932	67933	67934	67935	67936	67937	67938	67939
SiO_2	71.23	72.19	72.12	68.43	64.11	71.98	66.94	64.90	71.58	75.33	72.32	69.30	73.76	73.91
TiO_2	0.32	0.30	0.34	0.42	0.47	0.33	0.28	0.31	0.32	0.32	0.32	0.33	0.28	0.32
Al_2O_3	13.15	12.43	12.96	16.12	17.22	11.57	11.83	12.61	13.61	13.50	13.39	14.46	11.74	12.46
Fe_2O_3	2.14	2.22	3.03	2.80	3.55	2.29	2.03	2.40	2.20	2.02	2.34	2.60	2.89	2.65
MnO	0.64	0.58	0.53	0.19	0.22	0.17	0.14	0.16	0.08	0.05	0.11	0.20	0.24	0.26
MgO	0.66	0.69	0.95	1.07	1.81	1.11	0.48	0.70	0.55	2.28	1.52	1.35	0.97	1.03
CaO	3.36	3.34	1.24	1.64	2.61	3.92	7.24	6.95	1.52	1.16	1.63	1.79	1.45	1.24
Na_2O	0.15	0.61	0.77	3.55	1.59	3.13	2.29	2.93	3.44	0.15	1.70	0.79	0.15	0.15
K_2O	4.97	4.13	4.63	3.58	4.83	2.45	2.40	2.87	3.34	3.00	4.01	5.56	5.20	4.71
P_2O_5	0.04	0.01	0.04	0.06	0.03	0.01	0.01	0.01	0.01	0.04	0.01	0.03	0.01	0.01
ign. loss	4.88	2.27	4.51	3.21	4.63	4.62	6.38	6.61	3.07	2.85	3.58	4.65	3.91	4.07
total	101.55	98.77	101.13	101.08	101.07	101.57	100.02	100.46	99.72	100.70	100.94	101.06	100.60	100.81
Nb	14	15	13	16	15	10	13	12	13	13	13	13	11	13
Zr	239	244	249	305	293	195	192	215	240	247	238	267	229	250
Y	34	32	33	39	39	32	31	40	37	40	34	40	36	33
Sr	67	10	14	201	162	208	268	274	181	335	114	32	25	14
Rb	248	243	206	121	170	81	103	128	156	91	139	245	177	220
Pb	30	474	301	21	6	5	28	11	5	4	8	8	105	57
Zn	47	495	221	68	72	45	73	52	38	47	75	96	94	164
Cu	6	11	5	2	3	4	5	3	3	2	2	5	26	6
Ni	3	4	4	4	4	4	3	4	5	4	3	3	4	4
Co	2	3	2	4	1	1	3	1	3	1	2	2	1	1
Ba	470	530	440	370	520	450	450	590	380	1050	290	430	240	440
S	0.09	0.14	0.12	0.06	0.02	0.04	0.03	0.03	0.02	0.02	0.01	0.03	0.11	0.05
E	1	-8	-17	-32	-46	-59	-74	-87	-101	-115	-142	-166	-190	-214
N	847	846	846	846	846	846	845	845	845	845	843	831	819	807
	D	D	D	D	D	D	D	D	D	D	D	D	D	D
	C	C	C	C	C	C	C	C	C	C	C	C	C	C

	67940	67941	67942	67943	67944	67945	67946	67947	67948	67949	67950	67951	67952	67953
SiO_2	72.99	72.32	71.90	67.06	82.96	75.97	71.33	66.94	75.98	67.16	68.83	67.78	75.80	72.20
TiO_2	0.33	0.37	0.14	0.07	0.13	0.20	0.28	0.54	0.23	0.23	0.25	0.28	0.22	0.26
Al_2O_3	13.32	13.78	14.20	14.81	6.90	10.95	14.04	16.97	13.13	10.99	13.03	13.99	11.16	11.76
Fe_2O_3	2.74	2.80	1.99	3.29	3.59	6.20	6.62	3.22	1.52	4.28	2.15	4.67	5.92	7.53
MnO	0.06	0.18	0.19	0.56	0.05	0.16	0.14	0.38	0.28	2.40	0.30	0.80	0.24	0.52
MgO	0.86	1.20	0.76	0.68	0.32	0.55	0.61	2.20	1.07	2.06	3.00	3.16	0.69	1.14
CaO	0.95	1.56	1.86	1.27	0.07	0.21	0.16	0.90	0.49	3.91	3.79	0.95	0.06	0.49
Na_2O	3.59	0.15	0.15	0.60	0.40	0.15	0.15	0.90	0.15	0.15	0.15	0.15	0.15	0.15
K_2O	2.42	2.57	4.95	5.22	1.88	2.56	3.44	3.46	3.61	2.78	3.25	3.50	2.80	2.66
P_2O_5	0.01	0.06	0.01	0.01	0.03	0.03	0.05	0.12	0.03	0.03	0.05	0.03	0.03	0.03
ign. loss	2.48	4.35	4.61	4.89	2.26	2.67	3.49	3.90	2.73	6.93	5.34	4.54	2.83	3.28
total	99.76	99.34	100.76	98.46	98.59	99.64	100.32	99.52	99.21	100.91	100.15	99.85	99.89	100.03
Nb	13	15	11	13	10	14	17	15	15	12	14	15	12	16
Zr	234	257	139	238	108	168	211	252	189	174	222	221	169	189
Y	39	34	24	34	17	20	26	31	25	23	29	30	24	28
Sr	219	41	32	114	11	21	21	113	26	65	78	23	10	12
Rb	122	164	224	139	93	131	172	157	174	150	164	180	146	145
Pb	5	147	16	13	249	24	180	117	17	75	14	129	315	184
Zn	51	512	51	52	102	74	119	137	107	186	132	1223	817	266
Cu	2	11	3	4	1021	28	285	6	5	257	6	27	380	1158
Ni	5	3	5	7	4	7	1	3	1	4	3	3	4	2
Co	4	3	3	3	6	3	5	3	3	3	3	3	5	7
Ba	320	610	280	330	840	560	500	2800	2500	670	460	570	170	190
S	0.10	0.10	0.13	0.17	1.52	0.53	1.15	1.14	0.25	0.21	0.07	1.35	0.97	0.77
E	-241	-266	-290	-315	36	31	25	140	131	116	107	98	91	84
N	793	781	768	756	1103	1103	1103	854	854	854	854	854	854	854
rock dens.					2.75	2.79	2.77							
					FC	FC	FC	FC	FC	FC	FC	FC	FC	FC
	D	D	D	D	D	D	D	D	D	D	D	D	D	D
					SIMS	SIMS	SIMS							
	C	C	C	C										

	67954	67955	67956	67957	67958	67959	67960	67961	67962	67963	97964	97965	67966	67967
SiO_2	76.13	71.33	69.90	77.19	76.97	74.18	67.27	78.23	69.80	69.77	76.10	83.69	52.57	64.71
TiO_2	0.22	0.52	0.28	0.14	0.20	0.21	0.28	0.20	0.29	0.29	0.24	0.15	0.87	0.39
Al_2O_3	10.48	13.61	14.17	8.71	10.30	11.10	14.52	10.36	13.86	14.28	11.58	8.85	23.71	19.51
Fe_2O_3	5.75	4.22	3.20	6.20	5.60	6.26	2.95	2.74	2.14	2.30	1.75	1.16	4.52	3.12
MnO	0.35	0.08	0.10	0.23	0.26	0.16	0.70	0.08	0.10	0.08	0.17	0.10	0.38	0.08
MgO	0.60	0.67	0.81	0.30	0.61	0.62	1.35	0.81	2.65	3.94	3.21	0.62	2.10	2.30
CaO	0.27	2.53	3.36	0.44	0.43	0.27	2.16	0.29	2.79	1.55	1.37	0.39	2.29	0.99
Na_2O	0.15	2.24	1.27	0.15	0.15	0.15	0.40	0.15	0.85	0.71	0.15	0.65	1.28	0.91
K_2O	2.69	1.49	2.73	2.47	2.46	2.91	4.80	3.40	2.89	2.94	2.38	1.98	4.11	3.51
P_2O_5	0.04	0.08	0.05	0.04	0.03	0.03	0.03	0.03	0.05	0.05	0.03	0.03	0.24	0.09
ign. loss	2.64	2.36	3.60	4.19	3.10	4.29	3.87	2.50	4.10	3.92	3.40	1.85	6.34	4.07
total	99.30	99.12	99.47	100.06	100.11	100.18	98.33	98.77	99.51	99.83	100.38	99.46	98.40	99.67
Nb	13	10	12	14	13	13	21	12	15	15	13	10	20	18
Zr	166	187	176	117	159	164	201	156	232	234	184	127	298	365
Y	24	21	31	19	21	19	24	19	31	32	26	20	27	47
Sr	10	351	224	17	19	15	59	8	107	78	55	44	361	278
Rb	139	54	101	119	135	152	207	160	123	113	97	96	189	155
Pb	101	14	18	1236	619	23	3165	56	17	4	9	67	145	51
Zn	357	61	82	2045	154	54	4868	332	33	37	61	169	998	68
Cu	405	13	7	2538	18	15	95	27	4	5	5	6	24	9
Ni	3	3	3	6	3	3	3	3	2	2	3	7	11	8
Co	4	8	3	58	5	3	3	3	3	3	3	3	4	6
Ba	120	300	600	1270	860	860	1060	900	480	820	1280	1480	4200	1280
S	0.60	0.00	0.00	3.76	1.10	1.23	0.67	0.76	0.05	0.08	0.02	0.34	0.00	0.00
E	75	200	204	100	93	85	293	304	243	249	255	261	273	279
N	854	854	854	1099	1099	1099	1250	1250	853	853	853	853	853	853
rock dens.				2.84	2.79	2.80								
	FC			FC	FC	FC	FC	FC	FC	FC	FC	FC	FC	FC
	D			D	D	D	D	D	D	D	D	D	D	D
				SIMS	SIMS	SIMS								
		C	C								C	C	C	C

	67968	67969	67970	67971	67972	67973	67974	67975	67976	67977	67978	67979	67980	67981
SiO_2	16.59	67.12	71.74	68.29	71.14	64.71	69.10	65.78	69.31	78.15	85.20	56.55	59.82	55.02
TiO_2	0.70	0.25	0.26	0.32	0.29	0.35	0.30	0.29	0.34	0.20	0.10	0.66	0.51	0.54
Al_2O_3	8.40	13.85	12.90	15.67	14.78	17.08	14.61	14.32	16.94	10.88	6.49	22.38	19.19	14.03
Fe_2O_3	5.48	2.09	1.97	2.29	1.82	6.52	2.75	1.93	1.81	1.42	1.16	3.92	5.12	7.10
MnO	5.90	0.32	0.08	0.70	0.05	0.26	0.12	0.22	0.22	0.12	0.18	0.69	0.60	0.12
MgO	2.25	2.43	1.81	2.98	2.44	1.79	4.60	3.98	1.46	0.74	0.72	2.81	2.02	2.01
CaO	25.77	2.98	1.95	2.03	1.34	0.29	1.40	3.59	1.23	0.80	0.77	1.85	1.73	6.71
Na_2O	0.15	0.40	2.86	1.26	1.14	0.15	0.15	0.55	0.15	0.40	0.41	1.12	1.90	0.85
K_2O	2.21	3.71	3.70	3.21	3.03	4.32	2.89	2.80	4.37	2.95	1.64	3.36	3.24	2.54
P_2O_5	0.03	0.03	0.04	0.05	0.03	0.04	0.04	0.06	0.04	0.03	0.03	0.16	0.10	0.19
ign. loss	28.16	5.05	3.36	3.85	3.07	4.81	4.15	5.33	3.54	2.94	2.11	5.54	4.31	9.39
total	95.64	98.22	100.68	100.67	99.13	100.32	100.11	98.85	99.41	98.62	98.80	99.04	98.55	98.49
Nb	8	15	13	15	16	19	16	14	18	14	11	20	13	12
Zr	88	211	215	258	230	269	247	226	260	157	87	321	180	140
Y	35	28	27	32	30	40	33	29	34	24	14	34	21	27
Sr	206	76	79	107	104	118	72	355	100	36	36	396	192	192
Rb	91	161	145	135	122	136	117	105	188	145	88	198	142	101
Pb	548	15	16	4	5	4	4	12	9	445	216	106	22	100
Zn	761	60	35	34	29	39	52	72	60	1378	381	85	93	357
Cu	32	4	6	3	10	13	4	8	6	21	9	10	23	28
Ni	7	2	2	4	1	4	3	4	2	3	5	2	18	24
Co	5	3	3	3	3	4	3	3	3	3	4	3	6	12
Ba	340	600	620	660	760	1320	1020	1600	3700	1580	2600	1180	860	460
S	0.00	0.07	0.07	0.02	0.03	0.03	0.00	0.04	0.40	0.54	0.35	0.00	0.00	0.00
E	284	241	248	256	263	270	277	285	293	300	307	329	343	410
N	853	853	853	853	853	853	853	853	853	853	853	853	853	853
rock dens.		2.73												
		FC	FC	FC	FC	FC	FC	FC	FC	FC				
		D	D	D	D	D	D	D	D	D				
		SEMS												
		C	C	C	C	C	C	C	C	C				

	67982	67983	67984	67985	67986	67987	67988	67989	67990	67991	67992	67993	67994	67995
SiO_2	61.08	68.68	65.62	72.32	69.37	70.50	53.47	76.11	32.13	54.51	59.63	71.99	67.81	69.41
TiO_2	0.38	0.38	0.34	0.23	0.28	0.29	0.55	0.38	0.47	0.58	0.43	0.23	0.28	0.29
Al_2O_3	17.06	15.43	16.73	11.51	14.20	15.19	18.78	12.10	11.72	14.80	15.85	12.33	14.30	13.67
Fe_2O_3	3.97	3.01	6.20	6.66	5.78	6.19	6.72	1.96	1.88	6.78	4.61	2.74	7.05	7.29
MnO	0.37	0.10	0.21	0.15	0.08	0.17	2.02	0.02	0.01	0.27	0.16	0.26	0.14	0.10
MgO	2.35	1.67	3.32	2.07	1.16	1.82	2.52	1.04	0.81	3.95	2.54	1.20	1.97	1.16
CaO	4.71	1.70	0.21	0.14	0.30	0.21	2.60	0.10	0.06	6.41	5.12	1.51	0.25	0.62
Na_2O	0.46	1.60	0.15	0.15	0.15	0.15	0.15	0.40	0.76	0.50	0.90	0.40	0.15	0.15
K_2O	3.22	2.51	3.97	2.61	4.08	3.39	5.12	3.69	2.66	2.16	2.80	4.10	3.82	3.66
P_2O_5	0.10	0.07	0.04	0.04	0.03	0.04	0.12	0.08	0.05	0.17	0.14	0.03	0.03	0.04
ign. loss	5.91	3.51	3.79	3.51	5.09	3.35	8.23	2.41	4.55	8.10	6.55	3.85	4.35	4.19
total	99.61	98.65	100.59	99.38	100.52	101.32	100.27	98.28	55.10	98.23	98.73	98.64	100.15	100.59
Nb	18	10	18	13	14	18	18	14	17	15	13	15	15	15
Zr	291	175	263	181	219	253	262	184	158	195	153	186	225	234
Y	48	24	34	24	25	27	32	21	19	28	24	22	22	30
Sr	159	156	9	8	12	12	38	12	1665	132	167	19	12	12
Rb	141	101	215	129	225	194	254	155	138	79	104	198	181	175
Pb	256	62	44	141	192	44	380	285	756	925	1352	462	46	64
Zn	742	69	179	1100	187	131	681	898	2820	4879	3607	766	77	62
Cu	17	4	6	12	10	1224	40	11	10	21	19	193	32	38
Ni	9	5	4	3	4	4	3	5	1	43	23	3	3	5
Co	3	3	3	3	92	5	3	5	3	13	10	3	4	5
Ba	1260	640	330	260	270	350	4200	5200	230000	3300	650	1040	320	290
S	0.00	0.00	0.63	1.66	3.19	0.87	3.25	0.78	7.53	1.57	1.59	0.65	2.61	2.64
E	424	441	239	246	253	260	280	295	302	309	315	244	239	241
N	853	853	1097	1097	1097	1097	1097	1097	1097	1097	1097	960	1097	1097
rock dens.			2.76		2.78								2.78	2.80
			FC	FC	FC							FC	FC	FC
			D	D	D							D	D	D
			SEMS		SEMS								SEMS	SEMS
		C												

	67996	67997	67998	67999	68000	68001	68002	68003	68004	68005	68006	68007	68008	68009
SiO_2	72.79	70.02	65.05	63.54	46.60	77.40	75.88	78.34	73.28	70.60	69.45	70.73	68.15	37.27
TiO_2	0.25	0.29	0.47	0.52	1.02	0.21	0.22	0.22	0.26	0.29	0.27	0.29	0.42	0.75
Al_2O_3	12.14	13.64	18.04	18.05	27.34	11.12	9.84	9.96	11.56	13.28	11.83	12.18	14.52	18.92
Fe_2O_3	5.18	2.43	3.18	4.42	6.07	3.91	4.94	5.86	8.33	4.02	2.77	4.11	3.17	8.23
MnO	0.11	0.13	0.08	0.14	1.53	0.33	1.09	0.49	0.36	1.85	1.53	1.71	0.07	0.75
MgO	1.05	4.32	2.73	3.05	0.96	0.29	0.33	0.84	1.05	0.93	0.65	0.75	0.73	0.68
CaO	0.22	2.13	1.22	2.42	0.34	0.03	0.09	0.07	0.04	0.14	2.49	1.29	3.87	6.64
Na_2O	0.40	0.15	0.15	0.70	0.48	0.15	0.15	0.15	0.15	0.15	0.15	0.15	0.68	3.06
K_2O	3.16	2.89	3.87	3.01	8.29	4.13	3.23	2.47	2.96	4.52	4.13	4.32	3.59	3.62
P_2O_5	0.04	0.04	0.04	0.10	0.18	0.06	0.03	0.03	0.01	0.04	0.01	0.03	0.01	0.01
ign. loss	3.19	3.74	4.18	4.83	6.92	3.49	3.98	2.86	2.90	4.11	5.88	5.65	4.56	11.49
total	98.54	99.78	99.00	100.79	99.72	101.13	99.78	101.29	100.91	99.92	99.15	101.21	99.77	91.42
Nb	15	15	24	12	-	-	-	-	-	-	-	-	10	-
Zr	198	229	252	221	-	-	-	-	-	-	-	-	200	-
Y	23	24	29	28	-	-	-	-	-	-	-	-	44	-
Sr	10	11	74	181	-	-	-	-	-	-	-	-	147	-
Rb	161	182	134	118	-	-	-	-	-	-	-	-	125	-
PB	47	47	27	25	398	96	328	234	31	1627	52	363	4	1083
Zn	52	80	51	87	3990	64	5786	355	126	2438	891	444	58	4581
Cu	61	48	17	17	90	29	1412	90	538	17	5	5	5	29
Ni	4	1	10	9	4	4	7	4	4	4	5	4	5	3
Co	9	3	4	6	2	4	5	2	10	1	2	1	6	3
Ba	270	360	5600	2900	2800	1400	1200	350	370	280	320	330	420	14000
S	1.46	0.84	0.40	0.40	2.27	2.12	2.16	-	1.03	0.83	0.57	0.58	-	6.85
E	242	244	254	256	-30	-36	-41	-49	-58	-66	-75	-83	200	-107
N	1097	1097	1097	1097	844	840	837	831	826	821	816	810	792	870
	FC	FC				FC	FC	FC	FC	FC	FC	FC		
	D	D				D	D	D	D	D	D	D		
													C	

	68010	68011	68012	68013	68014	68015	68016	68017	68018	68019	68020	68021	68022	68023
TiO_2	83.77	85.74	73.84	57.51	55.83	65.40	56.27	82.88	71.14	81.02	79.51	74.47	81.31	33.78
SiO_2	0.16	0.20	0.29	0.35	0.21	0.22	0.35	0.21	0.25	0.15	0.21	0.24	0.18	0.54
Al_2O_3	8.00	8.97	10.32	16.82	10.27	9.70	14.89	7.37	11.53	6.96	10.00	12.05	8.82	17.25
Fe_2O_3	2.57	0.89	6.74	10.48	3.24	1.76	3.26	2.11	9.18	4.90	3.45	4.12	1.67	10.60
MnO	0.05	0.11	0.04	0.21	1.73	0.92	5.23	0.02	0.21	0.04	0.09	0.12	0.11	12.59
MgO	0.31	0.23	0.30	0.59	5.60	8.89	2.26	0.05	0.62	0.33	0.53	0.57	0.48	1.37
CaO	0.03	0.09	0.02	0.05	7.64	4.44	3.57	0.02	0.02	0.02	0.17	0.13	0.09	1.01
Na_2O	0.15	0.15	0.15	0.15	0.15	0.15	0.15	0.15	0.15	0.15	0.15	0.15	0.15	0.15
K_2O	2.23	2.44	3.85	5.95	2.93	1.39	4.65	2.61	3.47	2.55	3.67	4.31	3.24	5.57
P_2O_5	0.01	0.06	0.01	0.01	0.03	0.01	0.04	0.01	0.01	0.01	0.01	0.01	0.01	0.13
ign. loss	2.11	1.58	4.89	7.40	12.68	8.38	9.27	2.95	4.28	3.01	3.20	3.81	2.56	16.10
total	99.38	100.47	100.45	99.51	100.30	101.27	99.92	98.37	100.85	99.13	100.99	99.97	98.62	99.10
Nb	-	-	-	-	-	-	-	-	-	-	-	-	-	-
Zr	-	-	-	-	-	-	-	-	-	-	-	-	-	-
Y	-	-	-	-	-	-	-	-	-	-	-	-	-	-
Sr	-	-	-	-	-	-	-	-	-	-	-	-	-	-
Rb	-	-	-	-	-	-	-	-	-	-	-	-	-	-
Pb	160	80	188	6922	201	135	164	855	1517	836	849	91	292	991
Zn	391	419	1059	1218	1649	149	500	7814	1257	1673	2257	3248	8767	4250
Cu	9	21	42	206	23	3	20	638	3279	940	1872	239	211	15
Ni	5	5	8	6	3	3	4	6	6	5	5	4	4	7
Co	3	1	6	11	2	1	5	3	8	3	4	5	3	5
Ba	1900	280	1560	500	310	160	440	570	540	190	440	370	170	1120
S	1.45	0.17	4.83	6.24	0.97	0.04	0.25	3.36	3.37	2.74	1.74	2.21	1.39	4.22
E	-112	-121	-76	-83	-91	-100	-109	6	1	-4	-34	-36	-38	151
N	868	865	833	831	828	825	822	1112	1112	1112	1112	1112	1112	1098
rock dens.				2.73	2.74	2.70	2.75		2.84	2.78	2.76	2.79	2.77	
	FC	FC	FC	FC	FC	FC	FC		FC	FC	FC	FC	FC	
	D	D	D	D	D	D	D		D	D	D	D	D	
				CBMS	CBMS	CBMS	CBMS		SIMS	SIMS	SIMS	SIMS	SIMS	

	68024	68029	68030	68031	68032	68034	68035	68036	68027	68040	68041	68046	68085	68086
SiO_2	81.81	68.12	71.87	73.13	29.23	41.34	55.55	66.98	76.64	68.66	77.29	56.47	47.22	56.96
TiO_2	0.17	0.44	0.32	0.35	0.45	0.42	0.86	0.30	0.31	0.31	0.23	0.75	3.55	0.73
Al_2O_3	9.08	15.29	13.01	13.63	12.63	12.72	23.55	12.64	12.40	15.09	11.46	17.07	20.34	20.78
Fe_2O_3	2.87	2.00	3.21	2.55	21.55	2.50	3.92	10.80	5.33	4.59	2.11	4.27	11.10	5.47
MnO	0.33	0.09	0.12	0.07	11.38	0.41	0.07	0.48	0.21	0.49	0.17	0.09	0.10	0.51
MgO	0.48	0.93	0.48	0.45	1.47	1.67	2.14	1.73	0.79	0.67	0.58	1.68	2.57	3.28
CaO	0.02	3.42	3.56	1.57	0.75	19.93	0.85	0.05	0.06	0.08	0.54	6.55	1.44	1.21
Na_2O	0.15	1.08	1.69	3.36	0.15	2.33	2.63	0.15	0.15	0.15	1.65	2.68	2.86	0.95
K_2O	3.33	3.92	2.28	2.40	3.26	1.47	4.80	2.89	2.50	4.61	2.65	2.61	1.92	3.17
P_2O_5	0.01	0.01	0.01	0.01	0.10	0.13	0.14	0.03	0.01	0.01	0.01	0.16	0.35	0.11
ign. loss	2.58	5.19	4.08	2.50	18.16	17.01	4.84	4.12	2.49	3.99	2.85	7.28	7.81	5.07
total	100.84	100.49	100.65	100.02	99.13	99.92	99.36	100.18	100.89	98.64	99.53	99.62	99.25	98.24
Nb	-	11	10	11	-	10	14	12	12	-	10	22	44	17
Zr	-	191	200	210	-	110	218	238	228	-	155	339	264	331
Y	-	30	46	45	-	22	32	34	34	-	24	38	23	55
Sr	-	99	189	327	-	449	21	10	11	-	202	91	261	524
Rb	-	151	102	84	-	61	176	142	190	-	132	192	99	192
Pb	447	203	11	7	1351	69	1437	177	608	857	2110	11	50	56
Zn	3695	466	64	64	6806	265	2420	261	1157	532	3201	127	252	169
Cu	674	10	3	5	31	9	12	234	179	3110	55	15	16	8
Ni	6	5	6	5	96	11	3	4	4	4	4	42	20	7
Co	23	1	4	3	5	4	5	8	7	8	1	14	10	4
Ba	580	540	500	1460	2800	1560	6600	250	260	2900	5000	4500	7000	26000
S	1.32	-	-	-	-	0.91	1.95	1.70	0.38	1.53	-	-	6.82	2.35
E	142	170	209	229	80	151	149	88	79	71	48	71	156	148
N	1098	670	670	670	1097	792	792	792	792	1073	640	609	670	670
rock dens.	2.77													
	FC													
	D							D	D					
	SIMS													
			C	C				C	C		C			

	68087	68088	68089	68090
SiO_2	70.92	52.30	60.43	77.93
TiO_2	0.29	0.78	0.73	0.22
Al_2O_3	12.77	21.82	23.11	12.45
Fe_2O_3	3.61	5.38	3.03	1.72
MnO	0.58	0.16	0.27	0.18
MgO	2.58	2.43	1.91	0.72
CaO	0.42	2.70	0.27	0.16
Na_2O	0.15	3.76	0.15	0.15
K_2O	4.02	4.44	6.13	3.53
P_2O_5	0.01	0.21	0.17	0.03
ign. loss	3.55	6.38	4.39	2.63
total	98.89	100.37	100.59	99.72
Nb	13	14	20	16
Zr	227	257	320	166
Y	35	38	44	27
Sr	15	342	62	22
Rb	200	164	285	161
Pb	1179	25	10	1419
Zn	3630	66	56	1928
Cu	39	7	5	25
Ni	5	20	2	2
Co	3	8	7	3
Ba	600	7000	1160	870
S	0.98	-	1.22	0.53
E	94	80	69	58
N	670	762	853	853
				FC
	D			D
	C			

Key:

SC: used in surface contouring (chap. 8)

UA: used as unaltered pyroclastic in statistical methods (chap. 8)

SIL: used as massive siliceous rock in statistical methods (chap. 8)

SCH: used as schist in statistical methods (chap. 8)

D: used in dilution diagrams (chap. 12.1)

C: used in correlation of drill core samples (chap. 12.3)

SIMS: used as siliceous mine schist in element exchange (chap. 12.2)

SEMS: used as sericitic mine schist in element exchange (chap. 12.2)

CBMS: used as carbonaceous mine schist in element exchange (chap. 12.2)

FC: used in footwall contouring, underground (chap. 9.3.1.)

Coordinates E (east) and N (north) in metre for SC and FC, otherwise in feet

	68047	68048	68049	68050	68051	68052	68053	68054	68055	68056	68057	68058	68059	68062
Pb	203	9	17	61	51	60	18	97	406	587	624	1439	1777	88
Zn	65	76	42	131	51	116	61	149	455	2150	7268	2446	2566	101
Cu	6	0	1	0	1	3	1	3	1234	868	86	15	36	25
Ni	3	3	3	3	4	3	4	5	5	6	6	4	4	6
Co	3	3	0	0	0	2	0	0	5	0	3	2	0	3
Ba	460	560	330	360	210	220	420	210	4000	1900	3200	1140	1260	660
S	0.24	0.28	0.03	0.02	0.03	0.02	0.01	0.02	1.97	1.26	2.34	1.56	1.65	2.95
E	-235	-241	-248	-255	-263	-270	-276	-282	-161	-164	-103	-43	-41	140
N	963	960	957	953	949	945	942	939	998	997	976	991	991	975
	FC	FC	FC	FC	FC	FC	FC	FC	FC	FC	FC	FC	FC	FC

	68063	68064	68065	68066	68067	68068	68069	68070	68071	68072	68073	68074	68075	68076
Pb	24	78	11	30	326	97	38	30	67	54	1787	50	66	393
Zn	81	159	45	65	252	204	52	24	75	170	1602	115	818	2724
Cu	5	3	1	7	237	741	8	10	9	5	27	1	13	42
Ni	4	6	3	3	3	4	4	4	4	3	4	2	4	5
Co	0	3	3	3	2	4	0	0	0	0	2	0	25	6
Ba	760	2000	730	780	840	1140	880	820	440	500	370	380	440	395
S	0.40	1.16	0.09	0.33	0.73	0.95	0.27	0.50	0.75	0.37	0.59	0.09	0.16	0.85
E	134	128	298	300	304	308	311	314	-119	-126	-15	-21	-28	37
N	975	975	960	960	960	960	960	960	1159	1159	1219	1219	1219	1186
	FC	FC	FC	FC	FC	FC	FC	FC	FC	FC	FC	FC	FC	FC

	68077	68078	68079	68080	68081	68082	68083	68084
Pb	81	874	77	43	118	301	2114	851
Zn	165	6032	2410	958	976	447	4725	2736
Cu	1030	936	809	5	9	4	21	29
Ni	5	7	3	4	4	4	8	5
Co	8	2	7	4	0	0	6	0
Ba	420	800	680	490	790	560	540	520
S	1.62	1.51	1.00	0.86	0.42	0.35	0.56	1.60
E	88	134	125	289	291	294	296	298
N	1197	1234	1234	1250	1250	1250	1250	1251
	FC	FC	FC	FC	FC	FC	FC	FC

REE concetrations in ppm

Sample	La	Ce	Pr	Nd	Sm	Eu	Gd	Dy	Er	Yb	Y
				DDH 1121							
67921	27.3	55.9		24.0							24.7
	30.8	70.5	8.0	31.6	5.1	0.9	4.1	2.8	2.4	2.2	
67922	25.0	54.1		22.4							27.7
67923	57.1	128.8		49.6							54.4
	54.5	129.6	15.4	61.0	11.3	2.3	9.9	7.1	6.3	4.7	
67924	49.9	109.4		43.4							45.6
67925	35.1	76.1		31.9							30.5
67926	37.3	85.7		36.0							33.8
67927	36.6	77.0		31.8							31.6
	28.7	70.2	9.0	33.9	6.4	1.1	5.8	4.1	3.7	3.2	
67928	35.0	74.8		33.0							30.5
67929	53.8	121.4		46.6							39.1
	44.0	106.0	12.5	49.9	9.5	2.1	7.3	4.7	4.7	3.9	
67930	45.5	102.0		37.4							39.2
67931	36.2	76.2		33.5							32.2
67932	33.9	75.3		31.0							31.2
67933	39.8	86.7		35.3							40.1
67934	39.8	86.0		34.7							37.1
67935	40.1	95.3		37.1							39.5
67936	34.8	77.3		33.1							33.9
67937	44.5	98.2		40.1							39.5
67938	33.1	75.4		31.6							36.1
67939	43.4	89.1		36.8							33.3
67940	53.2	106.2		43.8							38.7
67941	33.6	69.8		28.9							33.9
67942	41.3	82.8		28.4							24.0
67943	36.0	75.4		26.3							30.1
				DDH 46R							
67912	52.7	113.4		47.6							58.9
	47.5	113.3	14.4	57.6	11.5	2.4	10.3	7.8	5.6	4.5	
67914	46.9	92.8		37.4							40.9
67916	42.2	87.5		36.4							46.2
	31.0	77.4	11.0	41.5	8.8	2.1	8.8	8.5	6.5	4.7	
67917	39.1	81.3		36.2							46.7
	27.3	68.6	9.6	37.4	8.3	2.3	8.7	8.8	7.9	4.9	
67918	30.7	66.4		26.6							29.7
	26.6	62.6	8.6	30.7	6.4	1.7	6.3	5.4	3.7	3.0	
67920	35.0	80.4		31.3							36.6

Sample	La	Ce	Pr	Nd	Sm	Eu	Gd	Dy	Er	Yb	Y
				Unaltered volcanics							
67802	47.7	93.5		37.1							46.6
	57.3	121.6	13.6	52.1	9.3	1.6	8.1	5.4	4.2	3.5	
67808	45.0	103.4		45.1							46.2
67795	31.4	69.1		29.4							33.0
67817	26.0	47.1		24.6							34.3
67832	30.9	58.3		21.7							27.6
67806	40.0	93.6		39.9							41.8
67850	45.4	98.2		42.2							38.4
67808	39.0	87.4		32.3							30.0
67797	32.2	69.4		27.6							26.2
67849	36.2	83.1		31.9							19.8
67857	45.2	121.7		44.1							27.3
67818	41.4	72.2		44.7							58.4
	37.2	73.3	11.1	48.2	9.7	1.7	10.9	10.8	7.7	4.1	
67823	42.4	80.9		31.0							40.1
67804	39.3	82.6		32.6							23.2
67847	66.0	136.8		60.3							47.9

Sample	La	Ce	Pr	Nd	Sm	Eu	Gd	Dy	Er	Yb	Y
7829	54.6	113.4		46.2							44.9
	36.1	88.8	10.7	47.6	9.6	1.9	8.8	6.7	4.5	3.8	
67861	46.6	97.9		41.2							35.4
67854	30.5	78.8		34.5							29.1
67891	49.5	80.6		45.0							39.4
	30.3	57.2	9.6	39.0	7.9	1.6	8.0	6.6	5.2	3.9	
67858	38.9	84.1		33.1							32.7
67838	38.1	86.0		35.4							40.8
67852	27.5	55.0		24.4							17.5
67886	42.2	101.7		39.5							37.1
67848	68.2	144.7		58.3							43.4
	53.8	127.0	15.0	60.5	12.1	2.9	11.2	9.6	7.3	4.3	
67878	23.6	46.5		20.2							30.4
67863	21.4	50.0		21.4							24.5
67811	55.0	114.5		51.1							37.2
	47.5	110.9	13.7	55.6	10.4	1.3	8.2	9.0	5.5	3.4	
67822	42.1	94.5		38.0							47.7
67864	28.5	59.7		27.8							23.6
67827	31.2	66.5		30.6							44.2
	27.4	66.0	7.6	34.9	7.4	1.6	7.6	7.7	5.4	3.5	

Sample	La	Ce	Pr	Nd	Sm	Eu	Gd	Dy	Er	Yb	Y
67826	42.5	71.5		29.2							22.2
67825	35.2	75.5		31.8							32.5
67864	28.7	63.6		26.3							24.5
67859	42.3	78.2		32.6							36.6
67867	75.1	103.9		62.8							42.5
67856	34.1	51.8		30.0							30.0
	16.5	32.9	7.5	28.2	5.6	0.9	5.8	5.5	5.6	3.8	
67874	11.8	30.5		20.3							37.6
	14.3	38.1	5.3	24.3	5.9	1.7	6.1	4.9	3.5	2.8	
				Surface schists							
67801	22.4	36.5		18.4							21.1
67833	10.4	18.3		8.9							25.9
	7.4	21.2	2.6	10.9	2.0	0.2	1.6	2.2	1.9	2.1	
67834	30.5	61.0		25.8							26.5
67835	32.6	66.6		27.9							20.0
	30.3	71.7	8.2	33.5	6.2	0.9	4.3	2.4	1.9	2.2	
67884	31.6	67.4		27.4							27.2
67882	31.1	71.5		29.9							26.4

Sample	La	Ce	Pr	Nd	Sm	Eu	Gd	Dy	Er	Yb	Y
67880	39.7	88.3		37.6							33.7
	20.0	55.1	7.7	31.5	6.4	1.5	6.7	6.1	5.8	3.9	
67876	10.2	24.9		9.7							34.8
	4.8	16.3	2.8	9.4	2.6	0.6	2.5	3.1	3.1	2.9	
67879	65.6	138.2		56.0							42.9
67883	55.0	110.7		45.6							27.9
	47.5	115.8	13.1	55.6	9.3	1.1	6.8	5.3	3.1	2.7	
67884	31.6	67.4		27.4							27.2
	16.5	42.7	5.8	23.8	5.3	0.8	4.7	5.3	4.0	3.3	
67880	8.3	12.7		5.6							23.5
67813	36.2	72.1		34.7							27.5
	42.4	89.0	9.9	46.7	7.7	0.8	5.4	4.0	3.0	2.9	
67816	17.5	39.6		16.4							20.5
	14.4	36.7	18.0	4.5	3.7	0.6	3.2	2.9	2.5	2.5	
67798	39.1	91.0		34.1							42.6
	20.7	61.5	31.2	7.5	6.6	1.5	6.2	5.9	5.2	4.1	
				Massive siliceous rocks							
67846	51.4	102.5		37.5							26.5
	42.1	93.0	9.8	37.7	7.3	0.9	5.2	2.8	2.8	2.6	
67840	44.8	91.3		31.3							32.7
	33.8	78.4	8.9	34.1	6.9	0.9	5.8	3.9	4.0	2.6	

Sample	La	Ce	Pr	Nd	Sm	Eu	Gd	Dy	Er	Yb	Y
67841	45.7	92.5		33.3							27.5
67843	49.5	95.7		32.6							19.7
67842	38.4	76.2		23.9							20.4
67830	31.2	66.5		24.4							29.0
				Mine schists							
68085	42.8	91.4		35.5							35.4
68037	40.8	88.6		35.8							33.7
68036	46.3	105.4		42.6							24.0
68090	32.0	60.4		23.5							27.2
67971	44.2	87.2		36.5							32.1
67970	32.2	71.2		29.7							26.8
67959	29.5	53.5		22.2							18.7
67986	43.9	99.4		41.1							25.3
67946	45.9	93.8		36.2							26.4
67958	25.2	61.8		22.9							20.9
67985	34.5	73.6		30.8							24.0
67920	35.0	80.4		31.3							36.6

APPENDIX 3

Normality diagrams for surface samples as indicated in tab.4 (chap. 8.3.1.3.2.)

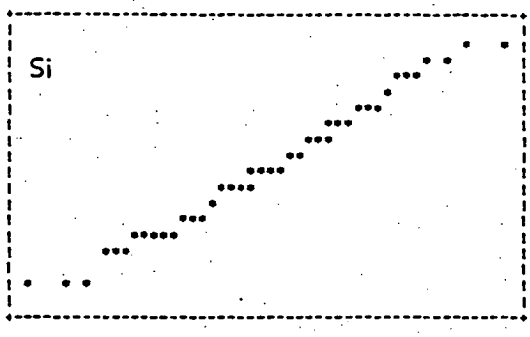

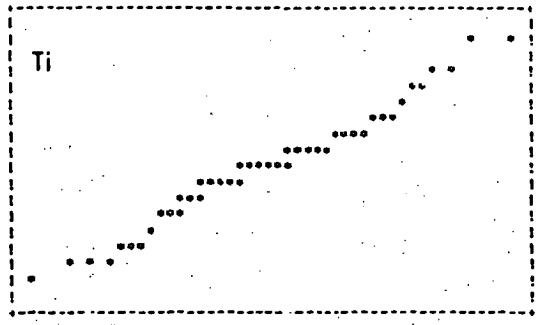

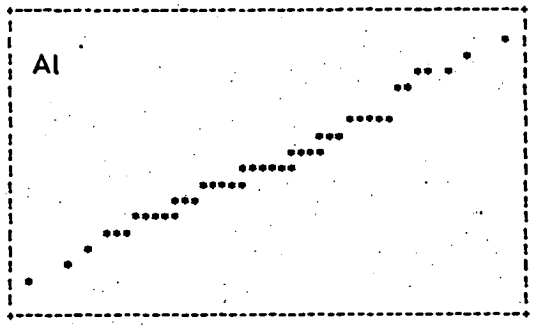

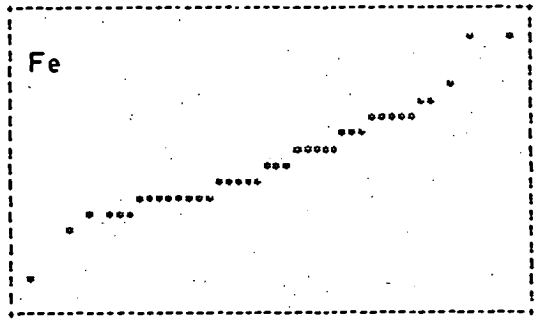

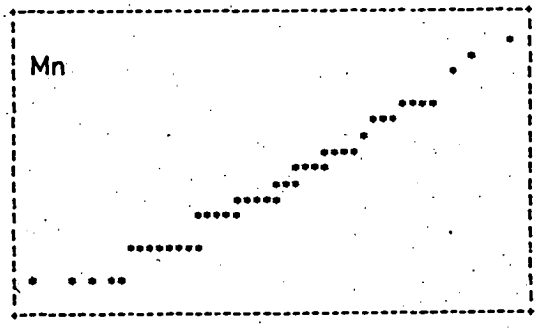

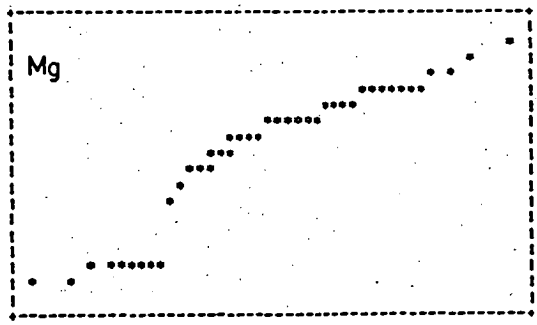

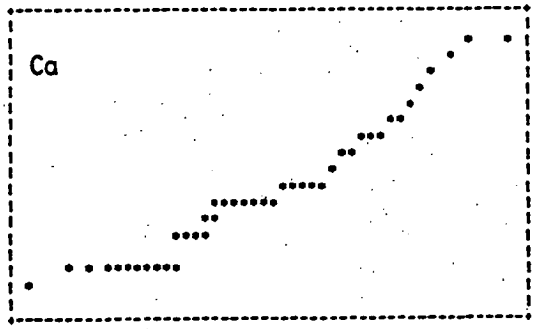

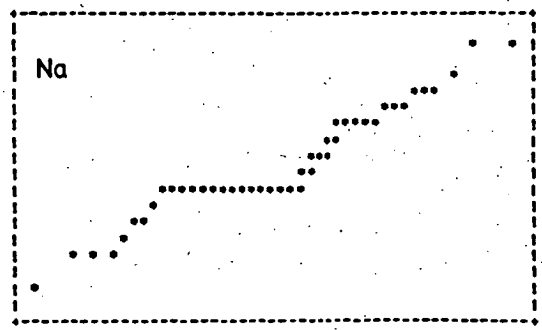

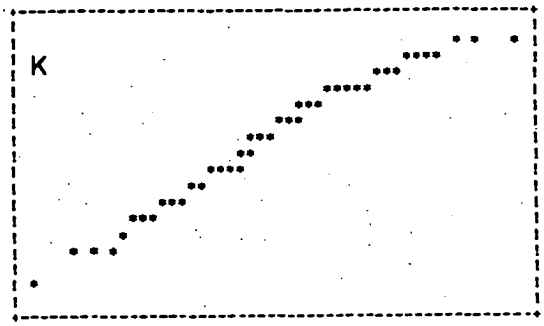
K

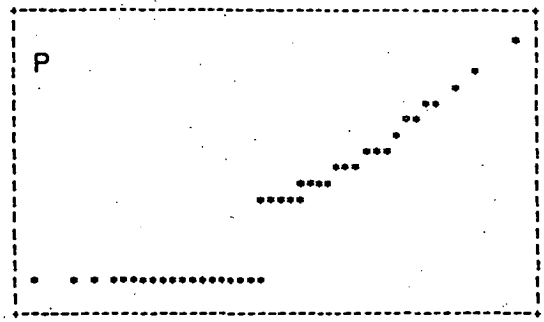
P

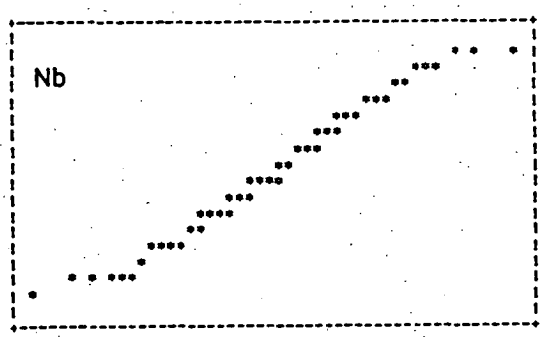
Nb

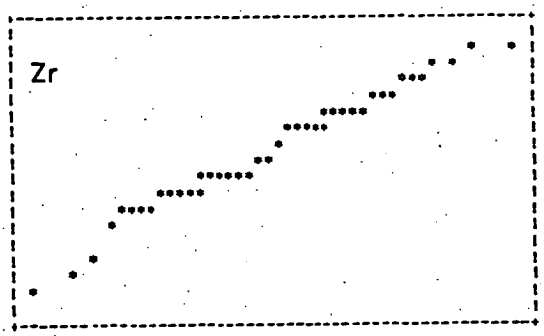
Zr

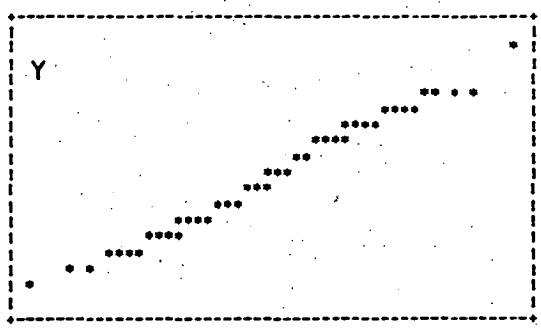
Y

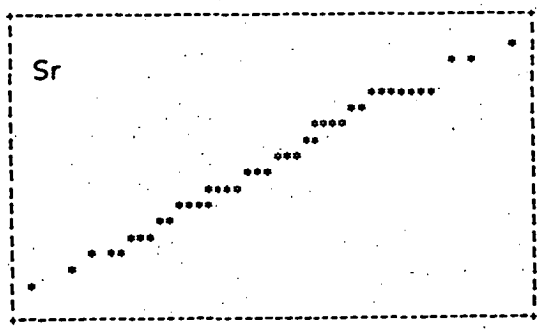
Sr

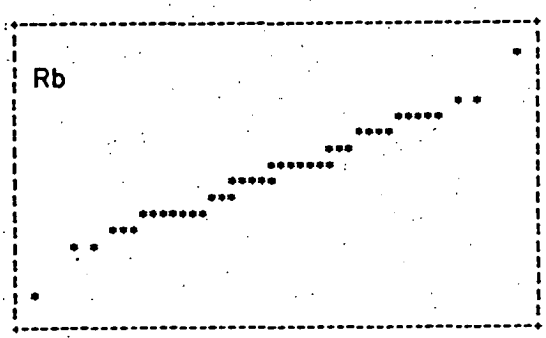
Rb

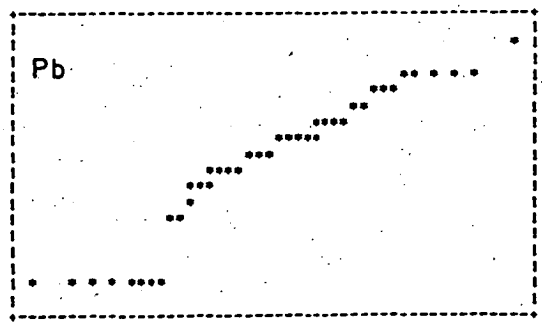
Pb

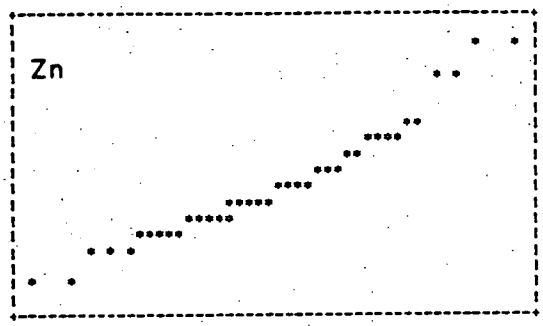
Zn

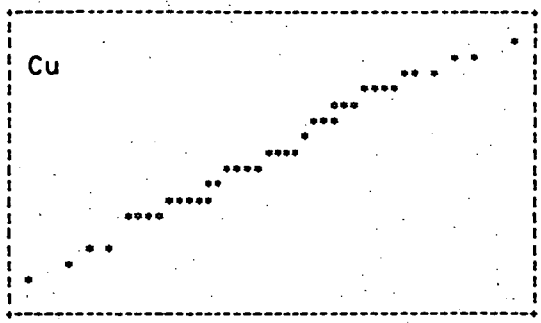
Cu

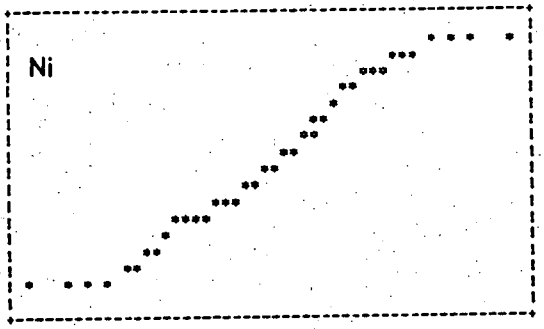
Ni

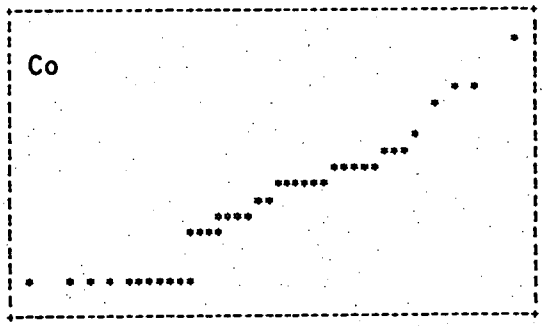
Co

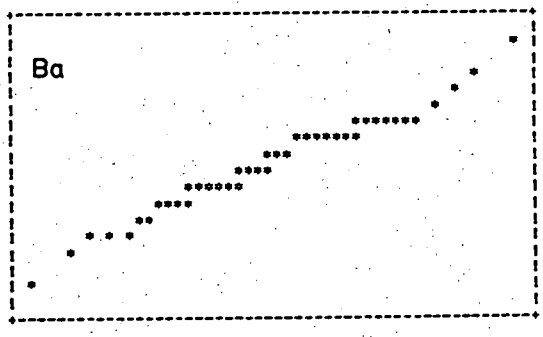
Ba

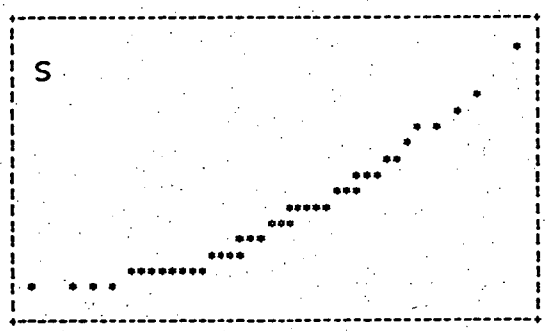
S

Normality diagrams for ore forming metals as indicated in chap.9.4.5.1

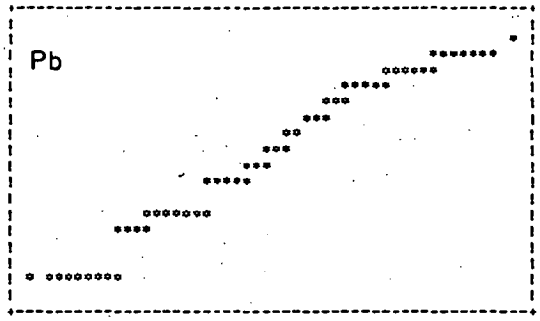

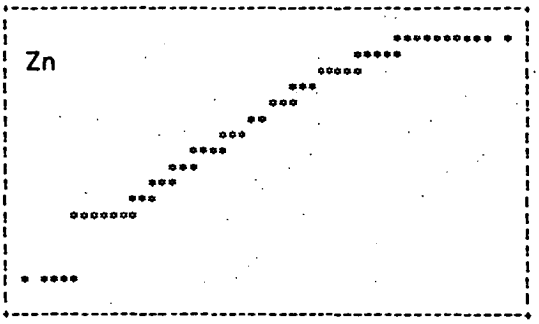

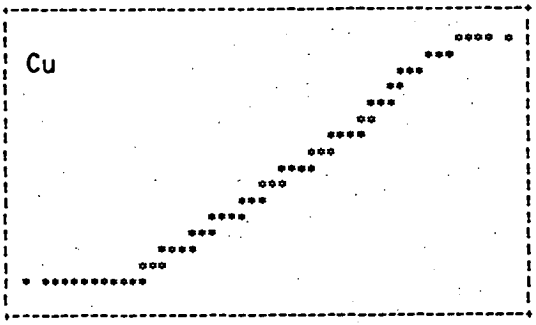

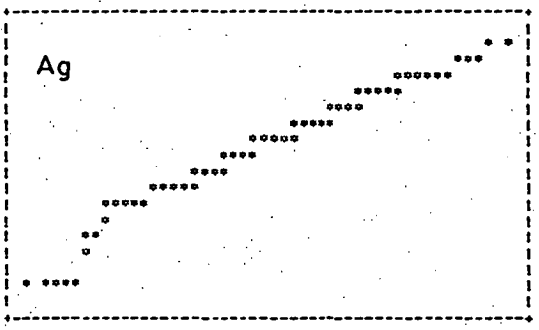

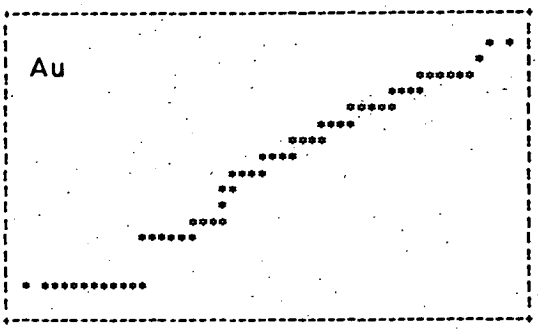

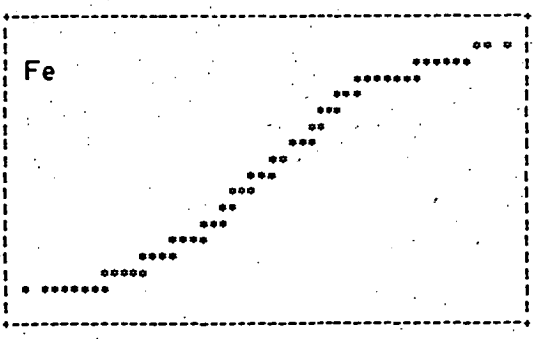

APPENDIX 4

Microprobe analyses

Chlorite: Averaged structure formulae

sample	type	Si	Ti	Al	Fe	Fe^{3+}	Fe^{2+}	Mn	Mg	Ca	Na	K	Fe^{2+}/R^{2+}	Mg/E	Struct.
67988	m, s	5.37	-	5.53	4.81	0.01	4.80	0.28	3.79	-	0.10	0.06	0.54	44.07	19.94
	n = 4, s:	0.21	-	0.15	0.35			0.03	0.31	-	0.02	0.12		0.36	0.21
67955	f, m	5.10	-	5.82	6.45	0.01	6.44	0.08	2.46	-	0.15	-	0.72	27.58	20.06
	n = 8, s:	0.05	-	0.09	0.08			0.01	0.09	-	0.09	-		0.97	0.05
67956	f, m	5.20	-	5.81	6.19	0.01	6.18	0.09	2.52	0.01	0.10	0.04	0.70	28.92	19.97
	n = 13, s:	0.16	-	0.11	0.26			0.02	0.16	0.02	0.10	0.10		1.28	0.15
67919	m	5.24	-	5.81	3.54	0.00	3.54	0.08	5.16	-	0.02	0.03	0.40	59.28	19.88
	n = 4, s:	0.09	-	0.05	0.16		0.02	0.14	-	0.04	0.05		1.04	0.08	
67913	m,v	5.28	-	5.69	6.11	0.00	6.11	0.18	2.58	0.02	0.03	-	0.69	29.68	19.89
	n = 7, s:	0.14	-	0.38	0.33		0.01	0.12	0.04	0.06	-		1.37	0.06	
"	v	5.42	-	6.04	7.00	0.00	7.00	0.05	1.05	-	-	-	0.86	13.07	19.56
	n = 1	-	-	-	-			-	-	-	-	-		-	-
67817	f	5.26	0.04	5.61	4.54	0.03	4.54	0.15	4.31	-	-	-	0.50	48.71	19.90
	n = 1	-	-	-	-			-	-	-	-	-		-	-
67954	m, s	5.32	0.01	5.86	6.59	0.07	6.52	0.31	1.56	-	-	0.11	0.78	19.14	19.77
	n = 4, s:	0.25	0.02	0.06	0.50		0.03	0.11	-	-	0.16		0.28	0.19	
67917	m, f	5.40	-	5.52	5.92	0.00	5.92	0.18	2.79	0.02	-	0.02	0.67	32.01	19.85
	n = 9, s:	0.11	-	0.09	0.16			0.01	0.07	0.03	-	0.05		0.72	0.07
"	m	5.77	0.02	5.62	6.90	0.04	6.90	0.00	1.04	0.02	-	0.10	0.87	13.07	19.46
	n = 2, s:	0.20	0.01	0.09	0.35			0.00	0.00	0.03	-	0.14		0.61	0.11
67916	m	5.40	-	5.59	6.11	0.01	6.10	0.19	2.46	0.04	-	0.02	0.70	28.68	19.81
	n = 4, s:	0.14	-	0.10	0.33			0.01	0.13	0.08	-	0.05		0.53	0.14
67817	m	5.21	0.01	5.65	6.63	0.01	6.62	0.24	2.21	-	-	-	0.73	25.03	19.95
	n = 6, s:	0.08	0.01	0.07	0.17			0.01	0.08	-	-	-		1.16	0.06
67891	m	6.22	0.01	5.22	3.92	0.01	3.91	0.16	3.53	0.04	0.02	0.09	0.51	47.39	19.22
	n = 5, s:	0.11	0.01	0.09	0.11			0.01	0.15	0.02	0.04	0.03		0.87	0.10
68000	m	5.18	-	5.77	5.40	0.03	5.40	0.52	3.08	-	-	-	0.60	36.29	19.94
	n = 6, s:	0.06	-	0.08	0.10			0.02	0.08	-	-	-		0.90	0.04
67804	m	5.46	-	5.47	6.20	0.01	6.19	0.21	2.42	-	-	0.08	0.70	28.09	19.84
	n = 6	0.26	-	0.17	0.32			0.02	0.14	-	-	0.07		0.76	0.21
67832	m	6.71	0.03	5.0	3.67	3.67	0.01	3.67	0.91	3.09	-	-	0.10	0.53	18.76
	n = 1	-	-	-	-	-	-	-	-	-	-	-	-	-	-
67818	f, m	5.46	-	5.03	4.80	0.01	4.79	0.10	4.63	-	-	-	0.50	49.08	20.02
	n = 2, s:	0.02	-	0.02	0.05			0.01	0.02	-	-	-		0.37	0.01
67912	cb	5.30	-	5.52	5.77	0.02	5.77	0.11	3.25	-	-	-	0.63	36.04	19.94
	n = 1	-	-	-	-		-	-	-	-	-		-	-	
67922	m	5.11	0.03	5.91	6.71	0.03	6.71	0.37	1.75	-	0.08	-	0.76	20.67	19.95
	n = 4, s:	0.04	0.02	0.11	0.09			0.01	0.04	-	0.06	-		0.31	0.07
68019	m	5.12	0.01	5.86	6.30	0.02	6.30	0.40	2.25	-	0.02	-	0.70	26.36	19.96
	n = 6, s:	0.04	0.01	0.07	0.04			0.02	0.04	-	0.05	-		0.42	0.02
68018	m	5.12	0.01	5.93	6.80	0.01	6.80	0.37	1.68	-	-	-	0.77	19.85	19.91
	n = 4, s:	0.07	0.02	0.14	0.10			0.02	0.12	-	-	-		1.38	0.02
68040	m	5.26	-	5.74	5.62	0.04	5.58	0.22	3.00	-	-	0.02	0.63	34.80	19.87
	n = 6, s:	0.05	-	0.04	0.12			0.01	0.22	-	-	0.05		2.04	0.04
67827	m, cb-v	5.49	-	5.08	4.51	0.00	4.51	0.12	4.77	-	-	-	0.48	51.41	19.97
	n = 4, s:	0.07	-	0.10	0.10			0.01	0.12	-	-	-		1.10	0.03
67826	m	5.59	-	5.07	5.71	0.03	5.71	0.10	33.9	0.03	-	-	0.62	37.21	19.88
	n = 3, s:	0.13	-	0.10	0.06			0.02	0.22	0.04	-	-		1.76	0.08
67805	m	5.10	-	5.69	6.81	0.06	6.75	0.30	2.12	-	-	0.01	0.74	23.73	20.05
	n = 8	0.06	-	0.08	0.16			0.03	0.08	-	-	0.02		0.87	0.07

68039	m	5.44	-	5.74	4.07	0.01	4.06	0.20	4.14	-	0.01	0.18	0.48	50.45	19.79
	n = 8, s:	0.26	-	0.13	0.40			0.02	0.40	-	0.02	0.22		0.55	0.21
67872	f	5.83	-	6.13	5.15	0.01	5.14	0.17	1.81	-	-	0.02	0.72	26.00	19.11
	n = 1	-	-	-	-			-	-	-	-	-		-	-
67904	m	5.46	0.03	5.02	4.74	0.03	4.74	4.60	0.09	0.06	-	-	0.50	49.30	20.00
	n = 4, s:	0.12	0.06	0.10	0.15			0.10	0.01	0.08	-	-		0.98	0.10
67874	m	5.36	0.02	5.24	5.23	0.04	5.23	4.19	0.00	-	-	-	0.56	44.45	20.03
	n = 2, s:	0.05	0.02	0.00	0.04		0.03	0.00	-	-	-		0.07	0.04	
106693	m	5.35	-	5.27	3.46	0.01	3.46	5.46	0.48	-	-	-	0.37	61.3	20.01
	n = 2, s:	0.03	-	0.06	0.25			0.10	0.00	-	-	-		2.12	0.06
106712	m, v	5.08	-	5.79	6.93	0.03	3.46	2.03	0.21	-	-	-	0.76	22.63	20.03
	n = 4, s:	0.03	-	0.04	0.07	0.03	6.93	0.08	0.01	-	-	-	0.76	0.87	0.01

Mica: Averaged structure formulae

Sample	Type	Si	Ti	Al	Fe	Fe^{3+}	Fe^{2+}	Mn	Mg	Ca	Na	K	Mg/E	Struct.
						Phengite								
67988*	a	6.77	0.10	4.39	0.36	0.00	0.36	-	0.64	-	0.16	1.14	63.54	13.57
	n = 3, s:	0.20	0.67	0.45	0.20	-	-	-	0.38	-	0.07	0.25	4.47	0.17
67955	d	6.66	0.01	4.89	0.21	0.00	0.21	-	0.22	-	0.03	1.66	50.42	13.78
	n = 2, s:	0.30	0.02	0.24	0.08	-	-	-	0.11	-	0.00	0.15	2.96	0.27
67956	c	6.46	0.04	5.09	0.18	0.00	0.18	-	0.20	-	0.23	1.74	52.41	13.94
	n = 2, s:	0.20	0.00	0.22	0.01	-	-	-	0.01	-	0.02	0.07	0.37	0.13
67913	d	6.79	0.03	4.59	0.32	-0.03	0.32	-	0.28	0.02	0.12	1.62	46.60	13.76
	n = 2, s:	0.09	0.01	0.18	0.07	-	-	-	0.06	0.02	0.18	0.12	0.69	0.04
68042	a	6.37	0.12	4.83	0.21	-0.10	0.21	0.01	0.45	-	0.53	1.78	67.55	14.19
	n = 4, s:	0.17	0.02	0.05	0.02	-	-	0.02	0.02	-	0.78	0.06	1.21	0.56
67954*	b	6.47	0.16	4.84	0.40	0.03	0.37	-	0.17	-	-	1.74	30.14	13.80
	n = 3, s:	0.39	0.12	0.25	0.09	-	-	-	0.01	-	-	0.09	3.58	0.17
67917	c	6.50	0.03	4.90	0.34	0.01	0.33	-	0.32	0.02	-	1.81	49.14	13.93
	n = 7, s:	0.13	0.00	0.16	0.05	-	-	-	0.02	0.04	-	0.05	3.59	0.06
67891	d	6.45	-	5.27	0.22	0.00	0.22	-	0.06	-	0.15	1.68	19.71	13.83
	n = 1	-	-	-	-	-	-	-	-	-	-	-	-	-
67919	a	6.11	0.02	5.85	0.02	-0.02	0.02	-	0.00	0.01	1.34	0.55	0.00	13.89
	n = 4, s:	0.05	0.02	0.02	0.02	-	-	-	0.00	0.02	0.04	0.05	0.00	0.06
"	a	6.27	0.09	5.43	0.11	0.00	0.11	-	0.16	0.01	0.25	1.46	61.60	13.78
	n = 12, s:	0.18	0.08	0.19	0.09	-	-	-	0.10	0.02	0.14	0.13	6.86	0.12
68000	a	6.15	0.06	5.23	0.54	-0.03	0.54	0.03	0.37	-	0.01	1.61	42.82	13.99
	n = 6, s:	0.21	0.01	0.05	0.33	-	-	0.03	0.14	-	0.03	0.14	7.37	0.14
67804	c	6.50	0.03	4.83	0.59	0.03	0.56	-	0.21	-	-	1.76	26.09	13.93
	n = 3, s:	0.09	0.00	0.02	0.12	-	-	-	0.04	-	-	0.06	1.37	0.06
67832	d	7.34	0.03	3.72	0.38	0.01	0.37	-	0.25	-	-	2.09	39.78	13.82
	n = 1,	-	-	-	-	-	-	-	-	-	-	-	-	-
67833	c	6.60	0.05	4.35	0.39	0.02	0.37	-	0.83	-	-	1.74	68.22	13.99
	n = 1	-	-	-	-	-	-	-	-	-	-	-	-	-
67837	c	6.38	0.04	5.25	0.14	0.00	0.14	-	0.23	-	-	1.83	62.11	13.87
	n = 6, s:	0.03	0.01	0.04	0.03	-	-	-	0.02	-	-	0.02	3.93	0.02
67822	d	6.53	0.07	4.77	0.37	0.00	0.37	-	0.36	-	0.04	1.79	49.48	13.94
	n = 3, s:	0.10	0.02	0.07	0.04	-	-	-	0.01	-	0.07	0.08	3.53	0.04
67818	d	1.63	0.02	0.34	0.57	-0.03	0.57	-	0.46	0.23	4.16	6.73	44.33	14.13
	n = 2, s:	0.27	0.02	0.19	0.05	-	-	-	0.00	0.28	0.22	0.17	2.29	0.17
68035	a	6.14	0.14	5.46	0.09	-0.02	0.09	-	0.35	-	0.21	1.43	79.0	13.81
	n =1,	-	-	-	-	-	-	-	-	-	-	-	-	-
68043	a	6.56	0.09	4.63	0.11	0.01	0.10	-	0.74	-	-	1.80	87.12	13.94
	n = 1	-	-	-	-	-	-	-	-	-	-	-	-	-
67912	d	6.72	0.03	4.54	0.39	0.00	0.39	-	0.31	-	0.30	1.68	43.99	13.98
	n = 2, s:	0.30	0.01	0.32	0.08	-	-	-	0.09	-	0.43	0.27	2.45	0.05
106728	a	5.67	0.14	5.21	0.26	-0.03	0.26	0.11	0.99	0.18	0.59	1.24	77.47	14.44
	n = 2, s:	0.10	0.01	0.55	0.05	-	-	0.04	0.58	0.06	0.00	0.08	7.12	0.11
68009	a	6.05	0.30	5.47	0.04	0.01	0.03	0.03	0.21	0.02	0.07	1.50	82.41	13.70
	n = 3, s:	0.06	0.04	0.04	0.01	-	-	0.00	0.02	0.03	0.00	0.02	5.93	0.03
68032	a	6.25	0.13	5.32	0.17	-0.02	0.17	-	0.20	-	0.07	1.73	55.01	13.87
	n = 1	-	-	-	-	-	-	-	-	-	-	-	-	-

Sample	Type	Si	Ti	Al	Fe	Fe^{3+}	Fe^{2+}	Mn	Mg	Ca	Na	K	Mg/Σ	Struct.
67824	d	6.64	0.03	4.51	0.45	-0.01	0.45	-	0.34	0.18	-	1.86	74.59	14.01
	n = 1	-	-	-	-	-	-	-	-	-	-	-	-	-
67826	d	6.47	-	4.61	0.81	0.00	0.81	-	0.48	0.02	-	1.67	40.44	14.05
	n = 2, s:	0.24	-	0.27	0.68	-	-	-	0.27	0.02	-	0.17	8.96	0.29
68045	a	6.61	0.08	4.86	0.11	-0.03	0.11	-	0.38	-	-	1.71	76.84	13.74
	n = 2, s:	0.22	0.00	0.20	0.00	-	-	-	0.08	-	-	0.09	3.18	0.16
67880	c	6.69	0.03	4.50	0.30	0.01	0.29	-	0.63	0.03	-	1.69	67.49	13.87
	n = 1	-	-	-	-	-	-	-	-	-	-	-	-	-
67901*	c	5.90	0.02	5.34	1.31	0.05	1.26	-	0.18	0.01	-	1.24	12.49	14.06
	n = 4	0.22	0.00	0.03	0.48	-	-	-	0.01	0.01	-	0.19	3.00	0.13
67878	d	6.90	0.03	4.45	0.29	0.02	0.27	-	0.15	0.06	0.69	1.16	37.13	13.77
	n = 6, s:	0.46	0.04	0.60	0.23	-	-	-	0.16	0.05	0.70	0.46	6.30	0.19
67880*	c	6.39	0.03	5.10	0.20	0.10	0.10	0.01	0.52	-	0.07	1.39	72.32	13.72
	n = 3, s:	0.54	0.01	0.59	0.06	-	-	0.01	0.16	-	0.02	0.28	1.86	0.42
67867	d	6.36	0.04	4.55	1.06	-0.01	1.06	-	0.41	0.01	-	1.80	27.96	14.23
	n = 2, s:	0.02	0.00	0.04	0.05	-	-	-	0.02	0.01	-	0.01	0.20	0.04
67885	c	7.10	0.10	3.27	0.69	-0.01	0.69	-	0.97	0.03	-	2.02	56.74	14.18
	n = 2, s:	0.00	0.06	0.75	0.35	-	-	-	0.67	0.01	-	0.05	5.38	0.30
67897	c	7.06	0.07	3.67	0.76	-0.01	0.76	0.01	0.55	0.02	0.01	1.76	41.80	13.92
	n = 3, s:	0.70	0.02	0.67	0.26	-	-	0.01	0.22	0.00	0.02	0.30	1.44	0.44
67795	d	7.26	-	4.08	0.09	0.02	0.07	-	0.17	-	1.46	0.72	65.56	13.79
	n = 1	-	-	-	-	-	-	-	-	-	-	-	-	-
"	d	6.68	-	4.75	0.25	0.00	0.25	-	0.38	-	-	1.77	60.20	13.83
	n = 2, s:	0.15	-	0.14	0.02	-	-	-	0.01	-	-	0.10	1.39	0.13
106716	a	6.35	0.04	5.22	0.27	-0.01	0.27	-	0.24	-	-	1.75	18.05	13.87
	n = 2, s:	0.05	0.00	0.05	0.12	-	-	-	0.04	-	-	0.02	6.44	0.08
						Biotite								
106693	a	6.14	0.26	1.93	0.00	0.00	0.00	-	15.51	-	-	1.59	00.00	15.43
	n = 2, s:	0.04	0.03	0.02	0.00	-	-	-	0.03	-	-	0.02	0.00	0.00
67833	c	5.88	0.08	2.53	1.33	-0.01	1.33	-	4.06	-	-	1.80	75.29	15.68
	n = 2, s:	0.03	0.00	0.03	0.10	-	-	-	0.05	-	-	0.06	1.62	0.01
67885	c	6.10	0.17	2.71	1.62	0.03	1.59	0.03	2.75	0.02	0.01	1.91	63.01	15.33
	n = 6, s:	0.50	0.04	0.10	0.44	-	-	0.02	0.69	0.01	0.02	0.14	1.45	0.45
67897*	c	5.59	0.19	3.14	2.83	0.01	2.83	0.03	1.94	0.01	-	1.83	40.67	15.58
	n = 6, s:	0.20	0.02	0.32	0.45	-	-	0.02	0.32	0.01	-	0.09	0.70	0.32
						Clay								
67817*	d	6.44	0.63	2.07	4.08	-0.01	4.18	0.23	0.00	0.06	0.28	0.21	0.00	14.12
	n = 1	-	-	-	-			-	-	-	-	-	-	-
67954	b	4.66	0.03	4.75	4.09	-0.03	4.09	0.19	0.98	-	-	0.50	19.32	15.19
	n = 1	-	-	-	-			-	-	-	-	-	-	-
67818	d	5.84	-	3.49	2.44	-0.01	2.44	0.03	2.22	0.04	0.28	0.44	47.63	14.78
	n = 1	-	-	-	-			-	-	-	-	-	-	-
68043	a	5.45	0.08	3.99	0.49	-0.03	0.49	0.13	3.27	0.60	-	0.96	87.11	14.96
	n = 2, s:	0.11	0.05	0.03	0.13			0.04	0.85	0.42	-	0.26	00.08	00.06
67912	d	5.46	0.03	4.0	2.94	0.02	2.92	0.04	1.60	-	0.25	0.61	35.17	14.94
	n = 2, s:	0.20	0.01	0.36	0.15			0.01	0.08	-	0.09	0.04	02.31	00.04

Key:
a = host rock
b = immediate footwall (underground)
c = altered hanging wall and surface alteration
d = unaltered volcanics
v = vein
* = minute amounts of P, Cl, S, Cr, not listed
n = number of analyses
s = standard deviation

$Mg/\Sigma = Mg/Mg + Fe^{2+} + Fe^{3+}$

$Fe^{2+}/R^{2+} = Fe^{2+}/Fe^{2+} + Mg + Mn$

Struct. = cations per structure formula

Averaged feldspars-oxide % normalized to 100%

Section	Type	Si	Ti	Al	Fe	Mg	Ca	Na	K	Others	Na/K/Ca	Struct.
67982	f	64.05	0.63	18.98	-	0.12	0.21	0.32	15.66	Cr 0.05	3.0/95.9/1.1	4.98
	n = 2, s:	0.16	0.31	0.21		0.04	0.08	0.07	0.25	Cr 0.06		0.01
67797	c	68.25	-	20.12	-	-	0.08	11.23	0.23	Cl 0.08	98.3/1.3/0.4	4.99
	n = 1	-	-	-	-	-	-	-	-			-
67847	f	66.99	-	17.65	-	-	-	-	15.36		0.0/100.0/0.0	4.91
	n = 1	-	-	-	-	-	-	-	-			-
	f	68.20	-	20.45	-	-	0.56	10.69	0.10		96.6/0.6/2.8	4.96
	n = 1	-	-	-	-	-	-	-	-			-
	v	68.40	-	20.34	-	-	0.47	10.06	0.72		93.2/4.4/2.4	4.94
	n = 1	-	-	-	-	-	-	-	-			-
	v	65.99	-	18.21	-	-	-	-	15.81		0.0/100.0/0.0	4.94
	n = 2, s:	1.13	-	0.75	-	-	-	-	0.37			0.03
	r	68.73	-	16.83	-	-	-	-	14.44		0.0/100.0/0.0	4.85
	n = 1	-	-	-	-	-	-	-	-			-
67874	l	68.29	-	20.24	-	-	0.66	10.81	-		96.7/0.0/3.3	4.96
	n = 1	-	-	-	-	-	-	-	-			-
	c	68.85	-	19.95	-	-	0.17	10.87	0.16		98.2/1.0/0.8	4.95
	n = 1	-	-	-	-	-	-	-	-			-
106707	f	68.59	-	20.14	-	-	0.32	10.85	0.09		97.9/0.5/1.6	4.96
	n = 1	-	-	-	-	-	-	-	-			-
67951	c	62.58	-	24.74	0.21	-	1.24	8.68	2.55		78.6/15.2/6.2	5.02
	n = 1	-	-	-	-	-	-	-	-			-
67951	c	66.74	-	20.15	-	-	1.21	11.69	0.21		93.5/1.1/5.4	5.05
	n = 1	-	-	-	-	-	-	-	-			-
	c	60.40	0.05	24.70	0.10	-	5.69	8.24	0.83		69.1/4.6/26.4	5.03
	n = 5, s:	0.55	0.12	0.32	0.13	-	1.33	0.32	0.79			0.01
	c	58.72	-	25.62	0.12	-	7.69	7.39	0.47		61.8/2.6/35.6	5.03
	n = 10, s:	0.80	-	0.51	0.16	-	0.58	0.46	0.09			0.01
67912	c	69.28	-	19.18	-	-	-	11.54	-		100.0/0.0/0.0	4.98
	n = 1	-	-	-	-	-	-	-	-			-
	v	67.67	-	17.15	-	-	-	-	15.18		0.0/100.0/0.0	4.89
	n = 1	-	-	-	-	-	-	-	-			-
67955	c	67.38	-	19.96	0.05	0.09	0.79	11.69	0.03		96.2/0.2/3.6	5.03
	n = 6, s:	0.73	-	0.56	0.12	0.14	0.50	0.37	0.08			0.02
	c	63.06	0.36	23.20	-	-	1.66	9.49	2.23		79.9/12.4/7.7	5.06
	n = 1	-	-	-	-	-	-	-	-			-
	c	63.58	-	22.51	0.18	0.05	3.47	9.89	0.33		82.2/1.8/16.0	5.03
	n = 5, s:	2.50	-	1.52	0.41	0.10	1.74	1.05	0.26			0.01
67913	v	66.99	0.14	17.48	-	-	-	-	15.39		0.0/100.0/0.0	4.91
	n = 5, s:	0.70	0.31	0.40	-	-	-	-	0.23			0.01
	f	68.15	-	16.99	-	-	-	-	14.86		0.0/100.0/0.0	4.88
	n = 3, s:	0.34	-	0.30	-	-	-	-	0.04			0.01
	v	67.60	-	20.25	0.54	-	0.73	10.89	-		96.4/0.0/3.6	4.98
	n = 2, s:	0.36	-	0.42	0.76	-	0.04	0.04	-			0.01
	f	67.34	-	20.76	0.21	0.21	0.63	10.06	0.79		92.0/4.8/3.2	4.97
	n = 2, s:	1.17	-	0.89	0.30	0.30	0.28	0.76	0.16			0.01
67913	c	67.17	-	20.79	0.09	-	1.09	10.57	0.29		93.0/1.7/5.3	4.98
	n = 4, s:	1.34	-	1.01	0.18	-	0.60	0.76	0.58			0.00
67817	c	68.36	-	19.83	0.03	-	0.45	11.23	0.10		97.3/0.6/2.1	4.98
	n = 7, s:	0.52	-	0.38	0.09	-	0.30	0.19	0.18			0.01
68040	f	69.42	-	19.52	-	-	-	11.06	-		100.0/0.0/0.0	4.95
	n = 5, s:	0.27	-	0.14	-	-	-	0.30	-			0.02
106693	f	62.96	-	19.35	-	-	-	11.38	-		100.0/0.0/0.0	4.97
	n = 3, s:	0.51	-	0.11	-	-	-	0.41	-			0.03

Section	Type	Si	Ti	Al	Fe	Mg	Ca	Na	K	Others	Na/K/Ca	Struct.
67917	c	65.61	2.49	18.76	-	-	2.63	10.50	-		87.8/0.0/12.2	4.98
	n = 1	-	-	-	-	-	-	-	-			-
	c	60.08	-	26.10	1.23	0.55	1.29	6.10	4.64		61.8/31.0/7.2	5.01
	n = 1	-	-	-	-	-	-	-	-			-
	c	67.25	-	20.68	-	-	1.53	10.55	-		92.6/0.0/7.4	4.97
	n = 2, s:	0.49	-	0.11	-	-	0.36	0.02	-			0.01
	f	68.35	-	19.86	-	-	0.45	11.08	0.18	P 0.07	96.8/1.0/2.2	4.98
	n = 5, s:	0.36	-	0.21	-	-	0.13	0.27	0.29	P 0.16		0.01
	f	66.77	0.32	17.75	-	-	-	0.06	15.08		0.6/99.4/0.0	4.90
	n = 7, s:	0.41	0.37	0.23	-	-	-	0.15	0.38			0.01
	r	68.23	-	16.98	-	-	-	-	14.79		0.0/100.0/0.0	4.87
	n = 1	-	-	-	-	-	-	-	-			-
67916	c	64.14	-	18.33	-	-	7.15	10.38	-		72.4/0.0/27.6	5.09
	n = 1	-	-	-	-	-	-	-	-			-
	f	67.87	-	20.34	-	-	0.92	10.87	-		95.5/0.0/4.5	4.97
	n = 1	-	-	-	-	-	-	-	-			-
67916	c	60.53	-	25.78	1.22	0.34	1.25	6.52	4.38		64.6/28.6/6.8	5.02
	n = 2	2.90	-	2.76	0.39	0.06	0.42	1.77	1.90			0.01
67891	f	65.08	-	18.71	-	-	-	0.36	15.20		3.5/96.5/0.0	4.94
	n = 1	-	-	-	-	-	-	-	-			-
67832	c	64.64	-	21.40	0.62	0.29	0.74	7.74	4.47	P 0.11	69.8/26.5/3.7	5.01
	n = 2, s:	2.18	-	2.18	0.88	0.41	0.04	0.92	2.31	P 0.15		0.01
	c	67.60	-	20.33	0.33	-	0.65	10.04	1.06		90.5/6.3/3.2	4.96
	n = 3, s:	0.46	-	1.64	0.05	-	0.29	0.43	0.47		0.02	
67822	c	66.21	-	22.18	0.31	-	-	9.77	1.53		90.7/9.3/0.0	4.98
	n = 1	-	-	-	-	-	-	-	-			-
	c	64.21	0.07	19.83	0.39	0.09	4.45	10.33	0.54	Mn 0.09	78.6/2.7/18.7	5.07
	n = 3, s:	1.73	0.12	1.51	0.34	0.16	3.10	0.68	0.94	Mn 0.16		0.07
67824	p	69.20	-	19.85	-	-	-	10.80	0.15		99.1/0.9/0.0	4.94
	n = 1	-	-	-	-	-	-	-	-			-
	p	67.38	-	17.58	-	-	-	0.11	14.93		1.1/98.9/0.0	4.90
	n = 3, s:	0.81	-	0.35	-	-	-	0.18	0.64			0.03
	c	68.99	-	19.82	-	-	0.08	11.00	0.11		99.0/0.6/0.4	4.96
	n = 4, s:	0.24	-	0.18	-	-	0.10	0.16	0.14			0.01
	c	66.02	-	18.80	-	-	-	2.53	12.65		23.3/76.7/0.0	4.97
	n = 1	-	-	-	-	-	-	-	-			-
	c	65.63	-	18.54	-	-	-	-	15.83		0.0/100.0/0.0	4.95
	n = 1	-	-	-	-	-	-	-	-			-
67881	c	64.42	0.42	18.82	-	0.11	0.26	0.23	15.70	Cl 0.05	2.2/96.5/1.3	4.98
	n = 5, s:	0.51	0.23	0.17	-	0.07	0.05	0.10	0.29	Cl 0.05		0.02
67878	r	66.00	0.15	18.04	-	0.03	0.27	0.18	15.33		1.7/96.9/1.4	4.93
	n = 8, s:	0.82	0.24	0.42	-	0.07	0.03	0.10	0.17			0.02
	r	68.31	-	20.30	-	-	0.08	11.12	0.18		98.6/1.0/0.4	4.98
	n = 1	-	-	-	-	-	-	-	-			-
	f	63.60	1.03	19.66	-	-	0.25	0.40	15.06		3.8/94.9/1.3	4.96
	n = 1	-	-	-	-	-	-	-	-			-
	c	64.26	-	23.28	0.50	0.18	1.02	8.93	1.83		83.5/11.2/5.3	4.99
	n = 1	-	-	-	-	-	-	-	-			-
	c	65.47	-	22.13	-	-	2.23	9.92	0.25		87.7/1.4/10.9	4.98
	n = 1	-	-	-	-	-	-	-	-			-
	c	65.23	-	22.33	0.22	0.13	1.15	9.56	1.29	Cl 0.09	86.6/7.7/5.7	5.00
	n = 1	-	-	-	-	-	-	-	-	-		-
	f	67.33	-	20.66	-	0.06	0.63	11.02	0.22	Cl 0.09	95.7/1.3/3.0	5.00
	n = 2, s:	0.32	-	0.16	-	0.07	0.04	0.01	0.05	Cl 0.00		0.01
	f	65.28	0.23	18.28	-	0.13	0.28	0.32	15.34	Cr 0.11 Cl 0.04	3.0/95.5/1.5	4.96
	n = 2, s:	0.81	0.00	0.27	-	0.01	0.08	0.13	0.66			0.03
67883	c	64.75	0.12	18.90	-	0.08	0.30	0.21	15.61	Cl 0.02	2.0/96.5/1.5	4.97
	n = 4, s:	0.39	0.17	0.14	-	0.06	0.02	0.18	0.08	Cl 0.04		0.01

Section	Type	Si	Ti	Al	Fe	Mg	Ca	Na	K	Others	Na/K/Ca	Struct.
67885	c	64.09	0.73	18.96	0.03	0.05	0.27	0.15	15.59	Cr 0.09 Mn 0.02	1.4/97.2/1.4	4.97
	n = 5, s:	0.59	0.51	0.25	0.07	0.07	0.06	0.09	0.27	Cr 0.05 Mn 0.05		0.01
67867	c	66.80	-	20.81	0.47	0.07	0.27	10.50	0.96		93.1/5.6/1.3	5.00
	n = 4, s:	0.80	-	0.22	0.42	0.09	0.12	0.37	0.47			0.02
67818	c	67.49	-	20.47	-	-	1.25	10.79	-		94.0/0.0/6.0	4.98
	n = 1	-	-	-	-	-	-	-	-			-
67818	f	68.74	-	19.93	0.25	-	0.21	10.58	0.29		97.2/1.7/1.1	4.95
	n = 1	-	-	-	-	-	-	-	-			-
68032	c	67.02	-	20.75	-	-	1.54	10.70	-		92.6/0.0/7.4	4.99
	n = 2, s:	0.11	-	0.21	-	-	0.18	0.29	-			0.01
67933	c	64.20	-	22.26	0.68	0.19	0.52	7.39	4.77		68.3/29.0/2.7	5.01
	n = 2, s:	2.72	-	2.87	0.64	0.27	0.16	0.40	1.30			0.02
	c	66.56	-	20.89	0.11	-	1.14	10.58	0.61	P 0.12	91.1/3.5/5.4	5.00
	n = 2, s:	0.28	-	0.50	0.16	-	0.28	0.10	0.08	P 0.16		0.00
67938	c	62.23	-	18.17	-	-	8.43	10.96	-		70.2/0.0/29.8	5.17
	n = 1	-	-	-	-	-	-	-	-			-
67827	c	67.60	-	20.31	-	-	1.14	10.96	-		94.6/0.0/5.4	4.99
	n = 2, s:	0.23	-	0.18	-	-	0.14	0.19	-			0.01
67826	c	67.15	-	20.07	-	-	0.82	9.23	2.73		80.4/15.7/3.9	4.99
	n = 1	-	-	-	-	-	-	-	-			-
	c	67.79	-	20.33	-	-	0.90	10.85	0.12		95.0/0.7/4.3	4.98
	n = 5, s:	0.27	-	0.23	-	-	0.16	0.42	0.11			-
	f	65.62	-	18.40	-	-	-	1.25	14.72		11.4/88.6/0.0	4.98
	n = 1	-	-	-	-	-	-	-	-			-
	f	68.53	-	20.06	-	-	0.68	10.73	-		96.0/0.0/3.4	4.95
	n = 1	-	-	-	-	-	-	-	-			-
	f	65.91	-	18.31	-	-	-	0.17	15.61		1.6/98.4/0.0	4.5
	n = 2, s:	1.00	-	0.57	-	-	-	0.24	0.68			0.02

Key:
c = coarse primary feldspar
f = fresh, small-medium grained feldspar, occasionally clear fields in coarse grained feldspar
l = lath
r = clear rim around coarse altered feldspar
p = perthite
n = number of analyses
s = standard deviation

Struct. = cations per structure formula

Carbonate: Averaged wt% and mol ratios normalized to 100%

Sample	Type	FeO	MnO	MgO	CaO	Ca	Mg	Mn	Ca	Fe	Mn
67988	a	0.39	1.77	-	97.84	98.6	0.0	1.4	98.3	0.3	1.4
	n = 5, s:	0.22	0.43	-	0.34						
67955	d	0.88	1.29	-	97.83	99.0	0.0	1.0	98.3	0.7	1.0
	n = 1	-	-	-	-						
67956	c	0.67	1.40	-	97.93	98.9	0.0	1.1	98.4	0.5	1.1
	n = 3, s:	0.13	0.13	-	0.16						
67919	a	0.68	1.91	-	97.40	98.5	0.0	1.5	97.9	0.5	1.5
	n = 1	-	-	-	-						
67913	d	1.92	2.52	-	95.56	98.0	0.0	2.0	96.5	1.5	2.0
	n = 4, s:	1.52	1.11	-	1.33						
68032	a,nd	7.08	89.66	-	3.25	4.4	0.0	95.6	4.1	6.9	89.0
	n = 13, s:	1.66	3.86	-	2.41						
"	a	5.43	46.93	2.65	44.99	52.4	4.3	43.3	52.1	4.9	43.0
	n = 3, s:	1.22	2.27	0.55	0.99						
106722	a	-	9.57	-	90.43	92.3	0.0	7.7	92.3	0.0	7.7
	n =3, s:	-	0.78	-	0.78						
106727	a	0.47	6.26	-	93.27	95.0	0.0	5.0	94.6	0.4	5.0
	n = 3	0.06	0.99	-	1.06						
106693	a	-	14.97	23.59	61.44	57.9	30.9	11.2	83.8	0.0	16.2
	n = 1	-	-	-	-						
"	a	-	5.46	-	94.54	95.6	0.0	4.4	95.6	0.0	4.4
	n = 3, s:	-	2.29	-	2.28						
67917	c	0.36	1.20	-	98.43	99.0	0.0	1.0	98.8	0.3	1.0
	n = 2, s:	0.51	0.66	-	1.18						
68000	a	43.88	51.96	0.86	3.29	2.6	7.2	90.2	4.2	43.5	52.3
	n = 5, s:	1.86	2.00	0.53	1.11						
67837	c	50.28	36.91	10.20	2.61	30.9	5.7	63.5	3.7	55.2	41.1
	n = 1	-	-	-	-						
67822	d	87.96	5.53	6.51	0.00	0.0	67.4	32.6	0.0	94.0	6.0
	n = 1	-	-	-	-						
"	d	33.41	1.36	9.34	55.90	79.9	18.6	1.5	67.3	31.4	1.3
	n = 4, s:	2.22	0.13	0.86	2.55						
67818	d	0.46	0.85	-	98.69	99.3	0.0	0.7	99.0	0.4	0.7
	n = 1	-	-	-	-						
68035	a	-	4.12	-	95.88	96.7	0.0	3.3	96.7	0.0	3.3
	n = 1	-	-	-	-						
68034	a	-	1.50	-	98.50	98.8	0.0	1.2	98.8	0.0	1.2
	n = 1	-	-	-	-						
68043	a, nd	5.74	5.77	25.04	63.44	61.7	33.9	4.4	87.5	6.2	6.3
	n = 2, s:	0.13	0.88	0.32	1.37						
68044	a	1.12	14.82	25.02	59.04	55.9	33.0	11.1	82.4	1.2	16.4
	n = 2, s:	0.44	2.90	2.32	1.01						
67912	d	2.34	2.71	-	94.94	97.8	0.0	2.2	96.0	1.8	2.2
	n = 2, s:	1.36	1.26	-	2.64						
106728	a	0.84	23.89	-	75.28	79.9	0.0	20.1	79.4	0.7	19.9
	n = 2	0.55	5.57	-	6.11						

Sample	Type	FeO	MnO	MgO	CaO	Ca	Mg	Mn	Ca	Fe	Mn
67940	b	34.22	2.89	9.25	53.64	78.0	18.7	3.3	64.9	32.3	2.8
	n = 1	-	-	-	-						
67931	b	-	2.38	-	97.64	98.1	0.0	1.9	98.1	0.0	1.9
	n = 1	-	-	-	-						
68032	a, nd	44.06	55.94	-	-	0.0	0.0	100.0	0.0	43.7	56.3
	n = 4	5.69	5.68	-	-						
68040	a	50.34	40.89	6.26	2.51	5.8	20.0	74.2	3.4	53.0	43.6
	n = 2, s:	4.70	0.87	2.60	1.23						
67827	d	-	0.94	-	99.06	99.3	0.0	0.7	99.3	0.0	0.7
	n = 1	-	-	-	-						
68045	a, nd	5.12	16.57	24.46	53.85	53.3	33.7	13.0	75.9	5.6	18.5
	n = 3	1.13	1.12	0.84	1.01						
67874	d	1.77	3.66	0.73	93.84	96.0	1.0	3.0	95.6	1.4	3.0
	n = 2	0.35	0.33	0.01	0.69						
68047	a	66.91	7.06	24.61	1.42	3.4	83.0	13.5	2.4	88.2	9.4
	n = 1	-	-	-	-						
106707	a	7.13	44.27	5.72	42.88	49.9	9.3	40.8	51.4	6.7	42.0
	n = 2, s:	0.93	1.48	1.04	1.38						
106726	a	8.39	17.19	24.70	49.72	50.9	35.2	13.9	71.2	9.4	19.5
	n = 2, s:	1.41	0.80	2.52	0.31						

Key:
a = host rock
b = immediate footwall (underground)
c = altered hanging wall and surface alteration
d = unaltered volcanics
nd = nodule
n = number of analyses
s = standard deviation

Averaged epidote group-oxide % normalized to 100%

Sample	SiO_2	TiO_2	Al_2O_3	Cr_2O_5	FeO	MnO	MgO	CaO	Na_2O	K_2O	P_2O_5
67916	39.95	0.76	24.76	-	12.78	1.14	0.05	20.23	0.06	0.05	0.23
n = 5, s:	0.59	0.49	0.98	-	1.39	0.27	0.11	1.19	0.13	0.11	0.13
67832	40.02	0.43	24.47	0.17	12.65	0.88	0.17	20.75	0.10	0.09	0.27
n = 7, s:	0.91	0.42	1.22	0.45	1.94	0.54	0.37	3.37	0.25	0.16	0.20
67818	39.36	-	26.11	-	10.10	-	0.05	24.28	-	-	0.10
n = 5, s:	0.18	-	0.47	-	0.50	-	0.12	0.29	-	-	0.13
67827	39.49	-	26.55	-	9.42	0.19	-	24.28	-	-	0.07
n = 4, s:	0.13	-	1.69	-	1.77	0.32	-	0.20	-	-	0.12

Key:
n = number of analyses
s = standard deviation

Trace elements in pyrite.

Section	n	Averages and standard deviations (s) As	s	Zn	s	Section	n	Averages and standard deviations (s) As	s	Zn	s
67988	11	0.72	0.21	1.33	0.11	67950	2	0.64	0.01	1.39	0.11
67919	4	2.20	1.96	1.35	0.16	106693	11	0.93	0.65	1.40	0.11
67954	10	0.54	0.12	1.40	0.09	67916	4	0.71	0.27	1.42	0.14
68000	5	0.74	0.39	1.43	0.08	67837	3	0.77	0.04	1.41	0.06
68035	10	0.68	0.24	1.38	0.08	68043	10	1.05	0.66	1.39	0.10
106728	10	0.61	0.18	1.50	0.08	67922	10	0.65	0.08	1.65	0.10
68009	9	0.60	0.08	1.33	0.44	68032	9	0.75	0.27	1.58	0.10
68012	9	0.66	0.13	1.63	0.17	68018	2	0.56	0.21	1.46	0.06
67880	4	0.67	0.11	1.52	0.05	68023	10	0.79	0.31	1.38	0.25
68017	10	0.76	0.42	1.46	0.12	68022	4	0.23	0.43	1.63	0.10
67965	5	0.00	-	1.74	0.08	67987	12	0.32	0.34	1.65	0.07
67942	12	0.00	-	1.69	0.09	68014	13	0.14	0.26	1.61	0.10
68020	11	0.13	0.12	1.69	0.01	67952	10	0.39	0.12	1.47	0.07
67942	10	0.97	0.70	1.35	0.06	68037	9	0.63	0.20	1.42	0.08

Trace elements in sphalerite.

Section	n	Averages and standard deviations (s) Fe	s	Cu	s	As	s	Mn	s
68000	10	4.33	1.10	1.50	1.41	0.68	0.15	0.02	0.06
68032	1	5.38	-	0.00	-	0.88	-	0.00	-
68040	1	5.80	-	0.00	-	0.00	-	0.00	-
67883	5	9.10	0.44	0.09	0.07	0.67	0.15	0.06	0.09
68017	1	6.19	-	0.41	-	0.21	-	0.00	-
68022	1	7.36	-	2.60	-	0.69	-	0.00	-
68020	1	6.30	-	1.99	-	0.00	-	0.00	-

APPENDIX 5

Element exchange in 100g rocks for Volume coefficients f_v =1.0 - 1.2 with unaltered pyroclastics as reference rocks. Exchange in gram/10^{-4} gram for major/trace elements (wt) and percent (%) of unaltered pyroclastics

		Surface schists		Siliceous mine schists, underground		Sericitic mine schists, underground		Carbonaceous mine schists, underground		Massive siliceous rocks (surface)	
	f	wt	%	wt	%	wt	%	wt	%	wt	%
SiO_2	1.0	2.90	3.92	7.14	9.65	-2.23	-3.02	-11.68	-15.77	8.39	11.34
	1.1	10.59	14.31	15.26	20.61	4.94	6.68	-5.44	-7.35	16.63	22.47
	1.2	18.29	24.70	23.37	31.58	12.12	16.38	0.80	1.07	24.87	33.60
TiO_2	1.0	-0.09	-25.13	-0.16	-43.12	-0.08	-20.76	-0.05	-14.63	-0.31	-83.28
	1.1	-0.07	-17.64	-0.14	-37.43	-0.05	-12.83	-0.02	-6.09	-0.30	-81.61
	1.2	-0.04	-10.16	-0.12	-31.74	-0.02	-4.91	0.01	2.45	-0.30	-79.94
Al_2O_3	1.0	-0.86	-6.07	-3.26	-23.10	1.63	11.56	-0.39	-2.76	-2.30	-16.31
	1.1	0.47	3.32	-2.18	-15.41	3.21	22.71	0.98	6.97	-1.12	-7.94
	1.2	1.80	12.71	-1.09	-7.72	4.78	33.87	2.36	16.69	0.06	0.43
Fe_2O_3	1.0	0.10	4.38	2.90	125.03	4.15	179.24	1.23	53.25	-1.03	-44.66
	1.1	0.34	14.81	3.42	147.53	4.80	207.17	1.59	68.57	-0.91	-39.13
	1.2	0.59	25.25	3.94	170.04	5.45	235.09	1.95	83.90	-0.78	-33.59
MnO	1.0	0.04	139.40	0.14	461.21	0.12	388.67	1.41	4692.68	-0.02	-65.64
	1.1	0.05	163.34	0.16	517.33	0.13	437.54	1.56	5171.95	-0.02	-62.20
	1.2	0.06	187.28	0.17	573.45	0.15	486.41	1.70	5651.22	-0.02	-58.76
MgO	1.0	0.13	21.73	-0.01	-1.91	1.48	249.64	3.69	623.70	-0.52	-87.77
	1.1	0.20	33.90	0.05	7.90	1.68	284.61	4.12	696.07	-0.51	-86.55
	1.2	0.27	46.07	0.10	17.71	1.89	319.57	4.55	768.44	-0.50	-85.32
CaO	1.0	-0.13	-75.86	0.00	-0.96	0.14	84.79	4.18	2450.12	-0.16	-93.94
	1.1	-0.13	-73.45	0.02	8.94	0.18	103.27	4.62	2705.13	-0.16	-93.33
	1.2	-0.12	-71.03	0.03	18.84	0.21	121.75	5.05	2960.14	-0.16	-92.72
Na_2O	1.0	-2.85	-94.87	-2.84	-94.39	-2.85	-94.76	-2.85	-94.55	-2.79	-92.78
	1.1	-2.84	-94.36	-2.82	-93.83	-2.84	-94.24	-2.83	-94.01	-2.77	-92.06
	1.2	-2.82	-93.84	-2.81	-93.27	-2.82	-93.72	-2.81	-93.46	-2.75	-91.34
K_2O	1.0	1.64	50.71	0.24	7.51	0.77	23.90	0.91	28.21	0.36	11.10
	1.1	2.12	65.78	0.59	18.27	1.17	36.29	1.33	41.03	0.72	22.21
	1.2	2.61	80.85	0.94	29.02	1.57	48.68	1.74	53.85	1.08	33.32
P_2O_5	1.0	0.00	2.60	0.00	5.23	0.00	4.72	-0.01	-27.38	-0.01	-31.27
	1.1	0.00	12.86	0.00	15.75	0.00	15.19	-0.01	-20.12	-0.01	-24.40
	1.2	0.01	23.12	0.01	26.27	0.01	25.66	0.00	-12.86	-0.01	-17.53
Nb	1.0	-1.75	-11.21	-2.03	-12.99	0.11	0.69	-	-	-2.41	-15.41
	1.1	-0.37	-2.33	-0.67	-4.28	1.68	10.76	-	-	-1.09	-6.95
	1.2	1.02	6.54	0.69	4.42	3.26	20.83	-	-	0.24	1.51
Zr	1.0	-17.43	-6.71	-86.38	-33.25	-23.04	-8.87	-	-	-160.53	-61.79
	1.1	6.80	2.62	-69.04	-26.57	0.63	0.24	-	-	-150.60	-57.97
	1.2	31.04	11.95	-51.70	-19.90	24.31	9.36	-	-	-140.67	-54.15

Y	1.0	-4.09	-12.46	-11.59	-35.32	-3.18	-9.69	-	-	-4.16	-12.67
	1.1	-1.22	-3.71	-9.46	-28.85	-0.22	-0.66	-	-	-1.29	-3.94
	1.2	1.66	5.05	-7.34	-22.38	2.74	8.37	-	-	1.57	4.80
Sr	1.0	-174.18	-92.41	-168.11	-89.19	-175.56	-93.15	-	-	-184.66	-97.97
	1.1	-172.75	-91.65	-166.08	-88.11	-174.27	-92.46	-	-	-184.28	-97.77
	1.2	-171.32	-90.89	-164.04	-87.03	-172.98	-91.77	-	-	-183.89	-97.56
Rb	1.0	72.84	51.46	1.38	0.98	48.38	34.18	-	-	40.68	28.74
	1.1	94.28	66.61	15.67	11.07	67.37	47.60	-	-	58.90	41.61
	1.2	115.71	81.75	29.97	21.17	86.36	61.01	-	-	77.12	54.49
La	1.0	-10.00	-25.55	-5.03	-12.85	6.99	17.87	-	-	7.72	19.75
	1.1	-7.08	-18.11	-1.62	-4.14	11.60	29.66	-	-	12.41	31.72
	1.2	-4.17	-10.66	1.79	4.58	16.21	41.45	-	-	17.09	43.70
Ce	1.0	-20.46	-24.40	-8.81	-10.51	20.55	24.51	-	-	11.18	13.33
	1.1	-14.12	-16.84	-1.31	-1.56	30.99	36.96	-	-	20.68	24.66
	1.2	-7.78	-9.28	6.20	7.39	41.43	49.41	-	-	30.18	35.99
Nd	1.0	-8.90	-26.24	-5.09	-15.01	9.27	27.33	-	-	-0.81	-2.40
	1.1	-6.40	-18.86	-2.21	-6.51	13.58	40.07	-	-	2.50	7.36
	1.2	-3.89	-11.49	0.67	1.99	17.90	52.80	-	-	5.81	17.12
Pb	1.0	3.21	36.41	463.11	5246.24	39.07	442.62	190.73	2158.95	6.68	75.73
	1.1	4.42	50.05	510.30	5780.86	43.86	496.88	210.69	2384.84	8.24	93.30
	1.2	5.62	63.69	557.49	6315.48	48.65	551.14	230.64	2610.74	9.79	110.87
Zn	1.0	8.40	24.50	1291.98	3766.01	46.05	134.23	904.88	2635.54	-14.04	-40.92
	1.1	12.68	36.95	1424.61	4152.61	54.09	157.66	998.80	2909.09	-12.01	-35.01
	1.2	16.95	49.40	1557.24	4539.21	62.12	181.08	1092.72	3182.64	-9.98	-29.10
Cu	1.0	0.37	5.86	294.93	4666.94	3.97	62.89	16.97	268.27	-1.46	-23.09
	1.1	1.04	16.44	325.06	5143.63	5.00	79.18	19.30	305.10	-0.97	-15.40
	1.2	1.71	27.03	355.18	5620.33	6.03	95.47	21.63	341.92	-0.49	-7.71
Ba	1.0	-76.47	-7.23	-487.29	-46.09	-721.15	-68.21	-648.06	-61.25	-465.76	-44.05
	1.1	21.61	2.04	-430.29	-40.70	-687.53	-65.03	-607.05	-57.37	-406.60	-38.46
	1.2	119.69	11.32	-373.29	-35.31	-653.92	-61.85	-566.05	-53.50	-347.45	-32.86

	SiO_2	TiO_2	Al_2O_3	Fe_2O_3	MnO	MgO	CaO	Na_2O	K_2O	P_2O_5	Nb	Zr	Y	Sr	Rb	La	Ce	Nd	Pb	Zn	Cu	Ba
A	73.79	0.37	14.08	2.31	0.03	0.59	0.17	3.00	3.22	0.03	16	259	33	188	141	39	84	34	9	34	6	1054
B	74.74	0.27	12.89	2.35	0.07	0.70	0.04	0.15	4.73	0.03	14	236	28	14	208	28	62	24	12	42	7	953
C	78.89	0.20	10.29	4.94	0.16	0.55	0.16	0.16	3.29	0.03	13	164	20	19	135	32	71	27	447	1257	285	540
D	68.34	0.28	15.00	6.16	0.14	1.97	0.30	0.15	3.81	0.03	15	225	28	12	181	44	99	41	46	77	10	320
E	57.06	0.29	12.57	3.25	1.32	3.92	3.98	0.15	3.79	0.02	-	-	-	-	-	-	-	-	183	859	21	375
F	79.69	0.06	11.43	1.24	0.01	0.07	0.01	0.21	3.47	0.02	13	96	28	4	176	45	92	32	15	20	5	572

A = Unaltered pyroclastics
B = Surface schists
C = Siliceous mine schists, underground
D = Sericitic mine schists, underground
E = Carbonaceous mine schists, underground
F = Massive siliceous rocks (surface)

median values

APPENDIX 6

Equilibrium constants: Silicates

Chemical Reaction	log K 200°C	250°C	300°C
fig 1: log K calculated from data by Henley et al., 1984, after Helgeson et al., 1978			
$2ab + H_2O + 2H^+ = kaol + 4qz + 2Na^+$	9.67	8.82	8.18
$ab + K^+ + H^+ = Kfs + Na^+ + H^+$	1.34	1.10	0.99
$3ab + K^+ + 3H^+ = musc + 6qz + 3Na^+ + H^+$	12.27	11.24	10.55
$3Kfs + 2H^+ = musc + 6qz + 2K^+$	8.26	7.95	7.56
$2musc + 3H_2O + 2H^+ = 3kaol + 2K^+$	4.48	3.96	3.25
fig 2: Data from same source as fig 1			
$2zoi + H_2O + 8H^+ = 3kaol + 4Ca^{2+}$	35.08	30.56	25.80
$zoi + K^+ + 4H^+ = musc + 2Ca^{2+} + H^+ + H_2O$	15.29	13.21	11.18
$zoi + 3K^+ + 4H^+ + 6qz = 3Kfs + 2Ca^{2+} + 3H^+ + H_2O$	7.03	5.26	3.62
fig 3: log K calculated from data by Helgeson, 1969			
$Mg\text{-}chl + 10H^+ = 5Mg^{2+} + 7H_2O + kaol$	40.30	36.29	33.2
$3Kfs + 2H^+ = musc + 6qz + 2K^+$	8.46	8.16	7.81
$Mg\text{-}chl + 4qz + 2K^+ + 10H^+ = 2Kfs + 2H^+ + 6H_2O + 5Mg^{2+}$	32.32	28.79	26.18
$Mg\text{-}chl + 9.56H^+ + 0.52K^+ = 0.87ill + 0.52H^+ + 4.78Mg^{2+} + 7.74H_2O$	37.21	33.61	30.90
$ill + 0.6H^+ + 0.5H^+ + 0.75H_2O = 0.6K^+ + 0.25Mg^{2+} + 1.2qz + 1.15\ kaol$	3.57	3.09	2.66
$2musc + 3H_2O + 2H^+ = 3kaol + 2K^+$	3.51	3.09	2.72
$2Kfs + 1.48H^+ + 0.22Mg^{2+} + 8H_2O = 0.87ill + 1.48K^+ + 0.44H^+ + 1.74H_2O$	4.89	4.82	4.71

qz = quartz
Kfs = feldspar
musc = muscovite
Mg-chl = Mg-chlorite
ab = albite
zoi = zoisite
ill = illite

Equilibrium constants: Sulphides

Chemical Reaction	$\log K_T$ (T in $^{\circ}C$) $\log K = A + B(10^4/T) + C(10^4/T)^2$ A	B	C	Source
$H_2S = H^+ + HS^-$	-21.8359	1.1448	-0.02120	Ripley & Ohmoto (1977, 1980) [2]
$HS^- = H^+ + S^{2-}$	-21.4022	0.8979	-0.01950	"
$2H^+ + SO_4^{2-} = H_2S_{(aq)} + 2O_{2(g)}$	51.09715	-6.2208	0.02950	"
$HSO_4^- = H^+ + SO_4^-$	-19.0477	1.0026	-0.01495	"
$KSO_4^- = K^+ + SO_4^{2-}$	-14.7077	0.9469	-0.01640	"
$NaSO_4^- = Na^+ + SO_4^-$	-14.7077	0.9469	-0.01640	"
$CaSO_4^0 = Ca^{2+} + SO_4^{2-}$	-16.2093	0.9106	-0.01505	"
$MgSO_4 = Mg^{2+} + SO_4^{2-}$	-14.3396	0.6749	-0.00940	"
$H_2S_{(aq)} + 1/2\ H_2O_{(g)} = H_2O_{(l)} + 1/2\ S_{2(g)}$	-3.9973	1.0278	-0.00060	"
$3FeS_2 + 2O_{2(g)} = Fe_3O_4 + 3S_{2(g)}$	14.8401	1.0443	0.00177	"

Chemical Reaction	log K_T (T in ^oC) $\log K = A + B(10^4/T) + C(10^4/T)^2$ A	B	C	Source
$2FeS_2 + 3/2\ O_{2(g)} = Fe_2O_3 + 2S_{2(g)}$	5.5043	1.3466	-0.00377	"
$3FeS + 2O_{2(g)} = Fe_3O_4 + 3/2\ S_{2(g)}$	-7.6752	3.3989	-0.00193	"
$6Fe_2O_3 = 4Fe_3O_4 + O_{2(g)}$	14.8949	-2.6110	0.00175	"
$4FeS_2 + Cu_5FeS_4 = 5CuFeS_2 + S_{2(g)}$	12.560	-1.1067		"
$FeS_2 = FeS + 1/2\ S_{2(g)}$	6.3611	-0.68857		Schneeberg(1973)
$BaSO_4 = Ba^{2+} + SO_4^{2-}$	8.8048	-0.33619	$-2.5138 \times 10^6\ xT^3$	Blount (1977)
$ZnS = Zn^{2+} + S^{2-}$	-35.456	1.2525	-0.02765	Helgeson (1969)
$Zn^{2+} + Cl^- = ZnCl^-$	21.009	-1.1145	0.015912	"
$Zn^{2+} + 2Cl^- = ZnCl_2^0$	24.482	-1.3516	0.019165	"
$Zn^{2+} + 3Cl^- = ZnCl_3^-$	28.214	-1.5905	0.022913	"
$Zn^{2+} + 4Cl^- = ZnCl_4^{2-}$	31.596	-1.8039	0.02603	"
$FeS_2 + 2H^+ + H_2O = Fe^{2+} + 2H_2S + 1/2\ O_{2(g)}$	84.105	-9.0405	1.8484	Walshe & Solomon (1981)
$CuFeS_2 + H^+ + 1/4\ O_2 = FeS_2 + Cu^+ + 1/2\ H_2O$	$\log K_{48} = -61.681 + 1913/T + 0.05819T$			"

APPENDIX 7

Analytical methods

1. Determination of major and trace elements by XRF method

Major and trace element contents except for sulphur were determined by X-ray fluorescence spectrometry. The XRF-spectrometer (Philips PW 1140/00) used at the Geology Department, University of Tasmania has four sample holders and is controlled by a TRS-80 micro computer.

For the analysis of major elements , fusion discs (Norrish& Hutton, 1969) of 1.5 g lithium borate, 0.02 mg sodium nitrate and 0.28 g powdered rock sample were used. Analysis of trace element contents was based on pressed powder pills (Norrish & Chappell, 1977) using $\geq$ 3 g of powdered rock sample and boric acid crystals. Part of the Ba-analyses were carried out by Analabs, div. of MacDonald Hamilton & Co. Pty Ltd. (Welshpool, Western Australia). Mass absorption coefficients were determined from major rock compositions. In the absence of this information, mass absorption coefficients for the analysis of Zn, Pb, Cu, Ni and Co were determined by the measurement of Compton-scatter intensities (Norrish & Chappel, 1977). Although this method is not strictly applicable for Co, differences in the Co contents determined by both methods lie within the analytical error (tab.18a). The analytical precision of sample duplicates, repeated standard measurements, and instrumental settings are listed in tab. 18a, b.

2. Determination of Sulphur

The sulphur content of powdered rock samples was determined by iodate titration (0.444 g KIO_3/l) using a LECO induction furnace (model no. 632-000) (Turnbull, 1980). Combustion for each sample lasted for 6 minutes under an oxygen stream of 1l/min. Sample weight varied between approximately 10 and 500 mg. Based on a standard of 3.84% sulphur content determmined by X-ray fluorescence spectrometry (P. Robinson, pers. comm., Geol. Dept., Univ. of Tasmania) 92.44% of sulphur was converted to SO_2 as indicated by the titration process. The remaining sulphur was converted to SO_3 and could not be detected by the iodate titration. Repeated measurements of this standard (n = 10) resulted in a sulphur content of

3.55 ± 0.03%. The half range of duplicates from samples was 1.31 ± 1.64% of the mean value. Part of the sulphur analyses was carried out by Electrolytic Zinc Co. Pty Ltd. in Rosebery. The results were in good agreement with repeated analyses by the writer.

3. Determination of REE

The determination of the extended set of REE (La, Ce, Pr, Nd, Sm, Eu, Gd, Dy, Er and Yb) was carried out by a combined ion exchange (IE)-XRF technique (Higgens et al., 1983; Robinson et al., in press). Powdered rock samples of 1 g were completely dissolved in 20 ml of concentrated HF and concentrated $HClO_4$. Subsequent use of ion-exchange resin (Bio-Rad AG50W-X8, 100-200 mesh) enabled the extraction of the REE which were absorbed in ion-exchange paper (Whatman, Reeve Angle, SA-2) after removal of Ba. The ion-exchange paper finally was analysed for REE by X-ray fluorescence spectrometry.

Using standards (TASGRAN, tab.19) from this study, the analyses were adjusted to a standard (TASGRAN, tab.19) determined by spark source mass spectrography (SSMS) (Dr. S.R. Taylor, 1981, ANU Research School of Earth Sciences, pers. comm. to Dr. N.C. Higgins, then Geol. Dept. of Tasmania).

The techniques described above generally achieved lower values for La, Ce and Nd than by XRF method using powder pills. In fig.70, 71, 74, 75, 76 and 77, the contents of La, Ce and Nd as determined by the latter method were used

4. Determination of oxygen isotope

The determination of oxygen isotope was carried out by Krüger Enterprises, Inc., Geochem. Laboratories Div. (Cambridge, Massachusetts). Two samples were analysed in duplicate:

sample	$\delta\,^{18}O$
67335	+12.1
	+11.9
67800	+12.4
	+12.3
Standard NBS28	+9.4

5. Determination of rock densities

The rock density was determined using a 25 ml pycnometer and 1-2 g finely chipped rock samples. The half range of duplicates was 0.63 $\pm$ 0.45% of the mean value.

6. Mineral analysis by electron microprobe

Mineral compositions were examined from polished thin sections using the scanning electron microscope - electron microprobe analyser (SEM - EMPA) in the Central Science Laboratory at the University of Tasmania. The instrument can perform wave length and energy dispersive analysis (multichannel analyser: EG & G ORTEC EEDS II, previously EDAX) and is controlled by a PDP 11/23, 34 computer. Bean current used was 7.10 x 10^{-10}A, calibrated on pure Cu. Silicate analysis required 15 kV acceleration voltage and 60 seconds counting time. For sulphide, 20kV and 100 seconds were used.

TASGRAN

	Run 1		Run 2		Run 3	Run 4	SSMS (Taylor, 1984)
La	38.1	37.6	25.7	24.0	38.1	35.6	34.2
Ce	92.3	89.0	65.9	61.6	93.1	88.6	80.1
Pr	9.1	10.2	7.4	7.3	9.6	9.0	9.7
Nd	36.2	35.6	28.1	27.2	36.3	35.6	37.3
Sm	7.2	6.9	6.3	6.5	7.1	7.3	7.5
Eu	0.7	0.9	1.2	1.2	0.8	0.8	0.8
Gd	6.1	5.7	6.4	6.5	5.9	6.2	6.7
Dy	4.2	4.0	4.6	4.6	4.1	4.2	5.5
Er	1.8	2.0	2.7	2.9	1.9	1.9	3.3
Yb	2.9	2.9	3.6	3.7	3.1	3.2	3.0

Tab.19: TASGRAN determined by IE-XRF method

ERRATA

References:

Robinson, P., Higgins, N.C. & Jenner, G.A., 1986: Determination of rare earth elements, Yttriun and Scandium in rocks by ion exchange - X-ray fluorescence technique, Chem. Geol., in press

Rui, I.J., 1973: Structural control and wall rock alteration at Killingdal Mine, Central Norwegian Caledonides, Econ. Geol., 68, 859-883

Shimazaki, Y., 1974: Ore minerals of the Kuroko-type deposits, Mining Geol. Spec. Issue, 6, 311-322

Fig. 54 Mineralogical cross section through northern orebody at 15L. Left half-column (S) represents sphalerite-galena ore and right half-column (P) represents pyrite-chalcopyrite ore.